2021

Using New and Long-Term Multi-Scale Remotely Sensed Data to Detect Recurrent Fires and Quantify Their Relationship to Land Cover/Use in Indonesian Peatlands

Yenni Vetrita
South Dakota State University

USING NEW AND LONG-TERM MULTI-SCALE REMOTELY SENSED DATA TO DETECT RECURRENT FIRES AND QUANTIFY THEIR RELATIONSHIP TO LAND COVER/USE IN INDONESIAN PEATLANDS

BY

YENNI VETRITA

A dissertation submitted in partial fulfillment of the requirements for the

Doctor of Philosophy

Major in Geospatial Science and Engineering

Specializing in Remote Sensing Geography

South Dakota State University

2021

DISSERTATION ACCEPTANCE PAGE

Yenni Vetrita

This dissertation is approved as a creditable and independent investigation by a candidate for the Doctor of Philosophy degree and is acceptable for meeting the dissertation requirements for this degree. Acceptance of this does not imply that the conclusions reached by the candidate are necessarily the conclusions of the major department.

Xiaoyang Zhang

Advisor Date

Mark Cochrane

Advisor Date

Robert Watrel

Department Head Date

Nicole Lounsbery, PhD
Director, Graduate School Date

This dissertation is dedicated to whom I should call "Doctor" rather than myself: my beloved husband, Ery.

ACKNOWLEDGEMENTS

As you read this book, consider it not just as a work of science, but also reflecting a period of my life, with all its sacrifices, tears and happiness. This book symbolizes a renewed awakening of my scientist life. I have met many good, caring people with such positive thoughts, through whom I have learned and improved and never gave up. I cannot list all their names here. For those not mentioned below, this does not mean you have contributed less to my PhD life. I contacted them privately to say how grateful I was for their help.

My first thanks go to my intelligent 'father', mentor, and dissertation advisor, Dr. Mark Alan Cochrane, who deserves the highest credit for this achievement. I know it was definitely not easy for him to supervise this first Indonesian student, seeking her own identity for over 5 years. All his time sacrifice, devotion, and best thoughts can never be paid back. He also helped me carry my happiness - my family - to live with me in Brookings, South Dakota.

LAPAN's full support, and the scholarship from the Ministry of Science, Technology and Higher Education (RisetPro) made this study trip even more possible and enjoyable. I would also like to thank:

- My committee members: Dr. Xiaoyang Zhang who supervised me after Dr. Cochrane left to UMCES in 2017; Dr. Geoffrey Henebry from whom I learned more about being an excellent scientist; Dr. Carol, whose real loving always helped to calm me down; and Dr. Christopher Schmit, who always made sure I was on my work path.
- Mark's team (Pak Prof. Bambang Hero and his team in Bogor University Indonesia, Dr. Laura Graham and her team at the Borneo Orangutan Survival, and also Dr. Israr Albar at the Indonesian Ministry of Environment and Forestry) and Dr. Wilfrid Schroeder (NOAA)
- Special thanks to Dr. Njoki Kahiu for always being such a great sister for me, Dr. Kamilya Kelgenbeva for her courage, Kaboro, Jianmin, Dr. Izaya Numata, Dr. Lan Nguyen, Suwarsono, and Dr. Nathan Serfling (the writing center coordinator)
- Former fellow members of GSCE, students and instructors (Dr. David Roy, Dr. Michael Wimberley)

- *Ayah-ibu dan anak-anakku tersayang*, *bapak-mamah Ciamis*, and all my family members for their endless love

So, this book isn't just an ordinary thesis that helped me to get the "PhD" stamp. And it doesn’t belong to me, but to my husband, Ery, who dreamed of taking this PhD to the U.S. Thanks for being the biggest supporter. *This stamp is yours.*

CONTENTS

ABBREVIATIONS

AF	Active Fire
AHI	Advanced Himawari Imager
ALOS	Advanced Land Observation Satellite
AMSR	Advanced Microwave Scanning Radiometer
APAB	Annual Percentage of Area Burned
AQI	Air Quality Index
BA	Burned area
BBSDLP	*Balai Besar Sumberdaya Lahan Pertanian*
BOSF	Borneo Orangutan Survival
BRDF	Bidirectional Reflectance Distribution Function
BRG	*Badan Restorasi Gambut* (Peat Restoration Agency)
CCI	Climate Change Initiative
CH_4	Methane
CO_2	Carbon dioxide
DAAC	Distributed Active Archive Center
DNB	Day/Night Band
ECV	Essential Climate Variables
ENSO	El Nino-Southern Oscillation
EOS	Earth Observing System
ESA	European Space Agency
ETM+	Enhanced Thematic Mapper Plus
EVI	Enhanced Vegetation Index

FC	Fire Cycle
FREL	Forest Reference Emissions Level
FRI	Fire Return Interval
FRP	Fire Radiative Power
GBBEP-Geo	Global Biomass Burning Emission Product-Geostationary-satellite
GFAS	Global Fire Assimilation System
GFED	Global Fire Emission Database
GHG	Greenhouse Gases
GWEM	Global Wildland Fire Emission Model
IGBP	International Geosphere-Biosphere Programme
IPCC	Intergovernmental Panel on Climate Change
ISRO	Indian Space Research Organisation
LAPAN	Lembaga Penerbangan dan Antariksa Nasional (Indonesian National Institute of Aeronatics and Space)
LULC	Land Use Land Cover
LULCC	Land Use Land Cover Change
MCD45A1	MODIS Burned Area Collection 5
MODIS	Moderate Imaging Spectroradiometer
MOEF	Ministry of Environment and Forestry
MRV	Measurable, Reportable, and Verifiable
MSAVI	Modified Soil Adjusted Vegetation Index
MSI	MultiSpectral Instrument
MTSAT	Multifunctional Transport Satellites

NASA	National Aeronautics and Space Administration
NBR	Normalized Burn Ratio
NDMI	Normalized Difference Moisture Index
NDVI	Normalized Difference Vegetation Index
NIR	Near Infrared
NISAR	NASA-ISRO Synthetic Aperture Radar
NOAA	National Oceanic and Atmospheric Administration
NPP	National Polar-orbiting Partnership
OLI	Operational Land Imager
PSF	Peat Swamp Forest
Radar	RAdio Detection And Ranging
REDD	Reducing Emissions from Deforestation and forest Degradation
RGB	Red, Green, Blue
SAR	Synthetic Aperture Radar
SAVI	Soil Adjusted Vegetation Index
SLSTR	Sea and Land Surface Temperature Radiometer
SMAP	Soil Moisture Active Passive
SPOT	Satellite Pour l'Observation de la Terre
SWIR	Short Wave Infrared
TIR	Thermal Infrared
TIRS	Thermal Infrared Sensor
USGS	The United States Geological Survey
VIIRS	Visible Infrared Imaging Radiometer Suite

VIIRS-AF	VIIRS 375 m gridded active fire

LIST OF FIGURES

LIST OF TABLES

ABSTRACT

USING NEW AND LONG-TERM MULTI-SCALE REMOTELY SENSED DATA TO DETECT RECURRENT FIRES AND QUANTIFY THEIR RELATIONSHIP TO LAND COVER/USE IN INDONESIAN PEATLANDS

YENNI VETRITA

2021

Indonesia has committed to reducing its greenhouse gases emissions by 29% (potentially up to 41% with international assistance) by 2030. Achieving those targets requires many efforts but, in particular, controlling the fire problem in Indonesia's peatlands is paramount, since it is unlikely to diminish on its own in the coming decades.

This study was conducted in Sumatra and Kalimantan peatlands in Indonesia. Four MODIS-derived products (MCD45A1 collection 5.1, MCD64A1 (collection 5.1 and 6), FireCCI51) were initially assessed to explore long-term fire frequency and land use/cover change relationships. The results indicated the product(s) could only detect half of the fires accurately. A further study was conducted using additional moderate spatial resolution data to compare two years of different severity (2014 and 2015) (Landsat, Sentinel 2, Sentinel 1, VIIRS 375 m). The results showed that MODIS BA products poorly discriminated small fires and failed to detect many burned areas due to persistent interference from clouds and smoke that often worsens as fire seasons progress. Although there are unique fire detection capabilities associated with each sensor (MODIS, VIIRS, Landsat, Sentinel 2, Sentinel 1), no single sensor was ideal for accurate detection of peatland fires under all conditions. Multisensor approaches could advance biomass-burning detection in peatlands, improving

the accuracy and comprehensive coverage of burned area maps, thereby enabling better estimation of associated fire emissions.

Despite missing many burned areas, MODIS BA (MCD64A1 C6) provides the best available data for evaluating longer term (2001-2018) associations between the frequency of fire occurrence and land use/cover change across large areas. Results showed that Sumatra and Kalimantan have both experienced frequent fires since 2001. Although extensive burning was present across the entire landscape, burning in peatlands was ~5-times more frequent and strongly associated with changes of forest to other land use/cover classes. If fire frequencies since 2001 remain unchanged, remnant peat swamp forests of Sumatra and Kalimantan will likely disappear over the next few decades. The findings reported in this dissertation provide critical insights for Indonesian stakeholders that can help them to minimize impacts of environmental change, manage ecological restoration efforts, and improve fire monitoring systems within Indonesia.

CHAPTER 1

INTRODUCTION

1.1 Indonesian peatlands: the importance, degradation, and related land use/cover change

Indonesia holds the highest proportion of tropical peat carbon (65%) with an estimated 28.1-57.4 Gt (Page et al. 2011; Warren et al. 2017). Natural peat swamp forests are relatively inaccessible mucky wetland ecosystems, posing challenges for human exploitation. These barriers promote the existence of unique flora and fauna, such as crocodile (*Crocodylus porosus*), gibbons (*Hylobates* spp), macaques (*Macaca* spp) and orang-utan (*Pongo pygmaeus*), freshwater fish, birds, and commercial timber species such as Ramin (*Gonystylus bancanus*), *Shorea* spp, etc (Phillips and Conservation 1998; Posa et al. 2011). This rich biodiversity is currently under risk, however, since access to these ecosystems has been permitted and facilitated, enabling exploitation of many peatlands.

In 1997, Indonesia's peatlands drew worldwide attention when extensive peatland fires were estimated to have emitted 0.81-2.57 Gt Carbon, equal to 13-40% of average annual global fossil fuel carbon emissions (Page et al. 2002b). Despite Indonesia having a one-fifth the land area of the United States, the percentage covered by peatlands is comparatively higher (Xu et al. 2018) (8-15% vs. 2-2.5%, respectively). This is a considerable amount of land area for this small country that has a poulation of more than 80% that of the United States. Burning is not a new practice for traditional agriculture (Chokkalingam et al. 2007; Dennis et al. 2005). However, since peatlands have been degraded and drained for uses other than natural forests, they have become increasingly flammable. Consequently, Indonesia's peatlands now have shifted from being a net carbon

sink, with a huge amount of carbon-storage in a fire-resistant environment, to becoming a vulnerable source of frequent and sometimes immense carbon emissions.

Forest conversion to plantations has been blamed for the large areas of peatland burned, though Cattau et al. (2016) found few fires to have originated in plantations. Following initial deforestation events, recurrent fires alter the composition and structure of plant communities; maintaining fire-dependent vegetation in a self-reinforcing positive feedback loop (Cochrane et al. 1999; Siegert et al. 2001). These conditions lead to easier fire spread, increasing amounts of fire occurrences, and greater probability of changing the fire regime over time (Cochrane and Barber 2009; Hoscilo et al. 2011). To date, little comprehensive analysis exists of the spatiotemporal patterns of recurrent fires in Indonesia (Hoscilo et al. 2011; Langner and Siegert 2009).

Human activities have been reported as the root cause of the problem, through activities such as forest conversion to agricultural land, land settlement, illegal logging, land tenure conflicts (DeFries et al. 2010; Geist and Lambin 2002; Hosonuma et al. 2012; Laumonier et al. 2010) that cause more fires to ignite and spread. Once ignited, peatland fires can be extremely difficult to extinguish, especially when surface fires persist long enough to ignite the underlying peat. The resultant ground fires that dominate in drained peatlands (Stockwell et al. 2016) produce heavy smoke and a greater amount of aerosol particles than flaming combustion (e.g., California fires). Indonesia has committed to reducing its greenhouse gases emissions by 29% (potentially up to 41% with international assistance) by 2030, making efforts to control fire in Indonesian peatlands crucial. This issue is made even more important because the abundant smoke from peatlands fires causes

serious health impact, human loss of life, and other socio-economic problems (Koplitz et al. 2016).

1.2 Satellite-based approach to estimate carbon emissions

Applications of satellite-based observation of carbon emissions (trace gases and aerosols) provide the most consistent and systematic approach for monitoring of MRV (measurable, reportable, and verifiable) projects. Satellites, including AURA (Ozone Monitoring Instrument (OMI)) and the Greenhouse Gases Observing Satellite (GOSAT) (see (Streets et al. 2013) for comprehensive review) have been developed to quantify emissions of trace gases and aerosols. However, the most widely used approach adopted by the Intergovernmental Panel on Climate Change (IPCC) for estimating emissions is to quantify the amount and type of fuel consumed and the combustion characteristics (Seiler and Crutzen 1980). The model variables include burned area, fuel loading (biomass density), combustion completeness or percentage of biomass consumed, and emission factors for trace gasses and aerosols per unit dry matter.

$$E = BA \times B \times CC \times EF \qquad \text{Equation 1}$$

where E represents emissions from biomass burning (kg), BA is total area burned (km^2), B is the fuel load (kg/km^2), CC is combustion completeness (unitless, range 0–1), and EF is any specific gas emission factor ($g\ kg^{-1}$).

Current satellite approaches do not supply all parameters, notably emission factors. These parameters are calculated from lab or field data (Akagi et al. 2011; Andreae and Merlet 2001; Christian et al. 2003; Yokelson et al. 2003). Among the four parameters in Equation 1, remote sensing analysis plays a critical role in providing burned area since it

is relatively simpler and less expensive than conducting widespread field assessments. However, burned area continues to be among the greatest sources of error.

The Global Fire Emission Database (GFED) (van der Werf et al. 2017) and Global Wildland Fire Emission Model (GWEM) (Hoelzemann et al. 2004) are two examples of products reliant on burned area maps. GFED currently uses the fourth-generation Global Fire Emission Database (GFED4), while GWEM uses the monthly Global Burnt Scar Satellite Product (GLOBSCAR) from the European Space Agency.

1.3 Satellite-based approach uncertainties to estimate the fire-related emissions from Indonesian peatlands

The primary source of errors in the emissions estimate approach (Equation 1) derive from quality of the input data (Hoelzemann et al. 2004; van der Werf et al. 2010). Ideally, parameters should be directly measured at each location in the field. However, considering the significant spatial and temporal extents involved this is unrealistic. Acquisition of such data remains essential, but field-based calculations of area burned are lacking in Indonesia (Shi et al. 2014) or available only through rough estimation before 2015 (MoEF 2020). Since 2015, the Indonesian government has been producing satellite-based annual burned area maps, primarily using visual analysis methods (Endrawati 2016; Endrawati et al. 2018). Systematic satellite-based burned area mapping methods are still needed.

Satellite-based burned area mapping and gridded active fire (burned area-based active fire) are two common approaches for estimating burned area, reported as burn scars or fire-affected areas in various publications (Garcia-Haro et al. 2001; Langner et al. 2007; Lohberger et al. 2017; Roy et al. 2005). The use of gridded active fire to estimate burned area is of debatable use because active fire product(s) only record the location and time of

fires during satellite overpasses, without mapping the actual areas burned across landscapes (Giglio et al. 2006; Roy et al. 2008). However, Wiedinmyer et al. (Wiedinmyer et al. 2011) argue that burned area estimates should be near real-time in order to effectively estimate emissions but currently available burned area products are unable to provide such rapid inputs. In addition, existing burned area products have reported limitations for peatland areas, including insufficient detections of small area or low-temperature smoldering fires and inability to detect flaming combustion under heavy smoke or cloud cover, or within gaps between orbits near the equator (MODIS product) (Csiszar et al. 2003; Csiszar et al. 2006; Giglio et al. 2006; Schroeder et al. 2008; Tansey et al. 2008).

Despite these limitations, active fire product(s) are useful for integrating with post-fire burned area maps (Chuvieco et al. 2018; Fraser et al. 2000; Giglio et al. 2018; Giglio et al. 2009). Overall, all fire products are to some degree under-sampling fire activity because they miss many fires, suggesting that accurate detection and mapping of fire activity in Indonesia's peatlands is doubtful. However, the Visible Infrared Imaging Radiometer Suite (VIIRS) 375 m active fire product (Schroeder et al. 2014), has recently been reported to reliably to detect peatland fires (Sofan et al. 2020), as well as mapping areas burned in global applications (Oliva and Schroeder 2015). However, no specific assessments have yet been conducted for Indonesia, let alone in peatland areas.

The second approach of satellite-based burned area mapping is derived from mapping the extent and spatial distribution of burn scars or fire-affected areas. Theoretically, surface spectral changes caused by fire are observable. Near infrared (~0,75-1,4 μm) and shortwave infrared (~1,4-3 μm) are the best spectral bands for separating burned and unburned vegetation (Huang et al. 2016). Other spectral bands are also used,

e.g. red (~0.6 to 0.7 μm), as the wavelength is sensitive to changes in vegetation-reflectance. Over the last two decades, large-scale burned area mapping has been studied using coarse (≥1 km^2) and medium-resolution (20–500 m) optical sensors (Boschetti et al. 2009; Boschetti et al. 2015; Chuvieco et al. 2018; Chuvieco et al. 2019; Roteta et al. 2019; Roy et al. 2008; Roy et al. 2019; Tansey et al. 2004). Accuracy from approaches relying on optical sensors suffer due to the inability to observe areas under clouds or smoke. Therefore, applications using active sensors (radar) that are capable of penetrating the clouds and smoke that frequently impede land cover/use mapping in the tropics offer great promise, particularly in cloud-prone areas such as Indonesia (Lohberger et al. 2017; Siegert and Ruecker 2000).

Leveraging the archive of NASA Earth observations and other free multi-resolution data (e.g., Landsat, Sentinel-2, Sentinel-1) provides promising opportunities to address burned area mapping challenges. Several efforts to develop systematic information have been proposed using Landsat (e.g., (Boschetti et al. 2015; Hawbaker et al. 2017), Sentinel-2 (Roteta et al. 2019; Roy et al. 2019), and Sentinel-1 (Carreiras et al. 2020; Lohberger et al. 2017)). Active and passive sensors may increase both spatial completeness and thematic detail (Reiche et al. 2013). To date, such comprehensive work integrating these approaches has not been attempted for Indonesia.

Beyond burned area uncertainties, fuel load and combustion completeness definitions vary among fuel load product-approaches, leading to substantial discrepancies among various satellite-based global products (Boschetti et al. 2004; Giglio et al. 2010; Roy and Boschetti 2009; van der Werf et al. 2010). The impact of using different (fuels) conversion factors illustrates the significant uncertainties among currently available

biomass burning emission estimates (Baldassarre et al. 2015). Emission factors and fuel/vegetation types are dependent on each other, so misclassifications of forest/land cover classes result in incorrect calculations. The most recent update of GFED (version 4) changed the emission factors, increasing emission estimates from the previous version (van der Werf et al. 2017). This further points to the critical influence of parameters in making emissions estimates.

Limited emission factors data from field measurements require making coarse extrapolations from limited sources in global products, potentially leading to inaccurate estimations. For Indonesian peatlands, emission factors used to estimate carbon emissions have been derived from a single peat sample from Sumatra burned in a laboratory setting (Christian et al. 2003), updated by Akagi et al. (Akagi et al. 2011). However, recent field-based measurements from dozens of smoldering peat fires in Kalimantan during 2015 (Jayarathne et al. 2018; Stockwell et al. 2016) support significant revision of several important peatland emission factors. Specific greenhouse gases requiring substantial revisions (decrease or increase) include CO_2 (-8 %), CH_4 (-55 %), NH_3 (-86 %), and CO (+39 %). This finding indicates potential for variable emission factors from peat at different locations (Reid et al. 2013), meaning extrapolations to other regions should be considered carefully.

Two additional remaining concerns for peat fire emissions involve the peat fuel source and the amount consumed by fire. The first issue regards uncertainty of peatland maps, including peatland area distribution, depth, and other biophysical characteristics. Mapping peatlands is difficult due to the problems with accessing and exploring these ecosystems (Page et al. 2002a). In Indonesia, the existing map from Wetland International

(Wahyunto and Subagjo 2003, 2004) is widely used but limited to Sumatra and Kalimantan only. An updated version issued by the Indonesian Ministry of Agriculture (Balai Besar Penelitian dan Pengembangan Sumberdaya Lahan Pertanian, BBSDLP) is available for 2011 (Ritung et al. 2011). The main discrepancy between the two is the exclusion of shallow peat (<0.5 m depth) from the updated version, which helps explain the greater peatland area in the Wetland International version (13.0 Mha vs. 11.2 Mha). The highest disparity is found in smallholder areas (3.1 Mha vs. 2.5 Mha) (Miettinen et al. 2017) where burning occurs more frequently (Miettinen and Liew 2010). The BBSDLP map was officially revised in 2019 (Gatra 2019), further decreasing peatland areas by another 1.5 million hectares, but the map product has not yet been made publicly available. This suggests the critical need for coherent peat definitions and peatland distribution information for making accurate carbon emissions estimations.

A second problem is uncertainty about the amount of peat actually consumed by fires throughout areas that are burned. Consumption rates depend on factors as varied as moisture levels to frequency of previous burning. Moisture levels largely constrain ignition probability of peat soils by surface fires, which are not constant (Aswin et al. 2004; Frandsen 1997). Typically, various factors affect peat burning rates, such as dry conditions, the intensity of fires, and whether rainfall occurs during fires. A consistent relationship between burned depth and distance to the water table in the peat layer (Ballhorn et al. 2009) suggests that peat hydrology should be considered when mapping burned area in peatlands (Taufik et al. 2017). However, degraded peat has reduced ability to hold and maintain water, altering ground water levels (Putra et al. 2018). Varied degrees of degradation have also raised the uncertainty regarding emissions from peat fires since the bulk densities of

the affected peat are altered to become denser (i.e. increased bulk density) but with lowered peat surfaces that are closer to water table depths (Sinclair et al. 2020). Peat burning to several meters below the original surface is improbable, even though fires can be located on peat domes of considerable depth (Ballhorn et al. 2009), because combustion proceeds ever slower as deeper peat becomes less flammable with rising moisture levels and fires become less oxygenated with the build-up of overlying char and ash (Aswin et al. 2004).

Depths of peat burning also varies with distance from drainage canals and prevalence of tree roots and buried logs (Ballhorn et al. 2009; Konecny et al. 2016; Simpson et al. 2016; Sinclair et al. 2020). Consequently, depth of peat burning is inconsistent and decreases with fire frequency (Konecny et al. 2016). Repeated burning not only affects depth of peat burned but also alters emissions (Kuwata et al. 2017). Charcoal, produced during previous burning, was found to lower methane emissions by more than an order of magnitude compared to burning of fresh peat. Heating of peat during smoldering combustion, to temperatures as high as 400^{o}C, can also play an important role in determining the constituent emissions from peatland burning (Kuwata et al. 2017). All these factors highlight the links between the dynamics of peatland fires and carbon emissions uncertainty as drawn in Figure 1-1.

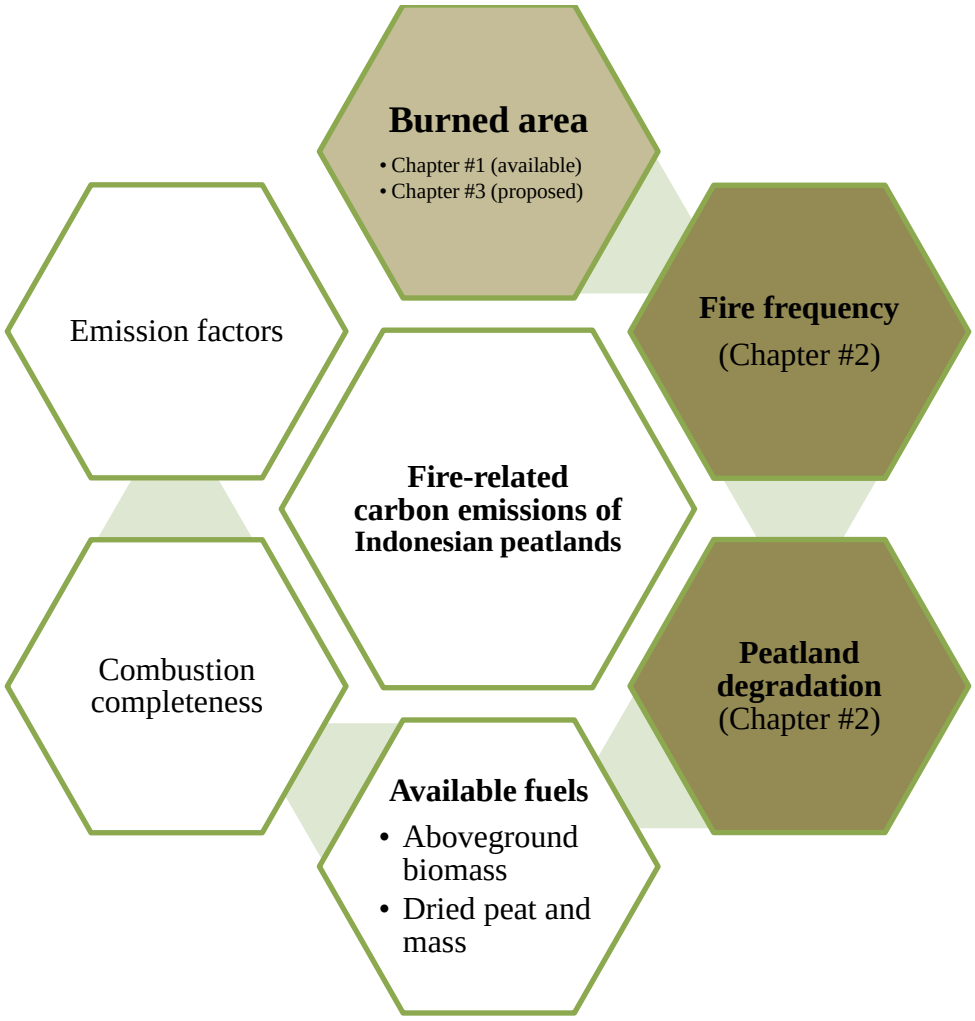

Figure 1-1. Key variables for estimating fire-related emissions in Indonesian peatlands. Remote sensing plays a major role in detecting and mapping burned areas, enabling spatial determination of the frequency of fire. Fire frequency not only affects the amount of emissions released from peat fires but is also interrelated with other drivers of peat depletion such as land use/cover transition following construction of drainage canals. Altering vegetation and hydrology ultimately modifies available fuels, both above- and belowground, affecting where and how remaining peat burns as well as changing the emissions being produced by the fires. These elements are linked to how much fuel is consumed and the quantity of emissions that are released. This dissertation focuses on the landscape level components (shaded brown) whereas the other factors are more site-specific.

1.4 Research objectives

In this dissertation, I focus on three interrelated main topics (shaded brown in Figure 1-1). These include an assessment of currently available burned area products and their potential to impact emissions estimates from fires in Indonesia's peatlands (Topic #1); construction of a long-term map (2001-2018) of fire occurrences in and around Indonesia's peatland across Sumatra and Kalimantan and linking fire occurrence and frequency to associated land use/cover changes (Topic #2); and future directions and potential for using multiscale optical and active sensor remote sensing products to improve mapping of burning in Indonesian peatlands (Topic #3). To be clear, site specific factors or combustion-related factors such as combustion completeness and emissions factors are discussed but not specifically explored in this research.

Topic #1. How accurate are existing moderate resolution burned area products for detecting and mapping peatland and non-peatland fires? To frame this research, I asked two specific questions:

- How do fire patch size and temporal window of detection (e.g. 8-10 day compositing) affect accuracy for the various products?
- What are the discrepancies among current MODIS-derived products and have there been improvements over preceding product versions?

This chapter was submitted to *Environmental Research Letters* (10.10.2020) and has now been accepted (12.18.2020). In this manuscript, I discuss the implications of my findings for fire-related emissions models and the need for development of improved burned area products.

Topic #2. How do long-term fire occurrences (fire frequency) vary between Indonesian peatland regions and what are their associations with land use/cover (LULC) changes? I used the most accurate available moderate resolution burned area product, from Topic #1, to answer three questions:

- How do fire occurrences differ spatially between peatland regions of Sumatra and Kalimantan?
- Which LULC types were most closely associated with burning, including determination of LULC connections to recurring fires?
- How does fire frequency differ between peatland regions and progress over time?

This chapter was accepted in late 2019 and published in early 2020:

Vetrita, Y. and Cochrane, M.A., 2020. Fire Frequency and Related Land-Use and Land-Cover Changes in Indonesia's Peatlands. Remote Sensing, 12(1), p.5. https://doi.org/10.3390/rs12010005

Topic #3. How can existing burned area (BA) products (MODIS burned area) and moderate-resolution imagery from Sentinel-2, Sentinel-1, Landsat, and gridded VIIRS 375 m active fire be used to improve the accuracy of BA mapping in Indonesian peatlands?

This topic follows up upon my recommendations made in Topic #1 based on my research findings to answer the questions below:

- How reliable/accurate are existing burned area products (MODIS) in peatlands over time as the fire season progresses?

- To what extent could available multisensor data (Sentinel-2, Sentinel-1, Landsat, gridded VIIRS 375-m active fire) be used to improve burned area estimation in peatlands?

I discuss the challenges and opportunities for producing a long-term burn history (1997-2015) for my test study site in Kalimantan and the potential for expanding the approach to create a national scale product.

These results were prepared for submission to ISPRS Journal of Photogrammetry and Remote Sensing.

1.5 Significance of the research

This research will fill the gap in our knowledge of 1) the landscape dynamics of peatland fires, 2) the uncertainty of carbon emissions from peatland fire activities, and 3) will provide a new approach to filling the existing uncertainty gap. The findings reported in this dissertation could help prioritize management activities in Indonesian peatlands (e.g. Indonesia's Peatland Restoration Agency (BRG) ongoing efforts to restore 2.5 million hectares of disturbed peatlands), strengthen early warning systems in Indonesia, and support ongoing climate change adaptation and mitigation processes (including REDD+) in the region. The results would also potentially be relevant for understanding and mitigating similar changes in peatlands worldwide.

1.6 Structure of the dissertation

The dissertation consists of five chapters, where the first chapter belongs to the introduction. Topic #1, #2, and #3 are discussed in Chapter 2 to 4, respectively. Finally, I conclude the research findings and address recommendations in Chapter 5.

References

Akagi, S., Yokelson, R.J., Wiedinmyer, C., Alvarado, M., Reid, J., Karl, T., Crounse, J., & Wennberg, P. (2011). Emission factors for open and domestic biomass burning for use in atmospheric models. *Atmospheric Chemistry and Physics, 11*, 4039-4072

Andreae, M.O., & Merlet, P. (2001). Emission of trace gases and aerosols from biomass burning. *Global biogeochemical cycles, 15*, 955-966

Aswin, U., Hashimoto, Y., Takahashi, H., & HAYASAKA, H. (2004). Combustion and thermal characteristics of peat fire in tropical peatland in Central Kalimantan, Indonesia. *Tropics, 14*, 1-19

Baldassarre, G., Pozzoli, L., Schmidt, C., Unal, A., Kindap, T., Menzel, W., Whitburn, S., Coheur, P.-F., Kavgaci, A., & Kaiser, J. (2015). Using SEVIRI fire observations to drive smoke plumes in the CMAQ air quality model: a case study over Antalya in 2008. *Atmospheric Chemistry and Physics, 15*, 8539-8558

Ballhorn, U., Siegert, F., Mason, M., & Limin, S. (2009). Derivation of burn scar depths and estimation of carbon emissions with LIDAR in Indonesian peatlands. *Proc Natl Acad Sci U S A, 106*, 21213-21218

Boschetti, L., Eva, H.D., Brivio, P.A., & Gregoire, J.M. (2004). Lessons to be learned from the comparison of three satellite-derived biomass burning products. *Geophysical Research Letters, 31*

Boschetti, L., Roy, D., & Hoffmann, A. (2009). MODIS Collection 5 Burned Area Product-MCD45. *User's Guide, Ver, 2*

Boschetti, L., Roy, D.P., Justice, C.O., & Humber, M.L. (2015). MODIS–Landsat fusion for large area 30m burned area mapping. *Remote Sensing of Environment, 161*, 27-42

Carreiras, J.M., Quegan, S., Tansey, K., & Page, S.J.E.R.L. (2020). Sentinel-1 observation frequency significantly increases burnt area detectability in tropical SE Asia, *15*, 054008

Chokkalingam, U., Permana, R.P., Kurniawan, I., Mannes, J., Darmawan, A., Khususyiah, N., & Susanto, R.H. (2007). Community fire use, resource change, and livelihood impacts: The downward spiral in the wetlands of southern Sumatra. *Mitigation and Adaptation Strategies for Global Change, 12*, 75-100

Christian, T.J., Kleiss, B., Yokelson, R.J., Holzinger, R., Crutzen, P., Hao, W.M., Saharjo, B., & Ward, D.E. (2003). Comprehensive laboratory measurements of biomass-burning emissions: 1. Emissions from Indonesian, African, and other fuels. *Journal of Geophysical Research: Atmospheres, 108*

Chuvieco, E., Lizundia-Loiola, J., Pettinari, M.L., Ramo, R., Padilla, M., Tansey, K., Mouillot, F., Laurent, P., Storm, T., & Heil, A.J.E.S.S.D. (2018). Generation and analysis of a new global burned area product based on MODIS 250 m reflectance bands and thermal anomalies, *10*, 2015-2031

Chuvieco, E., Mouillot, F., van der Werf, G.R., San Miguel, J., Tanase, M., Koutsias, N., García, M., Yebra, M., Padilla, M., Gitas, I., Heil, A., Hawbaker, T.J., & Giglio, L. (2019). Historical background and current developments for mapping burned area from satellite Earth observation. *Remote Sensing of Environment, 225*, 45-64

Cochrane, M.A., Alencar, A., Schulze, M.D., Souza, C.M., Nepstad, D.C., Lefebvre, P., & Davidson, E.A. (1999). Positive feedbacks in the fire dynamic of closed canopy tropical forests. *Science, 284*, 1832-1835

Cochrane, M.A., & Barber, C.P. (2009). Climate change, human land use and future fires in the Amazon. *Global Change Biology, 15*, 601-612

Csiszar, I., Abuelgasim, A., Li, Z.Q., Jin, J.Z., Fraser, R., & Hao, W.M. (2003). Interannual changes of active fire detectability in North America from long-term records of the advanced very high resolution radiometer. *Journal of Geophysical Research-Atmospheres, 108*

Csiszar, I.A., Morisette, J.T., & Giglio, L. (2006). Validation of active fire detection from moderate-resolution satellite sensors: The MODIS example in northern Eurasia. *IEEE transactions on Geoscience and Remote Sensing, 44*, 1757-1764

DeFries, R.S., Rudel, T., Uriarte, M., & Hansen, M. (2010). Deforestation driven by urban population growth and agricultural trade in the twenty-first century. *Nature Geoscience, 3*, 178

Dennis, R.A., Mayer, J., Applegate, G., Chokkalingam, U., Colfer, C.J.P., Kurniawan, I., Lachowski, H., Maus, P., Permana, R.P., & Ruchiat, Y. (2005). Fire, people and pixels: linking social science and remote sensing to understand underlying causes and impacts of fires in Indonesia. *Human Ecology, 33*, 465-504

Endrawati, E. (2016). *Analisis Data Titik Panas (Hotspot) dan Areal Kebakaran Hutan dan Lahan tahun 2016*. Jakarta: Direktorat Inventarisasi dan Pemantauan Sumber Daya Hutan, Ditjen Planologi Kehutanan dan Tata Lingkungan, Kementerian Lingkungan Hidup dan Kehutanan

Endrawati, E., Purwanto, J., & Nugroho, S. (2018). Identifikasi Areal Bekas Kebakaran Hutan Dan Lahan Menggunakan Analisis Semi Otomatis Citra Satelit Landsat. In, *Seminar Nasional Geomatika* (pp. 273-282)

Frandsen, W.H. (1997). Ignition probability of organic soils. *Canadian Journal of Forest Research, 27*, 1471-1477

Fraser, R., Li, Z., & Cihlar, J. (2000). Hotspot and NDVI differencing synergy (HANDS): A new technique for burned area mapping over boreal forest. *Remote Sensing of Environment, 74*, 362-376

Garcia-Haro, F., Gilabert, M., & Melia, J.J.I.J.o.R.S. (2001). Monitoring fire-affected areas using Thematic Mapper data, *22*, 533-549

Gatra (2019). Balitbangtan Luncurkan Peta Gambut, Luas Turun 1,5 Juta Ha. In. Jakarta: Gatra.com

Geist, H.J., & Lambin, E.F. (2002). Proximate causes and underlying driving forces of tropical deforestation: Tropical forests are disappearing as the result of many pressures, both local and regional, acting in various combinations in different geographical locations. *BioScience, 52*, 143-150

Giglio, L., Boschetti, L., Roy, D.P., Humber, M.L., & Justice, C.O. (2018). The Collection 6 MODIS burned area mapping algorithm and product. *Remote Sensing of Environment, 217*, 72-85

Giglio, L., Csiszar, I., & Justice, C.O. (2006). Global distribution and seasonality of active fires as observed with the Terra and Aqua Moderate Resolution Imaging Spectroradiometer (MODIS) sensors. *Journal of Geophysical Research-Biogeosciences, 111*

Giglio, L., Loboda, T., Roy, D.P., Quayle, B., & Justice, C.O. (2009). An active-fire based burned area mapping algorithm for the MODIS sensor. *Remote Sensing of Environment, 113*, 408-420

Giglio, L., Randerson, J., Van der Werf, G., Kasibhatla, P., Collatz, G., Morton, D., & DeFries, R. (2010). Assessing variability and long-term trends in burned area by merging multiple satellite fire products. *Biogeosciences, 7*

Hawbaker, T.J., Vanderhoof, M.K., Beal, Y.-J., Takacs, J.D., Schmidt, G.L., Falgout, J.T., Williams, B., Fairaux, N.M., Caldwell, M.K., & Picotte, J.J. (2017). Mapping burned areas using dense time-series of Landsat data. *Remote Sensing of Environment, 198*, 504-522

Hoelzemann, J.J., Schultz, M.G., Brasseur, G.P., Granier, C., & Simon, M. (2004). Global Wildland Fire Emission Model (GWEM): Evaluating the use of global area burnt satellite data. *Journal of Geophysical Research: Atmospheres, 109*

Hoscilo, A., Page, S.E., Tansey, K.J., & Rieley, J.O. (2011). Effect of repeated fires on land-cover change on peatland in southern Central Kalimantan, Indonesia, from 1973 to 2005. *International Journal of Wildland Fire, 20*, 578-588

Hosonuma, N., Herold, M., De Sy, V., De Fries, R.S., Brockhaus, M., Verchot, L., Angelsen, A., & Romijn, E. (2012). An assessment of deforestation and forest degradation drivers in developing countries. *Environmental Research Letters, 7*, 044009

Huang, H., Roy, D.P., Boschetti, L., Zhang, H.K., Yan, L., Kumar, S.S., Gomez-Dans, J., & Li, J. (2016). Separability analysis of Sentinel-2A multi-spectral instrument (MSI) data for burned area discrimination. *Remote Sensing, 8*, 873

Jayarathne, T., Stockwell, C.E., Gilbert, A.A., Daugherty, K., Cochrane, M.A., Ryan, K.C., Putra, E.I., Saharjo, B.H., Nurhayati, A.D., Albar, I., Yokelson, R.J., & Stone, E.A. (2018). Chemical characterization of fine particulate matter emitted by peat fires in Central Kalimantan, Indonesia, during the 2015 El Nino. *Atmospheric Chemistry and Physics, 18*, 2585-2600

Konecny, K., Ballhorn, U., Navratil, P., Jubanski, J., Page, S.E., Tansey, K., Hooijer, A., Vernimmen, R., & Siegert, F. (2016). Variable carbon losses from recurrent fires in drained tropical peatlands. *Glob Chang Biol, 22*, 1469-1480

Koplitz, S.N., Mickley, L.J., Marlier, M.E., Buonocore, J.J., Kim, P.S., Liu, T., Sulprizio, M.P., DeFries, R.S., Jacob, D.J., & Schwartz, J. (2016). Public health impacts of the severe haze in Equatorial Asia in September–October 2015: demonstration of a new

framework for informing fire management strategies to reduce downwind smoke exposure. *Environmental Research Letters, 11*, 094023

Kuwata, M., Kai, F.M., Yang, L., Itoh, M., Gunawan, H., & Harvey, C.F. (2017). Temperature and burning history affect emissions of greenhouse gases and aerosol particles from tropical peatland fire. *Journal of Geophysical Research: Atmospheres, 122*, 1281-1292

Langner, A., Miettinen, J., & Siegert, F. (2007). Land cover change 2002–2005 in Borneo and the role of fire derived from MODIS imagery. *Global Change Biology, 13*, 2329-2340

Langner, A., & Siegert, F. (2009). Spatiotemporal fire occurrence in Borneo over a period of 10 years. *Global Change Biology, 15*, 48-62

Laumonier, Y., Uryu, Y., Stüwe, M., Budiman, A., Setiabudi, B., & Hadian, O. (2010). Eco-floristic sectors and deforestation threats in Sumatra: identifying new conservation area network priorities for ecosystem-based land use planning. *Biodiversity and Conservation, 19*, 1153-1174

Lohberger, S., Stängel, M., Atwood, E.C., & Siegert, F. (2017). Spatial evaluation of Indonesia's 2015 fire affected area and estimated carbon emissions using Sentinel-1. *Global Change Biology*, n/a-n/a

Miettinen, J., Hooijer, A., Vernimmen, R., Liew, S.C., & Page, S.E. (2017). From carbon sink to carbon source: extensive peat oxidation in insular Southeast Asia since 1990. *Environmental Research Letters, 12*, 024014

Miettinen, J., & Liew, S.C. (2010). Status of peatland degradation and development in Sumatra and Kalimantan. *Ambio, 39*, 394-401

MoEF (2020). Sipongi, Karhutla Sistem. In, *Rekapitulasi Luas Kebakaran Hutan dan Lahan (Ha) Per Provinsi Di Indonesia Tahun 2015-2020*. Jakarta

Oliva, P., & Schroeder, W. (2015). Assessment of VIIRS 375m active fire detection product for direct burned area mapping. *Remote Sensing of Environment, 160*, 144-155

Page, S.E., Rieley, J.O., & Banks, C.J.J.G.c.b. (2011). Global and regional importance of the tropical peatland carbon pool, *17*, 798-818

Page, S.E., Siegert, F., Rieley, J.O., Boehm, H.D., Jaya, A., & Limin, S. (2002a). The amount of carbon released from peat and forest fires in Indonesia during 1997. *Nature, 420*, 61-65

Page, S.E., Siegert, F., Rieley, J.O., Boehm, H.D.V., Jaya, A., & Limin, S. (2002b). The amount of carbon released from peat and forest fires in Indonesia during 1997. *Nature, 420*, 61-65

Phillips, V.D.J.B., & Conservation (1998). Peatswamp ecology and sustainable development in Borneo*, 7*, 651-671

Posa, M.R.C., Wijedasa, L.S., & Corlett, R.T.J.B. (2011). Biodiversity and conservation of tropical peat swamp forests*, 61*, 49-57

Putra, E.I., Cochrane, M.A., Vetrita, Y., Graham, L., & Saharjo, B.H. (2018). Determining critical groundwater level to prevent degraded peatland from severe peat fire. In, *IOP Conference Series: Earth and Environmental Science* (p. 012027): IOP Publishing

Reiche, J., Souza, C.M., Hoekman, D.H., Verbesselt, J., Persaud, H., & Herold, M. (2013). Feature level fusion of multi-temporal ALOS PALSAR and Landsat data for mapping and monitoring of tropical deforestation and forest degradation. *IEEE Journal of Selected Topics in Applied Earth Observations and Remote Sensing, 6*, 2159-2173

Reid, J.S., Hyer, E.J., Johnson, R.S., Holben, B.N., Yokelson, R.J., Zhang, J., Campbell, J.R., Christopher, S.A., Di Girolamo, L., & Giglio, L. (2013). Observing and understanding the Southeast Asian aerosol system by remote sensing: An initial review and analysis for the Seven Southeast Asian Studies (7SEAS) program. *Atmospheric Research, 122*, 403-468

Ritung, S., Wahyunto, N.K., Sukarman, H., & Suparto, T.C. (2011). Peta Lahan Gambut Indonesia skala 1: 250.000. *Balai Besar Penelitian dan Pengembangan Sumberdaya Lahan Pertanian. Badan Penelitian dan Pengembangan Pertanian. Bogor, Indonesia*

Roteta, E., Bastarrika, A., Padilla, M., Storm, T., & Chuvieco, E. (2019). Development of a Sentinel-2 burned area algorithm: Generation of a small fire database for sub-Saharan Africa. *Remote Sensing of Environment, 222*, 1-17

Roy, D., Jin, Y., Lewis, P., & Justice, C. (2005). Prototyping a global algorithm for systematic fire-affected area mapping using MODIS time series data. *Remote Sensing of Environment, 97*, 137-162

Roy, D.P., & Boschetti, L. (2009). Southern Africa validation of the MODIS, L3JRC, and GlobCarbon burned-area products. *IEEE Transactions on Geoscience and Remote Sensing, 47*, 1032-1044

Roy, D.P., Boschetti, L., Justice, C.O., & Ju, J. (2008). The collection 5 MODIS burned area product—Global evaluation by comparison with the MODIS active fire product. *Remote Sensing of Environment, 112*, 3690-3707

Roy, D.P., Huang, H., Boschetti, L., Giglio, L., Yan, L., Zhang, H.H., & Li, Z. (2019). Landsat-8 and Sentinel-2 burned area mapping - A combined sensor multi-temporal change detection approach. *Remote Sensing of Environment, 231*, 111254

Schroeder, W., Oliva, P., Giglio, L., & Csiszar, I.A. (2014). The New VIIRS 375m active fire detection data product: Algorithm description and initial assessment. *Remote Sensing of Environment, 143*, 85-96

Schroeder, W., Prins, E., Giglio, L., Csiszar, I., Schmidt, C., Morisette, J., & Morton, D. (2008). Validation of GOES and MODIS active fire detection products using ASTER and ETM+ data. *Remote Sensing of Environment, 112*, 2711-2726

Seiler, W., & Crutzen, P.J. (1980). Estimates of gross and net fluxes of carbon between the biosphere and the atmosphere from biomass burning. *Climatic Change, 2*, 207-247

Shi, Y., Sasai, T., & Yamaguchi, Y. (2014). Spatio-temporal evaluation of carbon emissions from biomass burning in Southeast Asia during the period 2001–2010. *Ecological Modelling, 272*, 98-115

Siegert, F., & Ruecker, G. (2000). Use of multitemporal ERS-2 SAR images for identification of burned scars in south-east Asian tropical rainforest. *International Journal of Remote Sensing, 21*, 831-837

Siegert, F., Ruecker, G., Hinrichs, A., & Hoffmann, A. (2001). Increased damage from fires in logged forests during droughts caused by El Nino. *Nature, 414*, 437-440

Simpson, J.E., Wooster, M.J., Smith, T.E., Trivedi, M., Vernimmen, R.R., Dedi, R., Shakti, M., & Dinata, Y. (2016). Tropical Peatland Burn Depth and Combustion

Heterogeneity Assessed Using UAV Photogrammetry and Airborne LiDAR. *Remote Sensing, 8*, 1000

Sinclair, A.L., Graham, L.L.B., Putra, E.I., Saharjo, B.H., Applegate, G., Grover, S.P., & Cochrane, M.A. (2020). Effects of distance from canal and degradation history on peat bulk density in a degraded tropical peatland. *Science of the Total Environment, 699*, 134199

Sofan, P., Bruce, D., Schroeder, W., Jones, E., & Marsden, J. (2020). Assessment of VIIRS 375 m active fire using tropical peatland combustion algorithm applied to Landsat-8 over Indonesia's peatlands. *International Journal of Digital Earth*, 1-22

Stockwell, C.E., Jayarathne, T., Cochrane, M.A., Ryan, K.C., Putra, E.I., Saharjo, B.H., Nurhayati, A.D., Albar, I., Blake, D.R., & Simpson, I.J. (2016). Field measurements of trace gases and aerosols emitted by peat fires in Central Kalimantan, Indonesia, during the 2015 El Niño. *Atmospheric Chemistry and Physics, 16*, 11711-11732

Streets, D.G., Canty, T., Carmichael, G.R., de Foy, B., Dickerson, R.R., Duncan, B.N., Edwards, D.P., Haynes, J.A., Henze, D.K., & Houyoux, M.R. (2013). Emissions estimation from satellite retrievals: A review of current capability. *Atmospheric Environment, 77*, 1011-1042

Tansey, K., Beston, J., Hoscilo, A., Page, S., & Paredes Hernández, C. (2008). Relationship between MODIS fire hot spot count and burned area in a degraded tropical peat swamp forest in Central Kalimantan, Indonesia. *Journal of Geophysical Research: Atmospheres, 113*

Tansey, K., Gregoire, J.M., Binaghi, E., Boschetti, L., Brivio, P.A., Ershov, D., Flasse, S., Fraser, R., Graetz, D., Maggi, M., Peduzzi, P., Pereira, J., Silva, J., Sousa, A., & Stroppiana, D. (2004). A global inventory of burned areas at 1km resolution for the year 2000 derived from SPOT VEGETATION data. *Climatic Change, 67*, 345-377

Taufik, M., Torfs, P.J., Uijlenhoet, R., Jones, P.D., Murdiyarso, D., & Van Lanen, H.A. (2017). Amplification of wildfire area burnt by hydrological drought in the humid tropics. *Nature Climate Change*

van der Werf, G., Randerson, J., Giglio, L., van Leeuwen, T., Chen, Y., Rogers, B., Mu, M., van Marle, M., Morton, D., & Collatz, G. (2017). Global fire emissions estimates during 1997–2015, Earth Syst. Sci. Data Discuss. In

van der Werf, G.R., Randerson, J.T., Giglio, L., Collatz, G.J., Mu, M., Kasibhatla, P.S., Morton, D.C., DeFries, R.S., Jin, Y., & van Leeuwen, T.T. (2010). Global fire emissions and the contribution of deforestation, savanna, forest, agricultural, and peat fires (1997-2009). *Atmospheric Chemistry and Physics, 10*, 11707-11735

Vetrita, Y. & Cochrane, M. A. J. R. S. 2020. Fire Frequency and Related Land-Use and Land-Cover Changes in Indonesia's Peatlands. 12, 5.

Vetrita, Y. & Cochrane, M. A. 2019. Annual Burned Area from Landsat, Mawas, Central Kalimantan, Indonesia, 1997-2015. *ORNL DAAC, Oak Ridge, Tennessee, USA.* https://doi.org/10.3334/ORNLDAAC/1708

Vetrita, Y., Cochrane, M., A. , Suwarsono, Priyatna, M., Sukowati, K. A. D. & Khomarudin, M. R. 2020b. Evaluating accuracy of four MODIS-derived burned area products for tropical peatland and non-peatland fires. Environmental Research Letters. DOI: https://doi.org/10.1088/1748-9326/abd3d1

Vetrita, Y. & Cochrane, M. A. 2020c. Landsat-derived Land Use/Cover Maps, Mawas, Central Kalimantan, Indonesia, 1994-2019. *ORNL DAAC, Oak Ridge, Tennessee, USA.* https://doi.org/10.3334/ORNLDAAC/1838

Wahyunto, R.S., & Subagjo, H. (2003). Maps of area of peatland distribution and carbon content in Sumatera, 1990–2002. *Wetlands Int-Indonesia Programm and Wildl Habitat Canada, Bogor, Indonesia*

Wahyunto, R.S., & Subagjo, H. (2004). Map of peatland distribution area and carbon content in Kalimantan, 2000–2002. *Wetlands International—Indonesia Programme & Wildlife Habitat Canada (WHC), Bogor, Indonesia*

Warren, M., Hergoualc'h, K., Kauffman, J.B., Murdiyarso, D., Kolka, R.J.C.b., & management (2017). An appraisal of Indonesia's immense peat carbon stock using national peatland maps: uncertainties and potential losses from conversion, *12*, 12

Wiedinmyer, C., Akagi, S., Yokelson, R.J., Emmons, L., Al-Saadi, J., Orlando, J., & Soja, A. (2011). The Fire INventory from NCAR (FINN): a high resolution global model to estimate the emissions from open burning. *Geoscientific Model Development, 4*, 625

Xu, J., Morris, P.J., Liu, J., & Holden, J. (2018). PEATMAP: Refining estimates of global peatland distribution based on a meta-analysis. *Catena, 160*, 134-140

Yokelson, R.J., Bertschi, I.T., Christian, T.J., Hobbs, P.V., Ward, D.E., & Hao, W.M. (2003). Trace gas measurements in nascent, aged, and cloud-processed smoke from African savanna fires by airborne Fourier transform infrared spectroscopy (AFTIR). *Journal of Geophysical Research-Atmospheres, 108*

CHAPTER 2

ASSESSMENT OF AVAILABLE MODERATE-RESOLUTION BURNED AREA PRODUCTS IN PEATLAND AND NON-PEATLAND

Paper #1 Vetrita et al. 2020 (in press). Evaluating Accuracy of Four MODIS-derived Burned Area Products for Tropical Peatland and Non-peatland Fires. *Environmental Research Letters*. http://iopscience.iop.org/article/10.1088/1748-9326/abd3d1

Abstract

Satellite-based burned area products are accurate for many regions. However, only limited assessments exist for Indonesia despite extensive burning and globally important carbon emissions. We evaluated the accuracy of four MODIS-derived (Moderate Resolution Imaging Spectroradiometer) burned area products (MCD45A1 collection 5.1, MCD64A1 (collection 5.1 and 6), FireCCI51), and their sensitivity to burned-area size and temporal window length used for detection. The products were compared to reference burned areas from SPOT 5 imagery using error matrices and linear regressions. The MCD45A1 product detected <1% of burned areas. The other products detected 38-48% of burned area with accuracies increasing modestly (45-57%) when smaller burns (<100 ha) were excluded, with MCD64A1 C6 performing best. Except for the MCD45 product, linear regressions showed generally good agreement in peatlands (R^2 ranging from 0.6 to 0.8) but detections were less accurate in non-peatlands (R^2 ranging from 0.2 to 0.5). Despite having higher spatial resolution, the FireCCI51 product (250 m) showed lower accuracy (OE=0.55-0.88, CE=0.33-0.50) than the 500 m MCD64A1 C6 product (OE=0.43-0.79, CE=0.36-0.51) but it was comparable to the C5.1 product (OE=0.52-0.91, CE=0.37-0.67). Dense clouds and smoke limited the accuracies of all burned area products, even when the

temporal window for detection was lengthened. This study shows that emissions calculations based on burned area in peatlands remain highly uncertain. Given the globally significant amount of emissions from burning peatlands, specific attention is required to improve burned area mapping in these regions in order for global emissions models to accurately reflect when, where, and how much emissions are occurring.

Keywords: Tropical peatlands, fires, emissions, MODIS, burned area mapping

2.1 Introduction

In September 2019, vast amounts of smoke-related haze from regional peatland fires blanketed Sumatra and Kalimantan in Indonesia with the worst air conditions since 2015. Poor air quality in Sumatra (Riau) forced schools to close for weeks. Air Quality Index (AQI) and fine particles ($PM_{2.5}$) values in Kalimantan (Palangkaraya) exceeded 2,000 and 1,400 $\mu g/m^3$, respectively, greatly exceeding bounds of the index's worst anticipated conditions (Hazardous AQI >300-500, $PM_{2.5}$ >65 $\mu g/m^3$). This latest catastrophic event, emanating from the region's peatlands, pales in comparison to 2015 when the annual peat fires were exacerbated by El Niño drought and burned 2.6 million hectares, releasing greenhouse gases (GHGs) estimated at the CO_2-equivalent of 1.75 Gt (GFED 2015), greater than the annual emissions of Japan (Field et al. 2016). Tragically, the associated toxic regional haze is also estimated to have caused >100,000 premature human deaths (Johnston et al. 2012; Koplitz et al. 2016). Regional projections anticipate an annual average of 36,000 excess deaths if land management practices are not improved (Marlier et al. 2019). The regional health and economic impacts (Glauber et al., 2016) and globally significant GHG emissions make detection, monitoring, and ultimately mitigation of Indonesia's peatland fires crucial.

Heavy smoke from smoldering peat soils dominates emissions from burning peatlands (Page and Hooijer 2016; Turetsky et al. 2015). Smoldering peat fires produce many more gases and aerosol particulates than flaming surface components (Stockwell et al. 2016). Consequently, peatland fires are treated differently in emissions models (e.g., the Global Fire Emissions Database (GFED) (van der Werf et al. 2017) , Global Fire Assimilation System (GFAS) (Kaiser et al. 2012)) by incorporating higher emission factors (e.g., C, CO, CH_4) or organic matter burned than other land cover types (Andela et al. 2013). Uncertainties remain high for these variables, resulting in different estimates of fire-related emissions from various inventories for the Indonesian burning in 2015 (Heymann et al. 2017; Whitburn et al. 2016; Wooster et al. 2018). Burned area is the primary input for estimating associated emissions but providing it accurately is also the main challenge (Kaiser et al. 2012; van der Werf et al. 2010; van der Werf et al. 2017). In ecosystems, such as savannas, temperate and boreal forests, burned area may not be considered the main error source (French et al. 2002; Sparks et al. 2015), with phase of combustion and moisture content (Chen et al. 2007), or seasonality (Korontzi et al. 2003) being seen as more problematic. Unlike these ecosystems, burned area is of substantial uncertainty in tropical regions. Burned area monitoring over large areas is primarily reliant on satellite-based mapping. Given the central importance of burned area for assessing greenhouse gas emissions, it is critically important to validate and evaluate the accuracy of burned area products in Indonesia's peatlands.

Over the last two decades, Moderate Resolution Imaging Spectroradiometer (MODIS) imagery has been used to map global and regional fire activities (Alonso-Canas and Chuvieco 2015; Langner et al. 2007; Ramo and Chuvieco 2017; Vetrita and Cochrane

2020) and carbon emissions (Kaiser et al. 2012; van der Werf et al. 2010; van der Werf et al. 2017), providing an essential variable for climate models (Hollmann et al. 2013). MODIS burned area products, at 500 m resolution, have been modified over time to improve their accuracy with each newly released MODIS Collection of reprocessed imagery. The first MODIS burned area product, MCD45A1, used a "rapid changes bi-directional reflectance model" and time series of surface reflectance data to flag areas of rapid change as potential burned areas (Fornacca et al. 2017). It has been shown to have adequate accuracy for monitoring fires in some regions or biomes (Chang and Song 2009; Fornacca et al. 2017; Roy and Boschetti 2009; Ruiz et al. 2014; Tsela et al. 2014), with global omission and commission rates of 46% and 72%, respectively (Padilla et al. 2014). The MCD64A1 burned area product integrates 1 km MODIS active fire (MOD14/MYD14) detections with the 500 m reflectance data to reduce false detections. Resulting detections are subjected to additional algorithmic validity tests and masking. Although available from both Collection 5.1 and 6, the most recent burned area product (MCD64A1 C6) has algorithm changes designed to improve detection of small fires globally (Giglio et al. 2018). Product comparisons conducted in Brazil have found MCD64A1 C6 more reliable than the previous version, with lower omission errors and more fires detected (Rodrigues et al. 2019). Another MODIS-derived burned area product, FireCCI51, has a higher spatial resolution (250 m vs. 500 m) and was expected to have superior small fire detection capabilities than MCD64A1 C6 products (Chuvieco et al. 2018). However, global comparison of the FireCCI51 and MCD64A1 C6 products showed that detections varied spatially and temporally among regions (Humber et al. 2019).

Those assessments were largely conducted outside the Indonesian peatlands, where the fire characteristics are not necessarily equivalent to those on other peatlands. Limited studies exist that evaluate Indonesia's peatland areas (Albar et al. 2018; Miettinen et al. 2007; Miettinen and Liew 2009; Tansey et al. 2008), where fires are predominantly smoldering ground fires that are often small in area and frequently covered by clouds. Previous assessments have reported difficulty assessing accuracy for Indonesia due to the limited reference data, as compared to other regions (Shi et al. 2014). Providing reference data and determining standard accuracy methods are needed to get unbiased results (Boschetti et al. 2016). Lohberger et al. (2017) assessed one of the MODIS products (MCD64A1 C5.1) against a Sentinel-1 derived burned area map. Sentinel-1 satellites employ active remote sensing, using a C-band synthetic-aperature radar that can penetrate the clouds and haze in Indonesia at much higher spatial resolution (10 m) than MODIS. Without any specific validation of the MODIS product, Sentinel-1 detected nearly twice as much area burned as either the MODIS product or official burned area maps from the Indonesian government.

We initiated this research to assess which product(s) would be best for conducting a national fire frequency analysis. We concentrate here on the relative burned area mapping accuracies in the critical peatland areas and compare these to mapping accuracies in regional non-peatland areas. The frequency of fires is a critical parameter for calculating fire emissions from peat fires (Konecny et al. 2016). This parameter has been lacking in Indonesia, resulting in many satellite-based carbon emission models excluding this important component (e.g., GFED (van der Werf et al. 2017), GFAS (Kaiser et al. 2012),

the Fire INventory from NCAR (FINN) (Wiedinmyer et al. 2011), the Global Biomass Burning Emission Product-Geostationary-satellite (GBBEP-Geo) (Zhang et al. 2012)).

In this study, we conducted a comparative analysis of the detection accuracies of four global burned area products (MCD64A1 C5.1 and C6, MCD45A1 C5.1, and FireCCI51) acquired during 2014 in peatlands of Indonesia's Central Kalimantan province. We compared the burned area data from each product against a reference dataset derived from higher spatial resolution SPOT 5 imagery to determine errors of omission and commission in deep peatlands, shallow peatlands, and nearby non-peatlands of Indonesia. We also investigated how the exclusion of small area fire patches and lengthening the temporal window of detection affected accuracy. Finally, we addressed discrepancies among products, improvements over its predecessors (collection 5.1 versus 6), impact on fire-related emissions models, needs, and future studies.

2.2 Materials and Methods

2.2.1 Study site

The study area covered 1.6 million hectares (Mha), 10.4% of the total area of Central Kalimantan, Indonesia, that were delineated by available SPOT 5 imagery (figure 2-1Figure 2-1). Peatlands underlie 67% of this site, with 56% deep peat, 11% shallow peat, and 33% non-peatland. We derived these classes by aggregating the two peat maps currently available from the Indonesian Ministry of Agriculture (Ritung et al. 2011), and Wetland International peatland atlases (Wahyunto and Subagjo 2004). The Ministry of Agriculture peat maps do not include peaty soils (shallow peat areas <50 cm depth) since these areas are considered agricultural lands while Wetlands International maps peat regardless of depth. Therefore, if both maps agreed as being either peat or non-peat, we classified them as deep peat and non-peat, respectively, otherwise, as shallow peat. Here, the "deep" term does not imply a specific depth of the peat. The Indonesian government

peatland atlas is periodically updated. Although an updated 2019 version now exists, it was not yet publicly available, so our analyses are based on the available maps.

The 2014 MODIS annual land cover product (MCD12Q1) classified 60% of the study area as forests, 35% shrubs (including woody savannas and grassland), 2% croplands and the remainder as non-vegetated areas. The land cover classes were based on the International Geosphere-Biosphere Programme (IGBP) classification, available through the Earthexplorer (https://earthexplorer.usgs.gov/, last accessed on June 20, 2020). Based on the Ministry of Forestry and Environment land cover map of 2014, the majority land cover type was defined as bush/shrubs/regrowth, swamp, and secondary peat swamp forest (land use/cover map Ministry of Forestry and Environment, 2014)

The study region has been reported by Indonesian authorities as the greatest contributor to area burned in the country (MoEF 2020), particularly during the El Niño events of 2015 and 2019. El Niño drought events are associated with severe burning due to increased fire susceptibility (Siegert et al. 2001), extensive burning and recurring fire events. Although the 2014 burning event was less severe than the burning during El Niño years, the region has experienced frequent annual burning since 1997. Fire seasons usually occur from August to October every year.

Fires were reported to be associated with the “ex-Mega Rice Project (MRP)”, one million hectares of drained peat-swamp forest, converted into rice plantations in 1997, but later abandoned (Ballhorn et al. 2009; Konecny et al. 2016; Page et al. 2002; Stockwell et al. 2016). A grid-pattern of canals, thousands of kilometers in length, was constructed across the MRP, reducing water table levels in the peatlands, draining and drying near-surface peat, and providing open access to the remaining forests of the area, resulting in widespread human-induced fires. The site becomes prone to fire due to careless land use practices (e.g. logging and plantation establishment).

2.2.2 MODIS burned area products: brief algorithms, data sources, and processing

The MCD45A1 maps sudden changes of the earth's surface due to burning using bidirectional reflectance (BRDF) models from 500 m MODIS cloud-free surface reflectance data. The bidirectional effect shows changes that are not associated with the Earth' surface change (Roy et al. 2002), or variation in observed reflectance attributed to directional effects instead of surface change itself. The algorithm used a 16-day (with maximum 8 extra-day) time window before and after burning, with at least 7 of days of available imagery, to predict the reflectance. The MODIS 500 m infrared bands (858, 1240, 1640, and 2130 nm) were used to discriminate the changes due to fire from other types of change (see (Roy et al. (2005) for detailed information). The MCD45A1 datasets provided two layers on a monthly basis, i.e. burn date and the pixel confidence level. We clipped the imagery to match our study site extent and selected only the approximate date of burning with the most confidently detected pixels flagged in the Quality Assurance (QA) layer. The raster files were converted into a vector file by conserving the 500 m pixel size to calculate the intersected areas for our analysis.

The MCD64A1 (collections 5 and 6) algorithms integrate the 1-km MODIS active fire product (MOD14A1 and/or MYD14A1), MODIS reflectance data, and land cover product to detect area burned (Giglio et al. 2018; Giglio et al. 2009). The main differences between collection 5 (C5) and 6 (C6) products are summarized in (Giglio et al. 2018)) and include, changes to the input data, handling of cloud interference, temporal window change from 10 to 8 days, and changes in how training sample data is applied, among others. The HDF files were reprojected from sinusoidal to geographic coordinates to calculate the areas burned. The products provided the approximate burn date, burn date uncertainty, Quality Assurance, first day and last day layers. We selected all ordinal pixel days of burn (1-366), flagged in the QA layer as being in land grid cells flagged and having valid data.

FireCCI51 is the first updated version of FireCCI burned area products that are based on MODIS data from the Terra satellite platform. The product was developed under a Climate Change Initiative project of the European Space Agency (ESA). It has the longest time series, most improved algorithm, and the best validation results (Pettinari et al. 2020). This product is an improvement of the previous collection (FireCCI41, available from 2005-2011) to provide long-term data archives. This product is currently available and updated from 2001-2019 (last accessed on 16 July 2020). The main inputs to derive this product are the daily MODIS Surface Reflectance product (MOD09GQ) collection 6 images, MODIS Global Monthly Fire Location Product (MCD14ML collection 6), and the Land Cover Project of ESA Climate Change Initiative (ESA-CCI). Images were composited before the two-phase approaches were used. For each candidate burn pixel, pre and post images were defined based on the nearest active fire date with at least four valid post-fire observations within a specified time window. To minimize ambiguity, the standard search window was 10 days after selection of the post-fire date for each candidate pixel. Employing two MODIS bands at 250 m resolution (645 and 858 nm), the product provides higher spatial resolution than the other three burned area products assessed here (250 m versus 500 m). Detailed algorithms can be found at (Lizundia-Loiola et al. 2020; Pettinari et al. 2020).

We downloaded the pixel-version product (250 m spatial resolution, 6.25 ha areas equivalent), freely available since November 2018 at https://www.esa-fire-cci.org/FireCCI51 (accessed March 2020). Mimicking the other burned area products, FireCCI51 provides a monthly GeoTIFF dataset with three layers, estimated first day of burn (Julian-date), confidence level, and land cover type of a detected burn pixel. All burn pixels regardless the confidence level were used for our analysis.

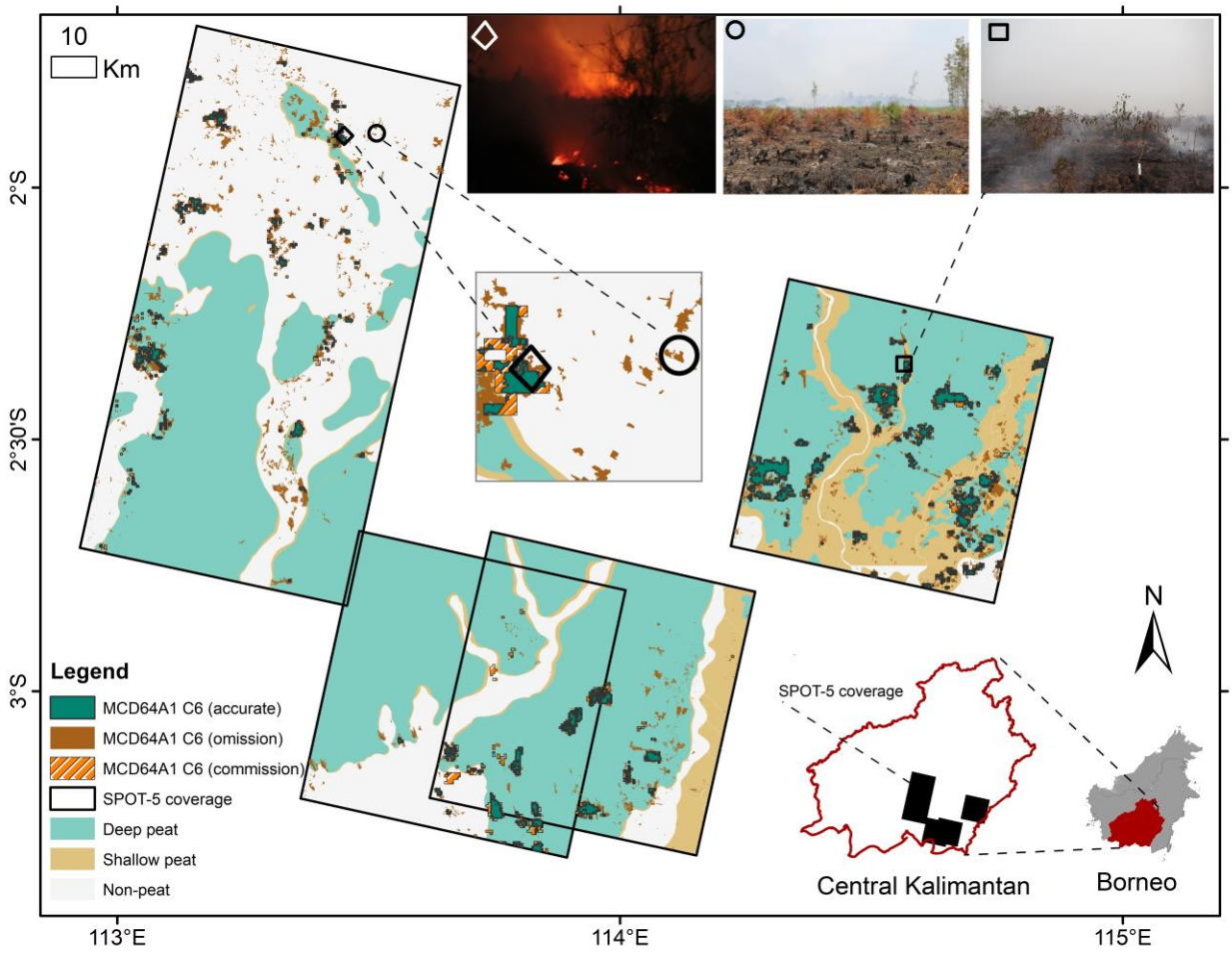

Figure 2-1 Study region in Central Kalimantan, Indonesia. Study areas were delineated by available SPOT 5 imagery footprints (black rectangles) covering 1.6 million hectares. Detected burned areas from SPOT 5, the MODIS burned area product collection 6 (MCD64 C6) accurately detected or missed in peatland (deep and shallow) and the non-peat cover is shown. Diamond, circle, and square symbols are associated with field assessments in 2014. Photo of burning in tall shrubs and cropland of the non-peatland area (diamond) was taken at nighttime (around 7 PM local time). Young oil palm that burned on non-peatland areas (circle). Burning in degraded areas on deep peat where Borneo Orangutan Survival Foundation (BOSF) measured depth of burn into the peat. Photo credits: LAPAN (diamond and circle) and BOSF (rectangle).

2.2.3 Reference map

The Indonesian National Institute of Aeronautics and Space (LAPAN) provided the burned area reference map (Zubaidah et al. 2017). The reference map was manually classified into burned and unburned classes. The protocol of the Southern African Fire

Network (SAFNet) was adopted to create the map. The committee on Earth Observations (CEOS) Land Product Validation Working Group has also approved the procedure for use by the international community (Boschetti et al. 2010). Brief methods and validation efforts were as follows.

Trained LAPAN image interpreters created the burned area reference map based on visual interpretation and classification of Orthorectified SPOT-5 imagery. Five relatively cloud-free (~10% coverage) SPOT images were acquired on September 3, 24 and 29, 2014. Several procedures were used to standardize evaluation conditions for each interpreter, such as using a fixed screen-scale (1:10,000), false composite bands (Short wave Infrared-Near Infrared-Red) and overlay of the MODIS active fire product (MOD14A1/MYD14A1). Visually, the area burned appeared as dark magenta, often with smoke visible, using visual interpretation. Due to limited availability of SPOT 5 images from before burning, Landsat 7/8 images were also used by the experienced interpreters to help them decide if areas had burned.

Many burned areas were located in remote locations restricting available locations for field validations. However, preliminary maps of the burned area were initially evaluated with local stakeholders. The research team conducted a week-long intensive (18-23 September 2014) field validation activity to evaluate the burned area map. Two validation sites are shown in our manuscript in Figure 2-1. Approximately 40 burn positions were marked with GPS (minimum 5-m accuracy) during the field trip, with all accurately detected in the SPOT 5 burned map. Safety and logistical access reasons precluded measurement of burn perimeters. A second validation analysis was conducted in September 2015 and one area erroneously mapped (dried pond) as being burned was discovered and

corrected in the final burned area map. Subsequently, map accuracy of more remote regions, accessible via canals, was assessed, with collaboration with the Borneo Orangutan Survival Foundation (BOSF), with data collected during parallel activities of a NASA project (Cochrane PI). BOSF manages a permanent site for hydrology and fire monitoring (1.2 million ha). In Figure 2-1, one photo was attached.

SPOT 5 mapped a total of 81,249 ha of burned area by September 2014, across both peatlands and non-peatlands, with 57%, 14%, and 29% occurring in deep peat, shallow peat, and non-peat, respectively. Most burned patches were small (85% ≤25 ha, or 94% < 100 ha) with only 6% of patches larger in size. However, although numerous, small burn patches only comprised 25% of the total area burned. For the study site, land cover was approximately 25% non-peat and 75% peatland. Comparable proportions of both land cover types burned, 4% of non-peatlands versus 5% of peatlands, respectively, indicating both land cover types are vulnerable to fires. In terms of vegetation, of all the areas burned, 68% were shrubs, woody vegetation, and grassland, ~30% was damaged forests and 1% was croplands that was almost entirely on non-peatland areas.

2.2.4 Burned area products accuracy analysis

Rules to select MODIS datasets for comparison to the SPOT 5-derived burned area reference map were: 1) all land pixels with a valid-data flag noted as having a “burn date” within the study region; 2) of those pixels, only those having detection dates from the beginning of fire season to a) the same date of the corresponding SPOT 5 image (hereafter defined as D0), b) eight-days after (D8), and c) ten days after the SPOT 5 images acquisition (D10). These three different temporal aggregation windows were considered to evaluate sensitivity to changed window lengths of the burned area products. Ideally, burned

areas are detected on the day when the burning occurred (D0). However, some areas may be covered by thick clouds or smoke, preventing detection, at the time of occurrence. MODIS products typically report aggregated findings over a period of days to improve detection likelihood by getting several potential observations of burned areas. Standard temporal window lengths vary between products but are all designed to reduce uncertainty (Giglio et al. 2018; Pettinari et al. 2020), with the MODIS C6 product using eight days (D8), while FireCCI51 and MODIS C5.1 use ten days (D10) instead. We evaluated the reliability of burned area detection for each product at the three observation periods, D0, D8, and D10. Longer window lengths were avoided because of increasing commission errors in detections. This approach may still be conservative, however, since SPOT 5 detected burned areas could have occurred several days before image acquisition. MODIS pixels corresponding to regions obscured by cloud cover in the SPOT imagery were excluded from the accuracy assessment.

Product reliability was quantified using an error matrix to compute commission (CE) and omission errors (OE). We followed (Tsela et al. 2014) using burned area intersection analysis to find the omission (Equation 1) and commission errors (Equation 2) for different burned area sizes. Overall accuracy (OA) was calculated as 1-OE. Since SPOT-5 has a spatial resolution with fifty times more detail than the MODIS products, we divided the error assessment into three groups based on burned area size, i.e., all burned areas regardless of burned area size (G1), all areas excluding small fires (G2, ≥25 ha), and all areas considered as large fires (G3, ≥100 ha).

We used linear regression to compare the proportion of the product's detected area burned to that shown in the reference data (Eva and Lambin 1998; Smith et al. 2007). A 5

x 5 km grid was created over the SPOT 5 coverage. This is the same grid size as used in previous analyses (Giglio et al. 2018; Roy and Boschetti 2009). We excluded grid cells covered by clouds and any land cover polygon ≤6.25 km^2. The fraction of the areas burned within each 5x5 km grid cell over each SPOT 5 image footprint was aggregated to effectively compare spatial agreement between the coarser scale MODIS-derived burned area products and higher resolution reference burned areas. For the final comparison, we had 481 peat grid cells (deep and shallow peat), and 253 grid cells of non-peat.

$$OE = 1 - \frac{MODIS\ accurately\ detected}{All\ BA\ SPOT\ 5} \quad \text{(Equation 1)}$$

$$CE = 1 - \frac{MODIS\ accurately\ detected}{All\ BA\ MODIS} \quad \text{(Equation 2)}$$

BA stands for burned area while OE and CE are omission, and commission error, respectively. Figure 2-2 describes the process used for evaluating MODIS BA product accuracy in this study.

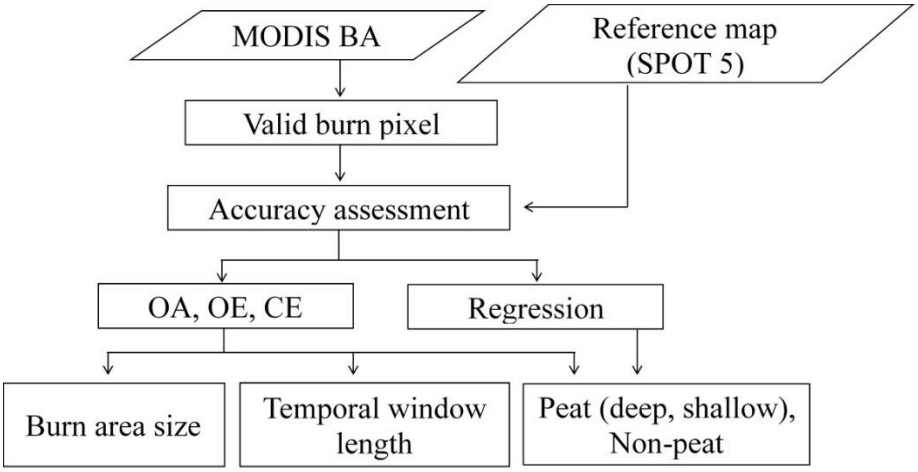

Figure 2-2 Assessment process for evaluating accuracies of four MODIS-derived burned area products in Central Kalimantan, Indonesia.

2.2.5 Temporal accuracy of burned area products

In order to determine which product(s) more accurately reflected when burned area was accumulating, we used Visible Infrared Imaging Radiometer Suite (VIIRS) 375 m active fire (VNP14IMG) to examine when the burning occurred at this site. The VNP14IMG product detects more fire pixels compared to the 1 km MODIS active fire (MOD14/MYD14) used by MODIS BA products (MCD64A1 and FireCCI51) due to its higher spatial resolution. This product is also superior for detecting smaller/cooler nighttime fires that are characteristics of fire on peatlands. The product includes burn pixel coordinates, Fire Radiative Power (FRP), and confidence level. The product is available at https://ladsweb.modaps.eosdis.nasa.gov/.

We downloaded a vector file of points representing the center of the burn pixel. We only selected the burn pixel with the type attribute "presumed vegetation fires" to limit the possible error due to other anomalies such as detection over water or other static land sources. These values were usually located along the river in our study site. Although burning along the river is possible, the number of pixels we removed was very low (1% of the total burn pixels during September and October 2014). We aggregated daily fire counts and then accumulated them from the beginning of September to the end of October. We also converted the points into a raster, pertaining to the original pixel size of 375 m. We aggregated the monthly FRP pixel (September and October only). When more than one point fell within a raster cell, the features were summed. FRP estimates the radiative energy component released during burning, which relates to combustion rate or fuel consumption (Wooster et al. 2005).

This dataset was independent from all of the evaluated product algorithms, but has recently been shown to reliably detect fires in Indonesia's peatlands (Sofan et al. 2020). The active fire product detects fire activity with low levels of commission errors (Schroeder et al. 2014). Aggregating the FRP pixels may be conservative, but it reliably represents month to month variations and thus verifies which month was the peak of the 2014 burning season.

2.3 Results

2.3.1 Temporal accuracy

MCD64A1 C6 had the highest single monthly burned area of the four products studied (154 km^2/month versus peaks of 126, 101, and 61 km^2/month for MCD64A1 C5.1, FireCCI51, and MCD45A1, respectively) as well as the most total burned area for 2014. This corroborates previous studies that concluded that the C6 product detected more burned areas than previous MODIS collections (Humber et al. 2019). The main difference between MCD64A1 C6 and the other products was that burned area was greatest in October as opposed to September for the other products (Figure 2-3).

We subsequently investigated possible double-counting of areas burned where the same pixel was labeled as being burned in consecutive months. For the MCD64A1 C6 product, 7.2% of the total area shown as burned in October had also previously burned in September. Surprisingly, the precursor product (MCD64A1 C5.1) had no pixels detected as potential double-counting across months. The FireCCI51 product had 3.2% of the total area burned in October marked as previously burning in September. The product's user guide indicates double counting is a known issue, specifically in high latitudes (Pettinari et

al. 2020), due to re-projection of the sinusoidal output to geographic coordinates, however, this is not applicable for this equatorial study site.

We examined independent fire detection data from the daily accumulated VIIRS 375 active fire (AF) product to corroborate whether large amounts of fires continued into October. The VIIRS data showed that fires continued after September and peaked in mid-October (figure 2-4). Total October AF counts were 13% higher than in September (6200 vs 5471 pixels, respectively). Fires predominantly occurred in peatlands (~73%), with 65% of all detections located on deep peat. Higher fire radiative power (FRP) values (>10 MW) were primarily clustered on deep peat regions (see figure 2-5) for both months. These findings support the MCD64A1 C6 product's representation of October as the peak of the burning season.

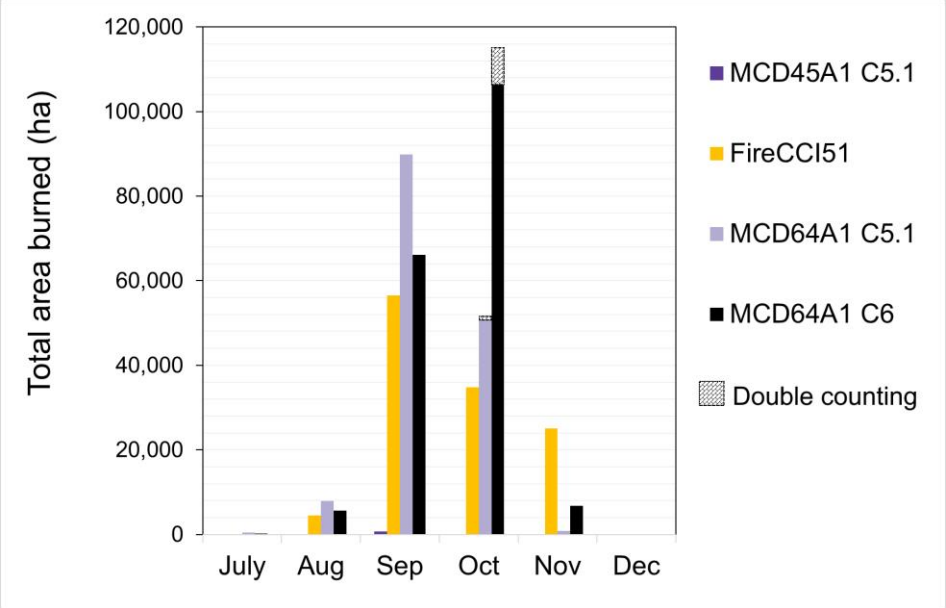

Figure 2-3 Monthly accumulated area burned, for all products, during the fire season of 2014 at the Central Kalimantan study site (Figure 2-1). Double counting indicates area of pixels labelled as burned in consecutive months (September and October) as detected by MCD64A1 C6, accounting for 7.2% of total area burned in October (114,616 ha). FireCCI51 showed a small area (~1600 ha) of double counting that is barely visible on the graph. The peak of the 2014 burning season for the

MCD64A1 C6 product was in October, while other products depicted it as occurring in September. Note that, by 24-29 September 2014, SPOT 5 showed 81,249 ha burned at this study site. Total accumulated area reported from July to September 2014 was underreported by both MCD64A1 C6 (88.6%) and FireCCI51 (75.1%). MCD64A1 C5.1, on the other hand, overestimated the area burned in September 2014 (120.8%).

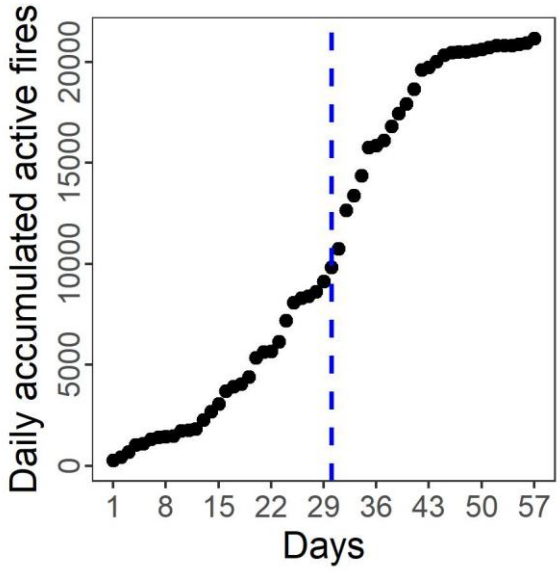

Figure 2-4. Daily accumulated VIIRS 375 m active fires (AF) from the first day of September (left of the dashed line) to the last day of October (right of dashed blue line). The AF increased steeply from the second week of September until a month later.

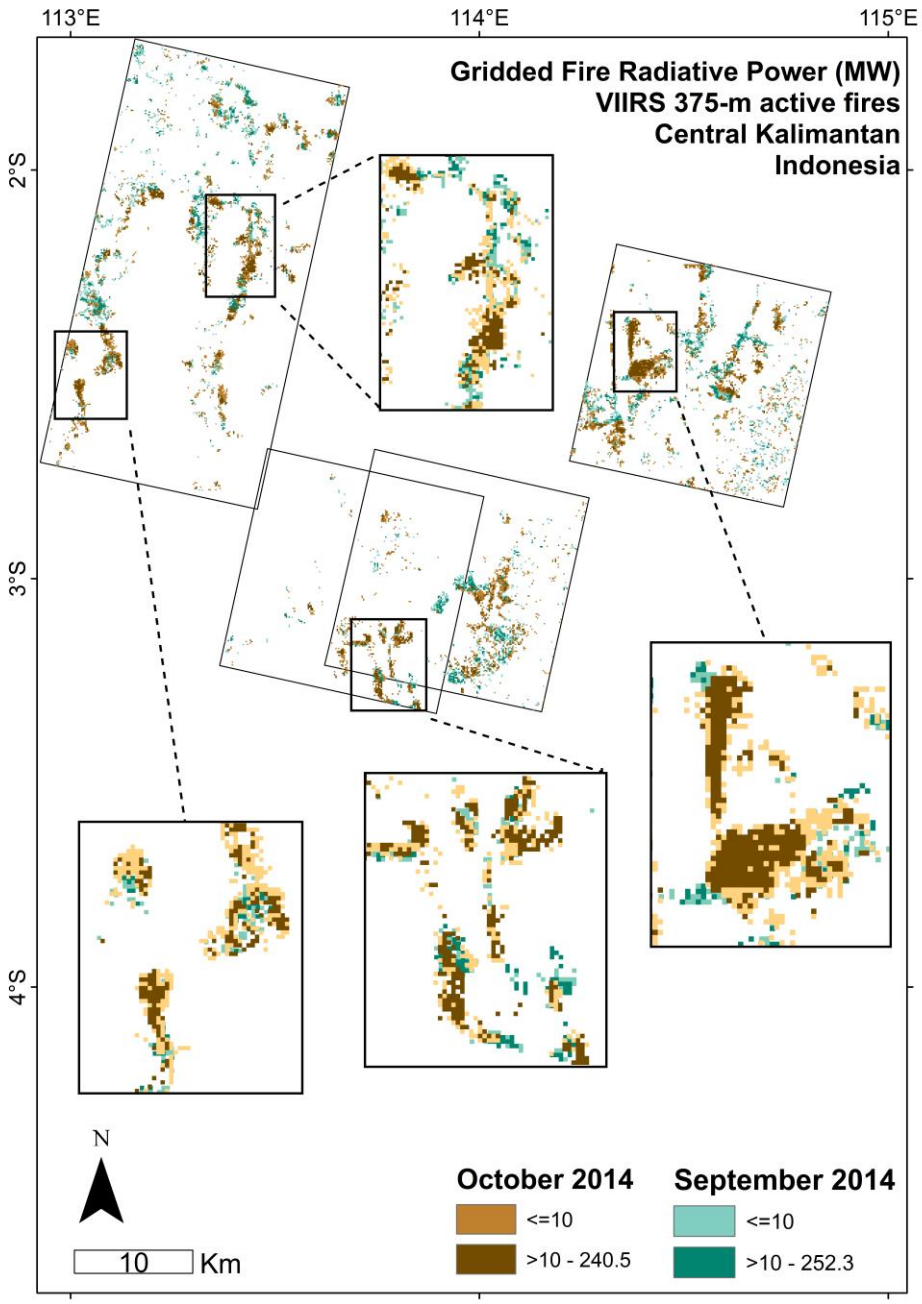

Figure 2-5. Gridded Fire Radiative Power (FRP) from VIIRS (Visible Infrared Imaging Radiometer Suite (VIIRS) 375 m active fire (VNP14IMG). Colors represent monthly sums of Fire Radiative Power (FRP) (Megawatt, MW) in October (brown) and September 2014 (cyan). The MCD64A1 C6 product estimated 66,160 ha burned in September and another 114,616 ha in October 2014 (7% of which were double counting of September burned areas). The other products analyzed in this study (MCD64A1 C5.1 and FireCCI51) showed less areas burned in October than in September.

Double-counted areas that burned in both September and October, as detected by MCD64A1 C6 and FireCCI51, persisted for one to two weeks after the first detected day of burning (figure 2-6). The majority of these long burning fires occurred on peatlands (88%), with most occurring in deep peat areas (63%). Only 12% occurred in non-peatlands.

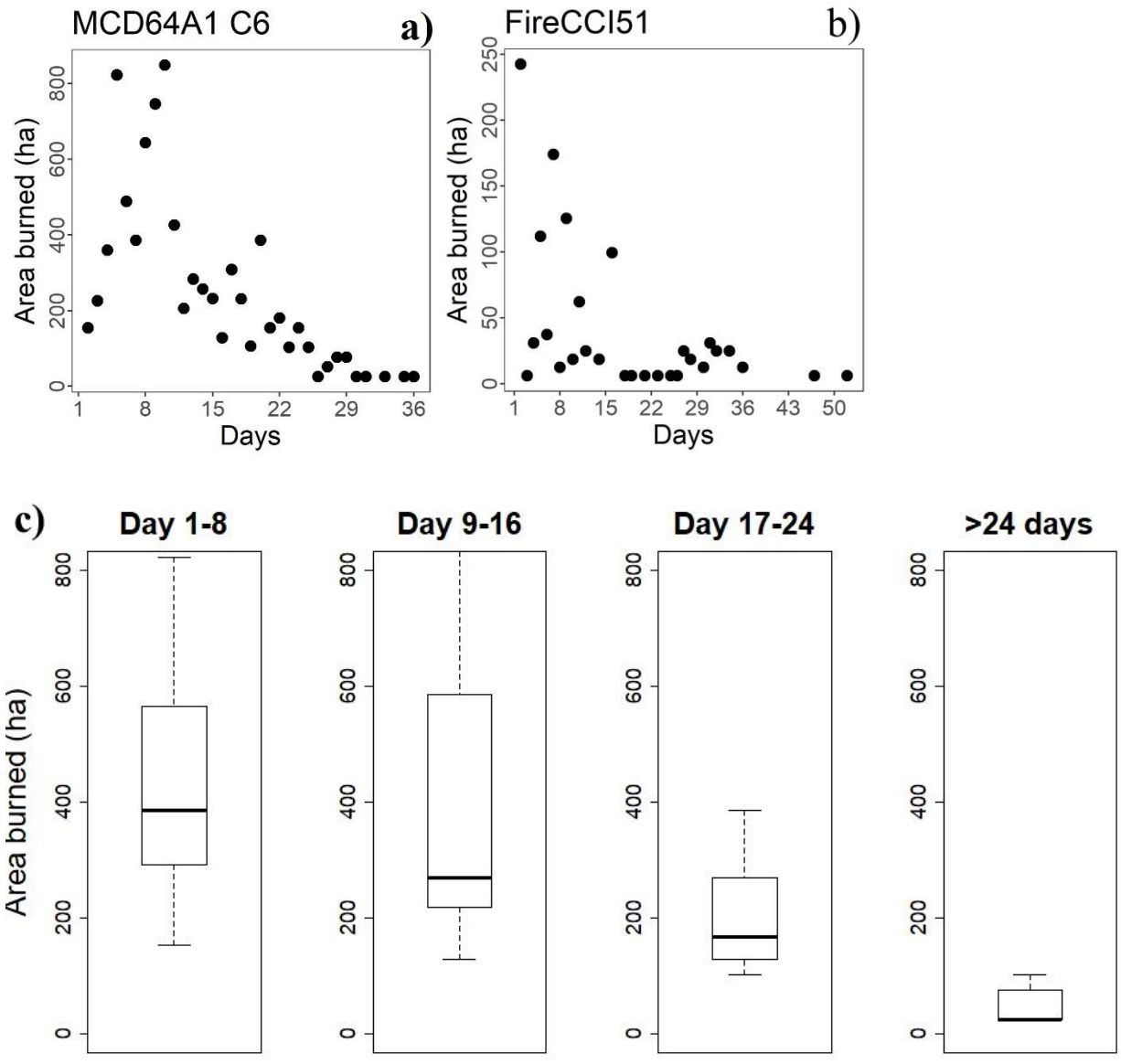

Figure 2-6 Persistence of detection over time for areas double counted in September and October by MCD64A1 C6 (a) and FireCCI51 (b) since the first detected day of burning. Both the range and median area of persistent detections drop rapidly 1 to 2 weeks after initial detection (c).

2.3.2 Areal uncertainty

The burned area from the MCD45A1 product detected <1% (735 ha) of burned areas in the study site, regardless of burn-size group or land cover types and was therefore excluded from further analysis. The other three product's accuracies were analyzed in terms of burned area, using three classes (≥100 ha, ≤25 ha, all burned areas), and using three different temporal aggregation windows, as defined in Table 2-1. These products approximated the total burned area in the study region more accurately for peatlands than for non-peatlands (Table 2-1).

The temporal window length was assessed by summing the area burned from the beginning of the burning season until the date of the corresponding SPOT 5 imagery (D0), as well as eight days (D8), and ten days afterward (D10). Product's (D0 temporal window) burned area accuracies were evaluated against the reference map (G1, all burned area size), first by comparing total reported burned areas and then in terms of spatial agreement of the mapped areas (overall accuracy, OA). In peatlands, total burned areas from MCD64A1 C6, MCD64A1 C5.1, and FireCCI51corresponded to 74%, 64%, and 56% of burned area, respectively. When constrained to areas of spatial agreement with the reference map, estimated burned areas only corresponded to 48%, 40%, and 38% of validated burned areas, respectively (Table 2-1, figure 2-7). In non-peatlands, all products had low correspondence for total area burned, all less than 40%, with very poor overall accuracy (21%, 9%, and 12% respectively for MCD64A1 C6, MCD64A1 C5.1, and FireCCI51). Of note, the collection 6 MCD64A1 product had somewhat reduced omission (OE) and commission errors (CE) by 12% and 3% in peatlands relative to the previous collection 5.1

product, as well as more substantial reductions of 13% and 18%, respectively, in non-peatland.

Lengthening the temporal window of observation affected the products differently. For MCD64A1 C5.1, omission levels were substantially reduced for both peat and non-peatlands. Conversely, the C6 product had the least reduction in omission, but the largest increases of commission errors. Overall, the FireCCI51 product had the lowest commission errors among the products, regardless of changes in the temporal window, most notably in peatlands. However, this has come at the cost of the largest omission errors in peatlands.

The exclusion of all burned areas smaller than 25 ha (G2) or 100 ha (G3) increased classification accuracy for all products, except for the MCD64A1 C5.1 in non-peatland (Table 2-1). Overall accuracy increased by approximately 8% and ~21% for all products when smaller fires in peatlands, <25 ha or <100 ha, were removed, respectively. This was due to large reductions in omission errors (~8%, -19%, Figure 2-8a) with much smaller increases in total commission errors (~2%, ~9%, figure *2-8*b). Significant differences were found in the fire detection of burned area products in non-peatlands where the MCD64 and FireCCI products showed ~57% increases in accuracy when only large fires were included, suggesting both products are missing large portions of small non-peatlands fires.

Linear regressions showed generally good agreement in peatlands (R^2 ranging from 0.6 to 0.8, Table 2-2 and figure 2-7) between the proportions of area burned in 5x5 km^2 cells of the burned area products and the reference SPOT-5 burned area of each grid cell. These results indicate roughly comparable spatial patterns among products and the validated burned map, despite underrepresentation of the proportions burned (positive slope <1).

The MCD64A1 C6 product had the best agreement for both peatlands (including deep and shallow peat) and non-peatland. The product most closely matched the proportional area burned of the reference map in peatlands, specifically in deep peat (Slope = ~0.84) but underestimated area burned, yielding moderate correspondence (R^2=0.78 and 0.50 for deep peat and non-peat, respectively). Despite having higher spatial resolution, the FireCCI51 product had accuracy similar to the MCD64A1 C5.1 product (both with R^2=~0.61), however, it was less accurate for non-peatland (R^2=0.31 versus 0.14, respectively).

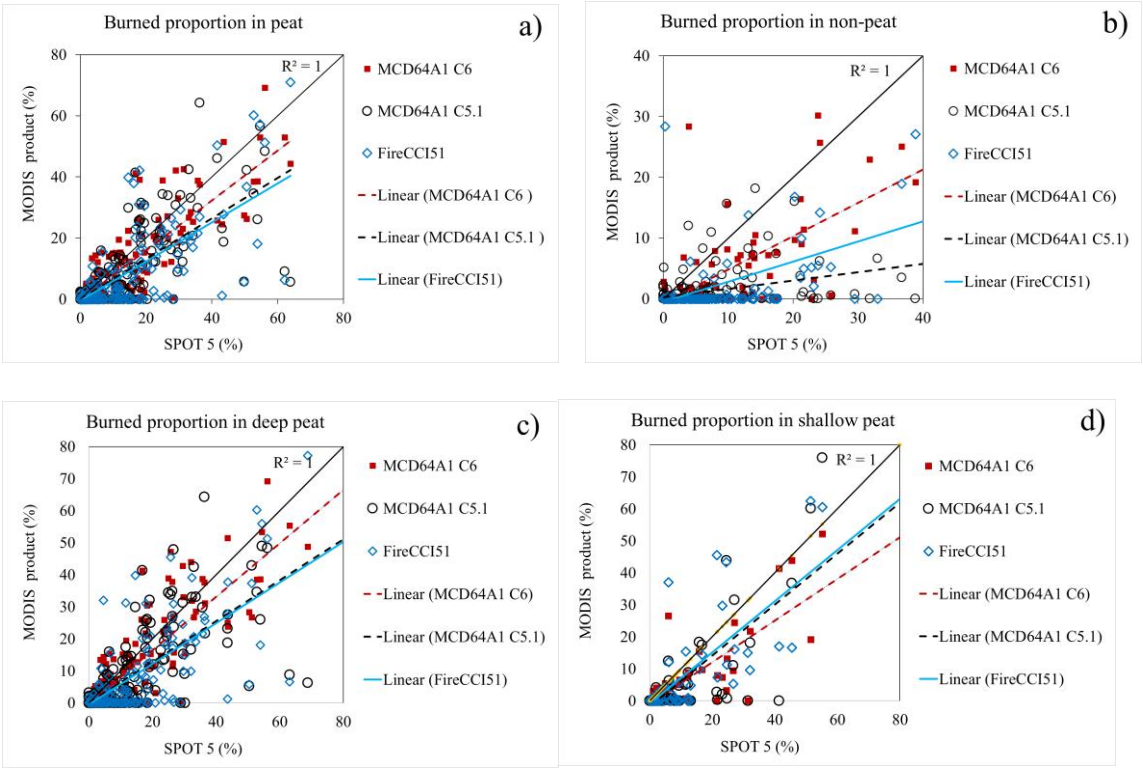

Figure 2-7. Regressions of the proportion of area burned in each 5x5 km^2 grid square of the various burned area products and the SPOT-5-derived reference map (Zubaidah et al. 2017) in Central Kalimantan, Indonesia, during the 2014 fire season. Markers denote proportions of area burned of each grid polygon over all peatlands (a), non-peat (b), deep peatland (c), and shallow peatland (d): MCD64A1 C6 = red rectangle; MCD64A1 C5.1= black hollow; and FireCCI51= blue diamond. Regression line colors correspond with associated product marker colors. Solid black (R^2=1) line

for comparison to product regressions. MCD64A1 C6 was the most accurate product for both peat and non-peat (slope=0.82, intercept=-0.34, $R^2 = 0.77$). A complete list of regression results can be found in Table 2-2.

Table 2-1 MODIS burned area (BA) product accuracy assessment in peatlands and non-peatland (OA=overall accuracy, OE=omission error, CE=commission error). Three BA classes and the temporal window lengths were assessed; all burned areas regardless of size (G1), all areas excluding small burned areas (G2, ≥25 ha), and all larger burned areas (G3, ≥100 ha). The temporal window length was assessed by summing the area burned from the beginning of the burning season until the date of the corresponding SPOT 5 imagery (D0), as well as eight days (D8), and ten days afterward (D10). The omission (burned areas not detected) and commission (burned areas erroneously detected) errors were calculated based on spatial comparisons to the reference map for each group and product. Total BA of the SPOT 5 reference maps in non-peat and peat for each BA size, respectively, were: G1=23,362 vs. 57,887 ha; G2=19,631 vs. 52,993 ha; and G3=14,589 vs. 46,280.

Temporal window	Peat class	MODIS Product	G1 (All areas)					G2 (≥25 ha)					G3 (≥100 ha)				
			Accurately detected	BA MODIS	OA	OE	CE	Accurately detected	BA MODIS	OA	OE	CE	Accurately detected	BA MODIS	OA	OE	CE
D0	Non-peat	MCD64A1 C6	4,864	8,923	0.21	0.79	0.45	4,764	8,923	0.24	0.76	0.47	4,373	8,923	0.30	0.70	0.51
		MCD64A1 C5.1	2,095	4,710	0.09	0.91	0.56	2,023	4,710	0.10	0.90	0.57	1,558	4,710	0.11	0.89	0.67
		FireCCI51	2,856	5,574	0.12	0.88	0.49	2,841	5,574	0.14	0.86	0.49	2,804	5,574	0.19	0.81	0.50
	Peat	MCD64A1 C6	27,522	42,729	0.48	0.52	0.36	27,300	42,729	0.52	0.48	0.36	26,598	42,729	0.57	0.43	0.38
		MCD64A1 C5.1	23,365	36,994	0.40	0.60	0.37	23,050	36,994	0.43	0.57	0.38	22,325	36,994	0.48	0.52	0.40
		FireCCI51	21,774	32,317	0.38	0.62	0.33	21,542	32,317	0.41	0.59	0.33	20,825	32,317	0.45	0.55	0.36
D8	Non-peat	MCD64A1 C6	5,627	14,597	0.24	0.76	0.61	5,427	14,597	0.28	0.72	0.63	4,868	14,597	0.33	0.67	0.67
		MCD64A1 C5.1	7,145	17,644	0.31	0.69	0.60	6,897	17,644	0.35	0.65	0.61	6,012	17,644	0.41	0.59	0.66
		FireCCI51	4,578	8,508	0.20	0.80	0.46	4,505	8,508	0.23	0.77	0.47	4,355	8,508	0.30	0.70	0.49
	Peat	MCD64A1 C6	33,230	71,359	0.57	0.43	0.53	32,683	71,359	0.62	0.38	0.54	31,336	71,359	0.68	0.32	0.56
		MCD64A1 C5.1	37,613	78,419	0.65	0.35	0.52	36,801	78,419	0.69	0.31	0.53	35,488	78,419	0.77	0.23	0.55
		FireCCI51	30,378	50,880	0.52	0.48	0.40	29,945	50,880	0.57	0.43	0.41	28,349	50,880	0.61	0.39	0.44
D10	Non-peat	MCD64A1 C6	5,735	16,178	0.25	0.75	0.65	5,533	16,178	0.28	0.72	0.66	4,973	16,178	0.34	0.66	0.69
		MCD64A1 C5.1	7,150	17,667	0.31	0.69	0.60	6,902	17,667	0.35	0.65	0.61	6,012	17,667	0.41	0.59	0.66
		FireCCI51	4,578	8,600	0.20	0.80	0.47	4,505	8,600	0.23	0.77	0.48	4,355	8,600	0.30	0.70	0.49
	Peat	MCD64A1 C6	33,683	76,039	0.58	0.42	0.56	33,082	76,039	0.62	0.38	0.56	31,670	76,039	0.68	0.32	0.58
		MCD64A1 C5.1	37,978	79,699	0.66	0.34	0.52	37,159	79,699	0.70	0.30	0.53	35,827	79,699	0.77	0.23	0.55
		FireCCI51	30,429	51,510	0.53	0.47	0.41	29,995	51,510	0.57	0.43	0.42	28,400	51,510	0.61	0.39	0.45

Table 2-2. Regressions of the proportion of area burned in each 5x5 km^2 grid square of the various burned area products and the SPOT-5-derived reference map for each land cover type (Zubaidah et al. 2017) in Central Kalimantan, Indonesia, during the 2014 fire season.

Product name	Peat									Non-peat (N=)		
	All peatlands (N=)			Deep peat only (N=)			Shallow peat only (N=)					
	Slope	Intercept	R^2	Slope	Intercept	R^2	Slope	Intercept	R^2	Slope	Intercept	R^2
MCD64A1 C6	0.82	-0.34	0.77	0.84	- 0.32	0.78	0.65	- 0.93	0.66	0.55	- 0.64	0.50
MCD64A1 C5.1	0.66	-0.04	0.61	0.64	0.06	0.59	0.80	- 1.77	0.59	0.14	0.26	0.14
FireCC51	0.64	-0.48	0.60	0.64	- 0.51	0.60	0.80	- 0.87	0.60	0.33	- 0.50	0.31

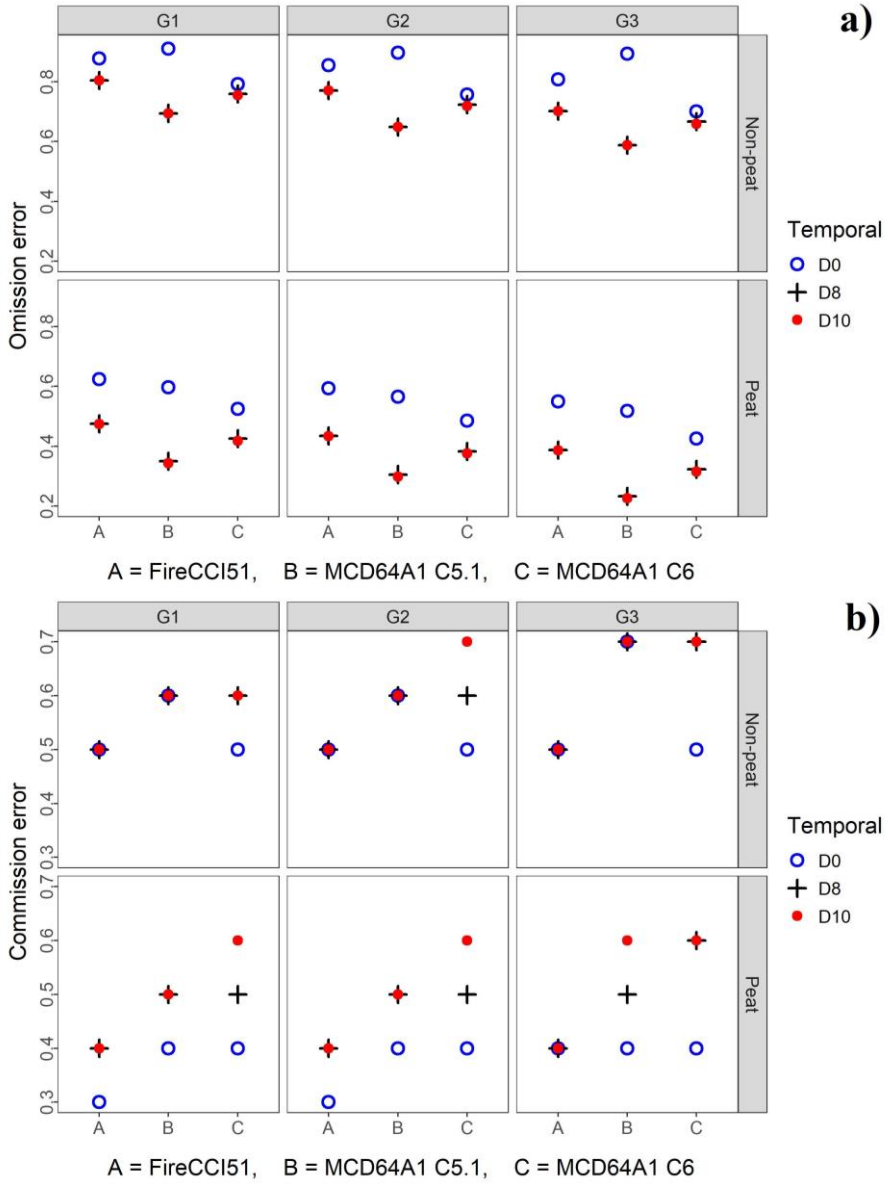

Figure 2-8 Omission (a) and commission error (b) comparison among burned area products respective to burned area (BA) size group and temporal window length in peatland and non-

peatland. G1, G2, and G3 represent the BA size: all burned areas regardless of size (G1), all areas excluding small burned areas (G2, ≥25 ha), and all areas considered as large burned areas (G3, ≥100 ha). D0, D8, and D10 refer to the temporal window length: summing the area burned from the beginning of the burning season until the same date as SPOT 5 scanned (D0), or eight days (D8), and ten days after the SPOT imagery collection (D10).

2.4 Discussion

All products underestimated validated burned areas by roughly half, on average. Fires smaller than 100 ha were only responsible for 2.9±0.9% and 2.5±1.6% of area underestimation in peatlands and non-peatlands, respectively, for all temporal window lengths. Burns in non-peatlands, primarily occurring in croplands, are frequently small and rapid fires that produce less char or ash, making detection difficult in this land cover type, as has been the case in other regions (Hall et al. 2016; Zhu et al. 2017). Our results corroborate the previous simulation (Miettinen & Liew, 2009) which showed that moderate to coarse resolution in Indonesian peatlands performed better than in non-peatlands, given the larger burn scars in peatland areas. Excluding small fires (<100 ha) from the analysis resulted in the greatest accuracy increases for MCD64A1 C5.1, indicating that this product has the worst small fires detection capability. FireCCI51 was least affected by small fire removal but it was less accurate overall than MCD64A1 C6.

The MODIS instruments on the Terra and Aqua satellites have known detection issues when dense clouds and smoke interfere (Giglio et al. 2003), common conditions in the study region. Since the FireCCI51 product is generated solely from Terra satellite MODIS data (Chuvieco et al. 2018), known issues of regular orbital space gaps at equatorial locations, such as Sumatra and Kalimantan, may partially explain the larger under-estimation of burned area by this product despite its higher spatial resolution.

Inclusion of detected active fires (MOD14/MYD14) into algorithms for more recent burned area products improves detection rates (Humber et al. 2019). The lack of

this feature in the algorithm of the older MCD45A1 product (Roy et al. 2008) may explain its apparent inability to detect burned areas in this perennially cloudy region. MCD64A1, which had the most accurate products, is more tolerant of cloud and aerosol contamination (Giglio et al. 2009) since the algorithm relies primarily on both thermal infrared bands and changes in vegetation indices using shortwave and near-infrared bands. These two bands discriminate areas burned and unburned more distinctly than other bands (Huang et al. 2016).

MCD64A1 is currently used by models for global carbon emissions estimation (e.g., GFED4 used MCD64A1 C5.1). The long time series (late 2000-present) and broad coverage of the MCD64A1 data make it ideal for producing global emissions estimates. Although there are uncertainties due to other variable model parameters (emissions factors, combustion completeness, peat burn depth) (Heymann et al. 2017; Whitburn et al. 2016; Wooster et al. 2018), our results indicate that burned area alone has contributed ~50% to the uncertainty of emissions estimates from fire activity in this region in 2014. Our study was limited to a year with moderate burning extent and intensity. Product accuracy varies spatially and temporally among regions (Humber et al. 2019) and this likely affects our study region as well. Accuracies in severe burning seasons (e.g. 2015), when thick smoke blankets the region for weeks on end may have even larger discrepancies because of the lack visibility that precludes burned area observations by all of these MODIS-based systems. We encourage further product accuracy assessment at various locations and seasonal periods of burning in Indonesian peatlands.

The frequency of fire activity at specific locations, which may directly relate to the amount of fire emissions in peatlands, has not been accounted for by most emissions models. However, such estimations can only be made if long-term annual burned area

maps, with better spatial resolution than MODIS, become easily available. Fire frequency at a site controls the risk of peat burns (high emissions rate) in peatlands. Konecny et al. (Konecny et al. 2016) suggest that the first time a peatland burns, peat is consumed to an average depth of (17±16 cm), while subsequent burns in the same area only burn roughly half as deeply. Lohberger et al. (2017) incorporated these results and found lower regional emissions rates than the GFED4 emissions model had reported. In 2015, GFED4 estimated a nearly doubled emissions rate for Indonesian fires (1.75 vs. 0.89 Gt CO_2e) despite the lower amount of burned area identified in their study using MODIS burned area. As shown here, current burned area products substantially underreport the amount of fire affected area. Uncertainties are largest in non-peatlands but the greatest impact on global emissions estimations from models comes from under detection of annual fire in peatlands, where smoldering fires lead to disproportionately large amounts of aerosol and gaseous emissions, and inability to account for recurrent fires in subsequent years. Improved burned area estimation, particularly in Indonesian peatlands, requires specific attention in order to improve the accuracy and precision of global carbon emissions estimates.

The challenges inherent in mapping burned areas in the cloudy and smoky peatlands of Indonesia make alternative approaches necessary to improve burned area map reliability. MCD45A1, for example, suffered from missing observations due to clouds and smoke, hampering systematic change-detection efforts using passive sensors to map this region (Roy et al. 2005). To overcome the issues with clouds and smoke obscuring the land surface some combination of more frequent visual observations, integration of burned area products, and methods that allow for imaging through clouds and smoke must be employed.

The amount of freely available satellite imagery has increased in recent years, providing cost-effective opportunities for developing integrated methods of burned area mapping and validation. With the launch of various free datasets with that have higher spatial, temporal, and spectral resolutions there is the potential to provide more comprehensive burned area maps (Boschetti et al. 2015; Lohberger et al. 2017; Miettinen et al. 2013; Roteta et al. 2019; Roy et al. 2019) in Indonesia. Additionally, the next generation of Terra/Aqua satellite successors, the Suomi NPP (National Polar-orbiting Partnership) (Justice et al. 2013) and NOAA-20—both under NOAA's Joint Polar Satellite System (JPSS), have a wider swath, without any orbital gaps at the equator, providing new prospects for detecting more of the burning (Sofan et al. 2020) when cloud-free conditions exist.

Studies are needed to explore the complementary nature of these various datasets for mapping burned areas, specifically in Indonesian peatlands, to overcome issues including cloud cover/shadow, small fires, and smoldering fires (low intensity). Recent studies have proven that these datasets improve burned area detection in this region and other fire-prone areas (Carreiras et al. 2020; Hawbaker et al. 2020; Lohberger et al. 2017; Roteta et al. 2019; Roy et al. 2019; Sofan et al. 2020). However, none of them can provide the long-term burning time series that MODIS does. Even Landsat, which has historically supplied long-term sequences of imagery, is lacking in this region. Newer systems such as Landsat 8 and Sentinel-2 may help rectify this for future years by providing many more potential observations throughout a burning season. Multi-sensor integration, including passive and active remote sensing sources may improve accuracy but, to the best of our knowledge, no studies have investigated this approach, specifically for Indonesian peatlands that are more vulnerable to fires (Vetrita and Cochrane, 2020).

2.5 Conclusion

We compared the accuracy of four MODIS-derived burned area products to a high resolution validated burned area reference map for 2014 in Central Kalimantan, Indonesia, including two decommissioned products (MCD45A1 C5.1 and MCD64A1 C5.1) and two currently available products (MCD64A1 C6 and FireCCI51, the product developed under a CCI project of European Space Agency). Currently available products were more reliable than the older ones, as expected. The standard burned area MODIS product, MCD64A1 C6, was the best, suggesting a better performance than its precursor (MCD64 C5.1). Despite the higher spatial resolution of FireCCI51 compared to MCD64A1, the burned area product showed lower improvements for detection of smaller burned areas (<100 ha).

Our findings bring new insight about the performance various MODIS satellite-based approaches for discriminating burned and unburned areas in tropical peatlands/non-peatlands. The globally significant emissions from frequent burning of Indonesian peatlands makes observation and quantification of these fires critical for effective monitoring and application of global emissions models. However, in this region, cloud cover and heavy smoke from persistent burning substantially degrades the effectiveness of existing MODIS-derived burned area mapping efforts. Our site in Central Kalimantan is one of the most severely fire-impacted regions in Indonesia, with recurrent burning prevalent for more than a decade (Vetrita and Cochrane, 2020). Our study was limited to the dry season of 2014 due to our available reference map which had less severe burning than what often occurs during El Niño events. Since smoke is even thicker and more persistent then, our results showing the inaccuracies of current global burned area products may be conservative.

We still recommend using currently available MODIS burned area products (MCD64A1 C6 and FireCCI51) for national scale monitoring. With nearly two decades of observations, the long time-series data provide unparalleled insight into Indonesia's fire history. However, mapping burned areas at higher spatial resolutions remains necessary in order to accurately detect changes and spatially locate peat fires. We urge use of both satellites with MODIS instruments, Terra and Aqua, to get better coverage and more chances to improve detection of burned areas in the frequently cloudy and smoke covered peatlands of Indonesia. Since the planned operational lifetime of the Terra and Aqua satellites is coming to an end, the next generation of satellites (e.g. Suomi NPP and NOAA-20) will continue monitoring of Indonesian burning. Having a wider swath, without any orbital gaps at the equator and higher spatial resolution than the MODIS precursors, the continuing burned area products, combined with multisensor satellites that are currently available, such as Sentinel-2, Sentinel 1, and Landsat 8 will ensure and improve future analyses of long-term burning history in Indonesian peatlands. These products will be useful for users with various applications, including fire frequency analysis, fire ecology, or fire-related and affected social assessments.

Strengthening monitoring systems by incorporating various additional data sources will help stakeholders to manage the land and improve the ability of emission-modelers to accurately map global emission levels, which remain highly uncertain. Indonesia has a critical need for accurate and timely burned area mapping to meet a variety of needs and different purposes, including fire-related emissions monitoring of burning peatlands, law enforcement, rapid assessment, and fire suppression efforts. However, clear guidelines for how to accurately interpret these datasets are essential.

2.6 Acknowledgements

We gratefully acknowledge the support from NASA funding #NNX13AP46G/NNX17AC95G/80NSSC18K0235 and the provision of field data and publication funds by the Indonesian National Institute of Aeronautics and Space (LAPAN). Y.V. was funded by the Research and Innovation Science and Technology Project (RISET-Pro), Ministry of Research, Technology and Higher Education of the Republic of Indonesia (Kemenristekdikti) under the World Bank Loan No. 8245-ID for her Ph.D. We would like to thank Dr. Carol Johnston, Ms. Any Zubaidah, and two anonymous reviewers for their constructive comments on earlier drafts this manuscript.

References

Albar, I., Jaya, I.N.S., Saharjo, B.H., Kuncahyo, B., & Vadrevu, K.P. (2018). Spatio-Temporal Analysis of Land and Forest Fires in Indonesia Using MODIS Active Fire Dataset. In K.P. Vadrevu, T. Ohara, & C. Justice (Eds.), *Land-Atmospheric Research Applications in South and Southeast Asia* (pp. 105-127). Cham: Springer International Publishing

Alonso-Canas, I., & Chuvieco, E. (2015). Global burned area mapping from ENVISAT-MERIS and MODIS active fire data. *Remote Sensing of Environment, 163*, 140-152

Andela, N., Kaiser, J., Heil, A., van Leeuwen, T., van der Werf, G., Wooster, M., Remy, S., & Schultz, M. (2013). Assessment of the Global Fire Assimilation System (GFASv1), MACC-II (Monitoring Atmospheric Composition and Climate) project. In, *Technical Memorandum No. 702*: ECMWF

Ballhorn, U., Siegert, F., Mason, M., & Limin, S. (2009). Derivation of burn scar depths and estimation of carbon emissions with LIDAR in Indonesian peatlands. *Proc Natl Acad Sci U S A, 106*, 21213-21218

Boschetti, L., Roy, D.P., Justice, C.O., & Humber, M.L. (2015). MODIS–Landsat fusion for large area 30m burned area mapping. *Remote Sensing of Environment, 161*, 27-42

Boschetti, L., Stehman, S.V., & Roy, D.P. (2016). A stratified random sampling design in space and time for regional to global scale burned area product validation. *Remote Sensing of Environment, 186*, 465-478

Boschetti, M., Stroppiana, D., & Brivio, P.A. (2010). Mapping Burned Areas in a Mediterranean Environment Using Soft Integration of Spectral Indices from High-Resolution Satellite Images. *Earth Interactions, 14*

Carreiras, J.M., Quegan, S., Tansey, K., & Page, S.J.E.R.L. (2020). Sentinel-1 observation frequency significantly increases burnt area detectability in tropical SE Asia, *15*, 054008

Chang, D., & Song, Y.J.J.o.G.R.A. (2009). Comparison of L3JRC and MODIS global burned area products from 2000 to 2007, *114*

Chen, L.W.A., Moosmüller, H., Arnott, W.P., Chow, J.C., Watson, J.G., Susott, R.A., Babbitt, R.E., Wold, C.E., Lincoln, E.N., & Hao, W.M. (2007). Emissions from Laboratory Combustion of Wildland Fuels: Emission Factors and Source Profiles. *Environmental science & technology, 41*, 4317-4325

Chuvieco, E., Lizundia-Loiola, J., Pettinari, M.L., Ramo, R., Padilla, M., Tansey, K., Mouillot, F., Laurent, P., Storm, T., & Heil, A.J.E.S.S.D. (2018). Generation and analysis of a new global burned area product based on MODIS 250 m reflectance bands and thermal anomalies, *10*, 2015-2031

Eva, H., & Lambin, E.F. (1998). Burnt area mapping in Central Africa using ATSR data. *International Journal of Remote Sensing, 19*, 3473-3497

Field, R.D., van der Werf, G.R., Fanin, T., Fetzer, E.J., Fuller, R., Jethva, H., Levy, R., Livesey, N.J., Luo, M., & Torres, O. (2016). Indonesian fire activity and smoke pollution in 2015 show persistent nonlinear sensitivity to El Niño-induced drought. *Proceedings of the National Academy of Sciences, 113*, 9204-9209

Fornacca, D., Ren, G., & Xiao, W.J.R.S. (2017). Performance of three MODIS fire products (MCD45A1, MCD64A1, MCD14ML), and ESA Fire_CCI in a mountainous area of Northwest Yunnan, China, characterized by frequent small fires, *9*, 1131

French, N.H.F., Kasischke, E.S., & Williams, D.G. (2002). Variability in the emission of carbon-based trace gases from wildfire in the Alaskan boreal forest, *107*, FFR 7-1-FFR 7-11

GFED (2015). 2015 Fire Season. [Online]. Available: http://www.globalfiredata.org/updates.html#2015_indonesia [Accessed 30 October 2020].

Giglio, L., Boschetti, L., Roy, D.P., Humber, M.L., & Justice, C.O.J.R.s.o.e. (2018). The Collection 6 MODIS burned area mapping algorithm and product, *217*, 72-85

Giglio, L., Descloitres, J., Justice, C.O., & Kaufman, Y.J. (2003). An enhanced contextual fire detection algorithm for MODIS. *Remote Sensing of Environment, 87*, 273-282

Giglio, L., Loboda, T., Roy, D.P., Quayle, B., & Justice, C.O. (2009). An active-fire based burned area mapping algorithm for the MODIS sensor. *Remote Sensing of Environment, 113*, 408-420

Glauber, A., Moyer, S., Adriani, M., & Gunawan, I. (2016). The Cost of Fire: An Economic Analysis of Indonesia's 2015 Fire Crisis. In, *Indonesia Sustainable Landscapes Knowledge Note No. 1*. Jakarta, Indonesia

Hall, J.V., Loboda, T.V., Giglio, L., & McCarty, G.W. (2016). A MODIS-based burned area assessment for Russian croplands: Mapping requirements and challenges. *Remote Sensing of Environment, 184*, 506-521

Hawbaker, T.J., Vanderhoof, M.K., Schmidt, G.L., Beal, Y.-J., Picotte, J.J., Takacs, J.D., Falgout, J.T., & Dwyer, J.L.J.R.S.o.E. (2020). The Landsat Burned Area algorithm and products for the conterminous United States, *244*, 111801

Heymann, J., Reuter, M., Buchwitz, M., Schneising, O., Bovensmann, H., Burrows, J., Massart, S., Kaiser, J., & Crisp, D. (2017). CO2 emission of Indonesian fires in 2015 estimated from satellite-derived atmospheric CO2 concentrations. *Geophysical Research Letters, 44*, 1537-1544

Hollmann, R., Merchant, C.J., Saunders, R., Downy, C., Buchwitz, M., Cazenave, A., Chuvieco, E., Defourny, P., de Leeuw, G., Forsberg, R., Holzer-Popp, T., Paul, F., Sandven, S., Sathyendranath, S., van Roozendael, M., & Wagner, W. (2013). The ESA Climate Change Initiative: Satellite Data Records for Essential Climate Variables. *Bulletin of the American Meteorological Society, 94*, 1541-1552

Huang, H., Roy, D.P., Boschetti, L., Zhang, H.K., Yan, L., Kumar, S.S., Gomez-Dans, J., & Li, J. (2016). Separability analysis of Sentinel-2A multi-spectral instrument (MSI) data for burned area discrimination. *Remote Sensing, 8*, 873

Humber, M.L., Boschetti, L., Giglio, L., & Justice, C.O.J.I.j.o.d.e. (2019). Spatial and temporal intercomparison of four global burned area products, *12*, 460-484

Johnston, F.H., Henderson, S.B., Chen, Y., Randerson, J.T., Marlier, M., DeFries, R.S., Kinney, P., Bowman, D.M., & Brauer, M. (2012). Estimated global mortality attributable to smoke from landscape fires. *Environmental Health Perspectives, 120*, 695

Justice, C.O., Román, M.O., Csiszar, I., Vermote, E.F., Wolfe, R.E., Hook, S.J., Friedl, M., Wang, Z., Schaaf, C.B., Miura, T., Tschudi, M., Riggs, G., Hall, D.K., Lyapustin, A.I., Devadiga, S., Davidson, C., & Masuoka, E.J. (2013). Land and cryosphere products from Suomi NPP VIIRS: Overview and status. *Journal of Geophysical Research: Atmospheres, 118*, 9753-9765

Kaiser, J., Heil, A., Andreae, M., Benedetti, A., Chubarova, N., Jones, L., Morcrette, J.-J., Razinger, M., Schultz, M., & Suttie, M.J.B. (2012). Biomass burning emissions estimated with a global fire assimilation system based on observed fire radiative power, *9*, 527

Konecny, K., Ballhorn, U., Navratil, P., Jubanski, J., Page, S.E., Tansey, K., Hooijer, A., Vernimmen, R., & Siegert, F. (2016). Variable carbon losses from recurrent fires in drained tropical peatlands. *Glob Chang Biol, 22*, 1469-1480

Koplitz, S.N., Mickley, L.J., Marlier, M.E., Buonocore, J.J., Kim, P.S., Liu, T., Sulprizio, M.P., DeFries, R.S., Jacob, D.J., & Schwartz, J.J.E.R.L. (2016). Public health impacts of the severe haze in Equatorial Asia in September–October 2015: demonstration of a new framework for informing fire management strategies to reduce downwind smoke exposure, *11*, 094023

Korontzi, S., Ward, D.E., Susott, R.A., Yokelson, R.J., Justice, C.O., Hobbs, P.V., Smithwick, E.A.H., & Hao, W.M. (2003). Seasonal variation and ecosystem dependence of emission factors for selected trace gases and PM2.5 for southern African savanna fires, *108*

Langner, A., Miettinen, J., & Siegert, F. (2007). Land cover change 2002–2005 in Borneo and the role of fire derived from MODIS imagery. *Global Change Biology, 13*, 2329-2340

Lizundia-Loiola, J., Otón, G., Ramo, R., & Chuvieco, E.J.R.S.o.E. (2020). A spatio-temporal active-fire clustering approach for global burned area mapping at 250 m from MODIS data, *236*, 111493

Lohberger, S.; Stängel, M.; Atwood, E.C.; Siegert, F. Spatial evaluation of Indonesia's 2015 fire affected area and estimated carbon emissions using Sentinel-1. Glob. Chang. Biol. 2017. doi:10.1111/gcb.13841.

Marlier, M.E., Liu, T., Yu, K., Buonocore, J.J., Koplitz, S.N., DeFries, R.S., Mickley, L.J., Jacob, D.J., Schwartz, J., & Wardhana, B.S.J.G. (2019). Fires, smoke exposure, and public health: An integrative framework to maximize health benefits from peatland restoration, *3*, 178-189

Miettinen, J., Hyer, E., Chia, A.S., Kwoh, L.K., & Liew, S.C. (2013). Detection of vegetation fires and burnt areas by remote sensing in insular Southeast Asian conditions: current status of knowledge and future challenges. *International Journal of Remote Sensing, 34*, 4344-4366

Miettinen, J., Langner, A., & Siegert, F. (2007). Burnt area estimation for the year 2005 in Borneo using multi-resolution satellite imagery. *International Journal of Wildland Fire, 16*, 45-53

Miettinen, J., & Liew, S.C. (2009). Burn-scar patterns and their effect on regional burnt-area mapping in insular South-East Asia %J International Journal of Wildland Fire, *18*, 837-847

MoEF (2020). Sipongi, Karhutla Sistem. In, *Rekapitulasi Luas Kebakaran Hutan dan Lahan (Ha) Per Provinsi Di Indonesia Tahun 2015-2020*. Jakarta

Padilla, M., Stehman, S.V., & Chuvieco, E. (2014). Validation of the 2008 MODIS-MCD45 global burned area product using stratified random sampling. *Remote Sensing of Environment, 144*, 187-196

Page, S., & Hooijer, A. (2016). In the line of fire: the peatlands of Southeast Asia. *Phil. Trans. R. Soc. B, 371*, 20150176

Page, S.E., Siegert, F., Rieley, J.O., Boehm, H.D., Jaya, A., & Limin, S. (2002). The amount of carbon released from peat and forest fires in Indonesia during 1997. *Nature, 420*, 61-65

Pettinari, M.L., Lizundia-Loiola, J., & Chuvieco, E. (2020). ESA CCI ECV Fire Disturbance: D4.2 Product User Guide - MODIS, version 1.0. In

Ramo, R., & Chuvieco, E. (2017). Developing a Random Forest Algorithm for MODIS Global Burned Area Classification. *Remote Sensing, 9*, 1193

Ritung, S., Wahyunto, N.K., Sukarman, H., & Suparto, T.C. (2011). Peta Lahan Gambut Indonesia skala 1: 250.000. *Balai Besar Penelitian dan Pengembangan Sumberdaya Lahan Pertanian. Badan Penelitian dan Pengembangan Pertanian. Bogor, Indonesia*

Rodrigues, J.A., Libonati, R., Pereira, A.A., Nogueira, J.M., Santos, F.L., Peres, L.F., Santa Rosa, A., Schroeder, W., Pereira, J.M., Giglio, L.J.I.J.o.A.E.O., & Geoinformation (2019). How well do global burned area products represent fire patterns in the Brazilian Savannas biome? An accuracy assessment of the MCD64 collections, *78*, 318-331

Roteta, E., Bastarrika, A., Padilla, M., Storm, T., & Chuvieco, E.J.R.S.o.E. (2019). Development of a Sentinel-2 burned area algorithm: Generation of a small fire database for sub-Saharan Africa, *222*, 1-17

Roy, D., Jin, Y., Lewis, P., & Justice, C. (2005). Prototyping a global algorithm for systematic fire-affected area mapping using MODIS time series data. *Remote Sensing of Environment, 97*, 137-162

Roy, D.P., & Boschetti, L. (2009). Southern Africa validation of the MODIS, L3JRC, and GlobCarbon burned-area products. *IEEE Transactions on Geoscience and Remote Sensing, 47*, 1032-1044

Roy, D.P., Boschetti, L., Justice, C.O., & Ju, J. (2008). The collection 5 MODIS burned area product—Global evaluation by comparison with the MODIS active fire product. *Remote Sensing of Environment, 112*, 3690-3707

Roy, D.P., Huang, H., Boschetti, L., Giglio, L., Yan, L., Zhang, H.H., & Li, Z. (2019). Landsat-8 and Sentinel-2 burned area mapping - A combined sensor multi-temporal change detection approach. *Remote Sensing of Environment, 231*, 111254

Roy, D.P., Lewis, P.E., & Justice, C.O. (2002). Burned area mapping using multi-temporal moderate spatial resolution data—a bi-directional reflectance model-based expectation approach. *Remote Sensing of Environment, 83*, 263-286

Ruiz, J.A.M., Lázaro, J.R.G., Cano, I.D.Á., & Leal, P.H.J.R.S. (2014). Burned area mapping in the North American boreal forest using terra-MODIS LTDR (2001–

2011): A comparison with the MCD45A1, MCD64A1 and BA GEOLAND-2 products, *6*, 815-840

Schroeder, W., Oliva, P., Giglio, L., & Csiszar, I.A. (2014). The New VIIRS 375m active fire detection data product: Algorithm description and initial assessment. *Remote Sensing of Environment, 143*, 85-96

Shi, Y., Sasai, T., & Yamaguchi, Y. (2014). Spatio-temporal evaluation of carbon emissions from biomass burning in Southeast Asia during the period 2001–2010. *Ecological Modelling, 272*, 98-115

Siegert, F., Ruecker, G., Hinrichs, A., & Hoffmann, A. (2001). Increased damage from fires in logged forests during droughts caused by El Nino. *Nature, 414*, 437-440

Smith, A.M.S., Drake, N.A., Wooster, M.J., Hudak, A.T., Holden, Z.A., & Gibbons, C.J. (2007). Production of Landsat ETM+ reference imagery of burned areas within Southern African savannahs: comparison of methods and application to MODIS. *International Journal of Remote Sensing, 28*, 2753-2775

Sofan, P., Bruce, D., Schroeder, W., Jones, E., & Marsden, J. (2020). Assessment of VIIRS 375 m active fire using tropical peatland combustion algorithm applied to Landsat-8 over Indonesia's peatlands. *International Journal of Digital Earth*, 1-22

Sparks, A.M., Boschetti, L., Smith, A.M.S., Tinkham, W.T., Lannom, K.O., & Newingham, B.A. (2015). An accuracy assessment of the MTBS burned area product for shrub–steppe fires in the northern Great Basin, United States %J International Journal of Wildland Fire, *24*, 70-78

Stockwell, C.E., Jayarathne, T., Cochrane, M.A., Ryan, K.C., Putra, E.I., Saharjo, B.H., Nurhayati, A.D., Albar, I., Blake, D.R., & Simpson, I.J. (2016). Field measurements of trace gases and aerosols emitted by peat fires in Central Kalimantan, Indonesia, during the 2015 El Niño. *Atmospheric Chemistry and Physics, 16*, 11711-11732

Tansey, K., Beston, J., Hoscilo, A., Page, S.E., & Hernandez, C.U.P. (2008). Relationship between MODIS fire hot spot count and burned area in a degraded tropical peat swamp forest in Central Kalimantan, Indonesia. *Journal of Geophysical Research-Atmospheres, 113*

Tsela, P., Wessels, K., Botai, J., Archibald, S., Swanepoel, D., Steenkamp, K., & Frost, P. (2014). Validation of the two standard MODIS satellite burned-area products and an empirically-derived merged product in South Africa. *Remote Sensing*, *6*, 1275-1293

Turetsky, M.R., Benscoter, B., Page, S., Rein, G., Van Der Werf, G.R., & Watts, A. (2015). Global vulnerability of peatlands to fire and carbon loss. *Nature Geoscience*, *8*, 11-14

van der Werf, G.R., Randerson, J.T., Giglio, L., Collatz, G.J., Mu, M., Kasibhatla, P.S., Morton, D.C., DeFries, R.S., Jin, Y., & van Leeuwen, T.T. (2010). Global fire emissions and the contribution of deforestation, savanna, forest, agricultural, and peat fires (1997-2009). *Atmospheric Chemistry and Physics*, *10*, 11707-11735

van der Werf, G.R., Randerson, J.T., Giglio, L., van Leeuwen, T.T., Chen, Y., Rogers, B.M., Mu, M., van Marle, M.J.E., Morton, D.C., Collatz, G.J., Yokelson, R.J., & Kasibhatla, P.S. (2017). Global fire emissions estimates during 1997–2016. *Earth Syst. Sci. Data*, *9*, 697-720

Vetrita, Y., & Cochrane, M.A.J.R.S. (2020). Fire Frequency and Related Land-Use and Land-Cover Changes in Indonesia's Peatlands, *12*, 5

Wahyunto, R.S., & Subagjo, H. (2004). Map of peatland distribution area and carbon content in Kalimantan, 2000–2002. *Wetlands International—Indonesia Programme & Wildlife Habitat Canada (WHC), Bogor, Indonesia*

Whitburn, S., Van Damme, M., Clarisse, L., Turquety, S., Clerbaux, C., & Coheur, P.F. (2016). Doubling of annual ammonia emissions from the peat fires in Indonesia during the 2015 El Nino. *Geophysical Research Letters*, *43*, 11007-11014

Wiedinmyer, C., Akagi, S., Yokelson, R.J., Emmons, L., Al-Saadi, J., Orlando, J., & Soja, A. (2011). The Fire INventory from NCAR (FINN): a high resolution global model to estimate the emissions from open burning. *Geoscientific Model Development*, *4*, 625

Wooster, M., Roberts, G., Perry, G., & Kaufman, Y. (2005). Retrieval of biomass combustion rates and totals from fire radiative power observations: FRP derivation and calibration relationships between biomass consumption and fire radiative energy release. *2012), 110*

Wooster, M.J., Gaveau, D., Salim, M.A., Zhang, T., Xu, W., Green, D.C., Huijnen, V., Murdiyarso, D., Gunawan, D., & Borchard, N.J.R.S. (2018). New tropical peatland gas and particulate emissions factors indicate 2015 Indonesian fires released far more particulate matter (but less methane) than current inventories imply, *10*, 495

Zhang, X., Kondragunta, S., Ram, J., Schmidt, C., & Huang, H.C. (2012). Near-real-time global biomass burning emissions product from geostationary satellite constellation. *Journal of Geophysical Research: Atmospheres, 117*

Zhu, C., Kobayashi, H., Kanaya, Y., & Saito, M. (2017). Size-dependent validation of MODIS MCD64A1 burned area over six vegetation types in boreal Eurasia: Large underestimation in croplands. *Sci Rep, 7*, 4181

Zubaidah, A., Sulma, S., Suwarsono, & Vetrita, Y. (2017). Akurasi Luas Areal Kebakaran dari Data Landsat-8 OLI di Wilayah Kalimantan (Accuracy of burned area derived from Landsat-8 OLI in Kalimantan). *MAJALAH ILMIAH GLOBE, 19*, 21-32

CHAPTER 3

FIRE FREQUENCY AND RELATED LAND-USE AND LAND-COVER CHANGES IN INDONESIA'S PEATLANDS

Paper #2: Vetrita, Y. and Cochrane, M.A., 2020. Fire Frequency and Related Land-Use and Land-Cover Changes in Indonesia's Peatlands. Remote Sensing, 12(1), p.5. https://doi.org/10.3390/rs12010005

Abstract

Indonesia's converted peatland areas have a well-established fire problem, but limited studies have examined the frequency with which they are burning. Here, we quantify fire frequency in Indonesia's two largest peatland regions, Sumatra and Kalimantan, during 2001–2018. We report, annual areas burned, total peatland area affected by fires, amount of recurrent burning and associations with land-use and land-cover (LULC) change. We based these analyses on Moderate Resolution Imaging Spectroradiometer (MODIS) Terra/Aqua combined burned area and three Landsat-derived LULC maps (1990, 2007, and 2015) and explored relationships between burning and land-cover types. Cumulative areas burned amounted to nearly half of the surface areas of Sumatra and Kalimantan but were concentrated in only ~25% of the land areas. Although peatlands cover only 13% of Sumatra and Kalimantan, annual percentage of area burning in these areas was almost five times greater than in non-peatlands (2.8% vs. 0.6%) from 2001 to 2018. Recurrent burning was more prominent in Kalimantan than Sumatra. Average fire-return intervals (FRI) in peatlands of both regions were short, 28 and 45 years for Kalimantan and Sumatra, respectively. On average, forest FRI were less than 50 years. In non-forest areas, Kalimantan had shorter average FRI than Sumatra (13 years vs. 40 years), with ferns/low shrub areas burning most frequently. Our findings highlight the significant influence of LULC change in altering fire regimes. If prevalent rates of burning in Indonesia's peatlands are not

greatly reduced, peat swamp forest will disappear from Sumatra and Kalimantan in the coming decades.

Keywords: fire regime; peatlands; deforestation; degradation

3.1 Introduction

Indonesia has committed to reducing its greenhouse gases emissions by 29% (potentially up to 41% with international assistance) by 2030. Achieving those targets requires many initiatives but controlling the fire problem is central to these efforts, since burning in Indonesia's peatlands is currently seen as being unlikely to diminish in the coming decades (Page et al. 2013). The peatland fires of 2015, which lasted for three months, were shocking, being referred to as the worst fire event on record since 1997 (Field et al. 2016). 2015's peatland fires burned more than 2.6 million hectares (Mha) of forest, peat, and other lands. The fires contributed CO_2 emissions equivalent to 5% of 2015's global fossil fuel emissions (GFED 2015), causing economic losses of at least US $16 billion in Indonesia alone, and resulting in roughly 100,300 excess deaths (World Bank 2016). Indonesia contains approximately 3.5 % of global peatlands that store at least 30 gigatons of carbon (Wahyunto et al. 2010; Wahyunto and Subagjo 2003, 2004; Xu et al. 2018). Monitoring carbon-fluxes from these peatlands is critical for both national and global carbon accounting.

Intact peatlands are wetlands that rarely burn. However, since peatlands have been drained for uses other than natural forest, peatlands have become flammable and progressively more degraded. Over the last two decades, fire events have become common. Several authors have investigated this fire activity and the underlying causes from social and political perspectives (Chokkalingam et al. 2007; Dennis et al. 2005; Murdiyarso and Adiningsih 2007), but the effects of physical constraints on the spatial

and temporal patterns of fire occurrence have been less studied (Miettinen et al. 2013), including the analysis of fire frequency itself.

Fire frequency, one of the key components characterizing a fire regime, is mostly described in publications using fire-affected area or fire density (for e.g. (Langner and Siegert 2009) (Miettinen et al. 2011), fire accumulation or occurrences (Numata et al. 2011), or annual mean frequency of fire (Barbosa and Fearnside 2005)). The common landscape approach for quantifying fire frequency is to quantify how many times fire affects a given amount of area over a defined time period, instead of the probability of burning across the entire landscape. We investigated fire frequency in Indonesia's peatlands, for the 2001-2018 period, to define how burning, and specifically recurrent fire, is associated with LULC types.

Understanding fire regimes is critical, not only to identify fire pattern changes in ecosystems but also to generate related assessments of forest regeneration potential (Graham et al. 2016), fire management (Tacconi et al. 2007), human impacts (Knorr et al. 2014), and fire-related emissions associated with the extent and depth of peat burned. A recent study suggests that fire frequency needs to be accounted for in fire-derived emissions calculations from peatlands since recurrent fires have lower emission levels and different compositions than the initial fires (Konecny et al. 2016). This finding increases uncertainty about emissions from peat fires and illustrates how critical it is to know the fire history.

Various studies have linked recurring fire events (Gaveau et al. 2016; Hoscilo et al. 2011; Langner and Siegert 2009) to positive feedbacks of increasing fire susceptibility in degraded forests (Cochrane 2001; Siegert et al. 2001) and increasing human land use activities (Dennis et al. 2005; Page et al. 2013). However, to our knowledge, studies emphasizing the spatiotemporal patterns of recurrent fires and their

relationship to the land cover change are scarce for this region. Earlier, Hoscillo *et al.* (Hościło 2009) analyzed fire frequency in a small part of Kalimantan using time series data (1978 to 2005). Langner and Siegert (2009) also explored fire-affected areas and its relationship to the land cover types (1997-2006) in Kalimantan. The studies excluded estimates of the time needed to burn the entirety of a specified area, with the consideration that some areas may not burn while others burn more than once during a cycle (Wagner 1978). Even for similar vegetation types, average fire-return intervals (FRI) can vary from region to region or over time (Cochrane and Ryan 2009).

Here, we compare the fire frequency in the two largest peatland regions in Indonesia, Sumatra and Kalimantan. The latest version of Moderate Resolution Imaging Spectroradiometer (MODIS) burned area products (MCD64A1 Collection 6) allowed us to create long-term and systematic burning-observations from 2001 to 2018. These consistent satellite-based burned area products have been increasingly used and validated in several ecosystems (Giglio et al. 2016; Mouillot et al. 2014; Roy and Boschetti 2009; Tsela et al. 2014). The collection 6 MODIS burned area product is believed to be superior to other products (the MODIS burned area product collection 5, both MCD64A1 and MCD45A1) because it includes more small fires. These products have not been well validated in many Indonesian biomes and may not accurately record all burned areas in this region. However, since our scope of analysis was regional in scale, covered several years (2001-2018), and used a consistent MODIS product over that time period, analyses should accurately reflect regional trends, and may be conservative.

We calculated the annual percentage of area burned (APAB) and average fire-return intervals (FRI) (the time required to burn an area equal to the study area) (Bond and Keeley 2005; Brown and Smith 2000) from these datasets to compare the fire

frequency in both regions. This approach has been widely used in different ecosystems (Júnior et al. 2014; Oliveira et al. 2012; Oliveira et al. 2013; Rogeau and Armstrong 2017; Steel et al. 2015), allowing for comparisons across types or sizes of landscape (Johnson and Gutsell 1994). We report area burned from 2001-2018 in Sumatran and Kalimantan peatlands, as well as linkages between burning and subsequent landcover changes. Our specific questions were: 1) How do fire occurrences differ between peatland regions? 2) Which LULC types were associated with the most burning, including which one's result in recurring fires? 3) How does fire frequency differ between peatland regions over time?

3.2 Materials and Methods

3.2.1 Study sites and peatlands maps

The study area covers 75% of Indonesian peatlands (Figure 3-1), roughly 7.2 million hectares (Mha) in Sumatra and 5.7 Mha in Kalimantan (Wahyunto and Subagjo 2003, 2004). The analyses used the peatland map published by Wetlands International (Wahyunto and Subagjo 2003, 2004). This map of peatlands differs from the recently updated one issued by the Ministry of Agriculture (Ritung et al. 2011) that excludes shallow peat (<0.5 m depth) areas. This exclusion is largely responsible for the disparity in total peatland area (13 Mha vs. 11.2 Mha) and smallholder area (3.1 Mha vs. 2.5 Mha) (Miettinen et al. 2017). Both maps are widely used for official uses. However, both maps have relatively low resolution (1:250,000), reducing certainties about accurate location and associated estimates of peat thickness.

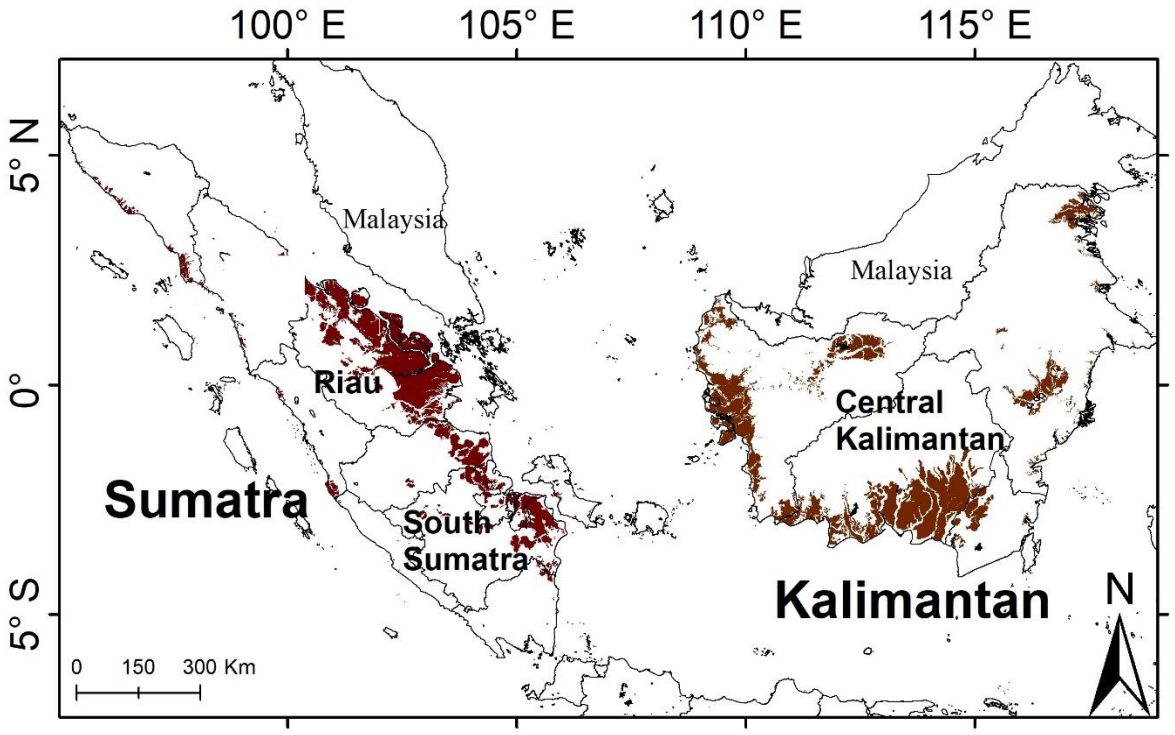

Figure 3-1 The study site (light grey) and peatland distribution (brown color).

The Wetlands International map shows that peatlands cover most of the eastern coast of Sumatra, with the most substantial portions in Riau and South Sumatra, while Kalimantan's peatlands are spread over southern and western parts of the island (Wahyunto et al. 2010; Wahyunto and Subagjo 2003, 2004). The peatlands vary in depth, with roughly 58% <2 m depth and 42% of > 2 m depth on both islands. Ages of the peats differ between the islands as well (Wahyunto et al. 2010).

Both regions have drawn international attention due to extensive peat burning and resultant haze impacts on neighboring countries. The two regions experience different land management practices, with Sumatra having more plantation areas (mainly oil palm (*Elaeis guineensis*) and pulp wood (*Acacia sp.*)) than Kalimantan (Miettinen et al. 2016) but both regions suffer near-annual burning crises. Natural peat forest areas were predominantly covered by *Dipterocarp sp* and *Gonysylus sp* trees in both regions before massive forest deforestation and degradation took place (see Table 3-2). The sites have different fire history time frames but, in each, land-use policies

related to forest clearing have been the primary cause of fires (Murdiyarso et al. 2004). Indonesia has experienced high rates of forest loss and degradation with 7.54 Mha lost from Sumatra (Margono et al. 2012) and 14.4 Mha from Kalimantan (Gaveau et al. 2016) since 1978. Forests being converted to plantations have been blamed for contributing to the large area burned. It is still unclear whether fires associated with plantation development affect landscape-level fire frequency (Gaveau et al. 2016).

Sub-regional differences exist. For example, Riau, has experienced persistent burning with heavy smoke that effects nearby countries and had the highest percentage of peat swamp forests converted to oil palm plantations by 2007 (Miettinen et al. 2012). In South Sumatra, on the other hand, fires have become part of Sonor, a traditional system of wetland rice cultivation (Chokkalingam et al. 2007). For Central Kalimantan, the fires have been associated with the one million hectares of drained peat-swamp forest—the so-called Mega Rice Project, converted into rice plantations that were later abandoned (Ballhorn et al. 2009; Konecny et al. 2016; Page et al. 2002; Putra et al. 2008; Stockwell et al. 2016). A massive network of drainage canals was built at this site, with a combined length of 4500 km, in peat with depths of up to 10m (Jaenicke et al. 2011).

Regardless of land use history, all peatland sites become prone to fire when drained before the establishment of new LULC or through careless logging techniques and plantation establishment. Severe droughts, especially those associated with El Niño-Southern Oscillation (ENSO) events, substantially increase fire susceptibility (Siegert et al. 2001) and recurrent fire events. El Niño corresponds to the warm phase of ENSO as opposed to La Niña in the cool phase. Here, we defined the El Niño/ La Niña conditions as anomalous sea surface temperatures (SST) in the Nino 3.4 region (5^{o}N-5^{o}S, 120^{o}-170^{o}W) that exceed 0.4^{o} C for at least 5 months. Impacts from El Niño-

related reductions in rainfall increase as anomalous SSTs rise and when the timing aligns with dry season periods, which usual begin in the June, July, August (JJA) period. Since 2001, El Niño events have been recorded in 2002, 2004, 2006, 2009, and 2015, with corresponding La Niña events in 2007, 2010, 2011, and 2016 (National Weather Service 2019). Kalimantan's peak fire season usually occurs from September to October while Sumatra's usually starts in June. However, in Riau, two peak fire seasons occur, February to April and June to August.

3.2.2 Satellite data and sources

We downloaded MODIS burned area Collection 6 (C6) products from July 2001 to September 2018 (207 months or 17.25 years) for the fire frequency analysis (Giglio 2015). To cover the entirety of Sumatra and Kalimantan, six scenes were composited including the tiles of h29v08, h29v09, h28v08, h28v09, h27v08, and h27v09. All pixels were selected based on two dataset layers provided with the products: "Burn Date" and Quality Assurance (QA). Day of burn (1-366) was extracted from the Burn Date layer. We filtered pixels so as to retain only those with valid-data flags (QA layer) located over land in all subsequent analyses. Active Fire Data (hotspot) MODIS Collection 6 were downloaded for the same period. The data is available at https://firms.modaps.eosdis.nasa.gov/download/. This product provides hotspot the coordinates and confidence levels. We removed all hotspots with confidence levels less than 30% from subsequent analyses. All datasets were processed using R software.

3.2.3 Land use and land cover maps

Peatland LULC maps were provided by the Centre for Remote Imaging, Sensing and Processing (CRISP) (Miettinen et al. 2016) for 1990, 2007, and 2015 (see Figure S 3-1, S3-2, and Figure S3-3). The map products used Landsat and SPOT 4

(*Satellite Pour l'Observation de la Terre,* 30 m and 20 m resolution, respectively) for classification of LULC (see the maps in the supplement materials). Manual classification was used with a final accuracy of 89%. The most problematic classifications involved separation of taller shrubs and secondary forest or confusion between open undeveloped land and newly established smallholder areas or industrial plantations.

Since the maps were produced at different times, slight classification differences exist between the 2007 map and the other two map years. For comparison purposes between years, the three 2007 LULC map categories (slightly, moderate, and highly degraded peat swamp forest) were combined into a single generic degraded peat swamp forest class. We divided the map into four groups for the fire frequency analysis: forests (including pristine and degraded forests), native-vegetated areas (low/tall shrubs, secondary forest), agricultural areas (smallholder and plantation areas), and other LULC types (water, seasonal water, built-up area, cleared/burned area, and mangrove). Table 3-1 describes the LULC group and types.

Table 3-2 Description of land use and land cover (LULC) types in this study

LULC groups	LULC types	Description
Forest	Pristine peat swamp forest (PSF)	PSF with no clear signs of human intervention. Dominant tree species include *Dipterocarp sp, Gonysylus sp* and *Dyera sp.*
	Degraded PSF	PSF with clear evidence of disturbance (e.g. logging), typically in the form of logging tracks and canals and/or opened canopy. In addition to PSF species, tall shrubs, such as *Melaleuca leucadendron* are also prevalent.
Native-vegetated areas	Tall shrub/secondary forest	Shrubland or secondary forest with an average height above 2 m. Dominant species include *Melaleuca leucadendron* and *Macaranga sp.*
	Ferns/low shrub	Ferns and grass or shrubland with average height less than 2 m. Dominant species include *Stenochlaena palustris, Blechnum indicum, Pandanus helicopus*, and *Melastoma malabathricum.*
Agricultural areas	Smallholder area	Mosaic of housing, agricultural fields, plantations, gardens, fallow shrubland, etc. Note that the name of the class refers to the patchy landscape patterns, typical in smallholder dominated areas but the actual land tenure of the areas is unknown.
	Industrial plantations	Large-scale industrial plantations assumed to have been already planted with the plantation species. Mainly oil palm (*Elaeis guineensis*) and pulp wood (*Acacia sp*.).
Other LULC types	Water	Permanent water bodies. This class also includes fish and crab farming ponds.
	Seasonal water	Areas that are inundated part of the year. Typically, either extremely degraded areas or flood zones of rivers. This class also includes smallholder mining sites.
	Built-up area	Towns, industrial areas, etc.
	Cleared/burned area	Open area with no vegetation, including recently burned areas.
	Mangrove	Areas determined to be mangrove forest in the satellite image interpretation although located within peatland areas of maps used in this study.

Source: (Miettinen and Liew 2010)

3.2.4 Fire occurrences, annual burned area, fire frequency, and related land use and land cover change

Fires accumulated (times burning) and annual burned area were calculated from the MODIS burned area product C6. Only a single fire occurrence per year/pixel was counted. Multi-year fire accumulations at a location of greater than 2 were categorized as recurrent burning. In addition to total annual burned area, burned surface areas were classified as either being extensive (fire accumulation $\leq$2) or recurrent (>2) in nature.

For the analysis, we divided fire events into two time periods to match the available LULC maps, 2001-2007 (period-I) and 2008-2018 (period-II). We used the 2007 LULC map for period-I and 2015 LULC map for period-II to relate LULC change and fire frequency. We divided the map into four groups: forests (including pristine and degraded forests), native-vegetated areas (low/tall shrubs, secondary forest), agricultural areas (smallholder and plantation areas), and other LULC types (water, seasonal water, built-up area, cleared/burned area, and mangrove).

Fire frequency was calculated from the annual percentage of area burned (APAB, Equation 1). Average fire-return intervals (FRI), time to burn the entire area, was then calculated (Equation 2), respective to each LULC type. We removed areas not covered in vegetation and grouped the LULC types into forest and non-forest. Our land cover-related calculations referenced the baseline map of 1990, when most of the region was still forested and forest degradation and conversion amounts were minimal, to assess subsequent fire-LULC change associations.

$$APAB_i = (\text{Annual burning rate})_i / (\text{Total peatland areas})_i \times 100\% \quad \text{(Equation 1)}$$

$$FRI_i = 1/(APAB)_i \quad \text{(Equation 2)}$$

where APAB is percentage of annual burned areas (%) over total peatland (ha) of specific LULC types (i) while FRI is annual fire-return intervals (year) of a specific land-cover type (i) defined as the inverse of APAB.

3.3 Results

3.3.1 Fire occurrences, total area burned, and area-affected by burning among regions

The MODIS burned area product (C6) shows areas burned one or more times in both peatlands and non-peatlands over the eighteen-year study period (Figure 3-2). At least 7.9% and 9.4% of the Sumatran and Kalimantan lands were affected by fires, respectively (Table 3-3), with the most area affected by burning found in Riau province, Southern Sumatra, and Central Kalimantan (see subsets Figure 3-2 and Figure 3-3). The average annual area burned decreased by 37% and 48% between the first (2001-2007) and second time (2008-2018) periods for Sumatra and Kalimantan, respectively. Although peatlands only cover roughly 13% of Sumatra and Kalimantan, burning affected these areas at rates five times higher than non-peatlands (2.8% vs. 0.6%).

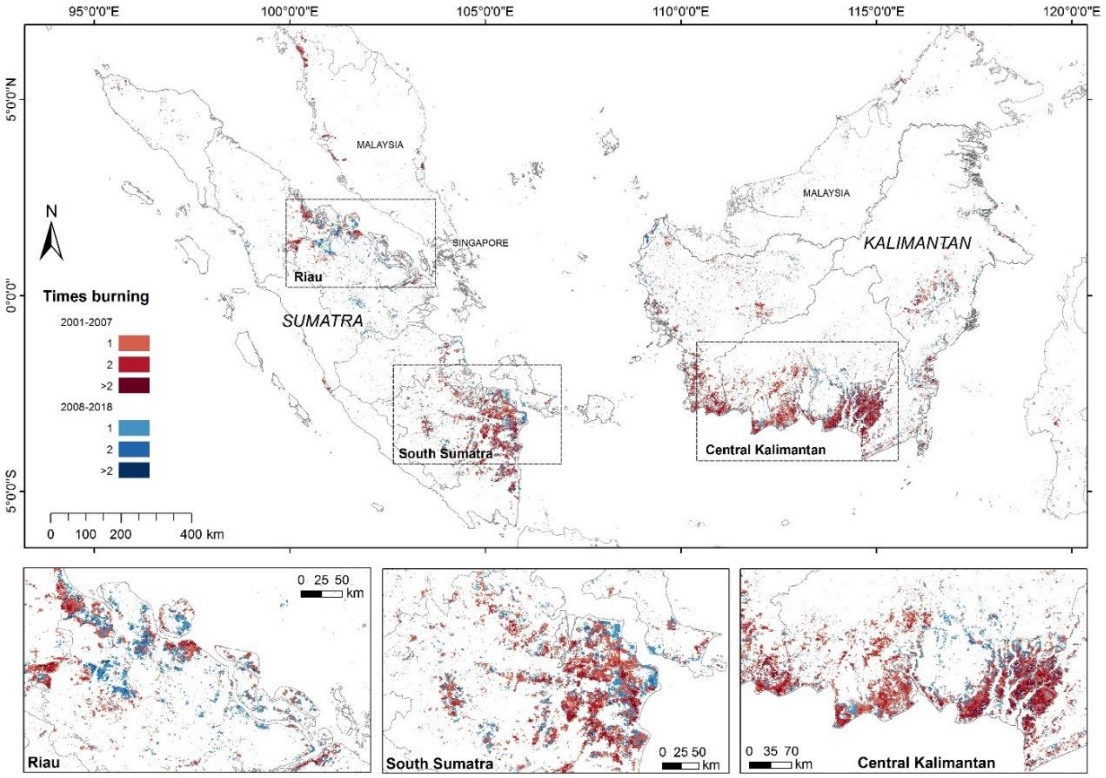

Figure 3-2 Spatial distribution of all burned areas of Sumatra and Kalimantan (including both the peatlands and non-peatlands). The map shows how frequently an area was affected by burning from 2001-2007 (represented by the reddish color) and from 2008-2018 (bluish color) regardless the land use and land cover types (see the supplement materials). Some areas burned once, twice or more for each period. The subsets are the three areas most prone to experiencing high frequency burning: Riau, South Sumatra, and Central Kalimantan.

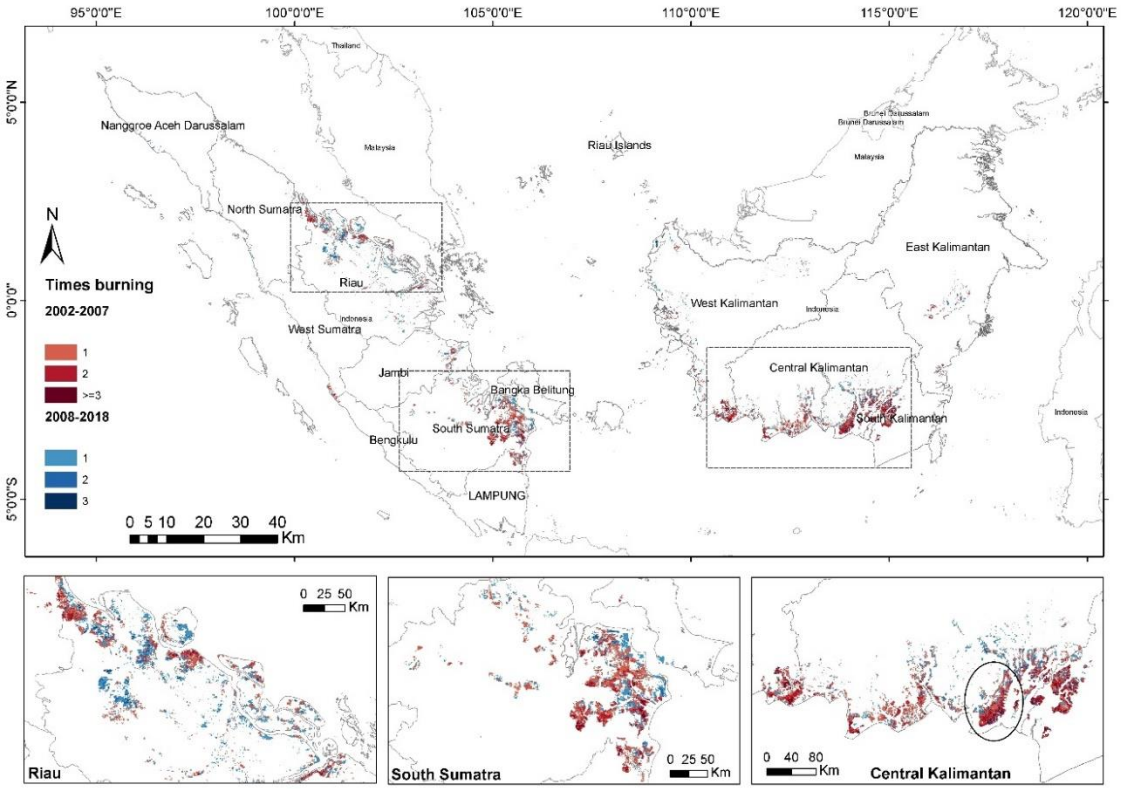

Figure 3-3 Spatial distribution of burned areas in peatlands of Sumatra and Kalimantan. The map shows how frequently an area was affected by burning from 2001-2007 (represented by the reddish color) and from 2008-2018 (bluish color) in peatlands only regardless the land use and land cover types. Some areas burned once, twice or more for each period. The subsets are the three areas most prone to experiencing high-frequency burning: Riau, South Sumatra, and Central Kalimantan. The black circle in the subset of Central Kalimantan shows the Mega Rice Project area (Hoscilo et al. 2011)

From 2001-2018, at least a quarter of the Sumatran and Kalimantan peatland areas were affected by fires. During the 6-year first period (2001-2007), nearly half million hectares (3.5% of the areas) burned annually in both peatland regions. These rates decreased by 29% during the 11-year second period (2008-2018). Inter-annual variability of area burned shows Kalimantan's burned areas exceeded Sumatra's in most years (Figure 3-4), with exceptions occurring during many non El Niño years (2005, 2008, 2010, 2011, 2013, and 2016). The greatest areas burned occurred during the El Niño conditions which lined up with dry seasons (2002, 2006, 2009, and 2015) except for 2014 (weak El Niño conditions) which was actually the early stage of the

2015 El Niño event (The Climate Prediction Center/National Weather Service 2019). Although Sumatra's peatland fires are less highly correlated with El Niño events than Kalimantan, large amounts of area burned during those events in both regions.

Table 3-3 Area affected by burning, total area burned, annual percentage area burned (APAB), and annual fire-return intervals (FRI) in peatlands and non-peatlands Sumatra and Kalimantan within three periods. The areas were calculated as percentage areas burned respective to each region. The difference of areas burned and fire frequency is presented for 1) all Sumatran and Kalimantan land, 2) peatlands only, and 3) in non-peatland only.

Percentage of area burned and surface affected fires	Sumatra			Kalimantan			Kalimantan and Sumatra		
	2001-2007	2008-2018	2001-2018	2001-2007	2008-2018	2001-2018	2001-2007	2008-2018	2001-2018
Surface area affected fires (%)									
Both the peatlands and non-peatlands	4.8	4.8	7.9	6.5	5.4	9.4	5.7	5.1	8.7
Peatlands only	13.4	15.9	23.6	19.3	20.8	28.6	16.0	18.1	25.8
1. All burned areas including both the peatlands and non-peatlands									
Accumulated area burned (%)	6.1	6.3	12.4	9.0	7.7	16.6	7.6	7.0	14.6
APAB (%)	0.9	0.6	0.7	1.4	0.7	1.0	1.2	0.7	0.8
FRI (years)	107	170	139	72	140	104	85	153	118
2.All burned areas in the peatlands only									
Accumulated area burned (%)	16.9	21.4	38.3	29.5	32.7	62.3	22.5	26.4	49.0
Burned once	10.4	11.8	14.7	12.1	13.0	13.5	11.2	12.4	14.1
Burned twice	4.9	6.0	10.9	9.6	9.5	12.8	7.0	7.6	11.7
Burned more than twice*	1.6	3.6	12.7	7.8	10.2	36.0	4.3	6.5	23.1
APAB (%)	2.6	2.0	2.2	4.5	3.0	3.6	3.5	2.5	2.8
FRI (years)	38	50	45	22	33	28	29	41	35
APAB in recurring* fires only (%)	1.4	1.5	1.9	4.0	2.9	3.3	3.0	2.3	2.7
FRI in recurring* fires only (years)	70	65	52	25	35	30	34	44	37

Percentage of area burned and surface affected fires	Sumatra			Kalimantan			Kalimantan and Sumatra		
	2001-2007	2008-2018	2001-2018	2001-2007	2008-2018	2001-2018	2001-2007	2008-2018	2001-2018
3. All burned areas in the non-peatlands only									
Accumulated area burned (%)	4.1	3.7	7.8	6.5	4.6	11.1	5.4	4.2	9.6
APAB (%)	0.6	0.3	0.5	1.0	0.4	0.6	0.8	0.4	0.6
FRI (years)	157	294	221	100	233	155	120	257	180

Total area of peatlands and non-peatlands: Sumatra: 47.6 Mha, Kalimantan: 53.6 Mha; Total peatlands area: Sumatra: 7.2 Mha, Kalimantan: 5.8 Mha. Note: *recurring events between the time periods make the sum of areas burned only once smaller and the areas burned more than twice larger than simple addition of values from the two time periods.

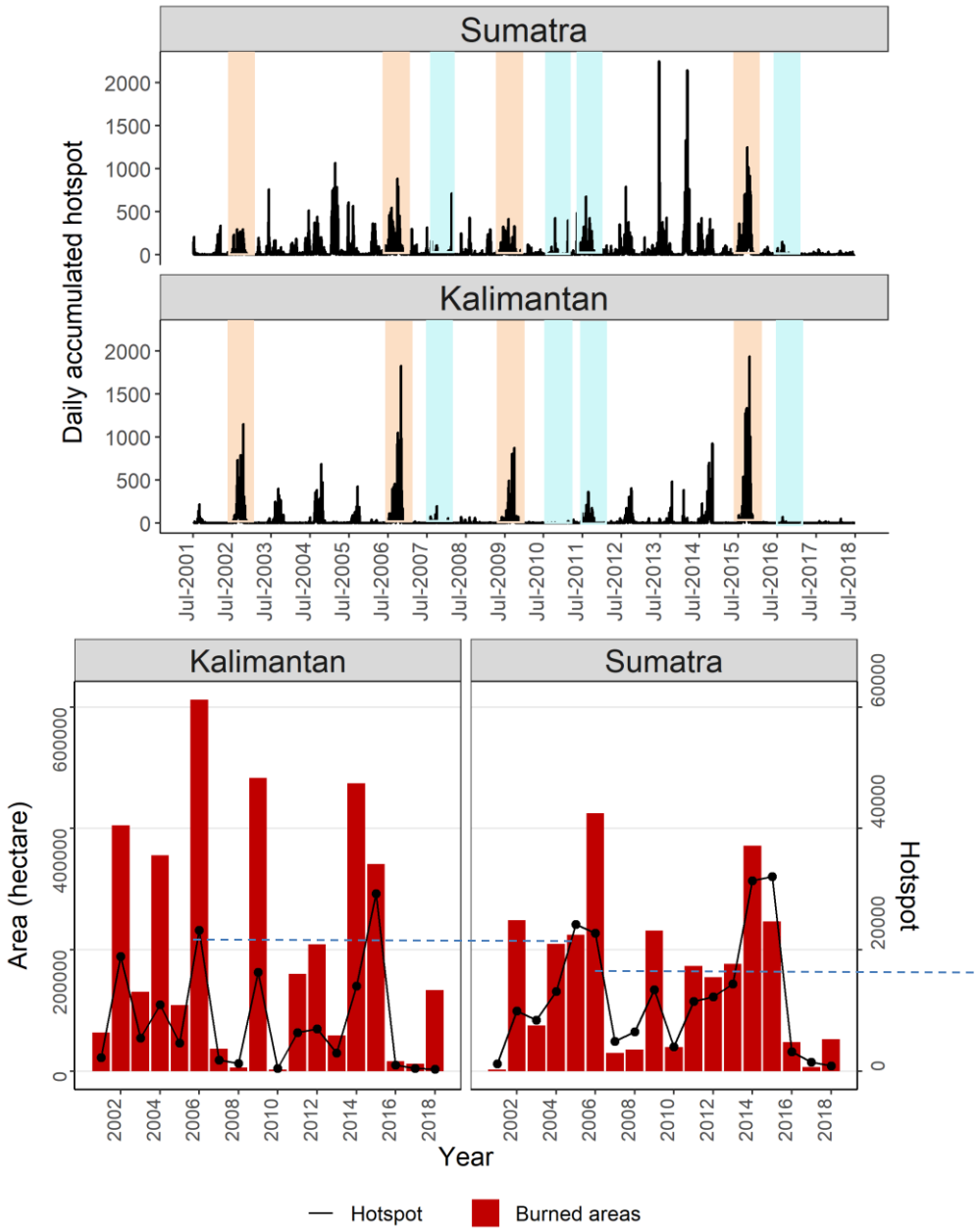

Figure 3-4 (a) Daily accumulated Moderate Resolution Imaging Spectroradiometer (MODIS) active fire in Sumatran and Kalimantan peatlands from July 2001 to June 2018 (confidence level >30%). Background color shows the El-Niño (orange) and La Niña (cyan) events; (b) Annual accumulated active fire and inter-annual burned area variability. A single annual peak burning period is evident in nearly every year during the dry season, between July-October, in Kalimantan. In Sumatra, with peatlands spanning the Equator and some regions having two dry seasons, the patterns are less evident. High rates of daily accumulation hotspots and longer seasonal persistence occur during El-Niño years (2002, 2006, 2009, and 2015) and other periods of prolonged drought. Kalimantan's areas burned exceeded those in Sumatra except for the La Niña years of 2010 and 2016, suggesting higher sensitivity of Kalimantan to dry El Niño and wet La Niña conditions. Although less highly correlated in Sumatra, high amounts of area

burned (above the annual average, showing by dotted lines) occurred during strong El Niño events in both regions.

We found that almost half of the areas burned in Sumatra and Kalimantan peatlands were recurrent burning (more than twice in the same location, Table 3-3). On average, the amounts of recurrent burning were nearly triple in Kalimantan compared to Sumatra. In the first 6-year period alone, more than one-quarter of burning was recurrent in Kalimantan, with a recurrent fire APAB nearly three times higher than in Sumatra. This rate disparity decreased in the second period but was still twice as high. The recurrent fire FRI is almost the same (slightly longer) than the overall peatland FRI for the entire peatlands from 2001-2018. Although there are some regional disparities, these findings reveal that previously burned areas burn nearly as frequently as other areas.

3.3.2 Fire related land use and land cover change in peatlands

Between 2001 and 2018, burning predominantly occurred in areas that had been forested in 1990, but these areas are now experiencing different land management practices in peatlands of Sumatra and Kalimantan (Figure 3-5). At least 70.5% and 63.8% of all fires occurred in peat swamp forests (pristine or degraded) of Sumatra and Kalimantan, respectively. Based on the LULC as of 2007, subsequent burning of standing forests was more prevalent in Sumatra (13.7%) than Kalimantan (6.9%). By 2015, 64% of these burned forests were converted to agriculture in Sumatra, while only 41% of such areas became agriculture in Kalimantan. Remaining burned forest areas transitioned to other native-vegetation (mostly shrubs). The disparity in plantation area located in peatlands between the regions has diminished in recent years from a ten-fold difference in 2007 to only a three-fold difference by 2015 (see Appendix Table S 3-1). At least 29% and 39% of the total plantation areas in Sumatra and Kalimantan

established by 2015, respectively, were associated with burning (Table S 3-2, Appendix).

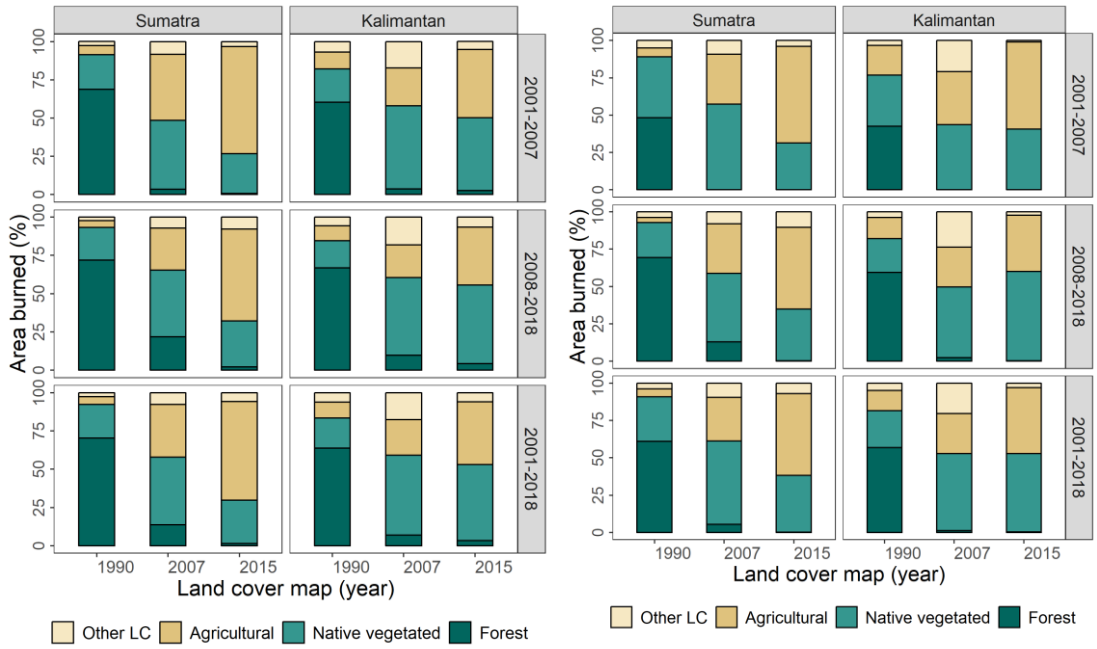

(a) (b)

Figure 3-5 Proportion of all area burned (a) and areas with recurrent burning (>2 fires) (b) within three burning periods (2001-2007, 2008-2018, and 2001-2018) as related to associated land use and land cover (LULC) for maps dating to 1990, 2007, and 2015 (a); While the majority of burning from 2001-2018 has occurred in areas that were forest in 1990, almost none of those areas are forests today, with progressively more being converted to either agriculture or non-forest vegetation. Aggregated LULC classes: forest (both pristine and degraded peat swamp forest); native-vegetated (ferns/low shrubs, tall shrubs/secondary forest); agricultural areas (smallholder and industrial plantations areas); other LULC types.

Based on the LULC map of 1990, the highest burning rate from 2001-2007 of non-forests occurred in ferns/low shrub for both regions (Figure 3-6 and Appendix Table S 3-3), with a higher annual burned rate in Kalimantan (32,902 ha/year) than Sumatra (29,575 ha/year). Burning rates in Kalimantan exceeded those in Sumatra for all LULC types other than industrial plantations, explaining the more rapid fire-return intervals in this region. In the early time period (2001-2007) burning was minimal in plantation areas with no detected fires Kalimantan and only a few burning in Sumatra

(4.3 ha/year). However, plantation burning rates increased in both regions during 2008-2018, most drastically in Sumatra (14,143 ha/year). Despite the increase, established plantations had the lowest average annual burning rate among all vegetated areas. The areas burned, detected as burn scars or bare land, were excluded from this calculation, accounting for 16% of the total area burned in Kalimantan. Those areas were subsequently converted to either agricultural or non-vegetated areas, as shown on the 2015 LULC map (Figure 3-5b).

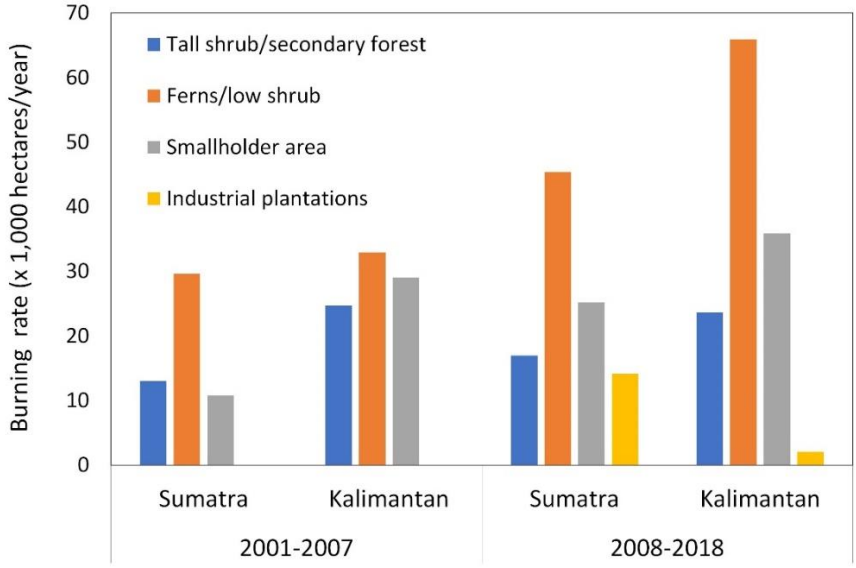

Figure 3-6 Annual burning rate in Sumatra and Kalimantan within two burning periods (2001-2007 and 2008-2018) in non-forest (native-vegetated areas).

LULC types other than native-vegetation or agricultural for both Sumatra and Kalimantan accounted for only 8% of total area burned during 2001-2018, on average (Figure 3-5b). Kalimantan had more prominent amounts of area burned in seasonal water locations than Sumatra (see Figure 3-7), usually located along rivers traversing peat swamp. Areas burned more than twice (2001-2018) predominantly occurred in either pristine or degraded peat swamp forest (extant in 1990) in both regions, accounting for 61% and 57% in Sumatra and Kalimantan, respectively (

Figure 3-5b). Native-vegetation of various types still constituted the majority of LULC in Kalimantan as of 2015 (

Figure 3-5a).

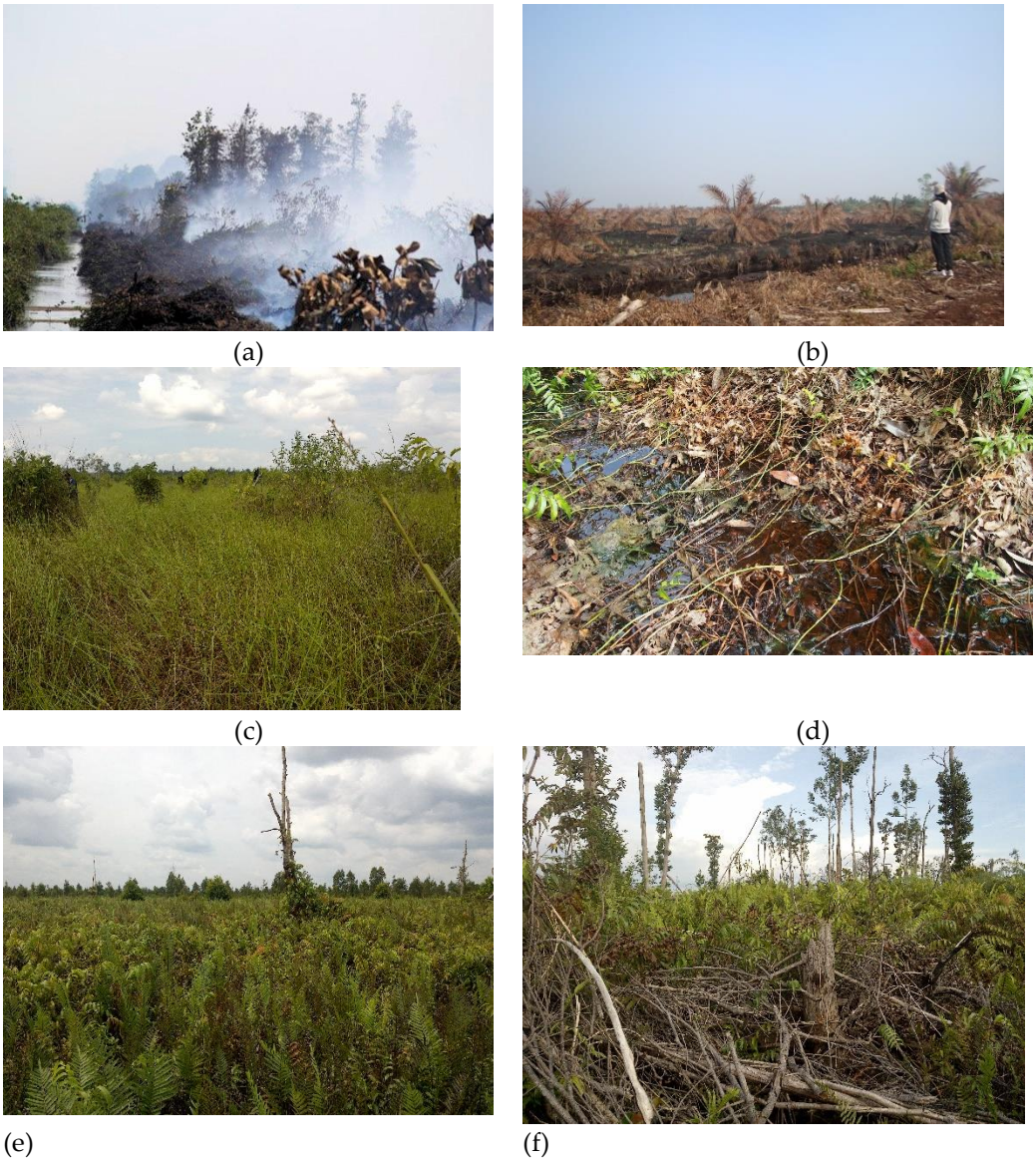

(a) (b)

(c) (d)

(e) (f)

Figure 3-7 Examples of various land use and land cover (LULC) types, burning situation, and regrowth after burning in the study regions. Burned areas in forest (a) and young plantation (b) (Photos were taken during survey in Riau by LAPAN in 2013 and 2014); (c) and (d) are seasonal water sites, with grass/ferns that flood during the rainy season; Peatland regrowth in areas with frequent burning (e) and in forest (f). Photos were taken during our survey in Central Kalimantan in August 2018.

3.3.3 Fire frequency analysis in peatland and their associated land use and land cover types

Overall, the FRI from 2001-2018 is short in both regions with shorter lengths in Kalimantan than Sumatra (28 vs. 45 years, Table 3-3). Shorter FRIs predominated during the first period of 2001-2007 but have lengthened somewhat in both regions during the second period, from 38 to 50 years in Sumatra and from 22 to 33 years in Kalimantan. This cycle equates to Sumatra's and Kalimantan's peatlands experiencing an average of 2.3% and 3.8% annual burning for the entire 2001-2018 period, respectively.

When associated with specific LULC types, both Kalimantan peatland forests and non-forest have the shortest FRIs (35 and 13 years, respectively). This indicates rapidly increasing amounts of deforestation/degradation in Kalimantan caused by burning. However, both Sumatra and Kalimantan have considerably short forest FRIs, less than 50 years on average (Figure 3-8). In forests, only 55 years and 47 years are required to burn areas equivalent to the entire pristine peat swamp forests of Sumatra and Kalimantan, respectively, while degraded PSF have even shorter FRIs, 34 and 25 years for Sumatra and Kalimantan, respectively. Annual fire-return intervals for non-forests are longer in Sumatra (40 years) than in Kalimantan (13 years).

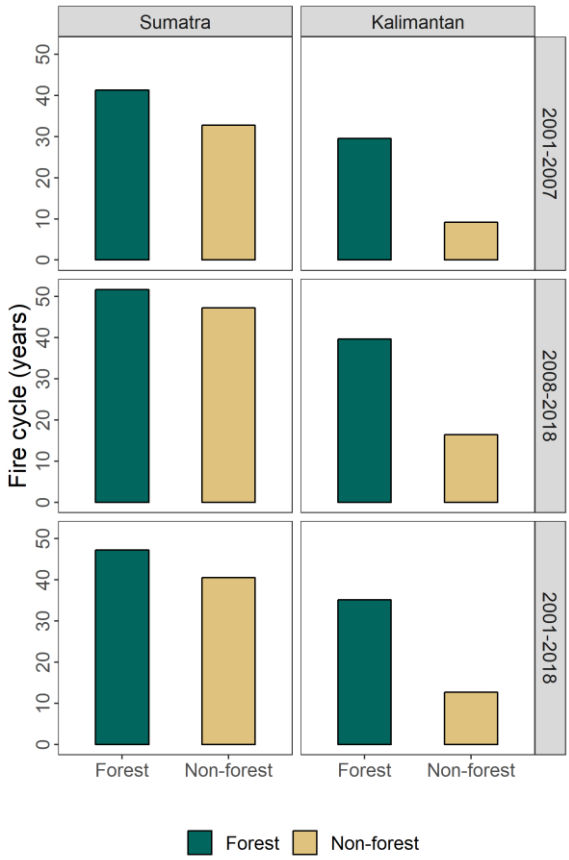

Figure 3-8 Annual fire-return intervals (FRI) in peatlands of Sumatra and Kalimantan based on the annual percentage of areas burned in 2001-2007, 2008-2018, and 2001-2018. The shortest forest FRI appeared in Kalimantan peatlands for both forest and non-forest.

3.4 Discussion

We found that burning was much more prevalent in peatlands than non-peatlands in both regions. Overall, Kalimantan and Sumatran peatlands both experienced extensive amounts and high rates of burning, but experienced different temporal and spatial patterns of fire. Kalimantan had both higher rates of annual burning and significantly higher percentages of recurrent fire events in the same locations than Sumatra. This suggests that extensive burning, such as was reported in 1982-1983 (Goldammer and Seibert 1990), has been increasingly replaced by recurrent fires, as reported by Hoscillo (Hościło 2009) for the Mega Rice Project areas of Central Kalimantan (see Figure 3-3). Our analysis indicated that these areas continue to be

subjected to recurring fire events. Both regions experience more fire during the intense droughts associated with El Niño periods, but Kalimantan's responses are more extreme increasing during El Niño droughts and decreasing during La Niña conditions.

Most areas burned were forested in 1990 but have been converted to a majority of either degraded native vegetation (Kalimantan) or agricultural lands (Sumatra). This indicates that, although development follows upon intentional burning, these areas partially suppress landscape-level fire spread, potentially explaining the modest reductions in overall annual area burned between the first and second periods. Lower burning rates in the plantation areas of both Sumatra and Kalimantan may be indicating that, although burning initiated agricultural conversion, different management practices may be helping to suppress fires once crops are established. This could support the recent findings (Cattau et al. 2016) that few fires originated from within plantations. Recurrent burning in Kalimantan, on the other hand, has been concentrated within non-managed shrublands, such as found in the drained peatlands of the now discontinued Mega-Rice Project.

With a moist microclimate, low-flammability soils (Turetsky et al. 2015) and waterlogged conditions, fire in natural peat swamp forests should be exceedingly rare. However, drained peatlands and degraded forest canopies allow the peat to dry and change both the above-ground biomass and the peat itself into more flammable fuels. The shorter FRIs of Kalimantan's forests indicate greater threat from fire than in Sumatra, but both are experiencing relatively high levels of burning compared to natural conditions. This supports the contention that continued losses of degraded primary forest from 2002-2012 might be fire-related (Margono et al. 2014). Burned forest area transitions to non-forest conditions indicate the critical role of fires in fostering LULC conversions.

Unlike burning in many other regions where natural causes, such as lightning, predominate, human-mediated activities drive altered fire regimes in Indonesian peatlands. However, the probability of burning is still strongly modulated by precipitation anomalies (Van der Werf 2008). Repeated fires, that are increasingly prevalent in Kalimantan, impede natural forest succession, particularly when trees are replaced by shrubs and other vegetation. Vegetation that spreads widely by seed, such as the woody species *Combretocarpus rotundatus* (Blackham et al. 2014), or ferns (*Stenochlaena palustris* and *Blechnum indicum*) act as invasive species that were not typically found in peat swamp forests, deflecting succession away from forest species (see Figure 3-7). The increasing prevalence of these degraded lands could lead to broader expansion of shrubs into degraded forests, even in the absence of additional fires. Natural reforestation may prove impossible unless more natural hydrological conditions and can be restored and fire prevalence greatly reduced.

Accurate burned area maps are critical for understanding LULC change and monitoring of land management efforts to reduce greenhouse gas emissions from Indonesia's peatlands. Although the MODIS Burned Area product, MCDA164 has been validated globally, few of the validation sites were specifically located in Indonesian peatlands and it is likely burned areas are substantially under-reported. In assessing the limited sites visited earlier in 2013, 2014, and 2018 (some of them can be seen in Figure 3-7) it was evident that there were many fires that the MODIS burned area product failed to detect (manuscript in preparation). This is evident from the 2015 fire season, when fires resulted in huge greenhouse gas (Stockwell et al. 2016) and particulate emissions (Jayarathne et al. 2018), exceeding those of previous years (GFED 2015), but MODIS burned area was less than the previous year. It is likely that the

MODIS burned area product failed to detect many areas burned in 2015 due to obstruction by thick smoke from many fires.

To date, unfortunately, a long-term archive of official national burned area maps does not exist. Official national burned area maps have been provided since 2015 by the Ministry of Environment and Forestry Republic of Indonesia (http://geoportal.menlhk.go.id/arcgis/home/). For earlier years, total annual areas burned are only available as rough estimations (MoEF 2016), since field assessments are costly and many sites are inaccessible.

Remote sensing is the only practicable avenue for extensive burned area mapping in the peatlands. However, the capabilities of the optical-sensor satellites used for burned area mapping (e.g., (Chuvieco et al. 2016; Giglio et al. 2013)) are limited by high amounts of cloud coverage, frequently small burn sizes, and thick smoke during the worst fire years. Consequently, systematic and consistent information has not been available. However, leveraging of the archive of NASA Earth observations and upcoming free multi-resolution data (e.g., Landsat, Sentinel-2, Sentinel-1) provide promising opportunities for addressing burned area mapping challenges. Several efforts to develop systematic information have been proposed using Landsat (e.g., (Boschetti et al. 2015; Hawbaker et al. 2017)), Sentinel-2 (e.g., (Roteta et al. 2019; Roy et al. 2019)) and Sentinel-1 (Lohberger et al. 2017)—an active sensor that is capable of penetrating the clouds that frequently impede LULC mapping in the tropics. The combined use of active and passive sensors may increase both spatial completeness and thematic detail (Reiche 2015) of coverage, allowing for more detailed characterization of fire impacts on both the vegetation and the underlying peat to complement burned area mapping efforts.

3.5 Conclusion

Nearly two decades of fire occurrences on the two biggest islands of Indonesia, Sumatra and Kalimantan, were synthesized from MODIS burned area products. We found Sumatra and Kalimantan experienced extensive fires with substantial amounts of recurring fire events. The initial LULC was predominantly forest, but most of these areas have been converted to other LULC types which experience different land management practices and rates of burning. Degraded shrublands have the most frequent rate of annual burning on both Sumatra and Kalimantan, precluding regeneration of native forests. Plantation areas are more established in Sumatra, but Kalimantan is experiencing rapid land conversion to plantations.

Our findings highlight the significant influence of LULC change in altering fire regimes in Indonesia. If the current rate of burning that is prevalent in Indonesia's peatlands is not greatly reduced, within less than half of century, peat swamp forest will likely disappear from Sumatra and Kalimantan.

3.6 Acknowledgements

We thank two anonymous reviewers for their valuable comments. We would like to thank Dr. Jukka Miettinen (CRISP) for sharing the peatland LULC map data and Indonesian National Institute of Aeronautics and Space (LAPAN) for field images. Y.V. thank the Research and Innovation Science and Technology Project, Ministry of Research, Technology and Higher Education of the Republic of Indonesia for funded her Ph.D. We also acknowledge the use of data and imagery from LANCE FIRMS operated by NASA's Earth Science Data and Information System (EOSDIS) with funding provided by NASA Headquarters.

References

Ballhorn, U.; Siegert, F.; Mason, M.; Limin, S. Derivation of burn scar depths and estimation of carbon emissions with LIDAR in Indonesian peatlands. *Proc. Natl. Acad. Sci. USA* 2009, *106*, 21213–21218. doi:10.1073/pnas.0906457106.

Barbosa, R.I.; Fearnside, P.M. Fire frequency and area burned in the Roraima savannas of Brazilian Amazonia. *For. Ecol. Manag.* 2005, *204*, 371–384. doi:10.1016/j.foreco.2004.09.011.

Blackham, G.V.; Webb, E.L.; Corlett, R.T. Natural regeneration in a degraded tropical peatland, Central Kalimantan, Indonesia: Implications for forest restoration. *For. Ecol. Manag.* 2014, *324*, 8–15.

Bond, W.J.; Keeley, J.E. Fire as a global 'herbivore': The ecology and evolution of flammable ecosystems. *Trends Ecol. Evol.* 2005, *20*, 387–394.

Boschetti, L.; Roy, D.P.; Justice, C.O.; Humber, M.L. MODIS—Landsat fusion for large area 30 m burned area mapping. *Remote Sens. Environ.* 2015, *161*, 27–42.

Brown, J.K. Introduction and Fire Regimes. In *Wildland fire in ecosystems: effects of fire on flora*, Brown, J.K.S., Jane Kapler, Ed. US Department of Agriculture, Forest Service, Rocky Mountain Research Station: Ogden, UT, 2000; Vol. 2 of Gen. Tech. Rep. RMRS-GTR-42, pp. 1-6.

Cattau, M.E.; Harrison, M.E.; Shinyo, I.; Tungau, S.; Uriarte, M.; DeFries, R. Sources of anthropogenic fire ignitions on the peat-swamp landscape in Kalimantan, Indonesia. *Glob. Environ. Chang.* 2016, *39*, 205–219.

Chokkalingam, U.; Permana, R.P.; Kurniawan, I.; Mannes, J.; Darmawan, A.; Khususyiah, N.; Susanto, R.H. Community fire use, resource change, and livelihood impacts: The downward spiral in the wetlands of southern Sumatra. *Mitig. Adapt. Strateg. Glob. Chang.* 2007, *12*, 75–100.

Chuvieco, E.; Yue, C.; Heil, A.; Mouillot, F.; Alonso-Canas, I.; Padilla, M.; Pereira, J.M.; Oom, D.; Tansey, K. A new global burned area product for climate assessment of fire impacts. *Glob. Ecol. Biogeogr.* 2016, *25*, 619–629. doi:10.1111/geb.12440.

Cochrane, M.A. Synergistic interactions between habitat fragmentation and fire in evergreen tropical forests. *Conserv. Biol.* 2001, *15*, 1515–1521.

Cochrane, M.A.; Ryan, K.C. Fire and fire ecology: Concepts and principles. In *Tropical Fire Ecology*; Springer: Berlin/Heidelberg, Germany, 2009; pp. 25–62.

Dennis, R.A.; Mayer, J.; Applegate, G.; Chokkalingam, U.; Colfer, C.J.P.; Kurniawan, I.; Lachowski, H.; Maus, P.; Permana, R.P.; Ruchiat, Y. Fire, people and pixels: Linking social science and remote sensing to understand underlying causes and impacts of fires in Indonesia. *Hum. Ecol.* 2005, *33*, 465–504.

Field, R.D.; van der Werf, G.R.; Fanin, T.; Fetzer, E.J.; Fuller, R.; Jethva, H.; Levy, R.; Livesey, N.J.; Luo, M.; Torres, O. Indonesian fire activity and smoke pollution in 2015 show persistent nonlinear sensitivity to El Niño-induced drought. *Proc. Natl. Acad. Sci. USA* 2016, *113*, 9204–9209.

Gaveau, D.L.; Sheil, D.; Husnayaen; Salim, M.A.; Arjasakusuma, S.; Ancrenaz, M.; Pacheco, P.; Meijaard, E. Rapid conversions and avoided deforestation: Examining four decades of industrial plantation expansion in Borneo. *Sci. Rep.* 2016, *6*, 32017. doi:10.1038/srep32017.

GFED. 2015 Fire Season. Available online: http://www.globalfiredata.org/updates.html#2015_indonesia (accessed on 15 October 2019).

Giglio, L.; Justice, C.; Boschetti, L.; Roy, D. *MCD64A1 MODIS/Terra+Aqua Burned Area Monthly L3 Global 500m SIN Grid V006*; NASA EOSDIS Land Processes DAAC, USGS Earth Resources Observation and Science (EROS) Center, Sioux Falls, South Dakota: 2015. doi:10.5067/MODIS/MCD64A1.006.

Giglio, L.; Randerson, J.T.; Werf, G.R. Analysis of daily, monthly, and annual burned area using the fourth-generation global fire emissions database (GFED4). *J. Geophys. Res. Biogeosci.* 2013, *118*, 317–328.

Giglio, L.; Schroeder, W.; Justice, C.O. The collection 6 MODIS active fire detection algorithm and fire products. *Remote Sens. Environ.* 2016, *178*, 31–41.

Goldammer, J.G.; Seibert, B. The impact of droughts and forest fires on tropical lowland rain forest of East Kalimantan. In *Fire in the Tropical Biota*; Springer: Berlin/Heidelberg, Germany, 1990; pp. 11–31.

Graham, L.L.; Giesen, W.; Page, S.E. A common-sense approach to tropical peat swamp forest restoration in Southeast Asia. *Restor. Ecol.* 2017, *25*, 312–321.

Hawbaker, T.J.; Vanderhoof, M.K.; Beal, Y.J.; Takacs, J.D.; Schmidt, G.L.; Falgout, J.T.; Williams, B.; Fairaux, N.M.; Caldwell, M.K.; Picotte, J.J. Mapping burned areas using dense time-series of Landsat data. *Remote Sens. Environ.* 2017, *198*, 504–522.

Hościło, A. Fire Regime, Vegetation Dynamics and Land Cover Change in Tropical Peatland, Indonesia. Ph.D. Thesis, University of Leicester, United Kingdom, 2009.

Hoscilo, A.; Page, S.E.; Tansey, K.J.; Rieley, J.O. Effect of repeated fires on land-cover change on peatland in southern Central Kalimantan, Indonesia, from 1973 to 2005. *Int. J. Wildland Fire* 2011, *20*, 578–588.

Jaenicke, J.; Englhart, S.; Siegert, F. Monitoring the effect of restoration measures in Indonesian peatlands by radar satellite imagery. *J Environ. Manag.* 2011, *92*, 630–638. doi:10.1016/j.jenvman.2010.09.029.

Jayarathne, T.; Stockwell, C.E.; Gilbert, A.A.; Daugherty, K.; Cochrane, M.A.; Ryan, K.C.; Putra, E.I.; Saharjo, B.H.; Nurhayati, A.D.; Albar, I.J.A.C., et al. Chemical characterization of fine particulate matter emitted by peat fires in Central Kalimantan, Indonesia, during the 2015 El Niño. *Atmos. Chem. Phys.* 2018, *18*, 2585.

Johnson, E.A.; Gutsell, S.L. Fire frequency models, methods and interpretations. *Adv. Ecol. Res.* 1994, *25*, 239-287.

Júnior, A.C.P.; Oliveira, S.L.; Pereira, J.M.; Turkman, M.A.A. Modelling fire frequency in a Cerrado savanna protected area. *PLoS ONE* 2014, *9*, e102380.

Knorr, W.; Kaminski, T.; Arneth, A.; Weber, U. Impact of human population density on fire frequency at the global scale. *Biogeosciences* 2014, *11*, 1085–1102.

Konecny, K.; Ballhorn, U.; Navratil, P.; Jubanski, J.; Page, S.E.; Tansey, K.; Hooijer, A.; Vernimmen, R.; Siegert, F. Variable carbon losses from recurrent fires in drained tropical peatlands. *Glob. Chang. Biol.* 2016, *22*, 1469–1480. doi:10.1111/gcb.13186.

Langner, A.; Siegert, F. Spatiotemporal fire occurrence in Borneo over a period of 10 years. *Glob. Chang. Biol.* 2009, *15*, 48–62.

Lohberger, S.; Stängel, M.; Atwood, E.C.; Siegert, F. Spatial evaluation of Indonesia's 2015 fire affected area and estimated carbon emissions using Sentinel-1. *Glob. Chang. Biol.* 2017. doi:10.1111/gcb.13841.

Margono, B.A.; Potapov, P.V.; Turubanova, S.; Stolle, F.; Hansen, M.C. Primary forest cover loss in Indonesia over 2000–2012. *Nat. Clim. Chang.* 2014, *4*, 730–735.

Margono, B.A.; Turubanova, S.; Zhuravleva, I.; Potapov, P.; Tyukavina, A.; Baccini, A.; Goetz, S.; Hansen, M.C. Mapping and monitoring deforestation and forest degradation in Sumatra (Indonesia) using Landsat time series data sets from 1990 to 2010. *Environ. Res. Lett.* 2012, *7*, 034010.

Miettinen, J.; Hooijer, A.; Shi, C.; Tollenaar, D.; Vernimmen, R.; Liew, S.C.; Malins, C.; Page, S.E. Extent of industrial plantations on Southeast Asian peatlands in 2010 with analysis of historical expansion and future projections. *GCB Bioenergy* 2012, *4*, 908–918.

Miettinen, J.; Hooijer, A.; Vernimmen, R.; Liew, S.C.; Page, S.E. From carbon sink to carbon source: Extensive peat oxidation in insular Southeast Asia since 1990. *Environ. Res. Lett.* 2017, *12*, 024014.

Miettinen, J.; Hyer, E.; Chia, A.S.; Kwoh, L.K.; Liew, S.C. Detection of vegetation fires and burnt areas by remote sensing in insular Southeast Asian conditions: Current status of knowledge and future challenges. *Int. J. Remote Sens.* 2013, *34*, 4344–4366.

Miettinen, J.; Liew, S.C. Status of peatland degradation and development in Sumatra and Kalimantan. *Ambio* 2010, *39*, 394–401.

Miettinen, J.; Shi, C.; Liew, S.C. Influence of peatland and land cover distribution on fire regimes in insular Southeast Asia. *Reg. Environ. Chang.* 2011, *11*, 191–201.

Miettinen, J.; Shi, C.; Liew, S.C. Land cover distribution in the peatlands of Peninsular Malaysia, Sumatra and Borneo in 2015 with changes since 1990. *Glob. Ecol. Conserv.* 2016, *6*, 67–78.

MoEF. Sipongi, Karhutla Sistem. Available online: http://sipongi.menlhk.go.id/hotspot/luas_kebakaran (accessed on 20 January 2019).

Mouillot, F.; Schultz, M.G.; Yue, C.; Cadule, P.; Tansey, K.; Ciais, P.; Chuvieco, E. Ten years of global burned area products from spaceborne remote sensing—A review: Analysis of user needs and recommendations for future developments. *Int. J. Appl. Earth Obs. Geoinf.* 2014, *26*, 64–79.

Murdiyarso, D.; Adiningsih, E.S. Climate anomalies, Indonesian vegetation fires and terrestrial carbon emissions. *Mitig. Adapt. Strateg. Glob. Chang.* 2007, *12*, 101–112.

Murdiyarso, D.; Lebel, L.; Gintings, A.; Tampubolon, S.; Heil, A.; Wasson, M. Policy responses to complex environmental problems: Insights from a science—policy activity on transboundary haze from vegetation fires in Southeast Asia. *Agric. Ecosyst. Environ.* 2004, *104*, 47–56.

Numata, I.; Cochrane, M.A.; Galvão, L.S. Analyzing the impacts of frequency and severity of forest fire on the recovery of disturbed forest using Landsat time series and EO-1 Hyperion in the Southern Brazilian Amazon. *Earth Interact.* 2011, *15*, 1–17.

Oliveira, S.L.; Pereira, J.M.; Carreiras, J.M. Fire frequency analysis in Portugal (1975–2005), using Landsat-based burnt area maps. *Int. J. Wildland Fire* 2012, *21*, 48–60.

Oliveira, S.L.; Turkman, M.A.; Pereira, J.M. An analysis of fire frequency in tropical savannas of northern Australia, using a satellite-based fire atlas. *Int. J. Wildland Fire* 2013, *22*, 479–492.

Page, S.; Rieley, J.; Hoscilo, A.; Spessa, A.; Weber, U. Current fire regimes, impacts and the likely changes–IV: tropical Southeast Asia. In *Vegetation Fires and Global Change – Challenges for Concerted International Action A White Paper directed to the United Nations and International Organizations*, Goldberg, J.G., Ed. Kessel Publishing House, Germany, 2013.

Page, S.E.; Siegert, F.; Rieley, J.O.; Boehm, H.D.; Jaya, A.; Limin, S. The amount of carbon released from peat and forest fires in Indonesia during 1997. *Nature* 2002, *420*, 61–65. doi:10.1038/nature01131.

Putra, E.I.; Hayasaka, H.; Takahashi, H.; Usup, A. Recent peat fire activity in the mega rice project area Central Kalimantan Indonesia. *J. Disaster Res.* 2008, *3*, 334–341.

Reiche, J.; Verbesselt, J.; Hoekman, D.; Herold, M. Fusing Landsat and SAR time series to detect deforestation in the tropics. *Remote Sens. Environ.* 2015, *156*, 276–293.

Ritung, S.; Wahyunto, N.K.; Sukarman, H.; Suparto, T.C. *Peta Lahan Gambut Indonesia Skala 1:250,000*; Balai Besar Penelitian dan Pengembangan Sumberdaya Lahan Pertanian, Badan Penelitian dan Pengembangan Pertanian: Bogor, Indonesia, 2011.

Rogeau, M.P.; Armstrong, G.W. Quantifying the effect of elevation and aspect on fire return intervals in the Canadian Rocky Mountains. *For. Ecol. Manag.* 2017, *384*, 248–261.

Roteta, E.; Bastarrika, A.; Padilla, M.; Storm, T.; Chuvieco, E. Development of a Sentinel-2 burned area algorithm: Generation of a small fire database for sub-Saharan Africa. *Remote Sens. Environ.* 2019, *222*, 1–17.

Roy, D.P.; Boschetti, L. Southern Africa validation of the MODIS, L3JRC, and GlobCarbon burned-area products. *IEEE Trans. Geosci. Remote Sens.* 2009, *47*, 1032–1044.

Roy, D.P.; Huang, H.; Boschetti, L.; Giglio, L.; Yan, L.; Zhang, H.H.; Li, Z.J. Landsat-8 and Sentinel-2 burned area mapping-A combined sensor multi-temporal change detection approach. *Remote Sens. Environ.* 2019, *231*, 111254.

Siegert, F.; Ruecker, G.; Hinrichs, A.; Hoffmann, A. Increased damage from fires in logged forests during droughts caused by El Nino. *Nature* 2001, *414*, 437–440.

Steel, Z.L.; Safford, H.D.; Viers, J.H. The fire frequency-severity relationship and the legacy of fire suppression in California forests. *Ecosphere* 2015, *6*, 1–23.

Stockwell, C.E.; Jayarathne, T.; Cochrane, M.A.; Ryan, K.C.; Putra, E.I.; Saharjo, B.H.; Nurhayati, A.D.; Albar, I.; Blake, D.R.; Simpson, I.J. Field measurements of trace gases and aerosols emitted by peat fires in Central Kalimantan, Indonesia, during the 2015 El Niño. *Atmos. Chem. Phys.* 2016, *16*, 11711–11732.

Tacconi, L.; Moore, P.F.; Kaimowitz, D. Fires in tropical forests—What is really the problem? Lessons from Indonesia. *Mitig. Adapt. Strateg. Glob. Chang.* 2007, *12*, 55–66.

The Climate Prediction Center/National Weather Service. Historical El Nino/La Niña Episodes (1950–present). Available online: https://origin.cpc.ncep.noaa.gov/products/analysis_monitoring/ensostuff/ONI_v5.php (accessed on 19 November 2019).

Tsela, P.; Wessels, K.; Botai, J.; Archibald, S.; Swanepoel, D.; Steenkamp, K.; Frost, P. Validation of the two standard MODIS satellite burned-area products and an empirically-derived merged product in South Africa. *Remote Sens.* 2014, *6*, 1275–1293.

Turetsky, M.R.; Benscoter, B.; Page, S.; Rein, G.; Van Der Werf, G.R.; Watts, A. Global vulnerability of peatlands to fire and carbon loss. *Nat. Geosci.* 2015, *8*, 11–14.

Van der Werf, G. Climate regulation of fire emissions and deforestation in equatorial Asia. *Proc. Natl. Acad. Sci. USA.* 2008, *105*, 20350–20355.

Wagner, C.V. Age-class distribution and the forest fire cycle. *Can. J. For. Res.* 1978, *8*, 220–227.

Wahyunto; Dariah, A.; Agus, F. Distribution, properties, and carbon stock of Indonesian peatland. In Proceedings of the International Workshop on Evaluation and Sustainable Management of Soil Carbon Sequestration in Asian Countries, Bogor, Indonesia, 28–29 September, 2010; pp. 187–204.

Wahyunto; Ritung, S.; Subagjo, H. *Peta Luas Sebaran Lahan Gambut dan Kandungan Karbon di Kalimantan/Map of Peatland Distribution Area and Carbon Content in Kalimantan, 2000–2002*; Wetlands International—Indonesia Programme & Wildlife Habitat Canada (WHC): Bogor, Indonesia, 2004.

Wahyunto; Ritung, S.; Subagjo, H. *Peta Luas Sebaran Lahan Gambut dan Kandungan Karbon di Pulau Sumatera/Maps of Area of Peatland Distribution and Carbon Content in Sumatera, 1990–2002*; Wetlands International—Indonesia Programme & Wildlife Habitat Canada (WHC): Bogor, Indonesia, 2003.

World Bank. *The Cost of Fire: An Economic Analysis of Indonesia's 2015 Fire Crisis*; The World Bank, Jakarta, Indonesia, 2016. Available online: http://pubdocs.worldbank.org/en/643781465442350600/Indonesia-forest-fire-notes.pdf (accessed on 10 October 2019).

Xu, J.; Morris, P.J.; Liu, J.; Holden, J. PEATMAP: Refining estimates of global peatland distribution based on a meta-analysis. *Catena* 2018, *160*, 134–140.

APPENDIX

Table S 3-1 Total areas of Sumatran and Kalimantan peatland for land cover maps dating to 1990, 2007, and 2015 (area in 1,000 hectares)

Land cover types	Sumatra			Kalimantan		
	1990	2007	2015	1990	2007	2015
Forest						
Pristine peat swamp forest (PSF)	3844.2	285.0	436.0	2861.9	99.2	426.0
Degraded PSF	1468.3	2045.3	956.5	1823.7	2760.9	2010.0
Non-forest (native-vegetated)						
Tall shrub/secondary forest	343.1	480.4	468.5	259.6	712.5	1032.6
Ferns/low shrub	474.1	742.2	330.3	236.5	915.2	443.9
Smallholder area	904.3	1880.1	2392.5	302.3	601.7	680.9
Industrial plantations	25.5	1506.7	2405.5	0.1	155.5	809.6
Other land cover						
Cleared/burned area	103.9	185.0	137.9	101.4	295.6	128.4
Seasonal water	31.6	44.2	38.5	169.8	212.6	220.5
Built-up area	0.5	4.9	7.7	1.2	2.6	3.8
Mangrove	29.4	28.3	29.0	22.5	21.5	20.8
Water	5.3	28.2	27.9	2.2	4.0	4.8

Table S 3-2 Accumulated area burned from 2001-2018 in Sumatra and Kalimantan peatlands as related to its associated land cover (LC) for maps dating to 1990, 2007, and 2015 (area in 1,000 hectares)

Land cover types	Sumatra			Kalimantan		
	1990	2007	2015	1990	2007	2015
Forest						
Pristine peat swamp forest (PSF)	1197.0	5.8	2.7	1053.4	0.8	7.2
Degraded PSF	744.6	370.9	37.7	1248.7	247.7	116.4
Non-forest (native-vegetated)						
Tall shrub/secondary forest	190.1	281.9	403.5	311.7	489.5	1101.8
Ferns/low shrub	415.4	938.7	377.8	401.1	1401.7	691.4
Smallholder area	138.9	542.4	883.6	372.2	752.2	824.7
Industrial plantations	0.0	404.3	889.8	0.0	81.9	656.7
Other land cover						
Cleared/burned area	40.4	176.9	127.8	112.5	546.8	115.1
Seasonal water	25.0	28.5	26.0	109.5	88.2	93.9
Built-up area	0.0	0.0	0.1	0.0	0.0	0.6
Mangrove	2.5	2.5	2.6	1.0	1.0	1.0
Water	0.2	2.4	2.5	0.3	0.6	1.6

Table S 3-3 Area burned in Sumatra and Kalimantan within two periods (2001-2007 and 2008-2018) and their related land cover types for maps dating to 1990 and 2007 (area in 1,000 hectares; burning rate in 1,000 hectares/year)

Land cover (LC) types	Burning from 2001-2007 dating to the 1990 LC map				Burning from 2008-2018 dating to the 2007 LC map			
	Sumatra		Kalimantan		Sumatra		Kalimantan	
	Area	Burning rate	Area	Burning rate	Area	Burning rate	Area	Burning rate
Forest								
Pristine peat swamp forest (PSF)	483.0	74.3	494.6	76.1	4.9	0.5	0.6	0.1
Degraded PSF	353.4	54.4	537.5	82.7	331.3	30.8	184.2	17.1
Non-forest (native-vegetated)								
Tall shrub/secondary forest	84.4	13.0	160.6	24.7	182.4	17.0	253.6	23.6
Ferns/low shrub	192.2	29.6	213.9	32.9	488.0	45.4	708.7	65.9
Smallholder area	70.1	10.8	188.6	29.0	270.8	25.2	385.8	35.9
Industrial plantations	0.0	0.0	0.0	0.0	152.0	14.1	22.2	2.1
Other land cover								
Cleared/burned area	22.9	3.5	64.2	9.9	88.2	8.2	295.6	27.5
Seasonal water	9.6	0.0	52.0	8.0	17.0	1.6	47.0	4.4
Built-up area	0.0	0.0	0.0	0.0	0.0	0.0	0.0	0.0
Mangrove	0.8	0.1	0.5	0.1	1.7	0.2	0.5	0.0
Water	0.1	0.0	0.1	2.2	1.1	0.1	0.0	0.1

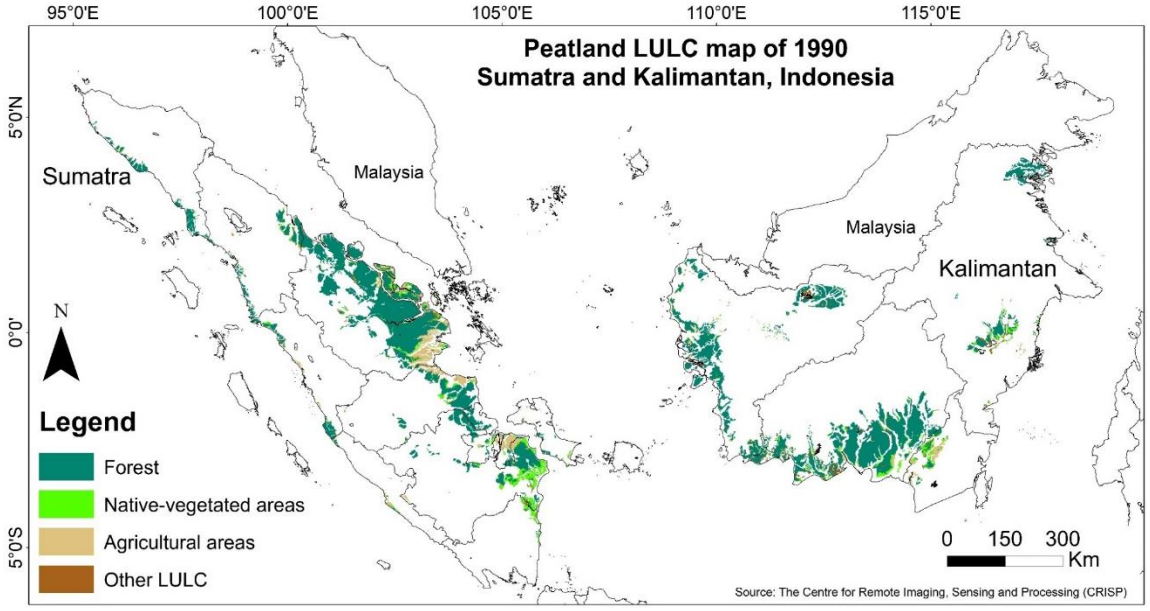

Figure S 3-1 Land-use and land-cover map of 1990 in peatlands of Sumatra and Kalimantan

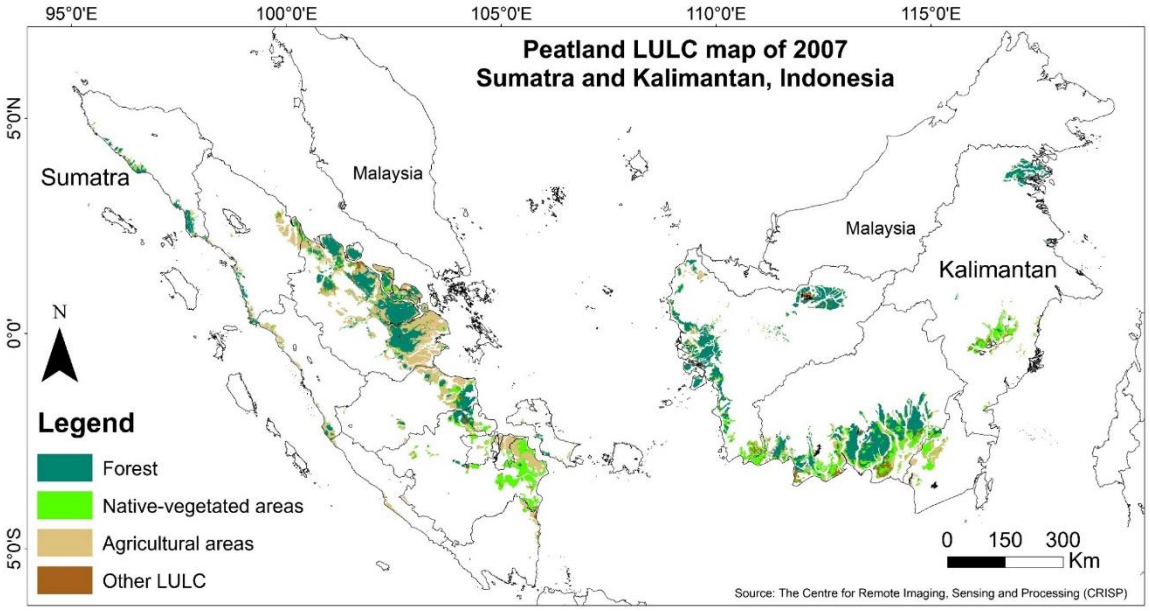

Figure S 3-2 Land-use and land-cover map of 2007 in peatlands of Sumatra and Kalimantan

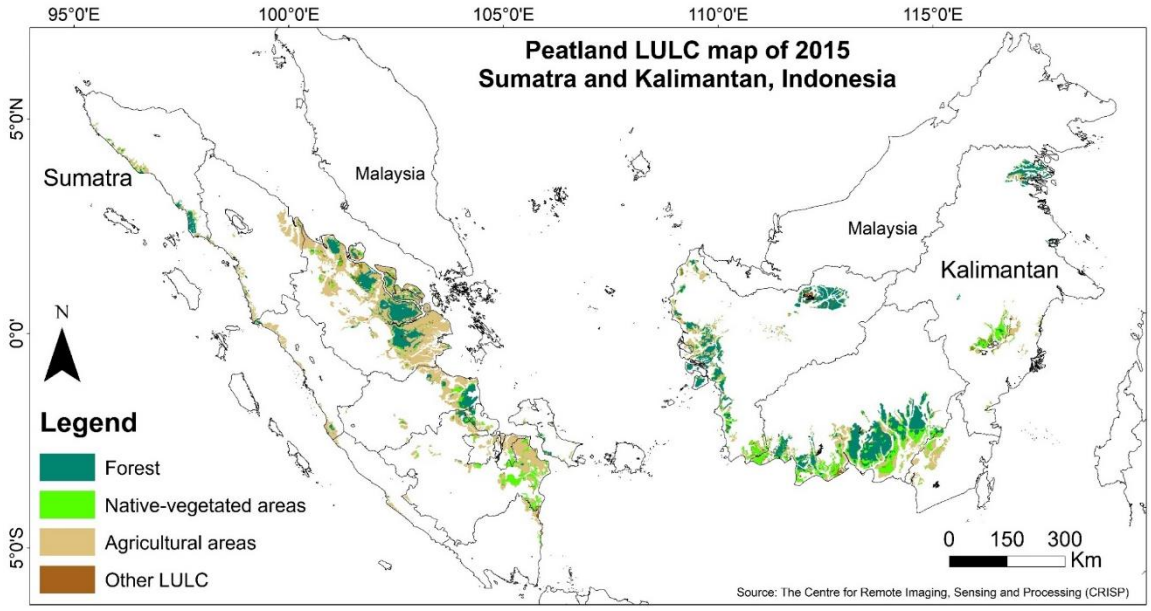

Figure S 3-3 Land-use and land-cover map of 2015 in peatlands of Sumatra and Kalimantan

CHAPTER 4

EVALUATING MULTISENSOR DATA FOR PRODUCTION OF BURNED AREA MAPS IN PEAT SWAMPS OF CENTRAL KALIMANTAN, INDONESIA: ASSESSING SEASONALITY DIFFERENCES

Manuscript #3: Vetrita et al. 2020. Evaluating multisensor data for production of burned area maps in peat swamps of Central Kalimantan, Indonesia: assessing seasonality differences

Datasets (Appendix):

1. Vetrita, Y., and M.A. Cochrane. 2019. Annual Burned Area from Landsat, Mawas, Central Kalimantan, Indonesia, 1997-2015. ORNL DAAC, Oak Ridge, Tennessee, USA. https://doi.org/10.3334/ORNLDAAC/1708
2. Vetrita, Y., and M.A. Cochrane. 2020. Landsat derived land use/cover maps across Mawas Central Kalimantan, Indonesia (under review). ORNL DAAC, Oak Ridge, Tennessee, USA. https://doi.org/10.3334/ORNLDAAC/1838

Abstract

Fires in Indonesian peatlands have become frequent and substantial contributors to global greenhouse gas emissions. Peat fires in Indonesia are often smoldering, small in size, and located under heavy cloud cover, making consistent production of annual burned area (BA) maps very challenging. We evaluated the Moderate Resolution Imaging Spectroradiometer (MODIS) BA product (MCD64A1) for two fire seasons of different intensity, moderate (2014) and severe burning (2015), in Central Kalimantan by comparing the results with the gridded VIIRS 375 active fire product and Landsat-based BA mapping based on Random Forest classifications of burned and unburned pixels. Several band indices and thermal Infrared bands were employed for the Landsat-based BA map derivations. In addition, we investigated how imagery from additional satellite sensors (Sentinel-1 and Sentinel-2) could improve BA estimations for the 2015 fire event. Cross-

validation of the Random Forest classification showed that the Out of Bag estimate of error rate was comparable for 2014 (when all available images until the year-end of 2014 were used) and 2015 (2.62% vs. 2.69%) but had a higher error rate (8.8%) when Landsat images being used did not extend beyond the date of the SPOT 5 image acquisition. Of the 180 ground truth points collected in 2015, only 140 corresponded to areas with available 2015 Landsat imagery, with 75% of them correctly discriminating actual burning. In our 50,000-hectare study site, incorporation of Sentinel-2 and Sentinel-1 imagery filled nearly all (99%) of the MODIS BA detection gap in 2015. Sentinel-1 was superior for detecting burned areas under heavy cloud cover but was of minimal use once the rainy season began. Combining Sentinel-2 and Landsat images improved monitoring of peat burning but was somewhat restricted by cloud cover. We also created annual burned area maps from 1997-2015 for our study site, along with these assessments, and discuss variables that are important for distinguishing burned and unburned pixels and possibilities for extending this approach to a national scale

Keywords: Burned scar, Peat, Random Forest, VIIRS, Indonesia

4.1 Introduction

Indonesia, with its unique flora and fauna and the third-largest amount of tropical forest in the world, has also become one of the largest threatened biodiversity hotspots (Myers et al., 2000). Increasingly, human activities have disrupted these ecosystems, converting forests into other land-use/covers (Curtis et al., 2018, Austin et al., 2019). In 1990, natural forest covered 60% of the country's land (113.2 Mha), with 10% in peatlands (MoEF, 2016). By 2012, annual forest loss rates exceeded those in Brazil by 83%, with an increasing trend in wetlands (including peatland) (Margono et al., 2014). Land degradation,

including illegal logging and fires, intensified forest loss rates. In 1990, Indonesia's two largest peat regions (13 Mha), Sumatra and Kalimantan, had 86% forest cover, but, by 2015, when a major fire season developed, only 29% remained (Miettinen et al., 2016). If peatland burning rates continue at levels seen in the last two decades, the remaining forests in those areas will most likely disappear in the coming decades (Vetrita and Cochrane, 2020a). Moreover, repeated burning and/or forest disturbance poses significant challenges for forest regeneration (Van Nieuwstadt et al., 2001).

Burning in peatland has not only threatened the forests and their biodiversity, but it has also affected human life through impacts on health, domestic travel, and school closures (Koplitz et al., 2016, Marlier et al., 2019, Glauber and Gunawan, 2016, The World Bank, 2014), despite ignitions from human activities being the primary cause of fires in the region (Medrilzam et al., 2014). Even without burning, degraded peatland has become a large carbon source as drainage has exposed peat to air, allowing year-round oxidization (Miettinen et al., 2017). Burning escalates the amount of carbon released from both above- and belowground biomass (peat) over a compressed time period. Carbon emissions from peatlands have been estimated to be as high as 13-40% in 1997 (Page et al., 2002) and 5% in 2015 (GFED, 2015) of the annual global carbon emissions from fossil fuels.

A study which compared the six available national inventories for carbon emission in Indonesia reported the main differences in inter-annual emissions among products were due to peat-fire emissions (Austin et al., 2018). Given the uncertainty in the estimates, levels of carbon emissions from peatland are debatable. The amount of peat consumed is highly uncertain, but inevitably depends on the peat moisture, bulk density, peat drainage, and fire frequency (Konecny et al., 2016, Putra et al., 2018, Sinclair et al., 2020). Remote

sensing plays an important role due to its ability to map both area and frequency of biomass burning. Field assessments are challenging due to the inaccessibility of most areas. Satellite-based approaches, however, are also problematic due to frequent cloud and/or smoke obscuring the ground and patchy burned areas (Vetrita et al., 2020). Remote sensing, however, provides a consistent, easier, and more cost-effective approach than direct field mapping. Various satellite-based burned area mapping methods have been developed over the past two decades (see Chuvieco et al. (2019) for a thorough review), although studies addressing use in Indonesian peatland environments have been relatively limited.

Satellite-based burned area mapping and gridded active fire (burned area-based active fire) are two common approaches for estimating burned area, reported as burn scars or fire-affected areas in various publications (Roy et al., 2005, Lohberger et al., 2017, Langner et al., 2007, Garcia-Haro et al., 2001). The use of gridded active fire to estimate burned area is of debatable use because active fire product(s) only record the location and time of fires during satellite overpasses, without mapping the actual landscape-burned areas (Roy et al., 2008, Giglio et al., 2006). Wiedinmyer et al. (2011), however, argue that burned area estimates should be near real-time in order to effectively estimate emissions; current burned area products are unable to provide such rapid inputs. In addition, current burned area products have reported limitations for peatland areas, including insufficient detections of small area or low-temperature smoldering fires and inability to detect flaming combustion under heavy smoke or cloud cover, or within gaps between orbits near the equator (MODIS product) (Giglio et al., 2006, Csiszar et al., 2003, Csiszar et al., 2006, Schroeder et al., 2008, Tansey et al., 2008, Vetrita et al., 2020). Most available national inventories use burned area-based active fire to estimate peat fires. Because of these

uncertainties in peatlands, one of the available inventories (e.g. FREL 2016) excluded peat-fire emissions from their estimate.

Despite these limitations, active fire product(s) are useful for integrating with post-fire burned area maps (Giglio et al., 2009, Fraser et al., 2000, Chuvieco et al., 2018, Giglio et al., 2018a). Overall, all fire products under-sample fire activity to some extent because they miss many fires, indicating that accurate detection and mapping of fire activity in Indonesia's peatlands is doubtful. However, the Visible Infrared Imaging Radiometer Suite (VIIRS) 375 m active fire product (Schroeder et al., 2014), was recently reported to accurately detect fire in peatland (Sofan et al., 2020), enabling mapping of areas burned in global applications (Oliva and Schroeder, 2015). As of yet, however, no specific assessments have been conducted for Indonesia using the approach, let alone in peatland areas.

The second approach for satellite-based burned area mapping is derived from mapping the post-fire extent and spatial distribution of burn scars or fire-affected areas. Theoretically, fire-induced surface-spectral changes are observed. Wavelengths from near infrared (~0.75-1.4 μm, NIR), shortwave infrared (~1.4-3 μm, SWIR), thermal infrared (~3-15 μm, TIR) bands and their associated indices (e.g., Normalized Burn Ratio) were commonly used for both single date or multitemporal approaches (Miettinen et al., 2007, Hoscilo et al., 2013, Sofan et al., 2019). NIR and SWIR are the best spectral bands for separating burned and unburned vegetation (Huang et al., 2016). The standard MODIS burned area product (MCD64A1 Collection 6 (Giglio et al., 2018a)) employed these bands in their algorithms.

Over more than two decades, large-scale burned area mapping has been studied using coarse (≥1 km^2) and medium-resolution (20–500 m) optical sensors (Roy et al., 2008, Boschetti et al., 2009, Boschetti et al., 2015, Tansey et al., 2004, Chuvieco et al., 2018, Chuvieco et al., 2019, Roteta et al., 2019, Roy et al., 2019). Accuracy from approaches relying on optical sensors suffer from an inability to observe areas under clouds or smoke. Therefore, applications using active sensors (radar) that are capable of penetrating the frequent clouds and smoke that impede land cover/use mapping in the tropics offer great promise, particularly in cloud-prone areas such as Indonesia (Siegert and Ruecker, 2000, Lohberger et al., 2017).

The Ministry of Environment and Forestry (MoEF) prefers using visual image analysis for deriving national land use/cover (Margono et al., 2014) and burned area maps. Active fire products are used to guide the interpreters who delineate the areas burned. Digital image classification techniques have not yet been used to provide long-term datasets such as provided by the U.S. Monitoring Trends in Burn Severity (Picotte et al., 2020). Integrating geo-statistics, object oriented, and machine learning methods remains a hot topic in remote sensing-based applications (Chuvieco et al., 2019), including burned area mapping. Random Forest model and Boosted Regression Trees are two examples that have recently been used with satisfactory results (Roy et al., 2019, Roteta et al., 2019, Ramo and Chuvieco, 2017, Hawbaker et al., 2017, Hawbaker et al., 2020, Ramo et al., 2018). However, all of the studies were conducted outside the Indonesian peatlands (Africa and the U.S.) where the fire regimes differ from this region. Though limited in scope, radar-based approaches and satellite-based active fire combinations have been used to map area burned in Indonesian peatlands. Some of the techniques used were pixel-based and object-

based approaches, also machine learning algorithms (e.g., Lohberger et al., 2017, Siegert and Hoffmann, 2000, Carreiras et al., 2020).

In recent years, the volume of free satellite imagery has risen, creating cost-effective opportunities to establish integrated approaches for mapping and validating burned area. The potential for comprehensive burned area mapping has increased with the launch of various free datasets (Landsat 8, Sentinel 2, Sentinel 1, VIIRS 375 m) with higher spatial, temporal, and spectral resolution. However, despite showing the potential for improved identification of burned areas in this region and other fire-prone areas, none of the studies provided long-term burning history, as provided by MODIS (Giglio et al., 2018a). When we prepared this manuscript, this region still lacked much data, even Landsat-based maps, which are historically available for long-term image sequences. The Indonesian government has been providing a satellite-based burned area estimates since 2015. Previously, only rough estimates were made (MoEF, 2020). The current map is viewable at http://webgis.menlhk.go.id:8080/kemenhut/index.php/id/peta/peta-interaktif.

Multi-sensor integration, including passive and active remote sensing, may improve accuracy but, to the best of our knowledge, no studies have investigated this approach, specifically for Indonesian peatlands that are more vulnerable to fires (Vetrita & Cochrane, 2020). Earlier, Vetrita et al (2020) assessed four MODIS-derived BA products for a moderately severe burning event in Central Kalimantan, Indonesia. But, the study did not take into account fire seasons differences which also affect accuracy (Humber et al., 2019). We intend to address these questions:

1. How does the accuracy of existing burned area products (MODIS) change between fire seasons of different severity?

2. To what extent could available multisensor data (Sentinel-2, Sentinel-1, Landsat, gridded VIIRS 375-m active fire) improve burned area estimation in peatlands?

We discuss the challenges in producing a long-term burn history (1997-2015) for this site and the opportunity to expand this activity to a national scale.

4.2 Materials and Methods

We compared two fire seasons of different severity, 2015 (severe) and 2014 (moderate). We assigned each year's severity class based on reported areas burned (MoEF, 2020) and impact of burning (The World Bank, 2014). We first assessed MODIS, Landsat, and VIIRS 375 aggregated active fires for the 2014 burning event. Since Sentinel-1, and Sentinel-2 sensors became operationally available as of late September 2015, their outputs were assessed for the 2015 burning event to determine whether they can potentially improve deficiencies found in the MODIS, VIIRS, and Landsat BA products. The following sections describe the study site (section 4.2.1), all input data and burned area production for each sensor. Figure 4-1 illustrates the approaches for 2014 and 2015 in a flow chart.

For the respective analyses, we first calculated the percentage of burned area detected or missed by each of the three sensors that were available for the 2014 fire event against a higher resolution (SPOT) validated reference map of burned area. For 2015, the comparative accuracies of the 5 sensor-derived products were assessed against 180 field-collected ground truth data points. Responsiveness of sensors between years of different fire severity, 2014 (moderate) and 2015 (severe), were assessed. Areas with no detection or erroneous detection were explored to find reasons or possible explanations.

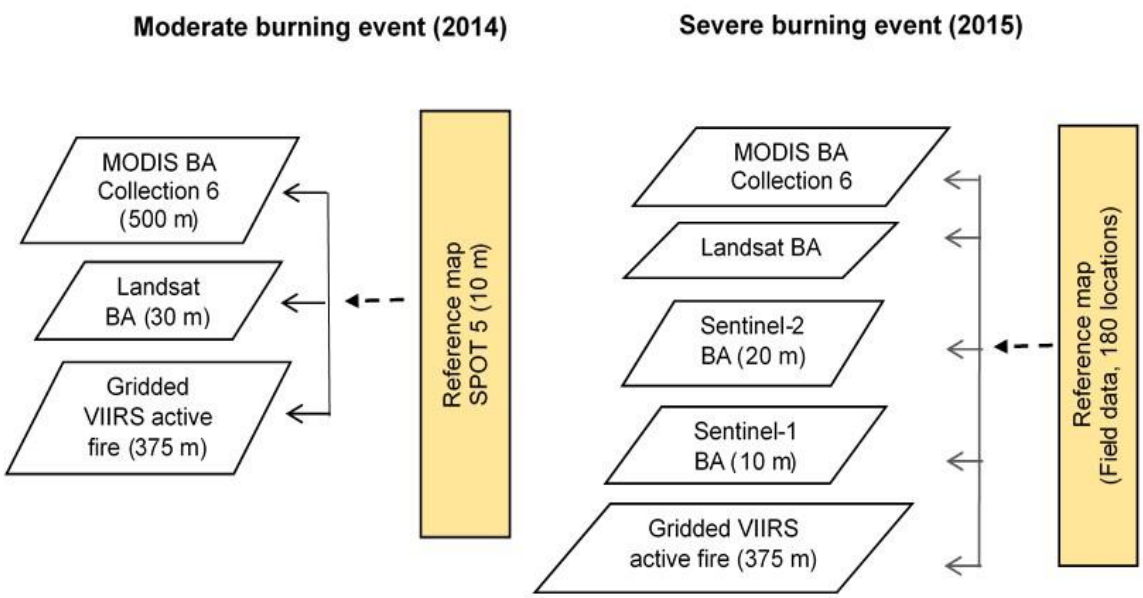

Figure 4-1 Evaluating multisensor data for production of burned area maps in peat swamps of Central Kalimantan, Indonesia.

4.2.1 Study site

The study site was located in Central Kalimantan, Indonesia (Figure 4-2), in one of the areas most affected by frequent fires during the last two decades (Vetrita and Cochrane, 2020a). The site has a tropical climate with a temperature range of 23.4-32.5 degrees Celsius and 64-95 percent relative humidity. The dry season typically starts in July and continues through October (Figure 4-3). The average annual rainfall for the area during 2010-2019 was 3177.5 mm (Badan Pusat Statistik, 2020). This site was in Block A of the Indonesian government's previous Mega Rice Project (MRP)—a million hectares of peat converted hydrologically through extensive drainage to facilitate landscape-scale rice

production. The MRP was started in 1996 and terminated unsuccessfully in 1999 (see Medrilzam et al. (2017) for more information on the study site).

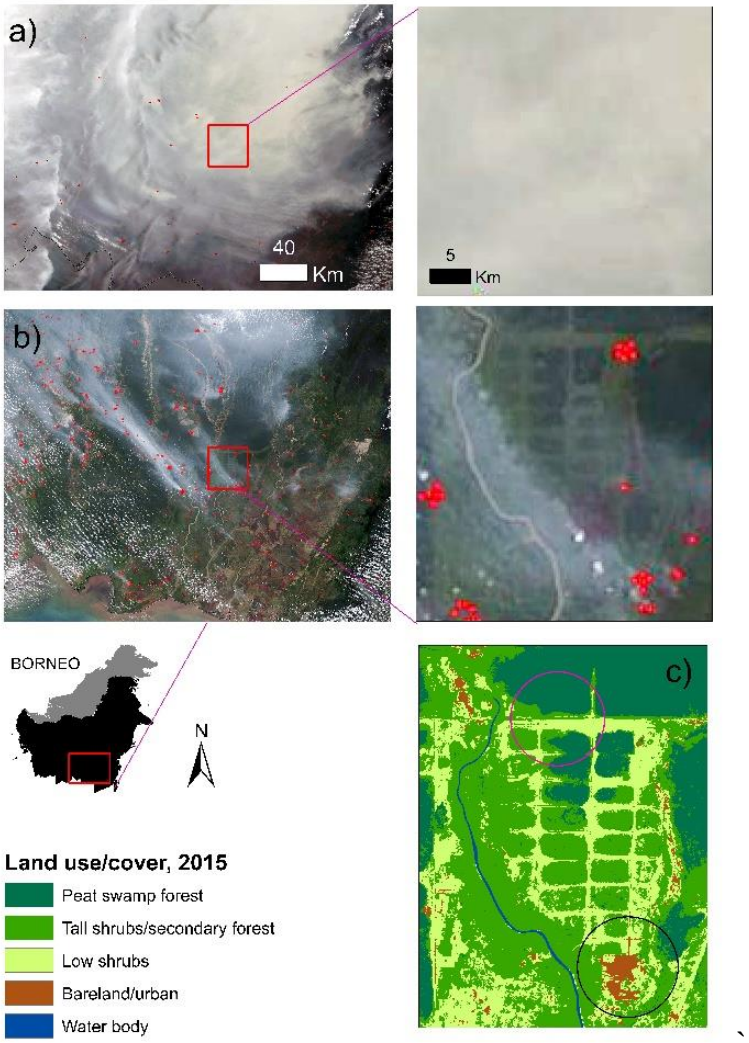

Figure 4-2. Intense smoke clouds combined to cover the study area on September 25, 2015 (a) as compared to moderate smoke/haze one the same date in 2014 (b) in central Kalimantan, on the island of Borneo. Natural color composites were downloaded from https://worldview.earthdata.nasa.gov/. The associated active fires (red dot) and focus site (red square) are shown. The magenta circle shows (c) the last remaining forest, half of which burned in 2015. The black circle shows bare land, burned in 2014, which was later converted to oil palm. The land use/cover for the site was downloaded from ORNL DAAC (https://doi.org/10.3334/ORNLDAAC/1838) (Vetrita and Cochrane, 2020b).

The study area covers almost 50 thousand hectares of peatland, 0.7% of the total Kalimantan peatland area (Ritung et al., 2011), and shares many characteristics with other degraded Indonesian peatlands. The area covers ~83% of a peat dome, most of which is greater than 3 meters depth. Shallower peat is found closer to the river, where five villages are also located. After the failure of the MRP, vast areas of cleared forest became dominated by shrubland and ferns, with isolated small managed land areas (Medrilzam et al., 2017) (Figure 4-2c), accessible through canals. The drainage canals were built through the peat swamp forest during the MRP, providing free access to the forests and facilitating human-induced fires. This site is one of the areas that has suffered the most frequent fires during the last two decades (Vetrita and Cochrane, 2020a). Since 2016, the region has been one of the Peat Restoration Agency (BRG) focus areas for 2.4 Mha of degraded peatland restoration. Canals have been blocked to rewet and restrict access to the site. The study area has also been the site of many interdisciplinary studies, with relevance not only to conservation activities but also to socio-political, biophysical, and peat-fire emissions assessments of degraded peatlands (Blackham et al., 2014, Goldstein et al., 2020, Sinclair et al., 2020, Medrilzam et al., 2017, Putra et al., 2019).

The area can become obscured with moderate to heavy smoke. For example, in 2014, the area was covered by a moderate level of smoke and haze, visible in satellite imagery (Figure 4-2a). During the same month in 2015, the area was completely obscured by heavy smoke/haze (Figure 4-2b). Smoke from southern areas of Kalimantan, nearer the coast, blows inland to the MRP region early in the fire season, before much of the local burning gets started. The study site's most recent major burn occurred in the 2015 El Niño year. In 2014, precipitation was low, but still wetter than in 2015, specifically during the

dry season (July – October) (Figure 4-3a-b). Less area burned during the 2019 El Niño year.

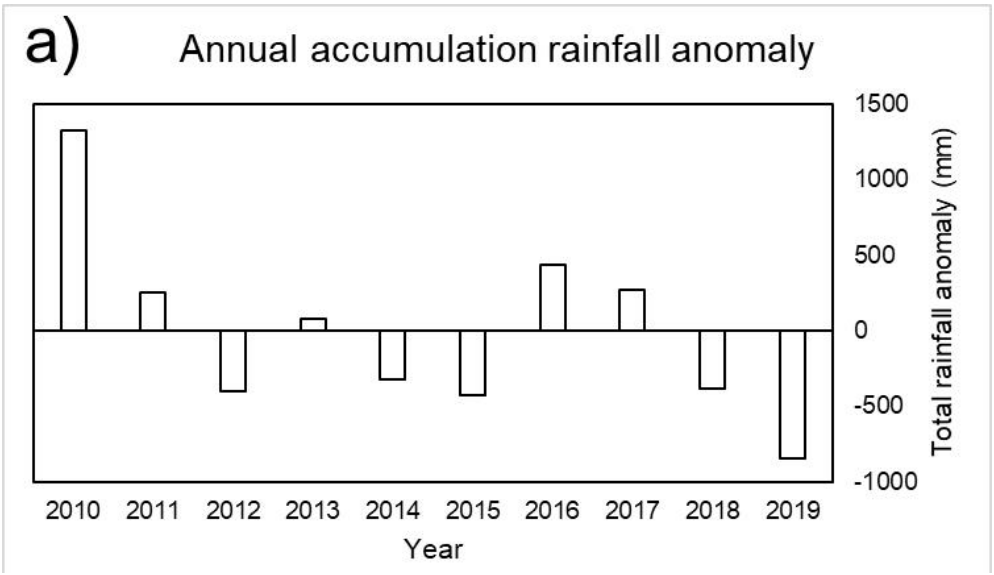

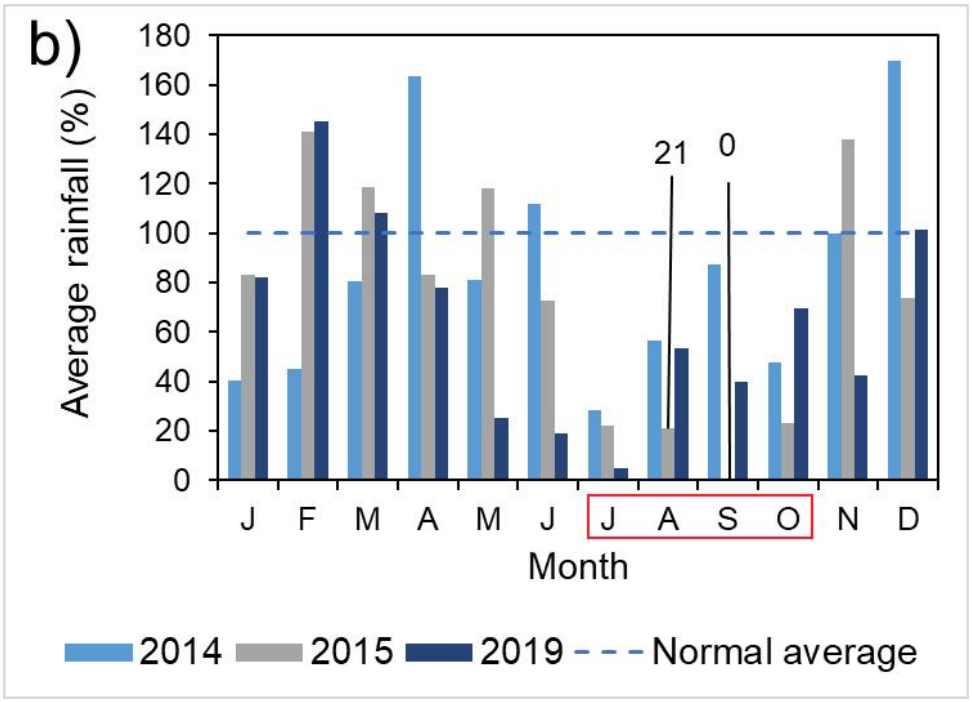

Figure 4-3 Annual accumulation rainfall anomaly from 2010 to 2019 (a) and percentage of average rainfall (b), comparing three different seasons at the Palangka Raya climate station, Central Kalimantan, Indonesia, the closest station to the study site. During this period, 2015 and 2019 were recorded as strong El Niño events in Indonesia. The lowest annual rainfall occurred in 2019 (a). However, during dry season (b, red rectangle) that normally starts in July and peaks in September,

the average rainfall in 2015 fell way below the normal average (b, dashed-lined) and the 2014 and 2019 rainfall amounts.

4.2.2 Data sources and selection for production of burned area

Table 4-1 Datasets and methods used to derive burned area products in this study

Satellite imageries datasets	Data selection and sources: Burning event of 2014	Burning event of 2015	Source	Temporal/spatial resolution	Method/ References
MODIS BA Collection 6	Sept 2014	July-Nov 2015	NASA	Monthly, 500 m	Thermal IR and multitemporal surface change approach (Giglio et al, 2018)
Landsat 7/8	Jan-Sep 25, 2014	Jan-Dec 2015	NASA	8-days, 30 m	Random Forest classifier (several indices) (Vetrita and Cochrane, 2019)
VIIRS 375 m active fire	Aug-Sep 24, 2014	July-Nov 2015	NOAA	Daily, 375 m	Gridded active fire (Schroeder et al., 2017, Oliva et al., 2015)
Sentinel 1	n/a	June-Oct 2015	ESA	6-12 days, 10 m	Multitemporal backscatter change approach (Lohberger et al, 2018)
Sentinel 2	n/a	Sept-Nov 2015 (three images)	ESA	5-10 days, 20 m	Threshold, Normalized Burned Ratio and Normalized Difference Moisture Index
Reference maps					
SPOT 5	Sept 24, 2014	-	LAPAN	10 m	Visual detection
Field data	-	Early Nov 2015	Cochrane's team		Field visit

4.2.3 Terra/Aqua MODIS burned area product

We assessed the latest version of MODIS burned area product (MCD64A1 collection 6) provided by NASA. This product more reliably detects small fires globally

than its precursor (Giglio et al., 2018a, Vetrita et al., 2020). This product integrates the active fire product (MOD14A1 and/or MYD14A1) (Giglio et al. 2016), multi-temporal vegetation indices, and land cover products into the algorithms (Giglio et al. 2009). The products provided the approximate burn date, burn date uncertainty, Quality Assurance, first day and last day layers. We selected all ordinal pixel days of burn (1-366) in land grid cells which flagged as valid data. MODIS datasets were then truncated to include only pixels having detection dates from the beginning of fire season to the same date of the SPOT 5 image used to derive the reference burned area map for the 2014 burning event. For the 2015 burning event, we selected the monthly products from July to November 2015, as opposed to the reference map. The product is available at https://earthexplorer.usgs.gov/.

4.2.4 VIIRS 375 m gridded active fire active fire (VNP14IMG)

The 375 m VIIRS level 2 active fire product (Schroeder et al., 2014) was used to detect active fire pixels (observation date, valid observation, related water/land/cloud pixels, and fire radiative power (FRP)) from each image analyzed (downloaded from https://ladsweb.modaps.eosdis.nasa.gov/). We quantified the persistence of cloud, land, water, and fire occurrences during the fire event of 2014 (1 July-24 September) and 2015 (1 July-5 November). All pixels were aggregated to derive the perimeter of fire-affected area (hereinafter, VIIRS-AF). We also summed values of all FRP pixels to explore the aggregate fire intensity for each burning season. FRP estimates the radiative energy portion released by burning related to combustion or fuel consumption (Wooster, Roberts, Perry & Kaufman, 2005).

4.2.5 Landsat-based burned area maps of 2014 and 2015 for accuracy assessment

All available scenes of level 1T (path/raw 118/62) were selected using the U.S. Geological Survey (USGS) Earth Explorer website (earthexplorer.usgs.gov), limited to cloud cover less than 80%. All selected scenes were submitted to the Earth Resources Observation and Science (EROS) Center Science Processing Architecture (ESPA) Ordering Interface (espa.cr.usgs.gov) for level-2 product processing. We ordered the surface reflectance, brightness temperature, and Quality Assurance (QA) layers, including indices that have previously been applied for BA applications (NDVI, NDMI, NBR, NBR2, SAVI, and MSAVI, see Table 4-2). Cloud and water pixels were removed based on the QA layer (flagged as good pixel) to derive the maps. Most of these indices have also been employed to create burned area maps using Boosting Regression Trees (Hawbaker et al., 2017). Here, we used Random Forest Model (Breiman, 2001) to classify burned and unburned pixels. Random forest is a machine learning approach that uses a collection of classifying trees to assign a class to a response variable. The predicted class is obtained by most “votes” from the classification trees Individual trees are derived using an original data set (called 'bagging'). Approximately two-thirds of the samples in the dataset are used for testing and the remaining third for model internal validation (i.e., out-of-bag error) (Collins et al., 2020). Models with all inputs were processed using the Random Forest package in R software (Liaw and Wiener, 2002). We used the default number of trees (500) because it is adequate for our relatively small area.

Table 4-2 Variables used to derive the Landsat-based burned area map. Parameters used included brightness temperature (BT) from the Thermal Infrared band (10.30-12.51 µm) and surface reflectance (ρ) of several bands: NIR=Near Infrared (0.77-0.9), $SWIR_1$=Shortwave Infrared (1.55-1.75µm), $SWIR_2$=Shortwave Infrared (2.09 - 2.35 µm), Red (0.63 - 0.69 µm), and Blue (0.45 - 0.52 µm).

Variable	Formula/parameters	Reference	Burned area applications examples
Normalized difference vegetation index (NDVI)	$\frac{\rho_{NIR}-\rho_{red}}{\rho_{NIR}+\rho_{red}}$	(Tucker 1979)	(Fraser et al., 2000, Navarro et al., 2017, Escuin et al., 2008)
Normalized difference moisture index (NDMI)	$\frac{\rho_{NIR}-\rho_{SWIR(1.6\mu m)}}{\rho_{NIR}+\rho_{SWIR(1.6\mu m)}}$	(Gao 1996)	(Fornacca et al., 2018)
Normalized burn ratio (NBR)	$\frac{\rho_{NIR}-\rho_{SWIR(2.2\mu m)}}{\rho_{NIR}+\rho_{SWIR(2.2\mu m)}}$	(Garcia and Caselles 1991)	(Giglio et al., 2018a, Fornacca et al., 2018, Escuin et al., 2008)
Normalized burn ratio 2 (NBR2)	$\frac{\rho_{SWIR(1.6\mu m)}-\rho_{SWIR(2.2\mu m)}}{\rho_{SWIR(1.6\mu m)}+\rho_{SWIR(2.2\mu m)}}$	(Key and Benson 2006)	(Hislop et al., 2018, Hawbaker et al., 2017)
Soil adjusted vegetation index (SAVI)	$[\rho_{NIR}-\rho_{red}(\rho_{NIR}+\rho_{red}+L)]x(1+L)$ L= soil correction factor, the value is depending on vegetation densities. The lower the density, the higher the correction factor	(Huete 1988)	(Chuvieco et al., 2002, Boschetti et al., 2010b, Norton et al., 2009)
Modified Soil Adjusted Vegetation Index (MSAVI)	$\frac{2\rho_{NIR}+1-\sqrt{\{(2\rho\}_{NIR}+1)^2-8(\rho_{NIR}-\rho_{Re}}}{2}$ MSAVI replaced the L soil correction factor used by SAVI with a function for calculating L	(Qi et al. 1994)	(Rogan and Yool, 2001)

Variable	Formula/parameters	Reference	Burned area applications examples
Enhanced Vegetation Index (EVI)	The function includes NDVI and weighted difference vegetation index $\frac{2.5x(\rho\}_{NIR}-\rho_{\{red)}}{\rho_{NIR}+6x\ \rho_{red}-7.5\ x\ \rho_{blue}+1}$	(Huete et al. 2002)	(Chen et al., 2011)
Brightness temperature of thermal infrared bands	Band 6 (Landsat 5/7), Band 10 and 11 (Landsat 8)	US Geological Survey (2018)	

To select the input for the model (see Figure 4-4), first we defined the post and pre fire images based on the timing information from the MODIS active fire product (MOD14/MYD14) occurring in the year of interest. Then, for each pixel of the Landsat indices (NDVI, NDMI, NBR, NBR2, SAVI, MSAVI, see Table 4-2), we selected the minimum value of post fire images and the maximum value of pre fire images. Unburned vegetation pixels prior to burning have higher indices values than burned pixels (see Figure S 4-1, supplementary material). For each of the indices, we calculated the pre-and post-fire differenced indices. We also selected the maximum brightness temperature of the Landsat thermal band (Band 6 for Landsat 7; Band 10 and 11 for Landsat 8) for only the post fire images since burn pixels should have higher values than non-burn pixels. Hawbaker et al (2017) found the Landsat thermal band was one of the most important variables for discriminating burned from unburned pixels. For the final inputs model, we kept the post-fire indices only (without denoted 'd'), indices differences (denoted with 'd'), and post-fire brightness temperature of the Landsat thermal band.

Burn samples were collected from the 2014 reference map of the SPOT 5 images (Zubaidah et al, 2017) from burn sizes greater than 100 ha. The unburned sample areas were visually digitized using Landsat and SPOT 5 images. Stratified random sampling was

used to create a balanced number of sample points from both sample classes (~2000) within a single SPOT 5 coverage. We used 80% of the sample points as training points and 20% as validating points to determine the overall accuracy of burned and unburned classes. Additional area-based accuracy assessment and regression of burned area proportion are described in Section 4.2.3. Training data samples for 2015 relied on visual interpretation. We carefully inspected pre-fire images and post images to select burn and unburned sample pixels. The predicted burned area was then derived from a probability map with pixel burn probability >= 95%. No pixels were removed or added manually.

Random Forest model allows us to investigate the most significant variables to differentiate the burn and unburned classes. To get a comprehensive understanding of how the time span of selected images affected burned area detection, we compared three models based upon all the available Landsat images acquired in a certain period. First, images available until the closest date of SPOT 5 acquisition date (September 24, 2014, hereinafter the first model). Second, images available until the end of 2015 (hereinafter, the second model) and 2014 (the third model). We report the out of bag and the six most significant variables for each model. We discuss these findings in Section 4.3.4.

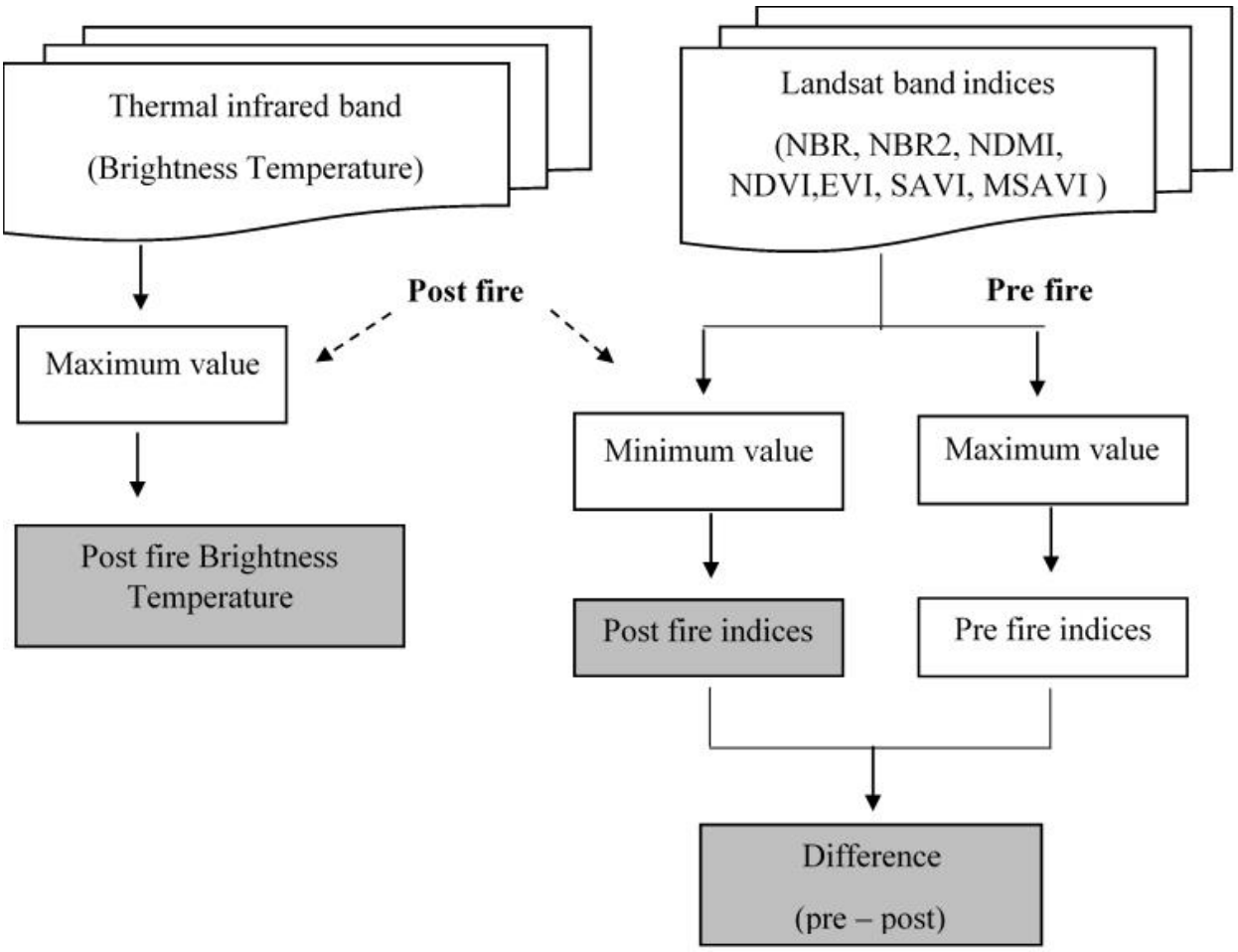

Figure 4-4 Compositing Landsat images to get the input variables for the Random Forest algorithm to separate burned and unburned pixels. Grey boxes represent all input variables used for the algorithm. Abbreviations: NDVI=Normalized Difference Vegetation Index; NDMI= Normalized Difference Moisture Index; NBR= Normalized Burn Ratio, NBR2= Normalized Burn Ratio 2, SAVI= Soil Adjusted Vegetation Index; MSAVI= Modified Soil Adjusted Vegetation Index.

4.2.6 Sentinel 2 and Sentinel 1

Sentinel-2A level 1C scenes, the top-of-atmosphere reflectance, were downloaded from the Copernicus Open Access Hub (http://scihub.copernicus.eu, last accessed January 2019). We used the Sen2Cor processor (downloaded from http://step.esa.int/main/third-party-plugins-2/sen2cor/, last accessed January 2019) to generate Bottom of Atmosphere reflectance images and Scene Classification (SCL) maps. The SCL maps were used to

exclude pixels that were flagged as high probability cloud, water, and saturated or defective pixels. We kept pixels with medium cloud likelihood, thin cirrus, and dark area pixels that have land surfaces visible through thin smoke/clouds.

Due to limited availability of imagery, only three images were used. The first image was acquired in September 2015, which was later defined as pre-fire, although a small number of places had already burned that year. The latter two images, defined as post-fire, were scanned on 23 November and 12 December (two weeks apart, or nearly two to three months after the pre-fire image). We drew some polygons to use for initial classification of burned and non-burned classes. We visually interpreted these polygon regions based on our knowledge of this study site using all pixels in pre-fire and post-fire images to delineate burned and unburned areas. The final burned area map for the whole scene was then classified using only two spectral indices, NBR and NDMI. Both indices were chosen based on our findings as discussed in Section 3. Image segmentation was then used then to derive the map using ENVI 5.1 software.

Indonesia 's 2015 burned area map from Sentinel-1 was available from the European Space Agency for Climate Change Initiatives (http:/www.esa-fire-cci.org/). We downloaded the Geotiff map and clipped out our study area. The map was reliable for Indonesia with an overall 83.85% accuracy (Lohberger et al., 2017).

4.2.7 Reference map and validating points

We used the 2014 burned area reference map from Vetrita et al (2020) cropped to our study site. This reference map was provided by the Indonesian National Institute of Aeronautics and Space (LAPAN) and derived from analyses of SPOT 5 images (Zubaidah, 2017). Following the protocol of the Southern African Fire Network (SAFNet), the images

were manually classified as burned and unburned classes. Of the approximately 50,000 ha areas, 9% had burned in our site by September 24, 2014 (the image date of acquisition).

Due to limited availability of high-resolution images during the 2015 burning event, we were unable to assess the burned area maps using the same approach as the 2014 fire event. Therefore, we evaluated the map classification using 180 field-visited ground truth points (89 burned and 91 unburned locations) that were collected early in November 2015, just before the beginning of the rainy season. Post-fire vegetation regrowth was limited and most of fire scars were still visible.

4.2.3 Accuracy assessment

Confusion matrices were used to define the product quality for both 2014 and 2015. For the 2014 burning event, each product's reliability was quantified using an area-based error matrix to compute the commission (CE) and omission errors (OE) of burned and unburned pixels (Equation 2 and 3, respectively). The SPOT 5 image was relatively clear without any cloud or smoke interference.

$$1\text{-OE}=\frac{\text{BA product and SPOT BA intersection}}{\text{All BA SPOT}} \qquad \text{(Equation 2)}$$

$$1\text{-CE}=\frac{\text{BA product and SPOT BA intersection}}{\text{All BA product}} \qquad \text{(Equation 3)}$$

BA stands for the burned area while OE and CE are omission and commission error, respectively. The products refer to MODIS, Landsat, and VIIRS 375 m gridded active fire (VAF-gridded).

Regression analysis was performed to find the relationship between the proportion of area burned within 3x3 km^2 grid cells (Eva and Lambin, 1998) of BA product and the reference map. We considered this grid size to be more appropriate for a relatively small

areas site rather than 5x5 km^2 that was used in previous MODIS validation efforts over larger regions (Giglio et al., 2018b, Roy and Boschetti, 2009). We had 59 grid cells for making final comparisons. Since the reference burned area map was unavailable during the 2015 study period, we used the combined burned area estimates from all sensors to find the relationship for each sensor. This might be a conservative approach; however, it gives perspective on the relative performance of each sensor compared to the others.

For 2015, we used the field-derived reference points to calculate the overall accuracy. If a ground truth point was located within a radius of two pixels of the estimated area burned/unburned by each product, we classified it as true burning/unburning. This range was chosen to minimize the error due to the difference in product spatial resolution and the size of the actual area burned—some burned areas were large, some were less than 100 ha.

If two or more reference points were located within a buffer, the majority class was selected. However, this condition only affected VIIRS-AF (MODIS was excluded from our assessment because almost zero burns were detected in 2015). Some of our ground truth points were less than 375 m from each other, the pixel size of VIIRS-AF. Therefore, for the VIIRS-AF validation, we first buffered each validating point at a radius of 375 m radius, and then selected the majority class of VIIRS-AF. Of the 180-ground truth point, 75 points were used for the assessment of this sensor. Overall accuracy for each product was defined as the percentage of accurately detected points.

4.2.4 Landsat-based burn history (1997-2015) and associated land cover change

For nearly two decades, Landsat series satellites have enabled a continuous Earth surface monitoring. We generated annual burned areas for this site using the Landsat data

series (TM, ETM+, OLI/TIRS) to explore the issues related to producing the burned area maps we assessed in Section 4.3. When available, two sensors were employed, including the SLC-off Landsat 7, to generate the maps. The products, available at The Oak Ridge National Laboratory Distributed Active Archive Center (ORNL DAAC, https://doi.org/10.3334/ORNLDAAC/1708), consisted of 16 datasets from 1997-2015. In this version, areas burned were estimated using predicted fitted Random Forest models, instead of probability maps, although the results were comparable. The salt-pepper noise of predicted burned areas were then removed using a 3x3 window majority filter.

Burned and unburned training data were largely dependent on visual imaging. During severe fire events or cloud cover, misclassifications were manually corrected (except 2002, 2006, 2009) mainly due to the failure of the quality assurance (QA) layer to remove cloudy/smoky pixels. The 1997 burn map was created from the 1997 - 1998 Landsat images as a continuous burning event during the 1997 El Niño event. There were no burning incidents in 1998, 2008, and 2010. Landsat-based land cover maps are also available for this study site at DAAC to analyze the relationship between fire frequency and land cover change (https://doi.org/10.3334/ORNLDAAC/1838) (Vetrita and Cochrane, 2020b).

4.3 Results

4.3.1 How do the accuracies of MODIS, VIIRS-AF and Landsat burned area products relate to each other and change between fire seasons of different severity?

In 2014, we found that the MODIS burned area (MCD64A1 Collection 6) product accurately detected 52% of burned areas (Table 4-3). Although some burned areas were not detected, likely due to the small size of fires, most of the detected areas were very well

spatially correlated with the SPOT 5 burned reference areas (Figure 4-5). On the other hand, under the extensive smoke cover of the severe 2015 fire season, hardly any burned areas were detected by the MODIS BA product. Conversely, in 2014, VIIRS-AF accurately detected 64% of burned areas, with a commission error nearly identical to that of MODIS (Table 4-3), but VIIRS was not similarly affected by the smoke cover of 2015, detecting >26,000 ha more burning (Table 4-4). Landsat had a very low commission error (0.07) but failed to detect 39% of areas burned in 2014 due to persistent cloud cover and much less frequent imaging than MODIS or VIIRS (Table 4-3).

Combining burned area detections from all sensors resulted in more area burned (142.76%) than the 2014 reference map, mainly due to the coarser resolution of the products (30-500 m) than the reference map (10 m). In 2015, combined detections derived from the passive sensor MODIS BA, VIIRS-AF, and Landsat products still missed 37.36% of the total area burned. Addition of VIIRS-AF and Landsat drastically improved upon the MODIS BA since it barely detected any areas burned during this fire season (Table 4-4, Figure 4-7).

Table 4-3 Burned area (in hectares) product accuracy assessment for 2014

Product	Total area burned	Area intersected	Overall accuracy	Omission error	Commission error
MODIS BA	3656	2393	0.52	0.48	0.35
VIIRS	4429	2944	0.64	0.36	0.34
Landsat	3052	2828	0.61	0.39	0.07
SPOT 5 (Reference)	4612	4612	1.00	0.00	0.00

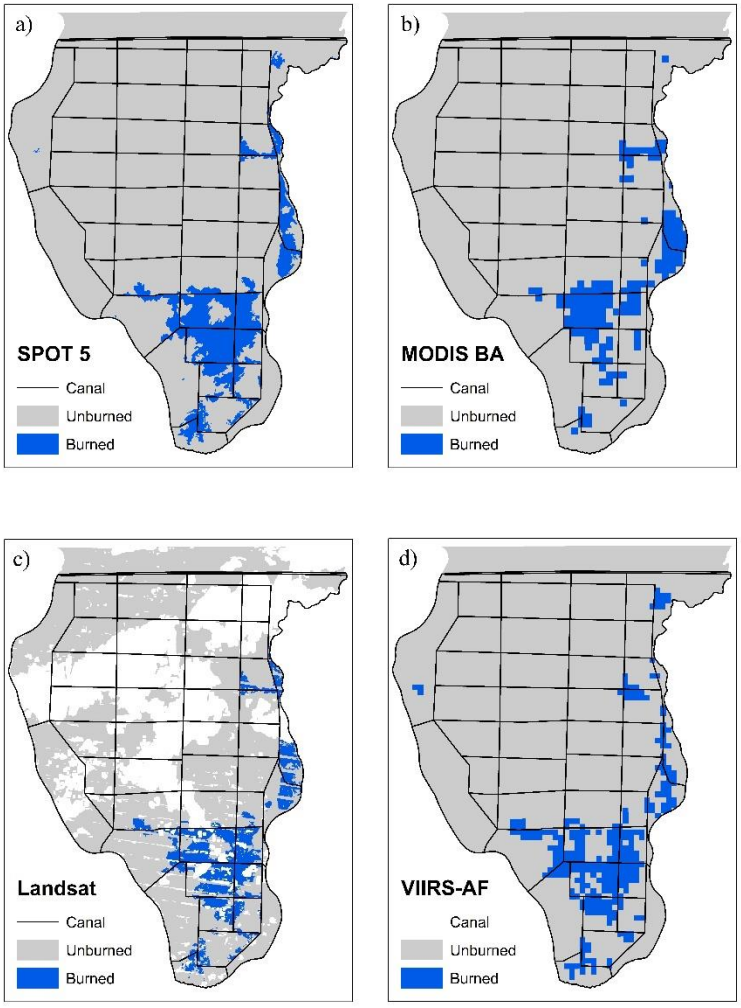

Figure 4-5 Comparison between SPOT 5 burned area map (a) and multiple satellite-based burned area (BA) products, derived during the moderate burning event of 2014 (b = MODIS Terra/Aqua combined BA product; c = Landsat 7 ETM+ and Landsat 8 OLI/TIRS, and d = gridded VIIRS 375 m active fire). Abbreviations: SPOT=Satellite Pour l'Observation de la Terre; ETM+ = Enhanced Thematic Mapper Plus; OLI/TIRS = The Operational Land Imager/Thermal Infrared Sensor; MODIS = Moderate Resolution Imaging Spectroradiometer; VIIRS=The Visible Infrared Imaging Radiometer Suite.

Table 4-4 Total area burned/unburned (in hectares) and the percentage burned for each burned area product in 2015

Product	Total area burned (ha)			Percentage burned[+]	Overall accuracy	Kappa	Number of validation points[++]
	Burned	Unburned	Not imaged[+++]				
VIIRS	26,162	22,029	-	78.6	0.89	0.73	75
Sentinel 2	12,134	19,547	16,510	36.4	0.82	0.64	101
Sentinel 1	28,130	20,061	-	84.5	0.92	0.84	180
Landsat	13,654	24,123	10,414	41.0	0.72	0.45	140
MODIS BA	41	48,150	-	0.1	0.00	0.00	None

[+]respective to combined BA (33,302.37 ha). [++]Of total 180 ground truth locations. [+++] This is due to cloud cover (and/or scan line corrector problems in Landsat 7).

Regressions of VIIRS-AF detections were comparable (R^2=0.94) to that of Landsat (R^2=0.99) but with closer correspondence to the SPOT reference map (slope=0.88 versus 0.64) (Figure 4-6). MODIS underestimated area burned as previously explored by Vetrita et al. (2020) with a less linear distribution (R^2=0.74).

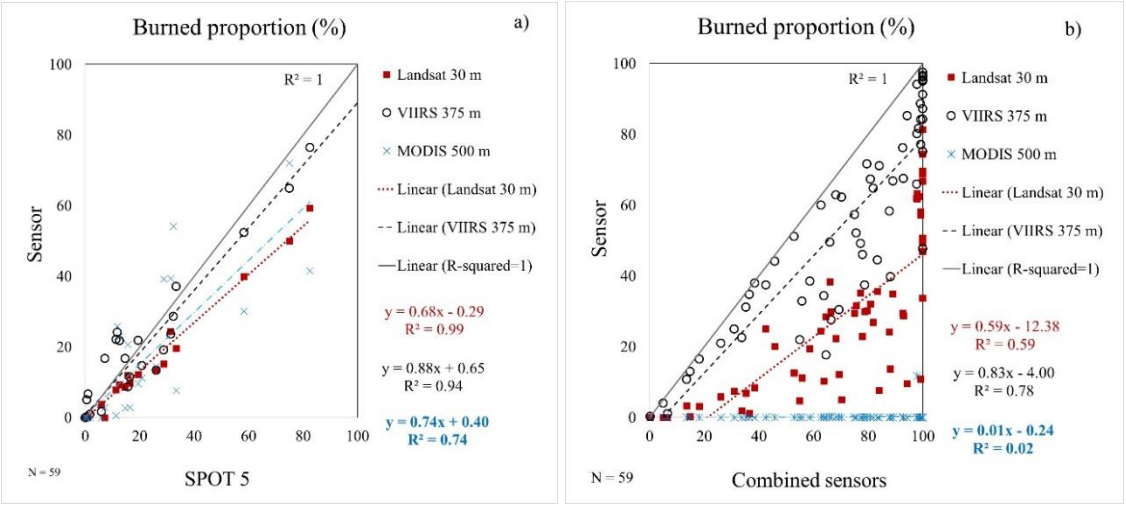

Figure 4-6 Linear regression of the burned area proportions between three satellite-derived burned area maps (Landsat, VIIRS 375 m, and MODIS-MCD64A1) and SPOT 5 in 2014 (a) and combined burned area detected by all sensors in 2015 (b).

4.3.2 To what extent could use of additional available multisensor data (Landsat, gridded VIIRS 375-m active fire, Sentinel-2, Sentinel-1) improve MODIS burned area estimation in peatlands?

In 2014, we investigated the intersections of the MODIS, VIIRS and Landsat burned areas and the SPOT-derived reference map (Figure 4-7a). For 2015, we investigated relationships between burned areas of individual sensors against the combined product of all sensors since no validated burned area map was available, but 180 field-based burned area points helped validate the various products. Figure 4-7b shows the comparisons and relative contributions of the MODIS, VIIRS and Landsat products used in Figure 4-7a. Figure 4-7c illustrates the potential unique burned area detections of each of the passive sensor systems (MODIS, VIIRS, Sentinel 2, Landsat) and the Sentinel 1 active sensor in comparison to an integrated burned area map from all products. Note, Sentinel 1 and 2 data were not available for 2014.

Of the 4,612 ha burned in 2014, only about 25% was detected by all three sensors and another ~45% by some combination of two sensors. The remaining 30% was detected by only one of the sensors with roughly 10% each from Landsat, MODIS BA and VIIRS-AF (Figure 4-7a). In 2015, MODIS BA only detected 41 ha of burning due to the persistent smoke and clouds so almost all detections were by VIIRS-AF and or Landsat. Figure 4-7b shows that over 40% of burned area came uniquely from one sensor, with over 30% from VIIRS-AF alone. The area commonly detected by all three sensors is too small to show on the figure.

In 2015, Sentinel 1 and 2 data became available for potential burned area mapping. A combined product from the five sensors indicates that 69.1% of the nearly fifty thousand hectares study area burned in 2015. Nearly half of the burned areas were detected by 3 or more sensors, while less than 20% were only detected by a single sensor. Sentinel 1 and VIIRS-AF were the greatest contributors of unique detections (Figure 4-7c).

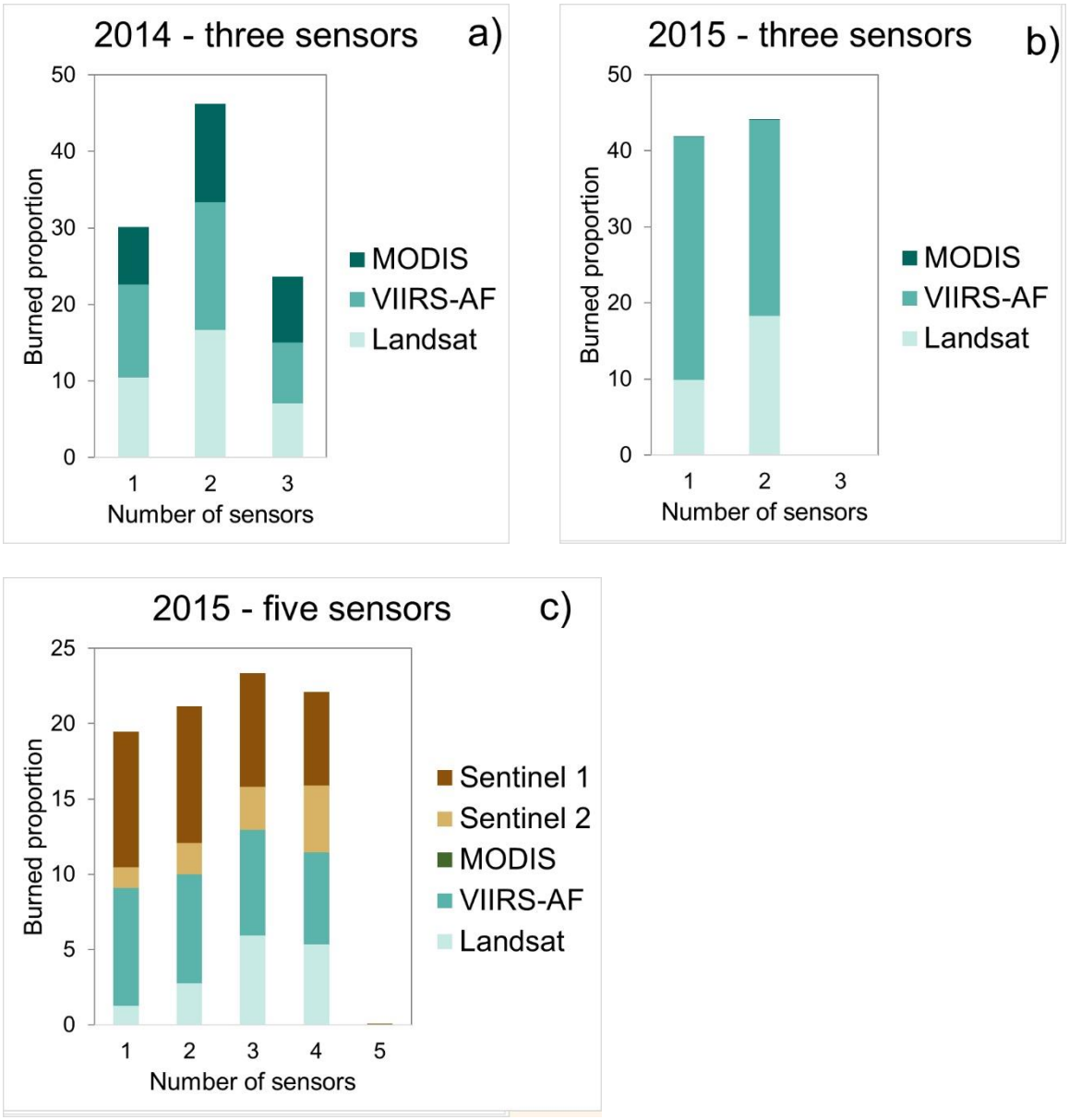

Figure 4-7 Burned area proportion contributed by each sensors uniquely or common areas between sensors. (a) burned proportion detected by Landsat, VIIRS-AF, and MODIS respective to total area burned in the validated SPOT 5 reference map in 2014. (b) the same comparisons but with respect to the combined BA of the three sensors in 2015. (c) burned proportion comparisons when Sentinel 1 and 2 sensors are added for 2015. Abbreviation: VIIRS-AF= Visible Infrared Imaging Radiometer Suite 375 m gridded active fire; MODIS= Moderate Resolution Imaging Spectroradiometer.

Figure 4-7 shows the combined and individual sensor-detected burned areas for 2015. Heavy smoke and clouds impacted optical sensor mapping of burned areas, nearly

completely disabling the MODIS BA product. Although smoke and clouds limited the observable area for both Landsat and Sentinel 2 and reduced available field validation points to 140 and 101, respectively, the overall accuracies of the imaged areas were 72 and 82%. The active radar system of the Sentinel 1 satellite was not inhibited by smoke and clouds and also had an overall accuracy of 92%. Despite not being an actual burned area product, VIIRS-AF benefitted from frequent imaging (daily) and had a greater overall accuracy (89%) than the other optical sensors, however, its larger pixel size limited the number of validation areas to 75 since multiple field points sometimes existed with a single pixel footprint.

Sentinel-1 was the most prominent sensor available to map the areas burned (84.5%) in 2015 for this site. Although, combining all the other sensors added >15% more areas possibly burned, much of it might be produced by the larger pixel sizes of each product than that of Sentinel-1. Sentinel 1 BA was limited, however, by late dry season rainfall that saturated the soils and made the sensor unable to observe subsequent burning, although peat fires could still have been ongoing. Landsat, Sentinel-2, and VIIRS-AF were unaffected by the soil moisture and able to observe burned scars after the onset of rains, depending on cloud or smoke cover (see examples in Figure 4-2 and Figure 4-12). In 2015, Landsat and Sentinel-2 mapped a total burned area roughly half of that detected by Sentinel-1 but 22-34% of these areas were misclassified due to cloud/smoke effects.

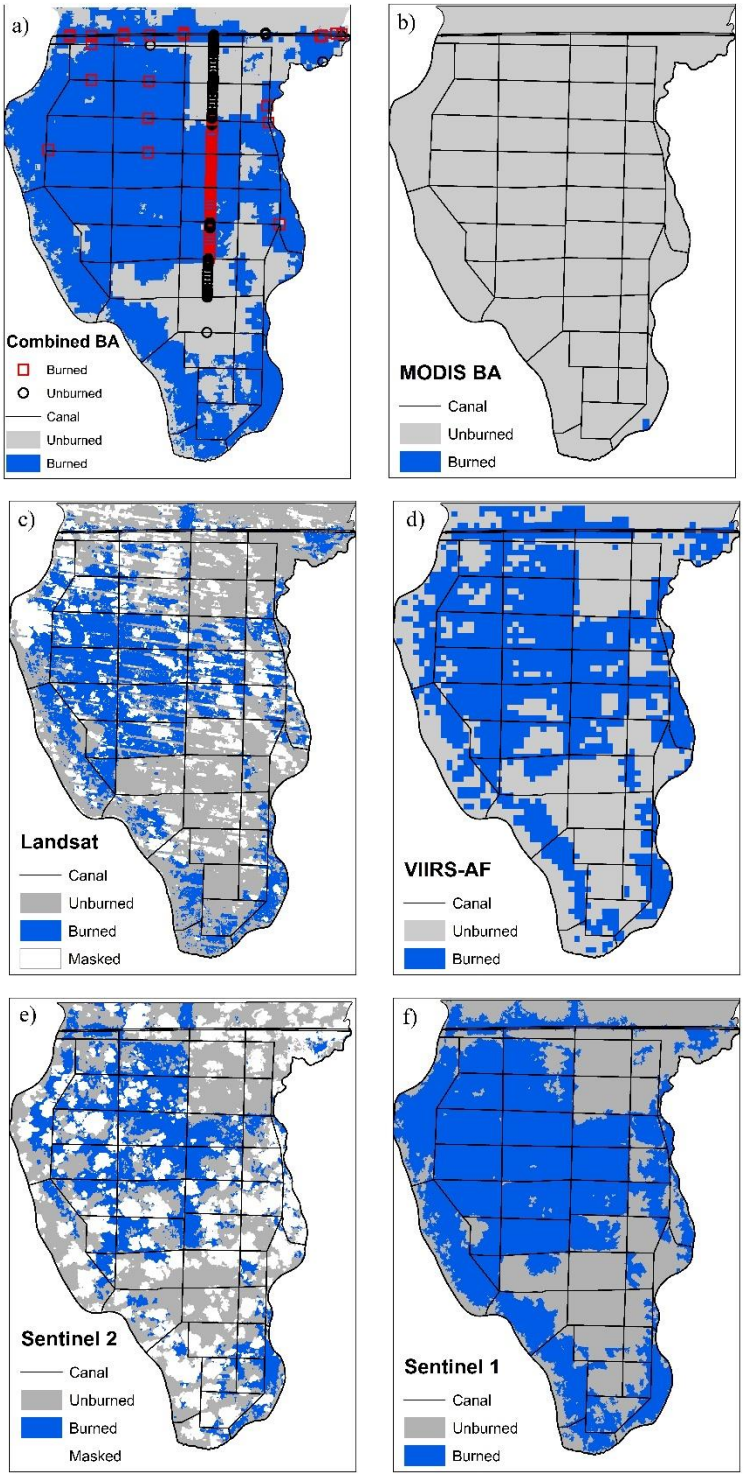

Figure 4-8 Combined burned area (BA) from all (a) and individual sensors (b-f) during the severe burning event of 2015 (b = MODIS Terra/Aqua combined product, MCD64A1 Collection 6; c = Landsat 7 ETM+ and Landsat 8 OLI/TIRS; d = Gridded VIIRS 375 m active fire (VIIRS-AF); e = Sentinel 2; and f = Sentinel 1). Areas obscured by cloud/haze (white). Abbreviations: SPOT=Satellite Pour l'Observation de la Terre; ETM+= Enhanced Thematic Mapper Plus;

OLI/TIRS= The Operational Land Imager/Thermal Infrared Sensor; MODIS=Moderate Resolution Imaging Spectroradiometer; VIIRS=The Visible Infrared Imaging Radiometer Suite; NBR= Normalized Burn Ratio; NDMI=Normalized Difference Moisture Index).

The gridded VIIRS 375 m active fires show sustained burning throughout the season, indicated by a persistent number of active fires and high Fire Radiative Power (FRP) accumulation during the burning period (Figure 4-9a-d). In 2015, fires began in early August from several places on the river boundaries of the peat dome where villages are located (Figure 4-9e blue) and along canals where people have easy access to the peatlands. However, sustained burning, indicated larger numbers of active fires or high FRP accumulation, were found in more central areas of the peatlands. This indicates widespread and intense burning of peat dome areas during this fire season. Usually, fires are mostly limited to the drier canal banks and can not spread to moister areas away from canal banks. However, during intense droughts, remote areas and deeper peat burning may occur.

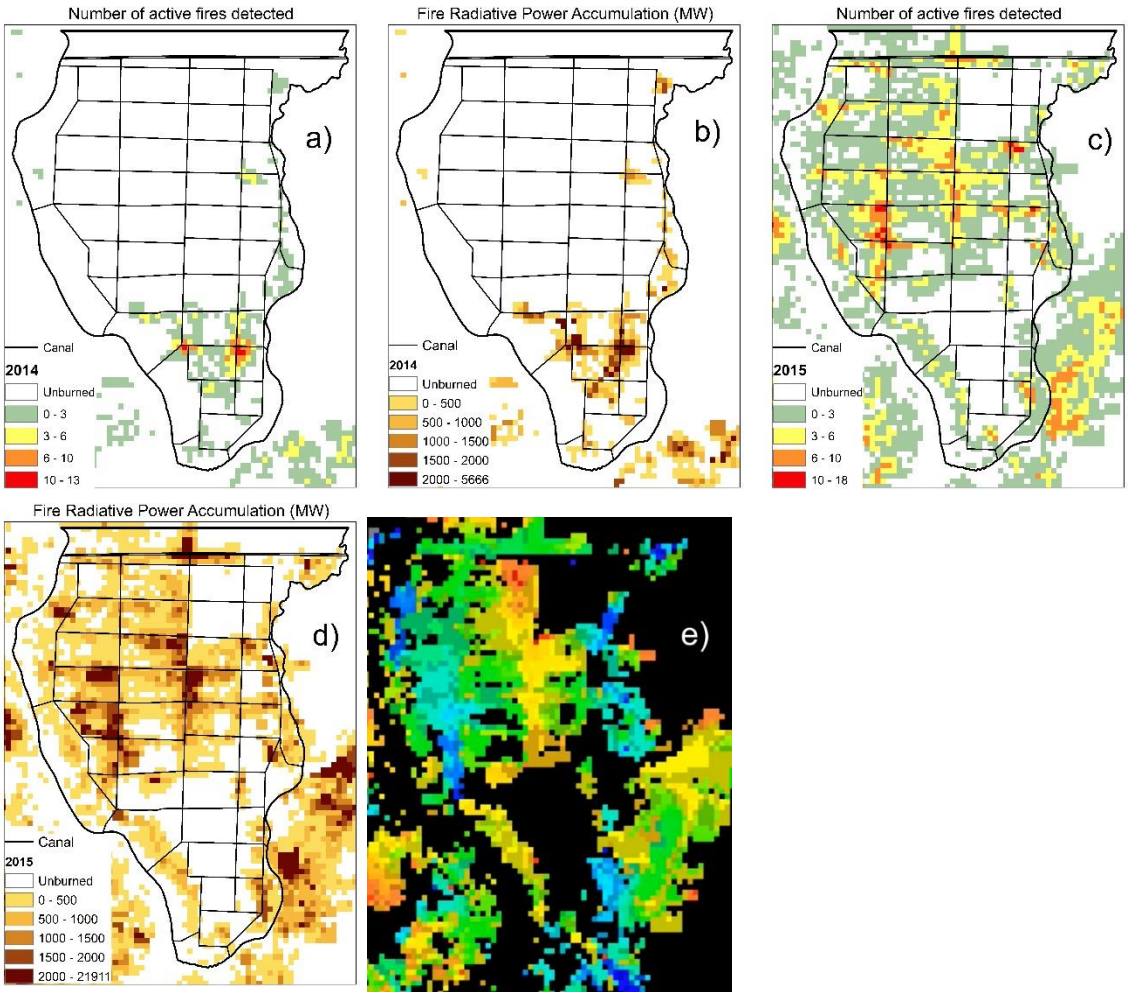

Figure 4-9 Number of VIIRS 375 active fires detected (a and c) and fire radiative power (FRP) accumulation (b and d) during 2014 and 2015. The highest number of active fires (red) and FRP (dark brown) are found along canals. In 2015 (e), fires began from several places (blue) near villages along rivers bounding the peat dome and spread more widely over time as the drought intensified.

4.3.4 Landsat-based burned area detection and the important variables

In our cross-validation of the classification, we found that the Out of Bag (OOB) estimate of error rate was comparable in 2014 and 2015 when all available images were used until the end of the year (2.6 % vs. 2.8%), but had a much higher rate (8.8%) when the Landsat images were restricted until the same date of SPOT 5 acquisition (first model). The probability maps for the two 2014 maps are shown in Figure 4-10. We found that the

first model had suffered from smoke (white color represents the unavailable Landsat pixels). It also decreased the predicted probability of the area being burned.

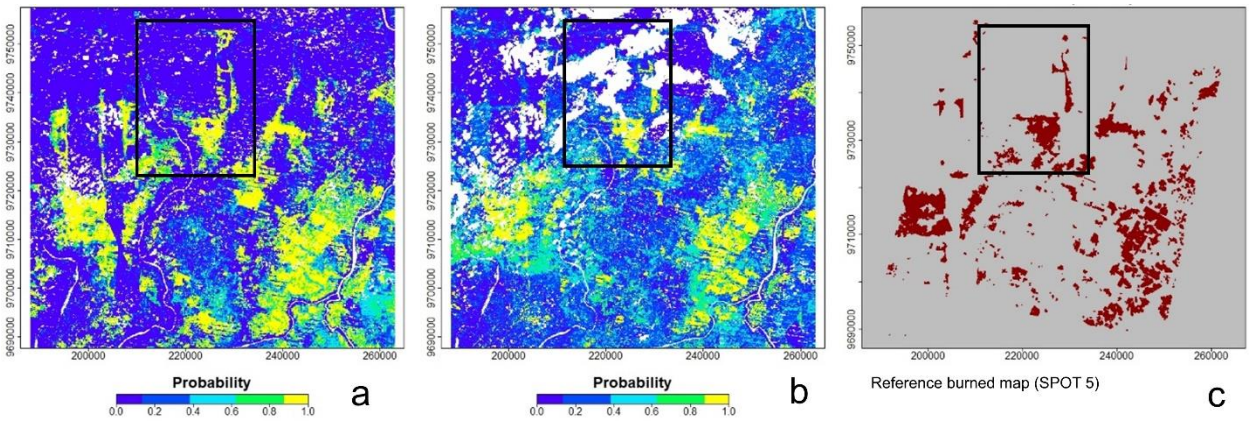

Figure 4-10 The 2014 burned area maps derived from the full year of available images (a) and restricted to the same date of acquisition of SPOT 5 (b) which can be compared to the 2014 SPOT 5 reference map (c). Black rectangle shows the study site. We found that those with less images (b) had suffered from smoke (white color represents the unavailable Landsat data). It also reduces the predicted probability of the region being burned (see b and c for comparison).

Of the three models run using Random Forest, we found that the post-fire NBR2 image and the pre- post-fire difference (denoted as 'd') of NBR image were the two most important variables agreed upon by all models (Figure 4-11), regardless of time span of imagery constraint. When the time span was extended to all available images through the end of the year, models for both years' fire seasons agreed on the utility of dNDMI and NBR (Figure 4-11b-c). MSAVI (model 1) and EVI (model 3) were the only two variables unique to an individual model. The two models are both from 2014 and correspond to the short- (date of SPOT 5 imagery) and long- (end of year) timespans of imagery collections (Figure 4-11a, and 4-11c).

a)

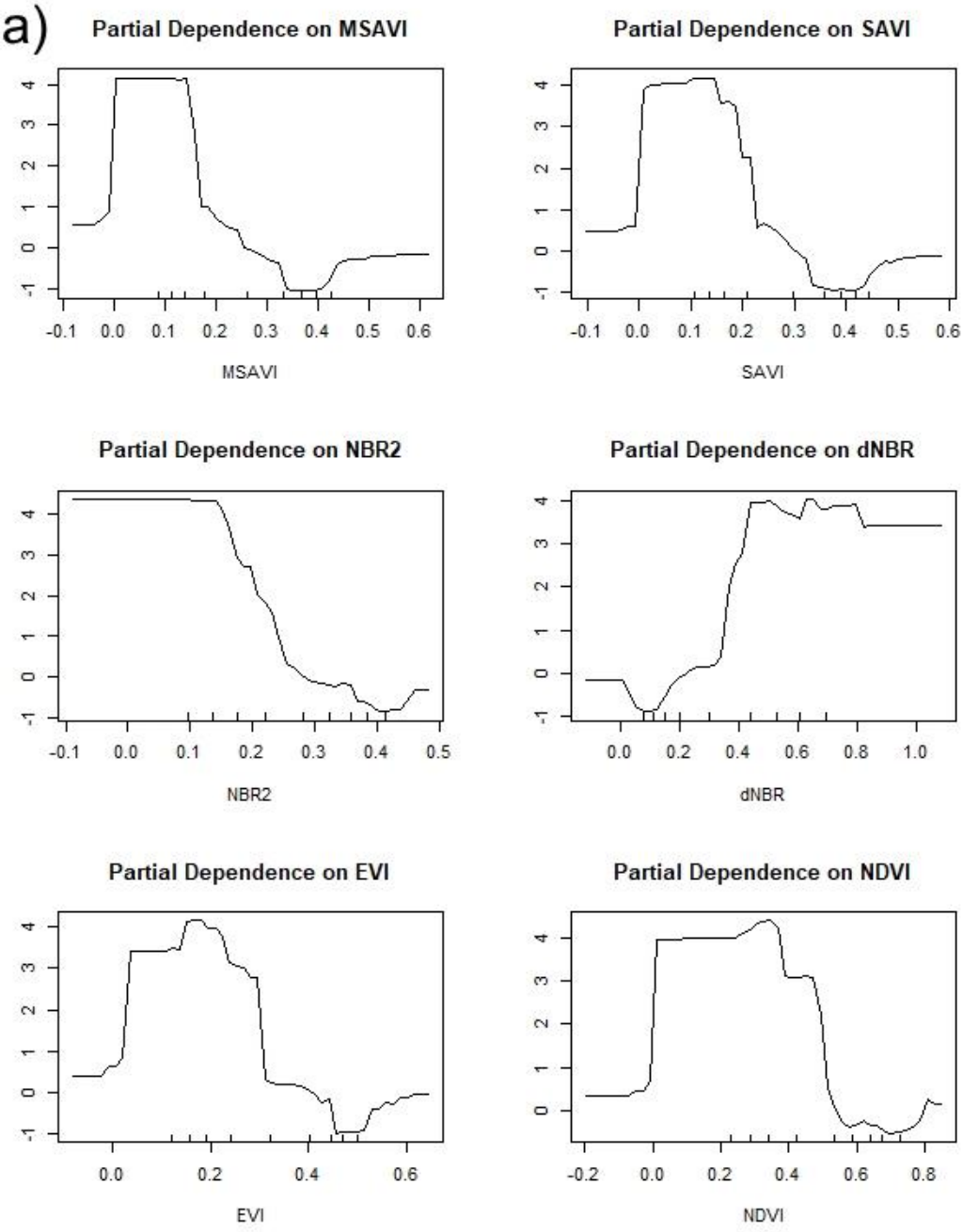
Partial Dependence on MSAVI
MSAVI
Partial Dependence on SAVI
SAVI
Partial Dependence on NBR2
NBR2
Partial Dependence on dNBR
dNBR
Partial Dependence on EVI
EVI
Partial Dependence on NDVI
NDVI

b)

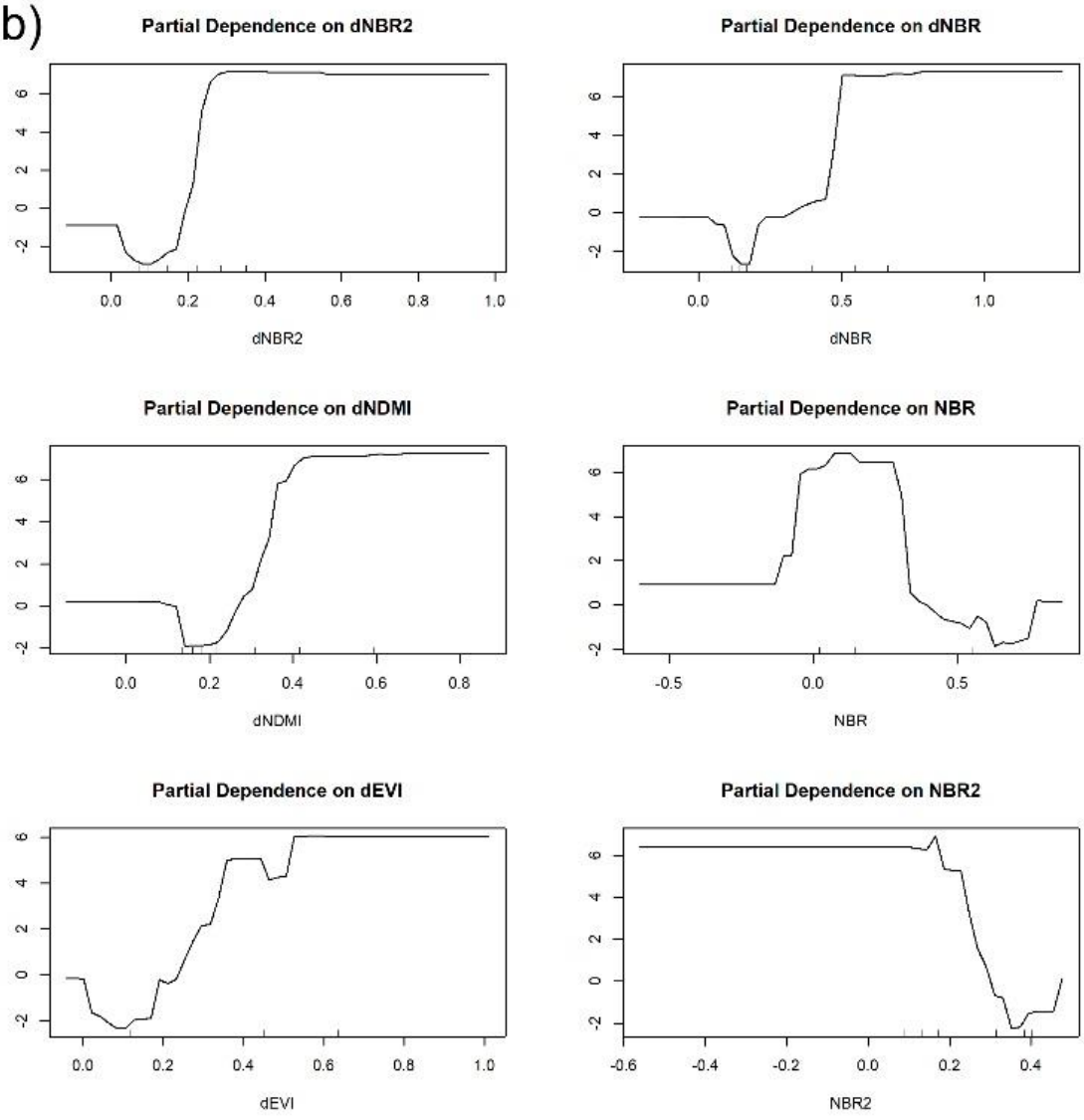
Partial Dependence on dNBR2
dNBR2
Partial Dependence on dNBR
dNBR
Partial Dependence on dNDMI
dNDMI
Partial Dependence on NBR
NBR
Partial Dependence on dEVI
dEVI
Partial Dependence on NBR2
NBR2

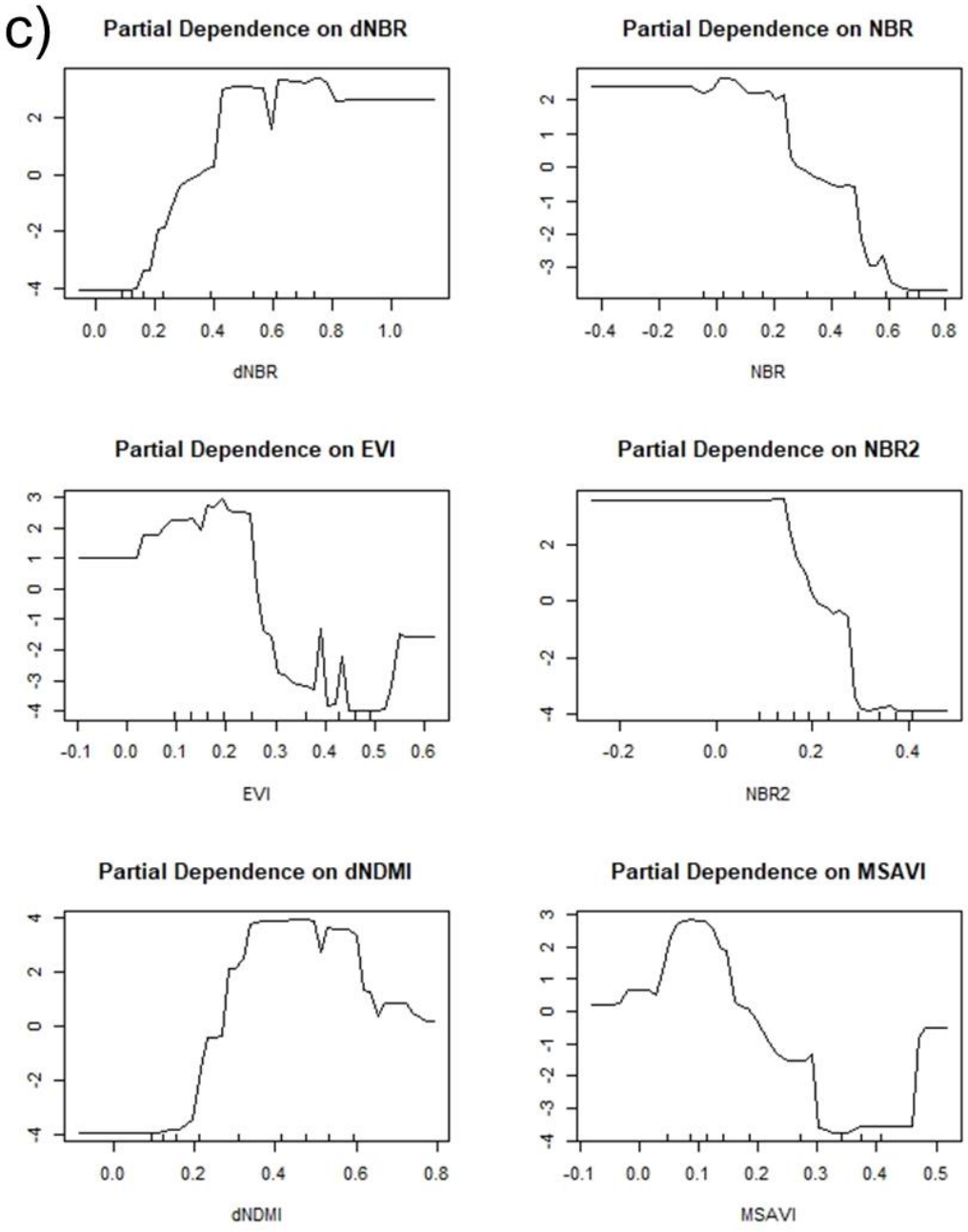

Figure 4-11 Partial dependency plots built from Landsat-derived burned area maps, based on the timespan of images selected for the input variables of the R package Random Forest Model: a =2014 (a, the selected images for the 2014 map were restricted to the closest SPOT 5 (reference-derived burned area map) acquisition date (24 September 2014); 2015 (b) and c (2014) were burned area derived from all images available until the year-end of each season. The plots display the top six significant variables distinguishing between burned and unburned classes: for 2014 (a) = MSAVI, SAVI, EVI, NDVI, NBR2, dNBR ("d" refers to the pre-and post-fire difference index;

without “d” means the post-fire image); 2015 (b) = dNBR2, dNBR, dNDMI, NBR, dEVI dSAVI; and for 2014 (c)= dNBR2, dNBR, dNDMI, NBR, dEVI, and NBR2. Y-axis represents the logit probabilities of burn class. Positive values of the y-axis mean that the burn class is more strongly predicted by the model variable while value≤0 means no average effect on the probability of burn classes. The larger the range, the stronger the overall impact.

4.4 Discussion

In this section, we discuss 1) the significance of using multisensor data and the effects of fire season severity on mapping areas burned; 2) lessons learned from deriving a Landsat-based burned area detection process and important variables to detect burn pixels; 3) the fire history and related land cover type at the study site, 4) satellite-based active fire (hotspot), burned area mapping, and their impact to the carbon emissions estimates; and finally 5) future directions for national burned area mapping.

4.4.1 The significance of using multisensor data and the effects of fire season severity effect on mapping areas burned

We have demonstrated how use of multisensor data could advance biomass-burning detection in peatlands of Central Kalimantan, Indonesia for fire seasons of different severity. Our findings are consistent with Humber et al. (2019) who concluded that burned area accuracy detection varies temporally. In tropical peatlands, where smoldering fires frequently dominate the fire-related emissions, small fire sizes and persistent cloud cover reduce the capabilities of optical sensors (e.g., Landsat and Sentinel 2) to map burned areas despite having much higher spatial resolutions than MODIS BA. Even with near-daily imaging, MODIS BA detects less than 50% of burned area during moderately severe fire season conditions and much less during severe fire seasons. Although the gridded active fire information provided by VIIRS-AF does not provide a real surface change map, as the

other sensors are capable of, this product alone can be a good approach for quickly mapping burned area, particularly during severe smoke/haze events. Among the other sensors, Sentinel 1 was superior during the extreme 2015 burning season, when conditions were considerably drier than during normal-moderate burning seasons. Combining information from all sensors improved MODIS BA detection significantly in 2015 (MODIS BA barely detected any areas burned during this fire season) and also substantially increased detection accuracy for 2014. These findings reveal that combining multiple satellite sensor imageries can improve burned area detection, specifically where and when extensive cloud cover and smoke from smoldering duff/peat consumption (ground fires) dominates.

Our results revealed that no single sensor is optimal for the accurate detection of fires in peatland. Sentinel 1 was unique, as seen in the incident of 2015. However, with its sensitivity to soil moisture, it may be a source of error during normal or wet conditions when sporadic rainfall events are not uncommon. Further research and assessments of burned area detection using Sentinel 1 imagery need to be undertaken for other fire seasons and different land cover or different fire regimes. The algorithm used here (Lohberger et al., 2017a) was accurate for Indonesian peatland but underestimated burning in Africa (Lohberger et al., 2017b).

VIIRS-AF was the next greatest contributor of unique detection beside Sentinel 1. However, this approach was a less accurate method for mapping actual areas burned due to VIIRS coarser resolution (375 m) than the other sensors. Therefore, combining results overestimated area burned, compared to the SPOT 5, in 2014. This indicates that caution should be used when interpreting coarser resolution burned area datasets, especially where smaller burn sizes predominate. Another concern with using this product is its inclusion

of ‘fire’ pixels from non-biomass sources (e.g. gas flares or volcanic activity) since the product was not designed for mapping only biomass burning. Masking such areas from available products should be done.

Multi-temporal images from multiple sensors allowed us to monitor how and in what direction burning spread over time. Burn directionality was not Each sensor has some capability to complement the others, making these datasets promising for detecting and characterizing peatland fires (see Figure 4-12). This approach reveals that the 2015 burned area map published by the government underestimated area burned by roughly 50% (Figure 4-12a), primarily due to limiting analyses to visual interpretation of a single sensor (Landsat 8; Figure 4-12d) which had no availability at the end of the fire season. From our analyzes of imagery from the various sensors, we found that Sentinel 1 may have slightly overestimated burned area in 2015. The black rectangle shown in Figure 10f highlights the one area of burning detected uniquely by the Sentinel 1 sensor (Figure 4-12h). However, area was open land, bare since May 2015, and had no signs of burning before October 14, 2015 (as the last date of Sentinel 1 only included the scanned of October 24, 2015) (Figure 4-12h). Since no other instruments corroborate either fire or burned area, this area was unlikely to have burned, especially since it was bare land.

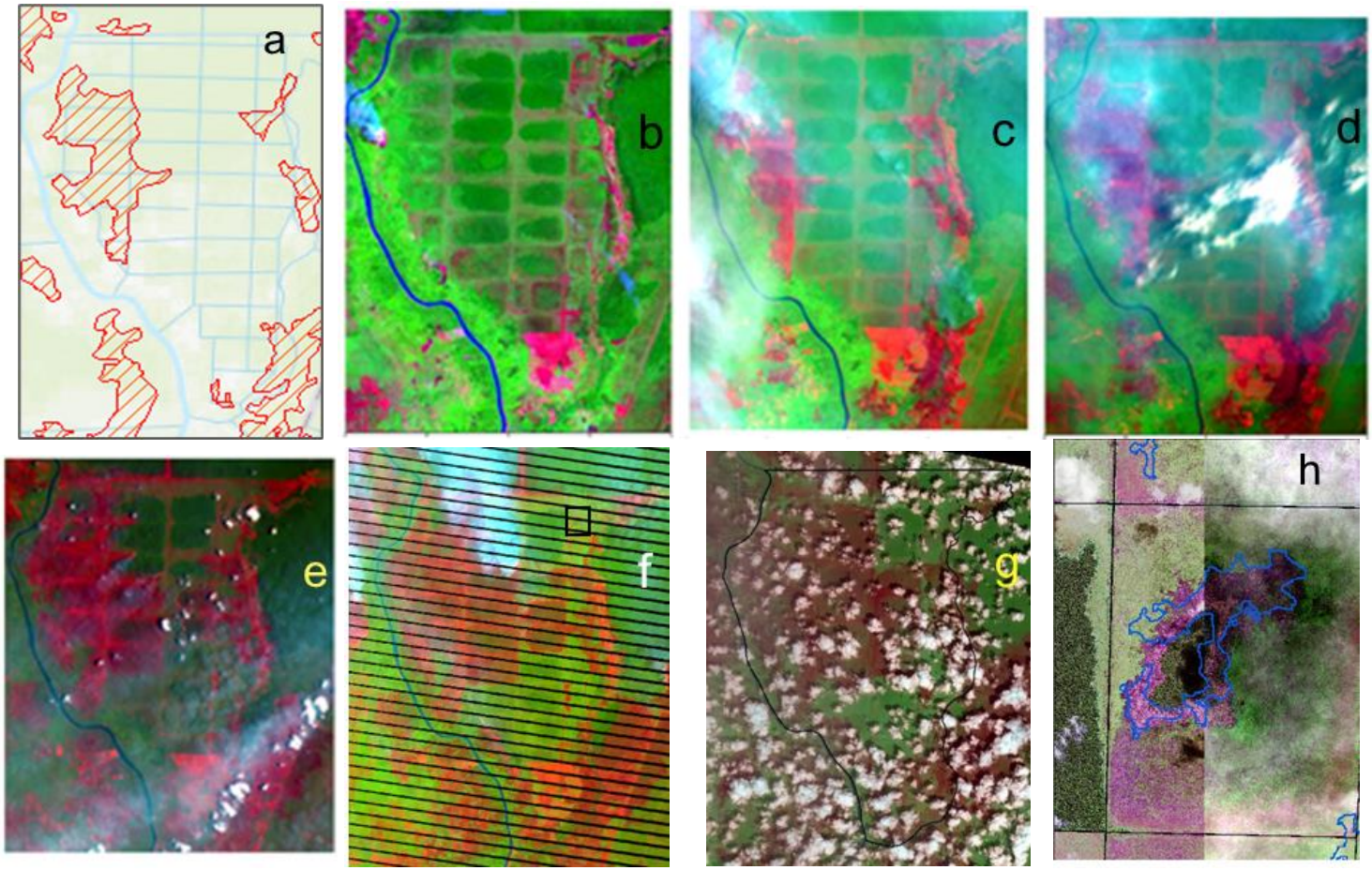

Figure 4-12 (a) Screenshot Landsat-based burned area (not scaled with other images, viewable at http://webgis.menlhk.go.id:8080/kemenhut/index.php/id/peta/peta-interaktif) published by the Indonesian authority (the Ministry of Environment and Forestry) in 2015, and burning progress shown by sequential dates and sensors. All images are displayed as RGB composites of surface

reflectance bands (shortwave infrared, near infrared, red bands) with image enhancement to accentuate burn locations (b= Landsat 8 OLI, 08/19/2015; c= Sentinel 2,09/14/2015; d=Landsat 8 OLI, 09/20/2015; e=Sentinel 2, 10/04/2015; f=Landsat 7 ETM+, 10/14/2015; g= Sentinel 2, 11/23/2015; h=WorldView-2, a left-right mosaic of twoimages, 05/15/2015 and 04/15/2015). (h) area corresponds to the black rectangle from image (f), showing the isolated area where only Sentinel 1 indicated burning. The area was cleared bare land months before the apparent burning occurred. Due to smoke/haze (bluish color) or cloud conditions (the white puffs, scattered without a cone shape), the color displayed in each image may not be the same. In general, the dark red/magenta shows burn scars in the Landsat and Sentinel 2 images.

4.4.2 Long-term Landsat-based burned area detection, important variables to detect burn pixel: a lesson learned

Landsat-based BA mapping allowed us to assess a long-term fire history from 1997 to 2015. In 2015, combined data from all sensors show that roughly 68% of the nearly 50,000 ha study area burned. Landsat alone only showed ~27% having burned but 21% of the study area was never imaged due to heavy smoke and cloud cover (Table 4-5). Similar to 2015, severe burning followed by a thick smoke restricted available cloud free imagery in 2002, 2006, and 2009, and 2015, preventing detection of burned area in many locations. We found that the cloud mask product failed to remove the thin clouds which affected the pre- and post-images during layer compositing. Multitemporal image compositing was needed to obtain a cloud-free imagery due to persistent clouds in this area. This technique strongly reduced the radiometric variability of a time-series of satellite data induced by changes in atmospheric conditions and viewing/illumination geometry (Stroppiana et al., 2002). Our technique used the minimum NBR (for post fire image) and maximum NBR (for pre-fire image) which is in line with the above concept. In addition, defining the training samples was also critical and challenging. The model was rerun by adding some samples until the errors were reduced.

The random forest model found that NBR and NBR2 images were the greatest contributors to Landsat-derived burned area maps. This result is unsurprising since NBR has been the most used index (Escuin et al., 2008; Huang et al., 2016) for discriminating burned from unburned pixels. Hawbaker et al (2017) also considered

NBR2 one of the most important contributing variables for the Landsat-derived BA map of the United States. The unique indices found to be important in both 2014 models (EVI and MSAVI) were likely the result of cloud pixel contamination. Considering the higher error rate of OOB for the 2014 first model (Figure 4-11a), the results might be less robust.

4.4.3 Fire history and related land cover type at the study site

Since the study area was made accessible by construction of an extensive network of drainage canals, fire has become the biggest threat to protecting native vegetation. The drainage through the canals has altered the peat hydrology and much of the original forest has been cleared or degraded (Graham et al., 2017). Most of the site has been progressively burned over the last two decades (see Figure 4-13), making this area ever more vulnerable to recurrent fires. Forest cover at the study site was 84% (Figure 4-13a) prior to the MRP, but intact peat swamp forest (PSF) had fallen to only 13.4% at the beginning of 2015 before the severe El Niño fires and was merely 6.3% by 2019 (Figure 4-13b). Fortunately, no major fire events have occurred since 2015, despite the extremely low amount of precipitation in 2019 (Figure 4-3). Between 1997 and 2015, ~91% of the study site was affected by burning at least once. Some areas have burned >5 times (up to twelve), with the majority located along the canals.

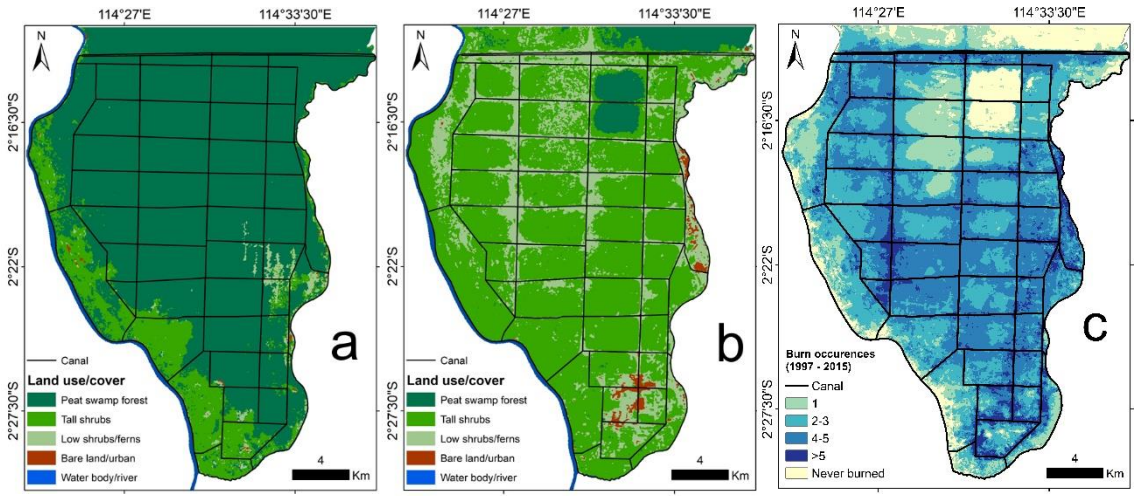

Figure 4-13 Land use/cover map of the study site in 1994 (a), 2019 (b), and the Landsat-derived burn occurrences from 1997 to 2015.

4.4.4 Satellite-based active fire (hotspot), burned area mapping, and their potential impacts on carbon emissions estimates

Fires in Indonesian peatlands have continued to occur over the last two decades, although there is evidence of a decrease after 2007 (Vetrita and Cochrane, 2020a), mostly due to the establishment of agricultural areas. Prior to 2015, the Indonesian government recorded only rough estimates of the total annual area burned, with no spatial information about where and how the fires spread. Indonesia has committed to providing burned area maps, beginning in 2015, but they are limited to imagery from a single sensor (Landsat 8 OLI), with additional active fire (widely known as hotspot) data used for interpreter and verification guidance. This approach is labor-intensive, expensive, and time-consuming. Additionally, the abilities of interpreters could be a source of uncertainty.

From mid-1996, NOAA AVHRR active fire data started being used for national and operational fire observations. The government began incorporating MODIS hotspot observations from the Terra and Aqua platforms in 2002. Albar et al., (2018) found that

NOAA's AVHRR and Terra/Aqua satellites data were valuable for creating new hotspot tracking information. The usage of hotspots as an effective fire suppression method was on the rise in the region. In Indonesia, hotspot data has been the primary source for early warning systems about fire and also been used in policy guidance. For example, prior to 2015, the accumulation of hotspots was used as a performance measure for various stakeholders, even though numbers of hotspots can be misleading, as they do not reflect the overall incidence of fire (Directorate of Forest and Land Fire Management, 2015). With knowledge that hotspots do not provide a solid base for decision-making, it has been recognized that the reliable provision of higher-resolution burned area mapping is crucial for indicating government performance in the 2020-2024 plan (The Indonesian Minister of Environment and Forestry, 2020).

Indonesia also incorporates hotspot monitoring from VIIRS (NOAA-20 and S-NPP satellites), which are successors to the MODIS (Terra, Aqua) sensors. VIIRS active fire products have been used nationally since 2017 (750 m) and 2019 (375 m). All such data is released by the Indonesian National Space Agency (LAPAN), which has authority over data collected from space-based satellites. The data has been implemented and published in forms designed to be easy to use by policymakers, researchers, the public, and firefighters (http://lowres-catalog.lapan.go.id/monitoring/, last accessed on 20 December 2020).

The gridded hotspot approach for burned area mapping has been used to calculate carbon inventories using MODIS active fire data (FREL 2016). However, because the 1 km^2 pixel footprints from hotspot detections overestimated the actual area burned, the resulting estimate for peat fires was omitted from the report. Active-fire-based burned area

mapping can be a large source of uncertainty in calculations of national carbon emissions estimates. The Indonesian calculations were biased since detected fires are often much smaller than the hotspot pixel size (e.g. 1 km^2 = 100 ha). In peatland and surrounding portions of Indonesia, most fires were found to have patch sizes of <100 ha, or even <25 ha (Vetrita et al., 2020). VIIRS 375 m (~14 ha) has finer spatial resolution for both day and night active fire detection (Schroeder et al., 2014, Schroeder and Giglio, 2018)). Our research has corroborated previous findings (Oliva and Schroeder, 2015) that VIIRS 375 m active fire offers an alternate source of knowledge for the near-real-time mapping of fire-affected areas in peatlands. These advancements in rapid mapping of fire occurrence and spread are more accurate than MODIS (1 km^2). However, numerous fires smaller than the VIIRS pixels (14 ha) can still lead to overestimates of area burned. Several carbon emissions models have used active fire in their methods (for example: GFAS (Kaiser et al., 2012)).

This study has shown that burned area estimations based solely on surface change methods from optical satellite imagery, is decreasingly reliable as the amount of burning increases. For example, in extreme cases when large areas of persistent burning occur, ubiquitous smoke and cloud cover can disable algorithms designed to map burned area, even though hotspots, especially from VIIRS, still show areas that are burning.

A study that compared several emissions models found that GFASv1.2 provided more reliable information for PM2.5 smoke detection during the 2015 Indonesian peat fire event in 2015 than other models (GFEDv4, FINNv1.5, QFEDv2.5r1, and FEERv1.0-G1.2) (Liu et al., 2020). VIIRS Active Fire (375 m) has created new opportunities to consider for the use of this data in similar models (e.g., MODIS

Blended Global Biomass Burning Emissions Commodity, VIIRS 750 m, and GBBEPx Geostationary Satellites; Zhang et al. 2014) or other regions than peatland (Li et al., 2020).

Tropical peat fires have been treated differently in some emission models, assuming that all fires in peat have substantially higher emissions than non-peat fires. Our studies (Vetrita et al., 2020) have shown that the most prevalently used MODIS-derived product (MCD64A1) can introduce great uncertainty to fire-related carbon emissions from the peatlands since it can miss 50% or more of the area burned. Another potential source of error in emissions estimates is from the lack of fire frequency analysis necessary to show where and when recurrent fires are happening. Lohberger et al. (2017) integrated recurring fires into their calculations and found lower regional emissions than that estimated by the GFED4 emissions model. GFED4 reported almost double the amount of emissions for Indonesian fires in 2015 (1.75 vs. 0.89 Gt CO_2e) despite using the low amount of burned area from the MODIS burned area product in the analysis.

4.4.5 Future direction

The goal for all users is to have burned area maps that have quick image processing methods and easily interpretable results that are accurate. The next few paragraphs discuss some of the relevant problems in creating such a system.

To date, the Indonesian government has been using visual detection methods to produce the burned area maps, but this is costly, labor intensive, and time consuming. An increasing amount imagery from relevant satellite sensors now becoming easily available. These data improve potential capability for conducting frequent measures of landscape

change (e.g. burned area mapping) at moderate resolutions, and build upon the decades of historic data that NASA's Landsat missions have provided (Wulder et al., 2019, Loveland and Dwyer, 2012). Landsat 8, which is currently active and operating as designed, will soon come to an end of its planned period of operation. Landsat 9 (expected to launch in 2021) and Landsat 10 will extend the provision imagery comparable to Landsat 8 for years to come. As a result, there is no foreseeable data gap in Landsat Earth observation. Even so, complementary data sources are very important redundancies that can be critical if any future problems such as loss of satellites (e.g. Landsat 6) or sensor errors (e.g. Landsat 7 SLC) arise. The Indonesian government utilizes Landsat 8 OLI for their monthly burned area product. While this material was being written, an anomaly occurred with the Landsat 8 satellite on November 1, 2020. This fault disabled image acquisition from the satellite for an anticipated period of 1-3 weeks. During such critical situations, other comparable data are needed. The ESA Sentinel program (http://www.esa.int/Applications/Observing_the_Earth/Copernicus/Overview4, last accessed 20 December 2020) provides both optical satellite data similar to Landsat (Sentinel 2) and active radar sensor data (Sentinel 1).

Over the last two decades, techniques of burned area mapping have improved from simple use of change detection, either using a single spectral index or a multi-temporalcomparison to the use of artificial intelligence (e.g, machine learning, deep learning) (Chuvieco et al., 2019). Although Random Forest (RF) modeling has been found to be reliable for mapping burned area (Roteta et al., 2019, Roy et al., 2019), this does not mean it will work for all circumstances. Ramo et al. (2018) found that RF was the best algorithm to map global MODIS-derived indices, but the result was less accurate than the

MODIS burned area product (MCD64A1). This shows that not only a reliable method was needed, but also variables or image selection, and training samples were critical. Here we highlight several important indices to map the areas burned in Indonesian peatland, (i.e., NBR, NDMI, and NBR2) that were similar to what Ramo et al (2018) used.

One of our experiments used object-oriented image analysis and two Sentinel-2 band indices (NDMI and NBR) or Landsat, which showed comparable results, regardless of cloud and smoke conditions in the images that were used. However, more experiments will be needed to determine which, if any, method(s) is readily applicable and reliable for depicting landcover change across Indonesia. The choice of optimal methods can be dependent on the time constraints for providing the required products (e.g., near real time, monthly or annual map) must also be addressed.

A perennial problem for optical imagery analyses is acquisition of cloud-freescenes. Thefore, image compositing is recommended (Pereira, 2003). The process requires proper cloud/shadow mask s that balance the need for imagery of the land surface with errors induced by clouds smoke and haze. Criteria that are too strict can result in masks that cover regions of thin clouds, overly limiting the number of pixels left for processing the burned area map. If criteria are are too loose, extensive classification errors can result.

Ever the increasing spatial resolution and numbers of imagery scenes provide opportunities for improving ground observations but comes with intensive computational impact (Roy et al., 2019). In Indonesia, several data sources have been supported by the Indonesian government (LAPAN) to makes use of the map burned areas (low to very high spatial resolution). Another option is the use of cloud computing, Google Earth

Engine, which has recently been widely used, including for the mapping of burned areas (Department of Planning, 2020, Long et al., 2019). One limitation to be addressed is the latency of the product available in the cloud. The author's experience shows that to obtain cloud-free data, considering either a single Landsat 8 or a combination of Sentinel 2, it is still very limited, with a record delay of more than 2 weeks in the acquisition of images (https://earthengine.google.com/, last accessed: October 2020).

4.5 Conclusion

This paper demonstrated the capabilities of medium-resolution satellite images to map burned peatlands in one of most vulnerable fire areas in Central Kalimantan, Indonesia. We assessed how well the satellite-derived map could fill the gap in the burned area of the available product (MODIS Burned Area Collection 6 product), based on currently accessible satellite data or widely used methods. Our emphasis was also how seasonality influenced this region's burned detection. MODIS product worked well during the moderate burning event in peatlands during 2014 but was less accurate during severe burning in 2015 due to heavy smoke produced by smoldering fires burning in the peatlands. Landsat and Sentinel 2 were suffered from cloud despite the higher spatial resolution than MODIS in both seasons. Sentinel-1 worked best for the severe 2015 burning event, with no rainfall during most of the burning season. Gridded active fire alone could be an alternative to mapping burned areas when no imagery is available to map burned area using surface reflectance change detection.

Adding Landsat and gridded VIIRS 375 m filled the MODIS burned area gap by 17% and about 80% in 2014 and 2015, respectively, indicating the importance of mutisensor approaches to mapping burned area in peatlands. Further assessments with

more representative areas, different fire regimes in both peatland and non-peatland are encouraged. Owing to cloud cover and related smoke interfere at different burning effect the optical sensors satellite imageries, strategy on which each sensor to be used with purpose and timely manner was crucial. Our experiments of restricting the range of dates of image acquisition have suggested that the optical sensor alone was ineffective. However, there was still a need to assess the use of radar during seasons with varying levels of drought and fire regimes (savanna, peat, etc.). The use of active fire data may be conservative, but it may also be an option if there are no sensors capable of providing information, as was the case in 2015. Our results have supported an alternative approach to the measurement of fire-related peatland burning in the calculation of the global model of carbon emissions.

References

Albar, I., Jaya, I.N.S., Saharjo, B.H., Kuncahyo, B., & Vadrevu, K.P. (2018). Spatio-Temporal Analysis of Land and Forest Fires in Indonesia Using MODIS Active Fire Dataset. In K.P. Vadrevu, T. Ohara, & C. Justice (Eds.), *Land-Atmospheric Research Applications in South and Southeast Asia* (pp. 105-127). Cham: Springer International Publishing

Austin, K.G., Harris, N.L., Wijaya, A., Murdiyarso, D., Harvey, T., Stolle, F., & Kasibhatla, P.S.J.E.R.L. (2018). A review of land-based greenhouse gas flux estimates in Indonesia, *13*, 055003

Austin, K.G., Schwantes, A., Gu, Y., & Kasibhatla, P.S. (2019). What causes deforestation in Indonesia? *Environmental Research Letters, 14*, 024007

Badan Pusat Statistik (2020). Central Kalimantan Climate Data (Tjilik Riwut). In: Central Bureau on Statistics

Blackham, G.V., Webb, E.L., & Corlett, R.T. (2014). Natural regeneration in a degraded tropical peatland, Central Kalimantan, Indonesia: Implications for forest restoration. *Forest Ecology and Management, 324*, 8-15

Boschetti, L., Roy, D., & Hoffmann, A. (2009). MODIS Collection 5 Burned Area Product-MCD45. *User's Guide, Ver, 2*

Boschetti, L., Roy, D.P., Justice, C.O., & Humber, M.L. (2015). MODIS–Landsat fusion for large area 30m burned area mapping. *Remote Sensing of Environment, 161*, 27-42

Boschetti, M., Stroppiana, D., & Brivio, P.A. (2010). Mapping Burned Areas in a Mediterranean Environment Using Soft Integration of Spectral Indices from High-Resolution Satellite Images. *Earth Interactions, 14*

Breiman, L.J.M.l. (2001). Random forests, *45*, 5-32

Carreiras, J.M., Quegan, S., Tansey, K., & Page, S.J.E.R.L. (2020). Sentinel-1 observation frequency significantly increases burnt area detectability in tropical SE Asia, *15*, 054008

Chen, X., Vogelmann, J.E., Rollins, M., Ohlen, D., Key, C.H., Yang, L., Huang, C., & Shi, H. (2011). Detecting post-fire burn severity and vegetation recovery using multitemporal remote sensing spectral indices and field-collected composite burn index data in a ponderosa pine forest. *International Journal of Remote Sensing, 32*, 7905-7927

Chuvieco, E., Lizundia-Loiola, J., Pettinari, M.L., Ramo, R., Padilla, M., Tansey, K., Mouillot, F., Laurent, P., Storm, T., & Heil, A.J.E.S.S.D. (2018). Generation and analysis of a new global burned area product based on MODIS 250 m reflectance bands and thermal anomalies, *10*, 2015-2031

Chuvieco, E., Martin, M.P., & Palacios, A.J.I.J.o.R.S. (2002). Assessment of different spectral indices in the red-near-infrared spectral domain for burned land discrimination, *23*, 5103-5110

Chuvieco, E., Mouillot, F., van der Werf, G.R., San Miguel, J., Tanase, M., Koutsias, N., García, M., Yebra, M., Padilla, M., Gitas, I., Heil, A., Hawbaker, T.J., & Giglio, L. (2019a). Historical background and current developments for mapping burned area from satellite Earth observation. *Remote Sensing of Environment, 225*, 45-64

Chuvieco, E., Mouillot, F., van der Werf, G.R., San Miguel, J., Tanase, M., Koutsias, N., García, M., Yebra, M., Padilla, M., & Gitas, I.J.R.S.o.E. (2019b). Historical

background and current developments for mapping burned area from satellite Earth observation, *225*, 45-64

Claverie, M., Ju, J., Masek, J.G., Dungan, J.L., Vermote, E.F., Roger, J.-C., Skakun, S.V., & Justice, C.J.R.s.o.e. (2018). The Harmonized Landsat and Sentinel-2 surface reflectance data set, *219*, 145-161

Cochrane, M.A., Alencar, A., Schulze, M.D., Souza, C.M., Nepstad, D.C., Lefebvre, P., & Davidson, E.A. (1999). Positive feedbacks in the fire dynamic of closed canopy tropical forests. *Science, 284*, 1832-1835

Collins, L., McCarthy, G., Mellor, A., Newell, G., & Smith, L. (2020). Training data requirements for fire severity mapping using Landsat imagery and random forest. *Remote Sensing of Environment, 245*, 111839

Csiszar, I., Abuelgasim, A., Li, Z.Q., Jin, J.Z., Fraser, R., & Hao, W.M. (2003). Interannual changes of active fire detectability in North America from long-term records of the advanced very high resolution radiometer. *Journal of Geophysical Research-Atmospheres, 108*

Csiszar, I.A., Morisette, J.T., & Giglio, L. (2006). Validation of active fire detection from moderate-resolution satellite sensors: The MODIS example in northern Eurasia. *IEEE Transactions on Geoscience and Remote Sensing, 44*, 1757-1764

Curtis, P.G., Slay, C.M., Harris, N.L., Tyukavina, A., & Hansen, M.C.J.S. (2018). Classifying drivers of global forest loss, *361*, 1108-1111

Darmenov, A., & da Silva, A. (2013). The quick fire emissions dataset (QFED)–documentation of versions 2.1, 2.2 and 2.4. *NASA Technical Report Series on Global Modeling and Data Assimilation, NASA TM-2013-104606, 32*, 183

Department of Planning, I.a.E. (2020). Google Earth Engine Burnt Area Map (GEEBAM). In: data.nsw.gov.au

Directorate of Forest and Land Fire Management (2015). Strategic plan (revised) of for Forest and Land Fire Management 2015-2019. In. Jakarta

Escuin, S., Navarro, R., & Fernández, P. (2008). Fire severity assessment by using NBR (Normalized Burn Ratio) and NDVI (Normalized Difference Vegetation Index) derived from LANDSAT TM/ETM images. *International Journal of Remote Sensing, 29*, 1053-1073

Eva, H., & Lambin, E.F. (1998). Remote sensing of biomass burning in tropical regions: Sampling issues and multisensor approach. *Remote Sensing of Environment, 64*, 292-315

Fisher, R., Bobanuba, W.E., Rawambaku, A., Hill, G.J., & Russell-Smith, J. (2006). Remote sensing of fire regimes in semi-arid Nusa Tenggara Timur, eastern Indonesia: current patterns, future prospects. *International Journal of Wildland Fire, 15*, 307-317

Fornacca, D., Ren, G., & Xiao, W.J.R.S. (2017). Performance of three MODIS fire products (MCD45A1, MCD64A1, MCD14ML), and ESA Fire_CCI in a mountainous area of Northwest Yunnan, China, characterized by frequent small fires, *9*, 1131

Fornacca, D., Ren, G., & Xiao, W.J.R.S. (2018). Evaluating the best spectral indices for the detection of burn scars at several post-fire dates in a mountainous region of Northwest Yunnan, China, *10*, 1196

Fraser, R.H., Li, Z., & Cihlar, J. (2000). Hotspot and NDVI differencing synergy (HANDS): A new technique for burned area mapping over boreal forest. *Remote Sensing of Environment, 74*, 362-376

Garcia-Haro, F., Gilabert, M., & Melia, J.J.I.J.o.R.S. (2001). Monitoring fire-affected areas using Thematic Mapper data, *22*, 533-549

GFED (2015). 2015 Fire Season. Available: http://www.globalfiredata.org/updates.html#2015_indonesia [Accessed on 2 December 2020].

Giglio, L., Boschetti, L., Roy, D.P., Humber, M.L., & Justice, C.O. (2018a). The Collection 6 MODIS burned area mapping algorithm and product. *Remote Sensing of Environment, 217*, 72-85

Giglio, L., Boschetti, L., Roy, D.P., Humber, M.L., & Justice, C.O.J.R.s.o.e. (2018b). The Collection 6 MODIS burned area mapping algorithm and product, *217*, 72-85

Glauber, A., Moyer, S., Adriani, M., & Gunawan, I. (2016). The Cost of Fire: An Economic Analysis of Indonesia's 2015 Fire Crisis. In, *Indonesia Sustainable Landscapes Knowledge Note No. 1*. Jakarta, Indonesia

Goldstein, J.E., Graham, L., Ansori, S., Vetrita, Y., Thomas, A., Applegate, G., Vayda, A.P., Saharjo, B.H., & Cochrane, M.A. (2020). Beyond slash-and-burn: The roles of human activities, altered hydrology and fuels in peat fires in Central Kalimantan, Indonesia, *41*, 190-208

Graham, L.L.B., Giesen, W., & Page, S.E. (2017). A common-sense approach to tropical peat swamp forest restoration in Southeast Asia. *Restoration Ecology, 25*, 312-321

Hawbaker, T.J., Vanderhoof, M.K., Beal, Y.-J., Takacs, J.D., Schmidt, G.L., Falgout, J.T., Williams, B., Fairaux, N.M., Caldwell, M.K., Picotte, J.J., Howard, S.M., Stitt, S., & Dwyer, J.L. (2017). Mapping burned areas using dense time-series of Landsat data. *Remote Sensing of Environment, 198*, 504-522

Hawbaker, T.J., Vanderhoof, M.K., Schmidt, G.L., Beal, Y.-J., Picotte, J.J., Takacs, J.D., Falgout, J.T., & Dwyer, J.L. (2020). The Landsat Burned Area algorithm and products for the conterminous United States. *Remote Sensing of Environment, 244*, 111801

Hiraishi, T., Krug, T., Tanabe, K., Srivastava, N., Baasansuren, J., Fukuda, M., & Troxler, T.J.I., Switzerland (2014). 2013 supplement to the 2006 IPCC guidelines for national greenhouse gas inventories: Wetlands

Hislop, S., Jones, S., Soto-Berelov, M., Skidmore, A., Haywood, A., & Nguyen, T.H. (2018). Using Landsat Spectral Indices in Time-Series to Assess Wildfire Disturbance and Recovery, *10*, 460

Hoscilo, A., Tansey, K.J., & Page, S.E. (2013). Post-fire vegetation response as a proxy to quantify the magnitude of burn severity in tropical peatland. *International Journal of Remote Sensing, 34*, 412-433

Huang, H., Roy, D.P., Boschetti, L., Zhang, H.K., Yan, L., Kumar, S.S., Gomez-Dans, J., & Li, J. (2016). Separability analysis of Sentinel-2A multi-spectral instrument (MSI) data for burned area discrimination. *Remote Sensing, 8*, 873

Humber, M.L., Boschetti, L., Giglio, L., & Justice, C.O.J.I.j.o.d.e. (2019). Spatial and temporal intercomparison of four global burned area products, *12*, 460-484

Kaiser, J., Heil, A., Andreae, M., Benedetti, A., Chubarova, N., Jones, L., Morcrette, J.-J., Razinger, M., Schultz, M., & Suttie, M.J.B. (2012). Biomass burning emissions

estimated with a global fire assimilation system based on observed fire radiative power, *9*, 527

Konecny, K., Ballhorn, U., Navratil, P., Jubanski, J., Page, S.E., Tansey, K., Hooijer, A., Vernimmen, R., & Siegert, F. (2016). Variable carbon losses from recurrent fires in drained tropical peatlands. *Glob Chang Biol, 22*, 1469-1480

Koplitz, S.N., Mickley, L.J., Marlier, M.E., Buonocore, J.J., Kim, P.S., Liu, T., Sulprizio, M.P., DeFries, R.S., Jacob, D.J., & Schwartz, J. (2016). Public health impacts of the severe haze in Equatorial Asia in September–October 2015: demonstration of a new framework for informing fire management strategies to reduce downwind smoke exposure. *Environmental Research Letters, 11*, 094023

Langner, A., Miettinen, J., & Siegert, F. (2007). Land cover change 2002–2005 in Borneo and the role of fire derived from MODIS imagery. *Global Change Biology, 13*, 2329-2340

Li, F., Zhang, X., & Kondragunta, S.J.R.S. (2020). Biomass Burning in Africa: An Investigation of Fire Radiative Power Missed by MODIS Using the 375 m VIIRS Active Fire Product, *12*, 1561

Liaw, A., & Wiener, M.J.R.n. (2002). Classification and regression by randomForest, *2*, 18-22

Liu, T., Mickley, L.J., Marlier, M.E., DeFries, R.S., Khan, M.F., Latif, M.T., & Karambelas, A. (2020). Diagnosing spatial biases and uncertainties in global fire emissions inventories: Indonesia as regional case study. *Remote Sensing of Environment, 237*, 111557

Lohberger, S., Stängel, M., Atwood, E.C., & Siegert, F. (2017a). Spatial evaluation of Indonesia's 2015 fire affected area and estimated carbon emissions using Sentinel-1. *Global Change Biology, 24*, 644-654

Lohberger, S., Wiedemann, W., & Siegert, F. (2017b). Cross-comparison of methods developed under small-fire databases applied in Tropical Africa. In, *Algorithm Intercomparison Document.* https://climate.esa.int/documents/253/Fire_cci_Ph2_RSS_D5_AID_V1_1.pdf (last accessed on 8 January 2021)

Long, T., Zhang, Z., He, G., Jiao, W., Tang, C., Wu, B., Zhang, X., Wang, G., & Yin, R.J.R.S. (2019). 30 m Resolution Global Annual Burned Area Mapping Based on Landsat Images and Google Earth Engine, *11*, 489

Loveland, T.R., & Dwyer, J.L.J.R.S.o.E. (2012). Landsat: Building a strong future, *122*, 22-29

Margono, B.A., Potapov, P.V., Turubanova, S., Stolle, F., & Hansen, M.C. (2014). Primary forest cover loss in Indonesia over 2000-2012. *Nature Climate Change, 4*, 730-735

Marlier, M.E., Liu, T., Yu, K., Buonocore, J.J., Koplitz, S.N., DeFries, R.S., Mickley, L.J., Jacob, D.J., Schwartz, J., & Wardhana, B.S.J.G. (2019). Fires, smoke exposure, and public health: An integrative framework to maximize health benefits from peatland restoration, *3*, 178-189

Medrilzam, M., Dargusch, P., Herbohn, J., & Smith, C. (2014). The socio-ecological drivers of forest degradation in part of the tropical peatlands of Central Kalimantan, Indonesia. *Forestry, 87*, 335-345

Medrilzam, M., Smith, C., Aziz, A.A., Herbohn, J., & Dargusch, P. (2017). Smallholder Farmers and the Dynamics of Degradation of Peatland Ecosystems in Central Kalimantan, Indonesia. *Ecological Economics, 136*, 101-113

Miettinen, J., Hooijer, A., Vernimmen, R., Liew, S.C., & Page, S.E. (2017). From carbon sink to carbon source: extensive peat oxidation in insular Southeast Asia since 1990. *Environmental Research Letters, 12*, 024014

Miettinen, J., Langner, A., & Siegert, F. (2007). Burnt area estimation for the year 2005 in Borneo using multi-resolution satellite imagery. *International Journal of Wildland Fire, 16*, 45-53

Miettinen, J., Shi, C., & Liew, S.C. (2016). Land cover distribution in the peatlands of Peninsular Malaysia, Sumatra and Borneo in 2015 with changes since 1990. *Global Ecology and Conservation, 6*, 67-78

MoEF (2020). Sipongi, Karhutla Sistem. In, *Rekapitulasi Luas Kebakaran Hutan dan Lahan (Ha) Per Provinsi Di Indonesia Tahun 2015-2020*. Jakarta

MoEF (KLHK) (2019). KLHK Terapkan Tiga Langkah Penguatan Penegakan Hukum Karhutla. In. Jakarta, Indonesia

Myers, N., Mittermeier, R.A., Mittermeier, C.G., Da Fonseca, G.A., & Kent, J.J.N. (2000). Biodiversity hotspots for conservation priorities, *403*, 853-858

Navarro, G., Caballero, I., Silva, G., Parra, P.C., Vazquez, A., & Caldeira, R. (2017). Evaluation of forest fire on Madeira Island using Sentinel-2A MSI imagery. *International Journal of Applied Earth Observation and Geoinformation, 58*, 97-106

Norton, J., Glenn, N., Germino, M., Weber, K., & Seefeldt, S. (2009). Relative suitability of indices derived from Landsat ETM+ and SPOT 5 for detecting fire severity in sagebrush steppe. *International Journal of Applied Earth Observation and Geoinformation, 11*, 360-367

Oliva, P., & Schroeder, W. (2015). Assessment of VIIRS 375m active fire detection product for direct burned area mapping. *Remote Sensing of Environment, 160*, 144-155

Pereira, J.M. (2003). Remote sensing of burned areas in tropical savannas. *International Journal of Wildland Fire, 12*, 259-270

Picotte, J.J., Bhattarai, K., Howard, D., Lecker, J., Epting, J., Quayle, B., Benson, N., & Nelson, K.J.F.E. (2020). Changes to the Monitoring Trends in Burn Severity program mapping production procedures and data products, *16*, 1-12

Putra, E.I., Cochrane, M.A., Saharjo, B.H., Graham, L., Thomas, A., Applegate, G., Saad, A., Setianto, E., Sutikno, S., & Prayitno, A. (2019). Developing better understanding on tropical peat fire occurrences and dynamics. *IOP Conference Series: Earth and Environmental Science, 394*, 012044

Putra, E.I., Cochrane, M.A., Vetrita, Y., Graham, L., & Saharjo, B.H. (2018). Determining critical groundwater level to prevent degraded peatland from severe peat fire. In, *IOP Conference Series: Earth and Environmental Science* (p. 012027): IOP Publishing

Ramo, R., García, M., Rodríguez, D., & Chuvieco, E. (2018). A data mining approach for global burned area mapping. *International Journal of Applied Earth Observation and Geoinformation, 73*, 39-51

Ritung, S., Wahyunto, N.K., Sukarman, H., & Suparto, T.C. (2011). Peta Lahan Gambut Indonesia skala 1: 250.000. *Balai Besar Penelitian dan Pengembangan*

Sumberdaya Lahan Pertanian. Badan Penelitian dan Pengembangan Pertanian. Bogor, Indonesia

Rogan, J., & Yool, S.J.I.J.o.R.S. (2001). Mapping fire-induced vegetation depletion in the Peloncillo Mountains, Arizona and New Mexico, *22*, 3101-3121

Rollins, M.G. (2009). LANDFIRE: a nationally consistent vegetation, wildland fire, and fuel assessment %J International Journal of Wildland Fire, *18*, 235-249

Roteta, E., Bastarrika, A., Padilla, M., Storm, T., & Chuvieco, E. (2019). Development of a Sentinel-2 burned area algorithm: Generation of a small fire database for sub-Saharan Africa. *Remote Sensing of Environment, 222*, 1-17

Roy, D.P., & Boschetti, L. (2009). Southern Africa validation of the MODIS, L3JRC, and GlobCarbon burned-area products. *IEEE Transactions on Geoscience and Remote Sensing, 47*, 1032-1044

Roy, D.P., Boschetti, L., Justice, C.O., & Ju, J. (2008). The collection 5 MODIS burned area product—Global evaluation by comparison with the MODIS active fire product. *Remote Sensing of Environment, 112*, 3690-3707

Roy, D.P., Huang, H., Boschetti, L., Giglio, L., Yan, L., Zhang, H.H., & Li, Z. (2019). Landsat-8 and Sentinel-2 burned area mapping - A combined sensor multi-temporal change detection approach. *Remote Sensing of Environment, 231*, 111254

Ryan, K.C., & Opperman, T.S. (2013). LANDFIRE – A national vegetation/fuels data base for use in fuels treatment, restoration, and suppression planning. *Forest Ecology and Management, 294*, 208-216

Schroeder, W., & Giglio, L. (2018). NASA VIIRS Land Science Investigator Processing System (SIPS) Visible Infrared Imaging Radiometer Suite (VIIRS) 375 m & 750 m Active Fire Products: product User's Guide Version 1.4. In

Schroeder, W., Oliva, P., Giglio, L., & Csiszar, I.A. (2014). The New VIIRS 375m active fire detection data product: Algorithm description and initial assessment. *Remote Sensing of Environment, 143*, 85-96

Siegert, F., Ruecker, G., Hinrichs, A., & Hoffmann, A. (2001). Increased damage from fires in logged forests during droughts caused by El Nino. *Nature, 414*, 437-440

Sinclair, A.L., Graham, L.L.B., Putra, E.I., Saharjo, B.H., Applegate, G., Grover, S.P., & Cochrane, M.A. (2020). Effects of distance from canal and degradation history on

peat bulk density in a degraded tropical peatland. *Science of the Total Environment, 699*, 134199

Sofan, P., Bruce, D., Schroeder, W., Jones, E., & Marsden, J. (2020). Assessment of VIIRS 375 m active fire using tropical peatland combustion algorithm applied to Landsat-8 over Indonesia's peatlands. *International Journal of Digital Earth, 13*, 1695-1716

Stroppiana, D., Pinnock, S., Pereira, J.M., & Grégoire, J.-M.J.R.S.o.E. (2002). Radiometric analysis of SPOT-VEGETATION images for burnt area detection in Northern Australia, *82*, 21-37

The Indonesian Minister of Environment and Forestry (2020). Rencana Strategis Kementerian Lingkungan Hidup dan Kehutanan Tahun 2020-2024. In. Jakarta: Ministry of Environment and Foresty of Indonesia

The World Bank (2014). Indonesia economic quarterly July 2014: hard choices. In A. Sienaert, A. Lnu, M. Adriani, M. Crystallin, F. Fitrani, A. Ihsan, E.A. Mileva, V. Vulovic, M. Ahmad, & I. Gunawan (Eds.): The World Bank

Vetrita, Y., & Cochrane, M.A. (2019). Annual Burned Area from Landsat, Mawas, Central Kalimantan, Indonesia, 1997-2015. *ORNL DAAC, Oak Ridge, Tennessee, USA*. DOI: https://doi.org/10.3334/ORNLDAAC/1708

Vetrita, Y., & Cochrane, M.A.J.R.S. (2020a). Fire Frequency and Related Land-Use and Land-Cover Changes in Indonesia's Peatlands, *12*, 5

Vetrita, Y., & Cochrane, M.A. (2020b). Landsat-derived Land Use/Cover Maps, Mawas, Central Kalimantan, Indonesia, 1994-2019. *ORNL DAAC, Oak Ridge, Tennessee, USA*. DOI: https://doi.org/10.3334/ORNLDAAC/1838

Vetrita, Y., Cochrane, M.A., Suwarsono, S., Priyatna, M., Sukowati, K.A.D., & Khomarudin, M.R. (2020). Evaluating accuracy of four MODIS-derived burned area products for tropical peatland and non-peatland fires. *Environmental Research Letters*. DOI: https://doi.org/10.1088/1748-9326/abd3d1

Wulder, M.A., Loveland, T.R., Roy, D.P., Crawford, C.J., Masek, J.G., Woodcock, C.E., Allen, R.G., Anderson, M.C., Belward, A.S., Cohen, W.B., Dwyer, J., Erb, A., Gao, F., Griffiths, P., Helder, D., Hermosilla, T., Hipple, J.D., Hostert, P., Hughes, M.J., Huntington, J., Johnson, D.M., Kennedy, R., Kilic, A., Li, Z., Lymburner, L.,

McCorkel, J., Pahlevan, N., Scambos, T.A., Schaaf, C., Schott, J.R., Sheng, Y., Storey, J., Vermote, E., Vogelmann, J., White, J.C., Wynne, R.H., & Zhu, Z. (2019). Current status of Landsat program, science, and applications. *Remote Sensing of Environment, 225*, 127-147

APPENDIX A

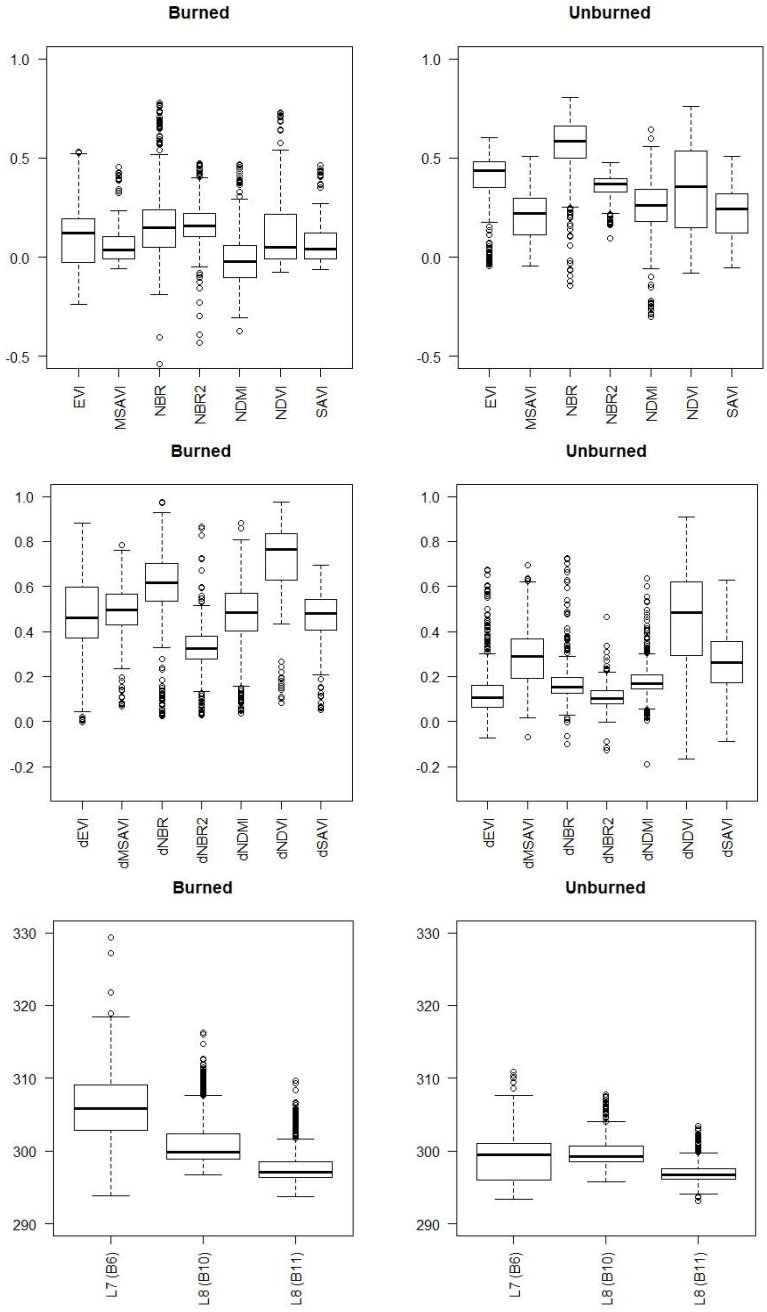

Figure S 4-1 Training pixel values of burn and unburn classes for the Random Forest model input to derive the burned area map of 2015: post-fire indices (top row), pre-and post-fire difference (middle), and post-fire temperature brightness (bottom row) for thermal infrared band Landsat 7 (band 6), Landsat 8 (band 10 and 11). Unburned vegetation pixels have higher indices values than burned pixels, so the difference in indices (pre-and post-fire) is higher for burned pixels than for unburned pixels. While a temperature brightness (in Kelvin) is considerably higher for burned pixels than for unburned pixels.

APPENDIX B.

LANDSAT DERIVED ANNUAL AREA BURNED MAPS ACROSS MAWAS, CENTRAL KALIMANTAN, INDONESIA

Citation: Vetrita, Y. & Cochrane, M. A. 2019. Annual Burned Area from Landsat, Mawas, Central Kalimantan, Indonesia, 1997-2015. *ORNL DAAC, Oak Ridge, Tennessee, USA.* https://doi.org/10.3334/ORNLDAAC/1708

Summary

This dataset contains annual burned area (or burn scars) maps at 30-m resolution derived from Landsat that occurred in Mawas, Central Kalimantan, Indonesia during 1997-2015. Random Forest classifications were used to separate burned and unburned pixels. Due to high cloud cover or smoke, some areas burned were manually added when visual-interpretation was possible.

Data File Information

There are a total of 16 shapefiles with this dataset, representing annual area burned from 1997 to 2015 (19 years). No fires were recorded in 2008 and 2010 with a special case for the 1997 map (see the methods).

File names

The files are named according to the following naming convention: Mawas.BA.YYYY.001.shp

where:

Mawas– refers to the site name

BA – refers to Burned Area

YYYY – refers to the year of burn.

001 – refers to the version of the product

Example file names: Mawas.BA.1997.001.shp

Table S 4-1 Data format for Landsat derived annual area burned maps

Data Type	Shapefile Feature Class
Geometry Type	Polygon
Projected Coordinate System	UTM Zone 50S
Projection	Transverse Mercator
Datum	WGS 1984
False_Easting	500000.0
False_Northing	10000000.0
Central_Meridian	117.0
Top left corner (x,y)	210465.000100 m, 9754987.830000 m
Bottom right corner (x,y)	233265.000100 m, 9727705.000000 m
Pixel size	30 m
Last modified	May 2019

Data Acquisition, Materials, and Methods

Landsat data series (TM, ETM+, OLI/TIR) from 1997 to 2015 were used to generate the annual burned areas. All available scenes of level 1T (path/raw 118/62) were selected using the U.S. Geological Survey (USGS) Earth Explorer website (earthexplorer.usgs.gov), limited to cloud cover less than 80%. All selected scenes were submitted to the Earth

Resources Observation and Science (EROS) Center Science Processing Architecture (ESPA) Ordering Interface (espa.cr.usgs.gov) for level-2 product processing. We ordered the surface reflectance, brightness temperature, and pixel QA, including indices (NDVI, NDMI, NBR, NBR2, SAVI, and MSAVI, see Table 1). Only good pixels (flagged in pixel QA, meaning, cloud and water mask out) were employed to derive the maps.

Table S 4-2 Variables used to derive the annual burned area maps

Variable	Abbreviation	Reference
Normalized difference vegetation index	NDVI	[1]
Normalized difference moisture index	NDMI	[2]
Normalized burn ratio	NBR	[3]
Normalized burn ratio 2	NBR2	[4]
Soil adjusted vegetation index	SAVI	[5]
Modified Soil Adjusted Vegetation Index	MSAVI	[6]
Brightness temperature	Band 6 (Landsat 5/7), Band 10 and 11 (Landsat 8)	

We used Random Forest classifications to separate the burned and unburned pixels. All band indices and thermal bands in that particular year were employed to derive the annual maps, except for the 1997 event. We generated the 1997 map from Landsat series from 1997 to early 1998, since the burning was considered as a continuous event during the El Nino of 1997-1998. The final inputs used to run the algorithm were composites of indices and thermal bands, based on the pre and post fire values (Figure S 4-2). MODIS active fire

(MCD14) was used to define when fires occurred. The highest difference of indices values between pre-fire and post fire periods were extracted. Post fire values were the minimum pixel value (indices) and the maximum brightness temperatures from the annual post-fire imagery set. Pre fire values were the maximum pixel value (indices) and the minimum brightness temperatures (BT) from the annual pre-fire imagery set. Burned and unburned training data depend largely on visual detection in imagery. We created a balanced number of training data points for both burned and unburned classes (~3000), with 80% as training points and 20% as validation points. The salt-pepper noise of predicted burned areas were then removed using a 3x3 windows majority filter. During severe fire events or cloud cover, misclassifications were manually corrected, mainly due to the cloud QA failure to remove cloudy/smoky pixels.

Quality Assessment

The SPOT 5—available from the Indonesian National Institute of Aeronautics and Space (LAPAN) for 2014—and our ground truth data from 2015 were used to verify the maps (manuscript nearing submission – Vetrita et al.). In our cross validation of the Random Forest classification, on average, the Out of Bag estimate of error rate was low (~1.5%) with overall accuracy of ~98% from validating points.

Caveats and Known Problems

Due to high cloud cover or smoke during fire events obscuring the land, some areas burned were likely to be undetected. For a number of fires, we added areas burned using visual-interpretation when possible. For the severe fire events of 2015, the annual map was merged with the Sentinel-1 burned area product provided by European Space Agency [7].

For the next version, we will include probability maps (likely/unlike burned) and add no burning or NAs pixel to the maps.

References

1. Tucker, C.J., Red and photographic infrared linear combinations for monitoring vegetation. Remote sensing of Environment, 1979. 8(2): p. 127-150.
2. Gao, B.-c., NDWI—A normalized difference water index for remote sensing of vegetation liquid water from space. Remote Sensing of Environment, 1996. 58(3): p. 257-266.
3. Garcia, M.L. and V. Caselles, Mapping burns and natural reforestation using Thematic Mapper data. Geocarto International, 1991. 6(1): p. 31-37.
4. Key, C. and N. Benson, Landscape assessment: remote sensing of severity, the normalized burn ratio and ground measure of severity, the composite burn index, in FIREMON: Fire effects monitoring and inventory system Ogden, Utah: USDA Forest Service, Rocky Mountain Res. Station, D.C. Lutes, Editor. 2006, United States Department of Agriculture.
5. Huete, A.R., A soil-adjusted vegetation index (SAVI). Remote sensing of environment, 1988. 25(3): p. 295-309.
6. Qi, J., et al., A modified soil adjusted vegetation index. Remote Sensing of Environment, 1994. 48(2): p. 119-126.
7. Lohberger, S., Stängel, M., Atwood, E. C., & Siegert, F. (2018). Spatial evaluation of Indonesia's 2015 fire-affected area and estimated carbon emissions using Sentinel-1. Global change biology, 24(2), 644-654.

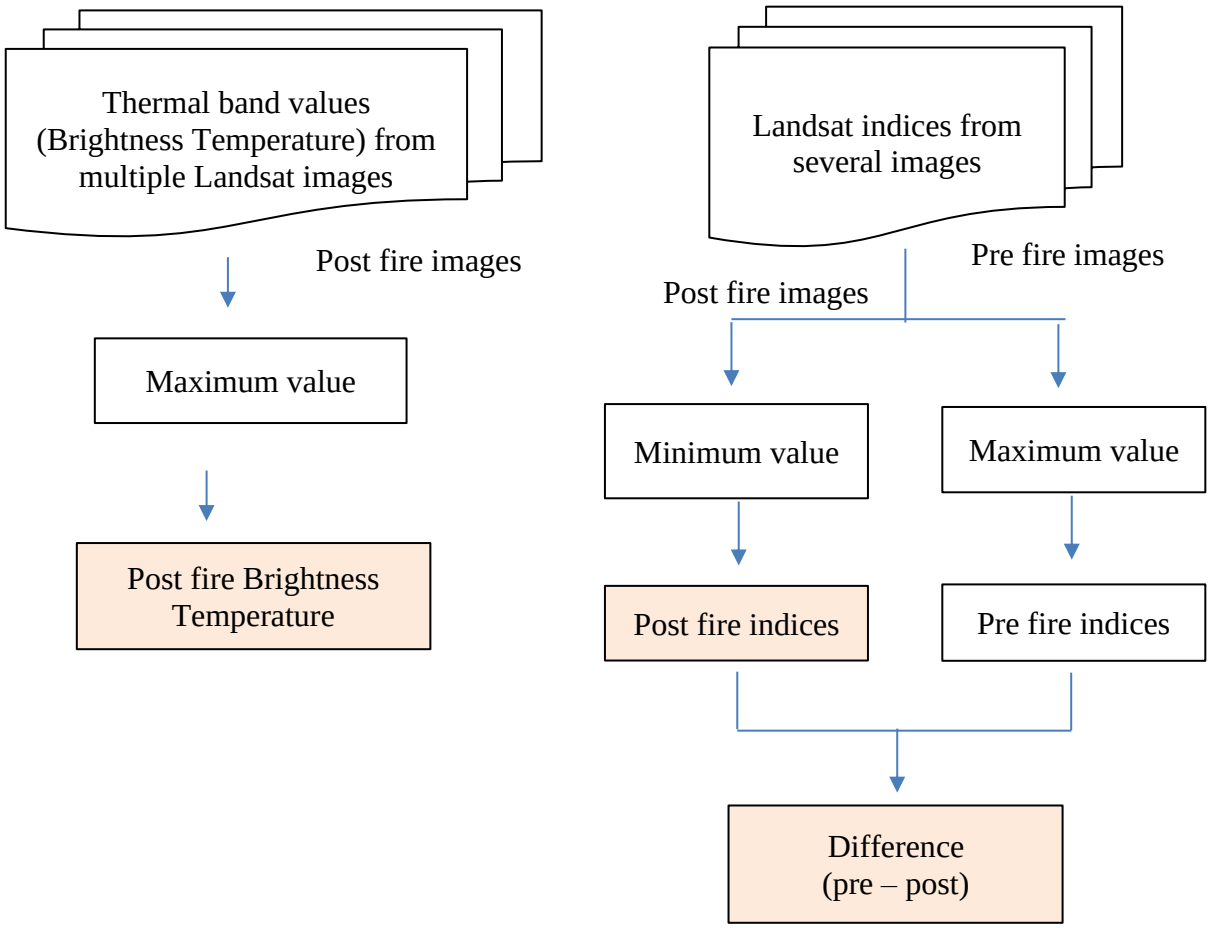

Figure S 4-2 Compositing Landsat images to get the input variables for Random Forest algorithm to separate burned and unburned pixels. First, we defined the post and pre fires based on the MODIS active fire product (MCD14) occurring in the year of interest. For each index (NDVI, NDMI, NBR, NBR2, SAVI, MSAVI), we selected the minimum value of post fire images and the maximum value of pre fire images. On the other hand, we selected the maximum brightness temperature of the Landsat thermal band (Band 6 for Landsat 7; Band 10 and 11 for Landsat 8). Shaded boxes represent all input variables used for the algorithm. Abbreviations: NDVI=Normalized Difference Vegetation Index; NDMI= Normalized Difference Moisture Index; NBR= Normalized Burn Ratio, NBR2= Normalized Burn Ratio 2, SAVI= Soil Adjusted Vegetation Index; MSAVI= Modified Soil Adjusted Vegetation Index.

APPENDIX C.

LANDSAT DERIVED LAND USE/COVER MAPS ACROSS MAWAS, CENTRAL KALIMANTAN, INDONESIA

Citation: Vetrita, Y. & Cochrane, M. A. 2020. Landsat-derived Land Use/Cover Maps, Mawas, Central Kalimantan, Indonesia, 1994-2019. *ORNL DAAC, Oak Ridge, Tennessee, USA.* https://doi.org/10.3334/ORNLDAAC/1838

Summary

This dataset contains an annual land use/cover map for every five-year period at 30-m resolution derived from Landsat that occurred in Mawas, Central Kalimantan, Indonesia, during 1994-2019. Classification and Regression Trees (CART) was used to classify the land use/cover types.

Data File Information

This dataset has a total of seven files, consisting of an annual map for each five-year period, including 1994, 1999, 2004, 2009, 2014, 2019 and 2015 for accuracy assessment.

File names

Files are named according to the following naming convention: Mawas_LUC_YYYY_001.tif

where:

Mawas– refers to the site name

LUC – refers to land use/cover

YYYY – refers to the year of the dataset

001 – refers to the version of the product

Example file names: Mawas_LUC_1994_001.tif

Table S 4-3 Data format for Landsat derived land use/cover maps

Data Type	Raster
Projected Coordinate System	UTM Zone 50S
Projection	Transverse Mercator
Datum	WGS 1984
False_Easting	500000.0
False_Northing	10000000.0
Central_Meridian	117.0
Top left corner (x, y)	205928.344807m, 9760767.6853m
Bottom right corner (x, y)	238388.344807 m, 9716697.6853 m
Pixel size	30 m

Data Acquisition, Materials, and Methods

Landsat data series (TM, ETM+, OLI/TIR) from 1994 to 2019 were used to classify the land use/cover types. We selected the surface reflectance Tier 1 product from several bands and indices (Table S 4-4). Image selection for each year used was based upon 1) selecting the same season to minimize sudden change in the land cover/use (e.g., burning). Here, the fire season typically begins from mid-August, so we restricted the images from January to August, 2) using a single image where cloud cover is less than 5%, or 3) using composite images available from January to August with only good pixels specified (flagged in pixel Quality Assurance (QA), meaning, cloud and water masked out). The

remaining cloud pixels (usually thin cloud) were removed using the <0.045 reflectance threshold in the blue band. Table S 4-5 describes the dataset selection list.

Table S 4-4 Variables used to derive the annual land use/cover area maps

Spectral bands/indices	Wavelength (μm)
Blue	0.45-0.51
Green	0.53-0.60
Red	0.63-0.68
Near Infrared (NIR)	0.85-0.88
Shortwave infrared (SWIR)	1.56-1.66 (center at 1.6)
Shortwave infrared	2.10-2.30 (center at 2.2)
Longwave infrared (Landsat 8 only)	10.30-11.30
Longwave infrared (Landsat 8 only)	11.50-12.50
Normalized difference water index (Gao, 1996)	$\frac{\rho_{NIR} - \rho_{SWIR(1.6\ \mu m)}}{\rho_{NIR} + \rho_{SWIR(1.6\ \mu m)}}$
Normalized burn ratio (Tucker, 1978)	$\frac{\rho_{NIR} - \rho_{SWIR(2.2\ \mu m)}}{\rho_{NIR} + \rho_{SWIR(2.2\ \mu m)}}$

Table S 4-5 Dataset selection for the annual land use/cover area maps

Year	Satellite/sensor	Acquisition date *
2015	Landsat 8 OLI/TIR	20150803
2019	Landsat 8 OLI/TIR	20190814
2014	Landsat 8 OLI/TIR	Composited image only
2009	Landsat TM 5	20090207

Year	Satellite/sensor	Acquisition date *
2004	Landsat TM 5	20040516
1999	Landsat TM 5	19990722
1994	Landsat TM 5	19940708

*The initial image classification. The pixels removed due to cloud masking were filled with the second classified image generated from the composite image in that particular year.

We used the Google Earth Engine platform to process all datasets (see Figure S 4-3). Classification and Regression Trees (CART) classifier (Breiman et al., 1984) divided land use/cover types into several classes (Table S 4-6). We initially created a map using the clearest image available for each year from January-August. Cloudy pixels were removed using the Quality Assurance (QA) pixels. Blue band reflectance <0.045 was used to remove thin cloud/cloud shadow interference that QA pixels could not detect. The sample polygons are drawn for five classes i.e. Pristine/degraded peat swamp forest (PSF), ferns/low shrubs, river/water body, tall shrubs, and secondary forest. Frequently the swamp/flooded tall shrubs were identified as PSF, so we added another class called swamp-shrubs and took polygon-samples to locate misidentified pixels. The majority pixels, 3x3 window, were used to remove the salt-pepper noise of the predicted classes. We merged three classes (tall shrubs, secondary forest, swamp/flooded tall shrubs) into one class (tall shrubs). The gap pixels produced by the cloud cover on the first map were filled with the second image classification produced from the composite image. Overall, very few land-use/cover types change from January to August, so we used the same polygon samples as the first image classification and added a few samples if needed. Because cloud cover also

influenced the water body pixels, we created a river map with the NDWI value <=-0.55 of the clearest image in 2015, and then overlaid it on all LUC maps.

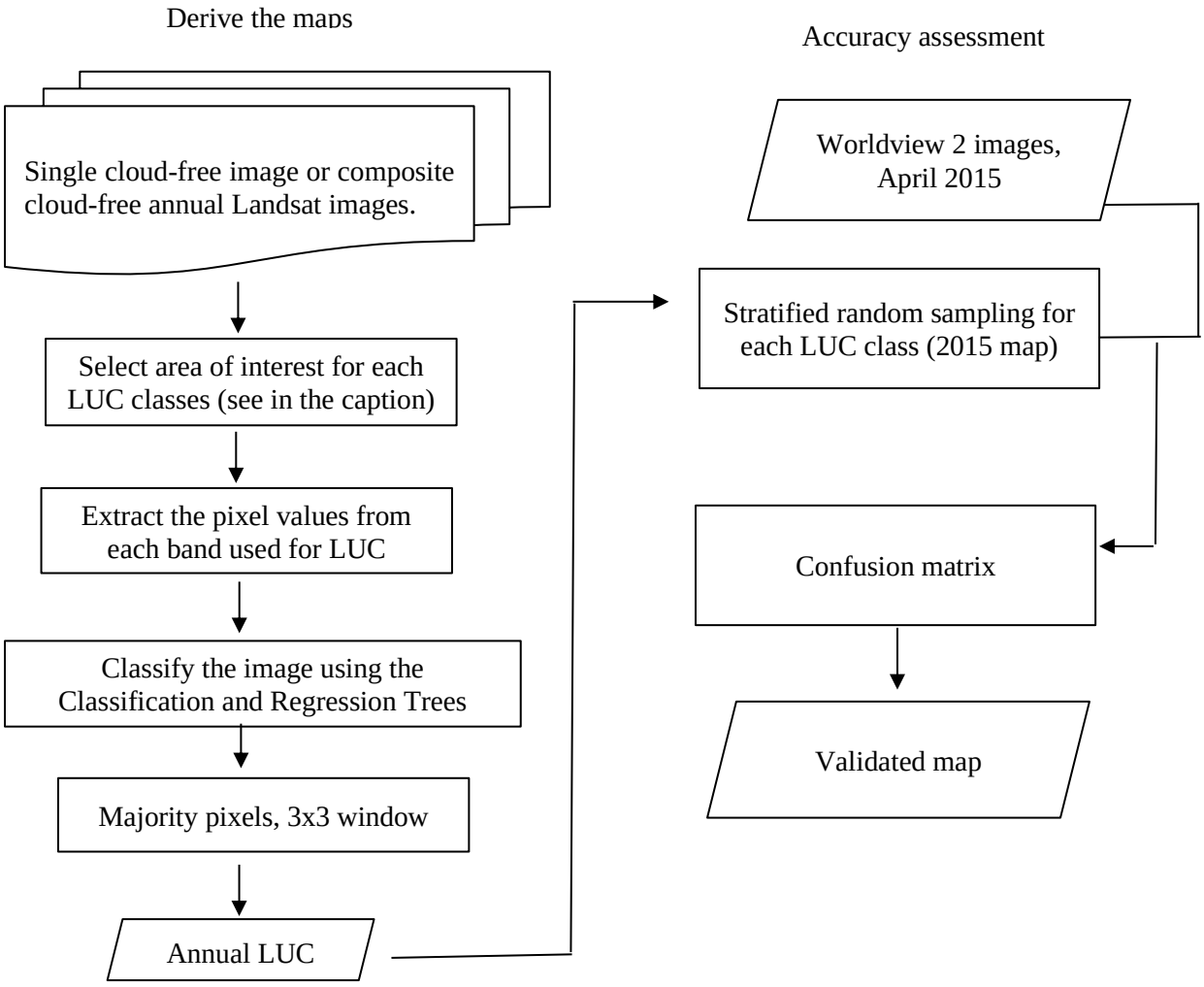

Figure S 4-3 Image processing to create a land use/cover (LUC) map across Mawas, Central Kalimantan, Indonesia. First, cloud-free Landsat images were derived from a single image or a composited annual pixel value. The image was used to select training points based on our knowledge for five LUC classes: Peat swamp forest, tall shrubs/ secondary forest, Low shrubs/ferns/grass, Urban/bare land/open flooded areas, and river (see Table 3). Finally, LUC classes were predicted using the Classification and Regression Trees (CART) method based on the training samples extracted from selected bands and indices: Blue (0.45 – 0.51 µm), Green (0.53–0.60 µm), Red (0.63–0.68 µm), Near Infrared (0.85 – 0.88 µm), Shortwave Infrared (1.56 – 1.66 µm and 2.10 – 2.30 µm), and longwave Infrared (only for Landsat 8 TIR, 10.30 – 11.30 µm and 11.50 – 12.50 µm)

Quality Assessment

The Worldview 2 and SPOT 6/7 images (multispectral imagery 1.84-meter and 6-meter spatial resolution, respectively) scanned in April, May, and early August of 2015—available from the Indonesian National Institute of Aeronautics and Space (LAPAN) for 2015 were used to verify the maps. Stratified random sampling was generated to verify the accuracy of each class. We removed the validation points that were 1) affected by cloudy pixels on either LUC map or the reference image; 2) located within the 3x3 pixel windows of our training points (none found), and 3) pixels detected later, after the reference image acquisition, as burned in our LC map (one pixel only). Of the initial 97 points created, a total of 17, 22, 17, 14, and 15 points remained, respectively, for peat swamp forest, tall shrubs, low shrubs, urban/bare land, and river. This number of validating points reaches a standard error of 0.01 within this relatively small site (50,000 ha). The confusion matrix indicates a 0.96 overall accuracy with the tall shrubs class as the least accurate (Table S 4-6).

Table S 4-6 Description of land use/cover map, the producer's and user's accuracies

ID	Class	Explanation	Producer's accuracy	User's accuracy
1	Peat swamp forest	Both pristine and degraded peat swamp forest	1.00	0.89
2	Tall shrubs	Shrubland or secondary forest with an average height above 2 m; including agricultural fields, plantation, and swamp shrubland	0.86	0.95
3	Low shrubs	Ferns and grass or shrubland with average height less than 2 m with soil/water exposed (just regrowth)	1.00	0.94

ID	Class	Explanation	Producer's accuracy	User's accuracy
4	Urban/bare land	Including open area with no vegetation, just burned, flooded area, and villages.	1.00	1.00
5	River	Permanent water bodies	0.93	1.00

Caveats and Known Problems

- Error sources could include: 1) thin cloud/cloud shadow interference that was not masked by QA pixels; 2) confusion between tall shrubs and peat swamp forest; 3) very few cloud-free images throughout 2014 that exacerbated the low quality of the LUC map.
- Canal (<10-meter width) or seasonal water along the river may each be classified differently. Users who need to identify the land use/cover change or identify the water canal should use the datasets cautiously.

References

Breiman, L., Friedman, J., Olshen, R. & Stone, C. 1984. Classification and Regression Trees.

Gao, B.-C. J. R. S. O. E. 1996. Ndwi—A Normalized Difference Water Index for Remote Sensing of Vegetation Liquid Water from Space. 58, 257-266.

Tucker, C. J. 1978. Red and Photographic Infrared Linear Combinations for Monitoring Vegetation.

CHAPTER 5

RESEARCH SUMMARY AND RECOMMENDATIONS

5.1 Research summary and key findings

The work presented in this dissertation advances our understanding of the dynamics of Indonesian peatland fires, the uncertainties associated with fire detection, burned area mapping and fire-related carbon emissions from peatland fire activities, and potential approaches for filling spatial and temporal gaps in available imagery gaps.

In chapter 2, I assessed the reliability of currently available burned-area products (MCD64A1 Collection 6 and FireCCI51), including two decommissioned products (MCD45A1 C5.1 and MCD64A1 C5.1), and their possible impact on estimates of burned area in Indonesian peatlands. As expected, the currently available products were more reliable than the older ones, with the standard MODIS burned area product working best for estimating burned area in Central Kalimantan's peatlands. FireCCI51 showed lower improvements for detection of smaller burned areas (<100 ha) than MODIS C6 and underestimated area burned in both peat and non-peat regions, despite having higher spatial resolution than the MCD64A1 product. Owing to use of fewer images for generating the FireCCI51 product, which uses Terra MODIS imagery only, cloud cover have more impact on detection of burned areas, as found in other tropical region (Pessôa et al., 2020).

Although MCD64A1 was the best performing product, it only detected half or less of the true burning in peatland areas, and even less in non-peatland. Despite this, the use of MODIS burned area is still recommended for national scale monitoring until better tools can be developed. However, findings from studies described in this dissertation bring new insight about remaining uncertainties for carbon emissions estimation from frequent burning of Indonesian peatlands. Therefore, accurate observation and quantification of

these fires remains critical for effective monitoring and application of global emissions models. With nearly two decades of observations, the long time-series MODIS burned area data has provided unparalleled insight into Indonesia's fire history.

In Chapter 3, I used the product and three epochs of Landsat/SPOT-4-derived land use/cover maps (1990, 2007, and 2015) to quantify fire frequency and its related land use/cover change in Indonesia's two largest peatland regions (Sumatra and Kalimantan) during 2001-2018. I reported the annual burned areas, total peatland area affected by fires, amounts of recurrent burning, and associations with land-use and land-cover (LULC) change. I found that Sumatra and Kalimantan experienced extensive fires with substantial amounts of recurring fire events. The initial LULC was predominantly forest, but most of these areas have been converted to other LULC types which experience different land management practices and rates of burning. Degraded shrublands had the most frequent rate of annual burning on both Sumatra and Kalimantan, precluding regeneration of native forests. Plantation areas were more established in Sumatra, but Kalimantan has experienced rapid land conversion to plantations. The findings have underlined the significant influence of LULC change in altering fire regimes in Indonesia. If the currently prevalent rate of burning in Indonesia's peatlands is not greatly reduced, within less than half of century, peat swamp forest will likely disappear from Sumatra and Kalimantan.

Currently available products have not answered to the need for accurate mapping of burned areas in Indonesian peatland. These fires have caused loss of peat and regional biodiversity over the last several decades. Therefore, in Chapter 4, I assessed the use of multiscale data at higher spatial resolutions for filling gaps in the currently available burned area product. I evaluated how well the satellite-derived map could fill the gap in the burned

area of the available product (MODIS Burned Area (BA) product Collection 6), based on freely accessible satellite data (Landsat, Sentinel 2, Sentinel 1, and VIIRS 375 m) or widely used methods (the use of spectral indices, simple change detection method, or Random Forest model). I also have emphasized how differences between fire seasons influence burn detection in this region, adding more insight from my first assessment in Chapter 2. I initially compared the MODIS BA product (MCD64A1) for two different fire seasons, moderate (2014) and severe burning (2015) in Central Kalimantan. I then compared the results with the gridded VIIRS 375 active fire product (VIIRS-AF) and Landsat-based BA mapping based on Random Forest classifications of burned and unburned pixels. Several band indices and thermal Infrared bands were employed for the Landsat-based BA map derivations. In addition, I investigated how imagery from additional satellite sensors (Sentinel-1 and Sentinel-2) could improve BA estimations for the 2015 fire event.

In 2014, I found that the MODIS burned area (MCD64A1 Collection 6) product accurately detected 52% of burned areas. Although some burned areas were not detected, likely due to the small size of fires, most of the detected areas were very well spatially correlated with the burned reference areas derived from SPOT 5 imagery. On the other hand, under the extensive smoke cover of the severe 2015 fire season, hardly any burned areas were detected by the MODIS BA product. Addition of VIIRS-AF and Landsat drastically improved upon the MODIS BA in 2015. Combining burned area detections from all sensors in 2014 (MODIS BA, VIIRS-AF, and Landsat) resulted in more area burned

(142.76%) than the 2014 reference map, mainly due to the coarser resolution of the products (30-500 m) than the reference map (10 m).

Despite having higher spatial resolution, Landsat and Sentinel-2 both suffered from cloud contamination to a greater extent than MODIS in both seasons due to the latter's greater temporal resolution (daily). Sentinel-1 worked best for the severe 2015 burning event, with no rainfall during most of the burning season. Gridded active fire alone could be an alternative to mapping burned areas when no imagery is available to map burned area using surface reflectance change detection. Along with the assessment, I analyzed the connection between the burning frequency and its relationship to the transition from forest to shrubs. The construction of drainage canals has promoted human access to the study area. The areas adjacent to the canals have experienced the highest observed frequency of recurrent fires. I have made the annual burned area product (1997-2015) and related land use/cover maps (1994-2019) derived from Landsat, freely accessible at the Oak Ridge National Laboratory Distributed Active Archive Center (https://doi.org/10.3334/ORNLDAAC/1708; https://doi.org/10.3334/ORNLDAAC/1838 (Vetrita and Cochrane, 2019, Vetrita and Cochrane, 2020b)). The guidelines for national mapping have also been discussed as part of my recommendations presented below.

5.2 Recommendations and limitations

The two main problems in tracking fire-derived emissions from Indonesian peatlands using optical imagery are (1) an inability to reliably image the land surface and (2) the difficulty of detecting changes that are often limited in area, ephemeral, and low in intensity. Persistent cloud cover and dense smoke, when fires are at their worst, obscure the ground surface for days or weeks, precluding optical imaging. When satellites can

observe the surface, the detection of fires and associated burned areas are challenging because fires typical of peatland burning are frequently smoldering and of small size. More frequent observations (higher temporal resolution) and finer spatial resolution imaging from satellites are needed to overcome these challenges in the future. At present, multi-scale approaches for addressing these issues are possible using imagery from many currently available and forthcoming satellite generations (Table 5-1).

Over the last two decades, imagery from the Terra/Aqua satellites has been used to provide tools for monitoring fire activity and burned area, enabling estimation of global emissions. Several MODIS-derived burned area products have been developed but the collection 5 products (MCD45A1 and MCD64A1) are now defunct, with the MCD64A1 collection 6 as the preferred standard product moving forward. The lifetime of the Terra and Aqua satellites are coming to an end, but the Suomi National Polar-orbiting Partnership (S-NPP) spacecraft that was launched in October 2011 will continue the missions. One of the sensors, the Visible Infrared Imaging Radiometer Suite (VIIRS) is intended to improve upon the long-used operational Advanced Very High-Resolution Radiometer (AVHRR) imagery and provide continuity with the EOS Moderate Resolution Imaging Spectroradiometer (MODIS). Various algorithms have been developed to ensure the smooth delivery of products following the transition from MODIS operations (Justice et al., 2013, Jackson et al., 2013), and provide long-term earth observation records. The spectral bands consist of 5 high-resolution imagery channels (I band), 16 moderate resolution (M band), and a single Day/Night band (DNB). VIIRS images have been promising, with finer spatial resolution than MODIS (375 and 750 m at nadir), and multispectral (22 bands) capabilities. VIIRS active fire and burned area algorithms employ

the same methods as MODIS at finer spatial resolution (~375 m and 750 m, respectively) (Schroeder et al., 2014, Giglio et al., 2019), ensuring the continuity of a long-term product for global fire monitoring.

Unlike MODIS, VIIRS imagery has no orbital gaps in its observations of the tropics. This synoptic coverage helps to reduce uncertainty about burned area estimates and provide more chances to observe during cloud-free conditions. Providing this data would help to ensure a consistent fire history record for Indonesia, which is critical given the lack of other comparable data sources. Since fire frequency is correlated with the amount of emissions generated by peat fires (Konecny et al., 2016), improved burned area estimates are still needed. The use of automated methods has reduced the need for visual classifications by less skilled labor to create burned area maps. Random Forest was tested in this study and shown to be a promising method for mapping burned area using Landsat data. Unlike visual interpretation techniques that are currently used by the Indonesian authority, the interpreter only needs to make decisions about a limited number of data samples. However, cloud-free data are required, which necessitates integrating several images into a cloud-free composite image. The ideal approach requires adequate cloud and shadow masking to ensure that not too many pixels are excluded due to strict criteria or included due to loose criteria that increase errors in burned area detection. I found that the quality assurance layer of the Landsat product was incapable of separating thin/small clouds and associated shadows, therefore causing masks that excluded much of the region.

Incorporation of various satellite datasets, which are spatially or temporally different, is crucial to filling imaging data gaps. The launch of geostationary satellites Himawari-8 and 9, which replaced MTSAT-1/2R, has great promise for integration to

improve emissions modeling by potentially providing higher temporal active fire or burned area detection (15-30 min). The Advanced Himawari Imager (AHI) onboard Himawari-8/9 has 16 channels with central wavelengths ranging from 0.47 µm to 13.3 µm. In addition to the additional 12 channels equipped with the AHI, the spatial resolution of AHI 0.65 µm channel increases to 0.5 km from 1 km. Other visible bands of AHI have a resolution of 1 km while its near-infrared and infrared channels have resolutions of 2 km (Da, 2015). AHI employs comparable spectral bands as VIIRS but has greater temporal resolution. Combining these two instruments for burned area mapping should prove valuable for reducing uncertainty about fire behavior and spread. There may also be potential for determining if smoldering deep peat fires are present based on persistent active fire detections of low fire radiative power and less pronounced diurnal cycles at a location over several consecutive days.

For burned area mapping at low-medium resolution (~30 m), combining Landsat and Sentinel-2 satellite imagery cuts overpass data gaps by half. Various studies have proven their combined reliability for mapping burned area and detecting active fire (Schroeder et al., 2016, Roy et al., 2019, Roteta et al., 2019). Sentinel-3, on the other hand, was designed primarily for ocean studies, but the spectral bands (see Table 5-1) are capable of observing fires as well, the stated second objective of the satellite (ESA, 2021).

In addition to optical sensors, radar-based approaches have been developed with currently available satellite in orbit. Our assessment in this study showed that, during severe 2015 burning season, the C-band data from Sentinel-1 (Lohberger et al., 2017, Carreiras et al., 2020) was superior to data from optical sensors, for mapping burned area, because of its ability to penetrate the thick clouds and smoke. Despite having lower

temporal resolution, several additional satellites with active remote sensing are currently available (also provided by LAPAN). These include TerraSAR-X/TanDEM-X, Radarsat, ALOS-2, Cosmosky-Med, and the constellation of ICEYE SAR satellites extending the range of potential radar data to be used. Additionally, free radar satellite data will be provided in the near future by NISAR (NASA-ISRO Synthetic Aperture Radar)(Sharma et al., 2018), which will be launched in September 2022. Carrying L- and S- band radar with a 12 day repeat cycle and high spatial resolution (3–10 m mode-dependent)(Xaypraseuth et al., 2015), NISAR may complement the C-band observations from Sentinel 1. Few studies have investigated the use of these satellites (with different wavelengths) (Tanase et al., 2010) in addition to Sentinel 1 (Belenguer-Plomer et al., 2019), in particular for burning in peatlands (Lohberger et al., 2017, Carreiras et al., 2020). Therefore, more research is merited, comparing their sensitivities at different degrees of burn severity, for both deep and surface peat fires, as a function of wavelength, polarization, incidence angle, and imaging mode.

To meet a range of different purposes, Indonesia has a critical need for accurate burned area mapping. These reasons include, fire-related emissions monitoring of peatland burning, law enforcement, rapid assessment, and efforts to suppress fire. As such, with more data available, guidelines for using these datasets are essential. Figure 5-1 describes an alternative framework for selecting data from currently available and expected future datasets, considering fire season severity and the scale of purpose. For example, radar can play an important role in burned area mapping, specifically when smoke/cloud obstruct visibility, precluding use of optical remote sensing. However, soil moisture influences the sensor's accuracy (Belenguer-Plomer et al., 2019), so its utility is greatest during very dry

seasons. VIIRS-AF is ideal for rapid mapping, when only an overall picture of a burning situation is required. Before any direct use of these data, persistent fire pixels (e.g., gas flare or active volcano) should be masked. This is a known problem. VIIRS gas flare sources (https://www.ngdc.noaa.gov/eog/viirs/download_global_flare.html, last accessed 10 January 2021) can be used as a guide. Roof tops have also been identified as a potential source of error (Sofan et al., 2020), so an additional land cover map for inhabited areas may be needed. This source of error was not a problem in the sparsely inhabited region I studied. Merging Landsat and Sentinel-2 could be a solution for monthly mapping purposes. Harmonized Landsat and Sentinel-2 are advantageous for minimizing intensive pre-processing (Claverie et al., 2018).

The use of geospatial-based scientific evidence has been rising lately for prosecuting illegal burning activities (MoEF (KLHK), 2019), including those reported for plantations. Data from multiple sensors data may assist the court in deciding cases. These data include images showing the trajectory of smoke (e.g., Figure 4-2), VIIRS 375 active fire showing fire spread progression (Figure 4-9e), and commercial very high-resolution images, currently funded by the Indonesian government, would be of great benefit for these purposes. Planet has also been a great source for daily high-resolution images. With 150+ satellites in orbit, Planet may answer the needs for high temporal and spatial resolution; however, they are potentially costly.

All these data will not be usable unless they are integrated into a mutually supportive platform. Awareness of the importance of geospatial data has increased substantially. Currently, however, the use of these data is haphazard by the user community for geospatial research in peatland of Indonesia. I urge the establishment of an integrated

platform, which will not only assist in locating remote sensing-based data, but also additional geospatial field data. These data include, but not limited to, land use/cover maps, soil moisture, disturbance history, ground water level, and air quality index data. Landfire (Landscape Fire and Resource Management Planning Resources Project (Ryan and Opperman, 2013, Rollins, 2009), http://www.landfire.gov (last accessed 26 December 2020)) is one of example of an initiative that generates consistent and detailed maps and data on vegetation, wildland fuel, fire regimes and ecological changes from historic conditions across the United States. This framework results from the incorporation of remote sensing, vegetation inventory and simulation of ecosystem processes. The inclusion of these data promotes preventive initiatives to restore burned areas as a single management entity, beginning with scientifically validated and interdisciplinary aspects.

In this study, I did not integrate the peat hydrology and land use/cover type in any method. Moisture levels determine the ignition probability of peat soils by surface fires, which are not constant (Aswin et al., 2004, Frandsen, 1997). Typically, various factors affect peat burning rates, such as dry conditions, the intensity of fires, and whether rainfall occurs during the fires. A consistent relationship exists between burn depth and groundwater table levels within the peat (Ballhorn et al., 2009). Therefore, geospatial peat hydrology information should be considered when mapping burned area or depth of burning in peatlands (Taufik et al., 2017). Combining such a moisture indication and an updated land use/cover map is critical for avoiding or correcting possible misclassifications due to either cloud shadow or seasonal water, both of which usually having a low value of spectral burn indices (e.g., Normalized Burn Ratio). Multitemporal data series will also be helpful for confirming that changes were not due to non-burning activities.

Since peatland fire vulnerability is primarily controlled by the peat moisture content, hydrology monitoring is essential. Satellite radar observation is a potentially useful tool for hydrological modeling (Hoekman, 2007). Soil moisture remote sensing-based data are available, such as Soil Moisture Active Passive (SMAP) and The Advanced Microwave Scanning Radiometer-EOS (AMSR-E and AMSR-2). AMSR-2 is superior for work under dry conditions (Kim et al., 2015) together with SMAP (Velpuri et al., 2016), making the products ideal for monitoring fire activity in drained peatlands. The Gravity Recovery and Climate Experiment (GRACE) satellite was also found reliable to assess water storage and fire management in regions with extensive biomass burning, such as Kalimantan (Han et al., 2017).

To date, our attention focuses on peatland because its effect on carbon emissions is greater than that of non-peatland fires. Burned detection in non-peatlands was much less accurate than in peatlands for MODIS-derived burned area products (Vetrita et al., 2020). Agricultural practices in these areas tend to generate smaller patchy fires. Non-peat areas, especially in the southern part of Indonesia, near Australia (Nusa Tenggara Timur Province), have been reported to have contributed to the highest consistent burned area in the last few years (MoEF, 2020). Fires in this dominant savannah grassland area were previously recorded in 2003-2004 (Fisher et al., 2006) with substantial damages and losses. With rougher topography (combining plains and rugged terrain) than the majority of Indonesian peatland, work in these areas may face the additional challenge of topographic effects on classifications. For example, shadow or layover effects on the processing of radar data or a bi-directional effect on the processing of optical sensors. The first MODIS-derived BA products (MDC45A1 Collection 5) used BRDF (bidirectional reflectance

distribution function) was found to be more accurate than BA's standard MODIS BA (MCD64A1 C6) in mountainous regions (Fornacca et al., 2017). However, MCD45A1 has suffered from missing observations due to cloud/smoke that could impair its accuracy in the tropics (Roy et al., 2008). Therefore, an alternative approach to BA-derived BRDF for the Indonesian region with a significant topography effect is merited. Further study should be conducted to find whether all models I explored here were peatland specific.

Table 5-1 Current and upcoming datasets to support a burned area mapping from Indonesian peatlands

Satellite (sensor)	Temporal resolution	Spatial resolution	Availability	Sources/references	Spectral bands/product name
High temporal resolution					
Terra/Aqua (MODIS)	Monthly	500 m	2001-present (end life time but still works)	NASA https://ladsweb.modaps.eosdis.nasa.gov/ (Giglio et al., 2018)	MCD64A1 Collection 6
Suomi-NPP (VIIRS)	Monthly	500 m	2013-present	NASA/USGS https://lpdaac.usgs.gov/ (Giglio et al., 2019)	VNP64A1 Collection 1
Suomi-NPP and NOAA-20 (VIIRS)	Daily	375 and 750 m	2014-present	NASA https://ladsweb.modaps.eosdis.nasa.gov/ (Oliva and Schroeder, 2015, Schroeder et al., 2014)	VNP14IMG
Sentinel-3 A and B (SLSTR)	1 day	500 m (VIS, SWIR), 1 km (MWIR, TIR)	2016-present	ESA https://sentinels.copernicus.eu/web/sentinel/home	Visible, NIR, SWIR, TIR
Himawari-8/9 (AHI)	15–30 min	~2 km	2015-present, available through the climatology bureau	Japan Meteorological Agency	Visible, NIR, SWIR, TIR
Medium resolution ≤30 m					
Landsat series	16 days	30 m	1995-present	NASA https://lpdaac.usgs.gov/	Visible, NIR, SWIR, TIR
Sentinel-2 A and B (MSI)	5-10 days	20 m (multispectral)	2015-present	ESA https://sentinels.copernicus.eu/web/sentinel/home	Visible, NIR, SWIR
Radar					

Satellite (sensor)	Temporal resolution	Spatial resolution	Availability	Sources/references	Spectral bands/product name
Sentinel-1 A and B	6-12 days	5-40 m (depending on acquisition mode and level of processing)	2014-present	ESA https://sentinels.copernicus.eu/web/sentinel/home	C-band
TerraSAR-X/TanDEM-X	11 days	0.25-18 m	2007-present	https://www.dlr.de/content/en/articles/missions-projects/terrasar-x/terrasar-x-earth-observation-satellite.html (accessed on 9 January 2021)	X-band
NISAR	12 days	5-10 m	2022	NASA-ISRO (Xaypraseuth et al., 2015)	L- and S-band
ALOS-2	14 days	Spotlight mode 1-3 m and high resolution mode 3-10 m	2014-present	https://www.eorc.jaxa.jp/ALOS-2/en/about/palsar2.htm (accessed on 9 January 2021)	L-band
RADARSAT	12 days	3-100 m	1995-present	https://www.asc-csa.gc.ca/eng/satellites/radarsat/default.asp (accessed on 9 January 2021)	C-band
PALSAR	46 days	7-10 m	2006-present	https://www.eorc.jaxa.jp/ALOS/en/about/palsar.htm (accessed on 9 January 2021)	L-band
ICEYE SAR	Tasked	~0.25-3 m	2018-present	https://www.iceye.com/ (accessed on 10 January 2021)	X-band
High resolution images					
SPOT 6/7, Geoeye, WorldView, Pleiades, Quickbird	Variable, ~25 days (tasked)	≤6 m	At least from 2011-present	LAPAN (https://www.lapan.go.id/)	Visible (mostly)
Planet	Daily	50 cm-3.7 m	2009/2014 (archive)-present	Planet monitoring https://www.planet.com/products/monitoring/ (accessed on 9 January 2021)	Visible, NIR, Panchromatic
Drone	Tasked				Visible

See list of abbreviations for AHI, ALOS, ESA, LAPAN, MODIS, NASA, NIR, NISAR, NOAA, NPP, SAR, SLSTR, SWIR, TIR, and VIIRS.

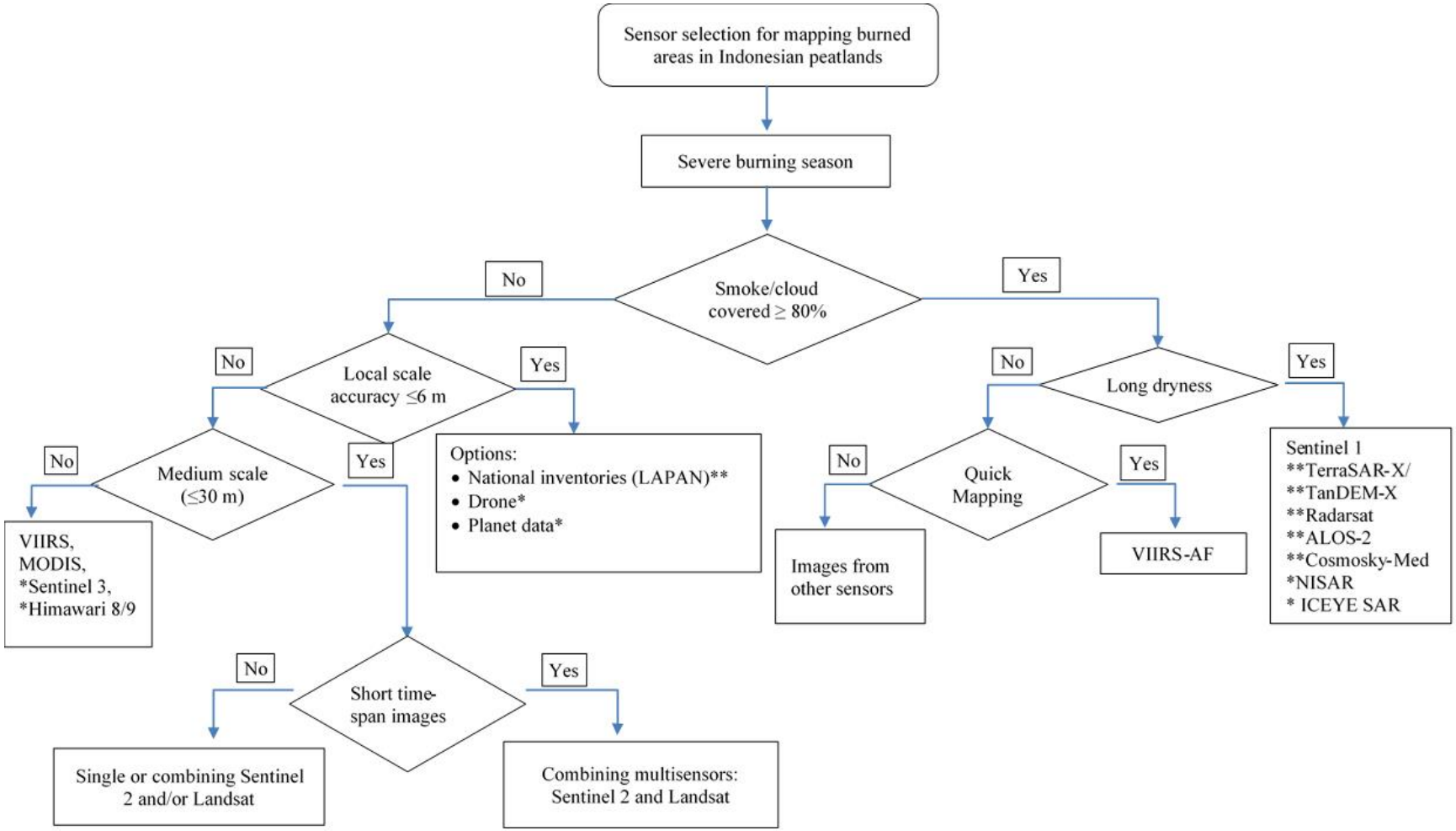

Figure 5-1 Decision tree as an alternate method for selecting among available satellite/sensor data for burned area mapping in Indonesian peatlands. The one-star (*) symbol indicates potentially useful satellites/tools that I have excluded from this study. National data inventories** currently

available for use in burning area mapping include SPOT-6/SPOT-7, Pleiades, Quickbird, Worldview, GeoEye and various radar-based satellites. Abbreviations: VIIRS-AF= Visible Infrared Imaging Radiometer Suite-Active Fire (the gridded active fire), VIIRS=NOAA-20 and Suomi NPP satellites; MODIS=; Moderate Resolution Imaging Spectroradiometer; ALOS= The Advanced Land Observing Satellite 2; NISAR= The NASA-ISRO Synthetic Aperture Radar.

References

Aswin, U., Hashimoto, Y., Takahashi, H., & HAYASAKA, H. (2004). Combustion and thermal characteristics of peat fire in tropical peatland in Central Kalimantan, Indonesia. *Tropics, 14*, 1-19

Ballhorn, U., Siegert, F., Mason, M., & Limin, S. (2009). Derivation of burn scar depths and estimation of carbon emissions with LIDAR in Indonesian peatlands. *Proc Natl Acad Sci U S A, 106*, 21213-21218

Belenguer-Plomer, M.A., Tanase, M.A., Fernandez-Carrillo, A., & Chuvieco, E. (2019). Burned area detection and mapping using Sentinel-1 backscatter coefficient and thermal anomalies. *Remote Sensing of Environment, 233*, 111345

Carreiras, J.M., Quegan, S., Tansey, K., & Page, S.J.E.R.L. (2020). Sentinel-1 observation frequency significantly increases burnt area detectability in tropical SE Asia, *15*, 054008

Claverie, M., Ju, J., Masek, J.G., Dungan, J.L., Vermote, E.F., Roger, J.-C., Skakun, S.V., & Justice, C.J.R.s.o.e. (2018). The Harmonized Landsat and Sentinel-2 surface reflectance data set, *219*, 145-161

Da, C. (2015). Preliminary assessment of the Advanced Himawari Imager (AHI) measurement onboard Himawari-8 geostationary satellite. *Remote Sensing Letters, 6*, 637-646

ESA. 2021. Sentinel-3 mission objectives. https://sentinels.copernicus.eu/web/sentinel/missions/sentinel-3/mission-objectives (accessed on 10 January 2021)

Fisher, R., Bobanuba, W.E., Rawambaku, A., Hill, G.J., & Russell-Smith, J. (2006). Remote sensing of fire regimes in semi-arid Nusa Tenggara Timur, eastern Indonesia: current patterns, future prospects. *International Journal of Wildland Fire, 15*, 307-317

Fornacca, D., Ren, G., & Xiao, W.J.R.S. (2017). Performance of three MODIS fire products (MCD45A1, MCD64A1, MCD14ML), and ESA Fire_CCI in a mountainous area of Northwest Yunnan, China, characterized by frequent small fires, *9*, 1131

Frandsen, W.H. (1997). Ignition probability of organic soils. *Canadian Journal of Forest Research, 27*, 1471-1477

Giglio, L., Boschetti, L., Roy, D., Humber, M., & Hall, J.V. (2019). Collection 1 VIIRS Burned Area Product User's Guide Version 1.0 (VNP64A1 Collection 1). In: NASA

Giglio, L., Boschetti, L., Roy, D.P., Humber, M.L., & Justice, C.O. (2018). The Collection 6 MODIS burned area mapping algorithm and product. *Remote Sensing of Environment, 217*, 72-85

Han, J.C., Tangdamrongsub, N., Hwang, C., & Abidin, H.Z. (2017). Intensified water storage loss by biomass burning in Kalimantan: Detection by GRACE. *Journal of Geophysical Research-Solid Earth, 122*, 2409-2430

Hoekman, D.H. (2007). Satellite radar observation of tropical peat swamp forest as a tool for hydrological modelling and environmental protection. *Aquatic Conservation-Marine and Freshwater Ecosystems, 17*, 265-275

Jackson, J.M., Liu, H., Laszlo, I., Kondragunta, S., Remer, L.A., Huang, J., & Huang, H.-C. (2013). Suomi-NPP VIIRS aerosol algorithms and data products. *Journal of Geophysical Research: Atmospheres, 118*, 12,673-612,689

Justice, C.O., Román, M.O., Csiszar, I., Vermote, E.F., Wolfe, R.E., Hook, S.J., Friedl, M., Wang, Z., Schaaf, C.B., Miura, T., Tschudi, M., Riggs, G., Hall, D.K., Lyapustin, A.I., Devadiga, S., Davidson, C., & Masuoka, E.J. (2013). Land and cryosphere products from Suomi NPP VIIRS: Overview and status. *Journal of Geophysical Research: Atmospheres, 118*, 9753-9765

Kim, S., Liu, Y.Y., Johnson, F.M., Parinussa, R.M., & Sharma, A. (2015). A global comparison of alternate AMSR2 soil moisture products: Why do they differ? *Remote Sensing of Environment, 161*, 43-62

Konecny, K., Ballhorn, U., Navratil, P., Jubanski, J., Page, S.E., Tansey, K., Hooijer, A., Vernimmen, R., & Siegert, F. (2016). Variable carbon losses from recurrent fires in drained tropical peatlands. *Glob Chang Biol, 22*, 1469-1480

Lohberger, S., Stängel, M., Atwood, E.C., & Siegert, F. (2017). Spatial evaluation of Indonesia's 2015 fire affected area and estimated carbon emissions using Sentinel-1. *Global Change Biology, 24*, 644-654

MoEF (2020). Sipongi, Karhutla Sistem. In, *Rekapitulasi Luas Kebakaran Hutan dan Lahan (Ha) Per Provinsi Di Indonesia Tahun 2015-2020*. Jakarta

MoEF (KLHK) (2019). KLHK Terapkan Tiga Langkah Penguatan Penegakan Hukum Karhutla. In. Jakarta, Indonesia

Oliva, P., & Schroeder, W. (2015). Assessment of VIIRS 375m active fire detection product for direct burned area mapping. *Remote Sensing of Environment, 160*, 144-155

Pessôa, A.C.M., Anderson, L.O., Carvalho, N.S., Campanharo, W.A., Junior, C.H., Rosan, T.M., Reis, J.B., Pereira, F.R., Assis, M., & Jacon, A.D.J.R.S. (2020). Intercomparison of Burned Area Products and Its Implication for Carbon Emission Estimations in the Amazon, *12*, 3864

Rollins, M.G. (2009). LANDFIRE: a nationally consistent vegetation, wildland fire, and fuel assessment %J International Journal of Wildland Fire, *18*, 235-249

Roteta, E., Bastarrika, A., Padilla, M., Storm, T., & Chuvieco, E. (2019). Development of a Sentinel-2 burned area algorithm: Generation of a small fire database for sub-Saharan Africa. *Remote Sensing of Environment, 222*, 1-17

Roy, D.P., Boschetti, L., Justice, C.O., & Ju, J. (2008). The collection 5 MODIS burned area product—Global evaluation by comparison with the MODIS active fire product. *Remote Sensing of Environment, 112*, 3690-3707

Roy, D.P., Huang, H., Boschetti, L., Giglio, L., Yan, L., Zhang, H.H., & Li, Z. (2019). Landsat-8 and Sentinel-2 burned area mapping - A combined sensor multi-temporal change detection approach. *Remote Sensing of Environment, 231*, 111254

Ryan, K.C., & Opperman, T.S. (2013). LANDFIRE – A national vegetation/fuels data base for use in fuels treatment, restoration, and suppression planning. *Forest Ecology and Management, 294*, 208-216

Schroeder, W., Oliva, P., Giglio, L., & Csiszar, I.A. (2014). The New VIIRS 375m active fire detection data product: Algorithm description and initial assessment. *Remote Sensing of Environment, 143*, 85-96

Schroeder, W., Oliva, P., Giglio, L., Quayle, B., Lorenz, E., & Morelli, F. (2016). Active fire detection using Landsat-8/OLI data. *Remote Sensing of Environment, 185*, 210-220

Sharma, P., Doubleday, J.R., & Shaffer, S. (2018). Instrument commissioning timeline for NASA-ISRO Synthetic Aperture Radar (NISAR). In, *2018 IEEE Aerospace Conference* (pp. 1-13): IEEE

Sofan, P., Bruce, D., Schroeder, W., Jones, E., & Marsden, J. (2020). Assessment of VIIRS 375 m active fire using tropical peatland combustion algorithm applied to Landsat-8 over Indonesia's peatlands. *International Journal of Digital Earth, 13*, 1695-1716

Tanase, M.A., Santoro, M., de La Riva, J., Fernando, P., Le Toan, T.J.I.T.o.G., & Sensing, R. (2010). Sensitivity of X-, C-, and L-band SAR backscatter to burn severity in Mediterranean pine forests, *48*, 3663-3675

Taufik, M., Torfs, P.J., Uijlenhoet, R., Jones, P.D., Murdiyarso, D., & Van Lanen, H.A. (2017). Amplification of wildfire area burnt by hydrological drought in the humid tropics. *Nature Climate Change*

Velpuri, N.M., Senay, G.B., & Morisette, J.T. (2016). Evaluating New SMAP Soil Moisture for Drought Monitoring in the Rangelands of the US High Plains. *Rangelands, 38*, 183-190

Vetrita, Y., & Cochrane, M.A. (2019). Annual Burned Area from Landsat, Mawas, Central Kalimantan, Indonesia, 1997-2015. *ORNL DAAC, Oak Ridge, Tennessee, USA*. DOI: https://doi.org/10.3334/ORNLDAAC/1708

Vetrita, Y., & Cochrane, M.A. (2020). Landsat-derived Land Use/Cover Maps, Mawas, Central Kalimantan, Indonesia, 1994-2019. *ORNL DAAC, Oak Ridge, Tennessee, USA*. DOI: https://doi.org/10.3334/ORNLDAAC/1838

Vetrita, Y., Cochrane, M.A., Suwarsono, S., Priyatna, M., Sukowati, K.A.D., & Khomarudin, M.R. (2020). Evaluating accuracy of four MODIS-derived burned area products for tropical peatland and non-peatland fires. *Environmental Research Letters*. DOI: https://doi.org/10.1088/1748-9326/abd3d1

Xaypraseuth, P., Satish, R., & Chatterjee, A. (2015). NISAR spacecraft concept overview: Design challenges for a proposed flagship dual-frequency SAR mission. In, *2015 IEEE Aerospace Conference* (pp. 1-11): IEEE